AUSTRALIAN NATIONAL ANTARCTIC RESEARCH EXPEDITIONS

A N A R E

R E S E A R C H

N O T E S

28

Australian Glaciological Research; 1982 - 1983

Edited by T.H. Jacka

ANTARCTIC DIVISION
DEPARTMENT OF SCIENCE

ANARE RESEARCH NOTES (ISSN 0729-6533)

This series allows rapid publication in a wide range of disciplines. Copies of this and other ANARE Research Notes are available from the Antarctic Division. Any person who has participated in Australian National Antarctic Research Expeditions is invited to publish through this series. Before submitting manuscripts authors should obtain a style guide from:

The Publications Office
Antarctic Division
Channel Highway
Kingston
Tasmania 7150
Australia.

Published September 1985
ISBN: 0 642 07625 1

CONTENTS

PREFACE

The short papers in this volume were presented at a three day informal meeting held at The University of Melbourne from May 23-25, 1984. The purpose of the meeting was to review advances made in Australia in glaciological and related research projects in 1982 and 1983. The work presented represented recent Antarctic field studies, laboratory experiments, modelling studies, and analysis of earlier data.

While the majority of the participants at the meeting were members of either the Antarctic Division Glaciology Section or The University of Melbourne Meteorology Department, a total of eight different organisations were represented at the meeting. Further organisations were represented by co-authors of papers resulting from co-operative research projects. Because of the wide interdisciplinary interest that the meeting generated, a number of papers were presented and are published here that, while not directly glaciological, are in related fields such as Antarctic meteorology or oceanography.

The majority of papers published in this volume are preliminary. They are published in this short form so that the larger Australian research community working on Antarctic projects, and the international glaciological community, can be kept informed of current and planned future directions of Australian glaciological research. It is expected that most of the papers will be published in a fuller form in appropriate journals in the not too distant future.

Finally, on behalf of all participants, I would like to thank Jo Jacka, Lynette Christou and Siew F. Ho for their efficient organisation of the meeting, their efforts in pursuing participants until they finally produced written versions of the papers, and for producing the edited version of this volume. The meeting was not only productive, but also enjoyable, and we hope to hold a similar meeting in another two or three years.

Ian Allison
Glaciology Section
Antarctic Division

LIST OF PARTICIPANTS

I. Allison	Antarctic Division.
W. Budd	Meteorology Department, The University of Melbourne.
L. Christou	Meteorology Department, The University of Melbourne.
B. Cook	Meteorology Department, The University of Melbourne.
E. Davis	Antarctic Division.
F. DeSilva	CSIRO; Division of Atmospheric Research.
D. Etheridge	Antarctic Division.
R. Francey	CSIRO; Division of Atmospheric Research.
P. Geissler	Meteorology Department, The University of Melbourne.
I. Goodwin	Antarctic Division.
T. Hamley	Antarctic Division.
J. Ivy	Australian Government Analytical Laboratories.
T. Jacka	Antarctic Division.
P. James	National Mapping.
D. Jenssen	Meteorology Department, The University of Melbourne.
D. Jones	Antarctic Division.
T. Medhurst	Antarctic Division.
J. Mitchell	Geology Department, The University of Melbourne.
V. Morgan	Antarctic Division.
B. Murphy	National Mapping.
G. Pearman	CSIRO; Division of Atmospheric Research.
H. Phillpot	Meteorology Department, The University of Melbourne.
P. Quilty	Antarctic Division.
D. Russell-Head	Faculty of Engineering, The University of Melbourne.
I. Simmonds	Meteorology Department, The University of Melbourne.
I. Smith	Meteorology Department, The University of Melbourne.
B. Van Meurs	Meteorology Department, The University of Melbourne.
E. Wehrle	Antarctic Division.
S. Williams	Meteorology Department, The University of Melbourne.
T. Wishart	Meteorology Department, The University of Melbourne.
J. Wilson	Bureau of Meteorology.
M. Wolff	Antarctic Division.
N. Young	Antarctic Division.

A. ANTARCTIC ICE CORE AND BOREHOLE STUDIES

Ice core and borehole studies can be considered to include three separate research areas. Firstly, access to ice from deep within the ice cap permits comprehensive measurement of its flow determining properties. The effects of crystal fabric alignment and temperature are known from laboratory measurements and results from such measurements are discussed in this volume in the section on ice mechanics. Significant flow enhancement can be produced by well aligned crystal c-axes. This means the effects of the well developed, but variable fabrics found in deep cores must be included in ice cap modelling studies.

Secondly, measurements of the borehole deformation (inclination change, extension or compression, and closure) can give, at least at the borehole location, a detailed and direct picture of the ice flow. This information, together with the crystal structure cannot be obtained by any means other than by drilling into the ice. Due to interactions between the flow and the crystal structure it is important that both are measured together. Results presented here from the Law Dome ice drilling show how the feedback mechanism (whereby the crystal structure controls the flow but is itself determined by the previous strain history) can produce complicated ice flow patterns apparently as a result of stress variations over the rough bedrock.

The third use arises because the ice cap is composed entirely of atmospheric fallout material. Included in the snowfall are dust particles, chemicals dissolved in the snow crystals and radioactive materials. Gas is also trapped as air bubbles in the ice during the process by which the snow is compressed into ice. All these materials are deposited as layers which are preserved, apart from minor mixing on the surface and thinning due to the ice flow at depths. Entrapped gases are investigated to provide data on past atmospheric conditions and compositions, and past climate conditions over periods ranging from a few years to 100 000 years.

In the near future work will include further investigations of the complicated ice flow patterns near Cape Folger on the Law Dome, the establishment of detailed atmospheric CO_2 levels over the last 20 000 years and the extension back in time of the oxygen isotope - climate record using the well dated Law Dome summit core. Further drilling, using a new mechanical drill instead of the thermal drill, will allow deeper boreholes in the most favourable locations such as the Law Dome summit, where annual layers easily detectable by oxygen isotope analysis allow accurate dating. After this, drilling on the main East Antarctic ice cap, where ice thicknesses of 4000 m are accompanied by an annual accumulation of only a few centimetres of ice, will allow records to be extended back several hundreds of thousand years in substantially undistorted strata.

V.I. Morgan

1. ENHANCED SHEAR ZONES IN ICE FLOW - IMPLICATIONS FOR ICE CAP MODELLING AND CORE DATING

V.I. Morgan and A.P. McCray
Antarctic Division, Department of Science
Kingston, Tasmania, 7150.

ABSTRACT

Oxygen isotope profiles for Law Dome boreholes can be used to deduce ages for the deep ice either by detecting annual layers or by comparison of known climatic features. Preliminary data from a recent ice drilling program is presented which will be used with a simple ice particle flow model to try to duplicate these ages by adjustment of various parameters, principally the vertical velocity profile to compensate for stagnant basal ice layers and the amount of snow accumulation in line with variations suggested by the ice core data.

1.1 INTRODUCTION

In ice dynamics studies (e.g. Nye, 1957; Budd and others, 1971) it is generally assumed that shear strain rates in an ice sheet increase monotonically with depth as a result of the concurrent increases in temperature and stress, and thus that they are greatest at the ice rock interface. This form of flow pattern is also usually assumed in ice cap modelling, and because there are as yet no direct dating methods for the deep ice, is commonly used to compute age-depth relationships within the ice cap.

Recent ice drilling work at Cape Folger on the Law Dome (see also Etheridge and McCray, this volume; Budd and Rowden-Rich, this volume) shows that due to bedrock irregularities and the non-uniform plasticity of glacier ice, more complicated flow patterns than have previously been assumed can arise and be self sustaining, presumably as a result of the feed forward effects of crystal development (Budd, 1972). The substantial errors in flowlines and ages calculated from models which make no allowance for bedrock blocking are illustrated by comparing ages from such a model (Pfitzner, 1980) with ages obtained by oxygen isotope analysis of Law Dome ice cores. The model ages are all found to be much lower (20 to 100%) than those found from the independent dating. In this note data are collected from various Law Dome drilling programs and used to deduce ages of the ice at depth. A simple two-dimensional model is to be used to try to duplicate these ages by adjustment of various parameters, principally the vertical velocity profile and the snow accumulation. The vertical velocity profile can be specified in detail (e.g. to include zones of stagnant ice) although only as an average for the whole flow line. Otherwise, the model calculates particle paths and isochrones for a steady state (i.e. constant size and shape) ice cap using the surface and bedrock profiles, ice accumulation and ice surface velocity. For the flow line from the Dome summit to the edge of the ice cap at Cape Folger (Figure 1) the present day parameters are well known. It is also considered that with the exception of the accumulation these have not changed very significantly since the ice cap revealed to its present size at

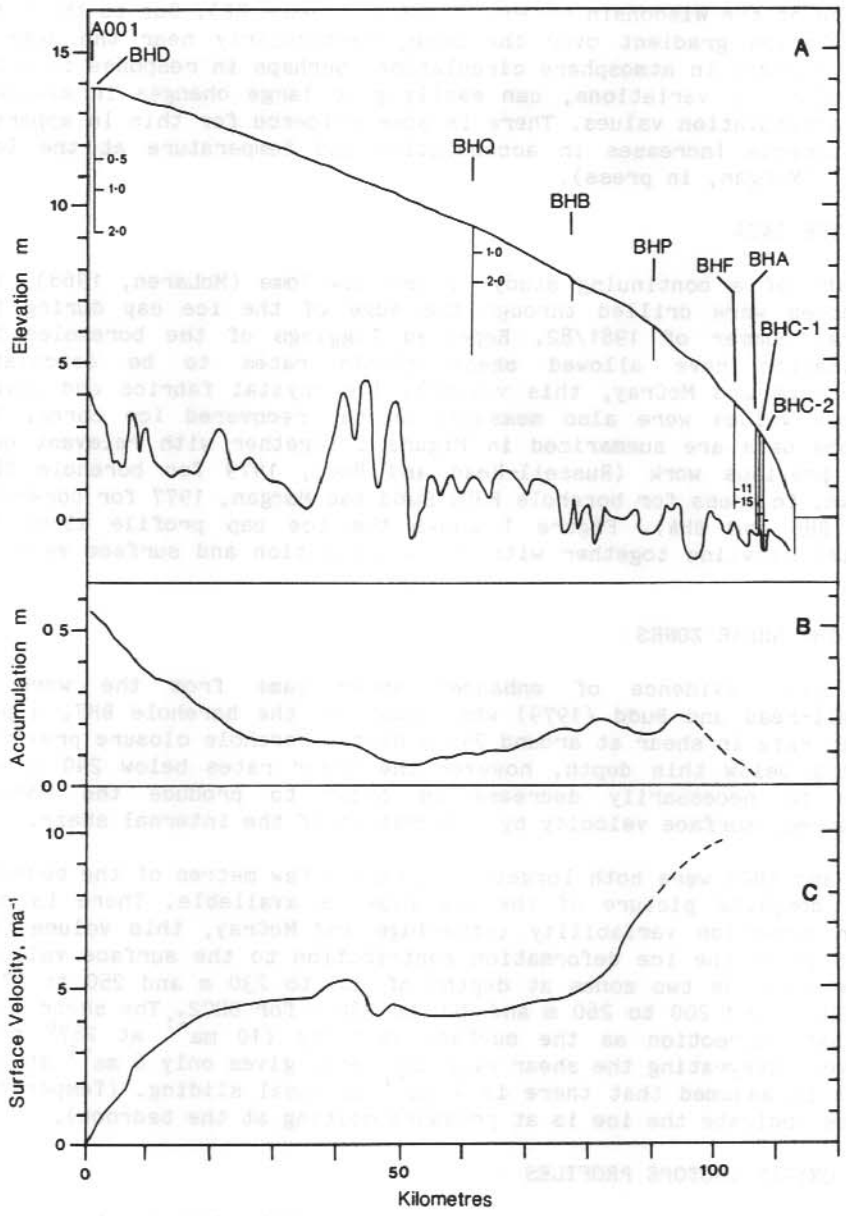

Figure 1. The profile of the Law Dome from its summit A001 to its edge at Cape Folger. The line A001 to Cape Folger approximates a surface flowline and is considered as one in the flow model.
Boreholes are indicated by vertical lines with ages determined from oxygen isotope data in thousands of years. The summit borehole (BHD) is approximately 1 km from the summit survey point A001. The measured snow accumulation over the last few years in ice equivalent is shown in B and the measured surface velocity in C.

the end of the Wisconsin period (11-15 000 years BP). Due to the large accumulation gradient over the Dome, particularly near the summit, small changes in atmosphere circulation, perhaps in response to short term climatic variations, can easily give large changes in measured snow accumulation values. There is some evidence for this in apparent simultaneous increases in accumulation and temperature at the Dome summit (Morgan, in press).

1.2 THE DATA

As part of a continuing study of the Law Dome (McLaren, 1968), two boreholes were drilled through the edge of the ice cap during the austral summer of 1981/82. Repeated loggings of the boreholes for inclination have allowed shear strain rates to be calculated (Etheridge and McCray, this volume). Ice crystal fabrics and oxygen isotope values were also measured on the recovered ice cores. The isotope data are summarized in Figure 2 together with relevant data from previous work (Russell-Head and Budd, 1979 for borehole BHF; Morgan, in press for borehole BHD; Budd and Morgan, 1977 for boreholes BHP, BHB and BHA). Figure 1 shows the ice cap profile along the studied flowline together with ice accumulation and surface velocity data.

1.3 THE SHEAR ZONES

The first evidence of enhanced shear came from the work of Russell-Head and Budd (1979) who found for the borehole BHF, a peak strain rate in shear at around 240 m depth. Borehole closure prevented logging below this depth, however the shear rates below 240 m were shown to necessarily decrease in order to produce the correct (measured) surface velocity by integration of the internal shear.

BHC1 and BHC2 were both logged to within a few metres of the bedrock, so a complete picture of the ice flow is available. There is some shear direction variability (Etheridge and McCray, this volume) but the bulk of the ice deformation contribution to the surface velocity comes from the two zones at depths of 200 to 230 m and 250 to 270 m for BHC1, and 200 to 260 m and 300 to 330 m for BHC2. The shear is in the same direction as the surface velocity (10 ma^{-1} at 287^{o} true) however integrating the shear over the depth gives only 6 ma^{-1} at 287^{o} so it is assumed that there is 4 ma^{-1} of basal sliding. (Temperature curves indicate the ice is at pressure melting at the bedrock).

1.4 OXYGEN ISOTOPE PROFILES

Oxygen isotope ratios (δ values) in Antarctic ice samples can be regarded as indicators of prevailing atmospheric conditions which existed when the particular piece of ice was formed from atmospheric water vapour. Once the ice has been consolidated into the snow pack, its δ value remains unchanged indefinitely. Patterns of variations in one ice core can therefore be matched with those in another to provide a method of assigning simultaneous dates of deposition (and hence ages) to the cores. In addition if any of these variations can be identified as being associated with known (i.e. dated) climatic

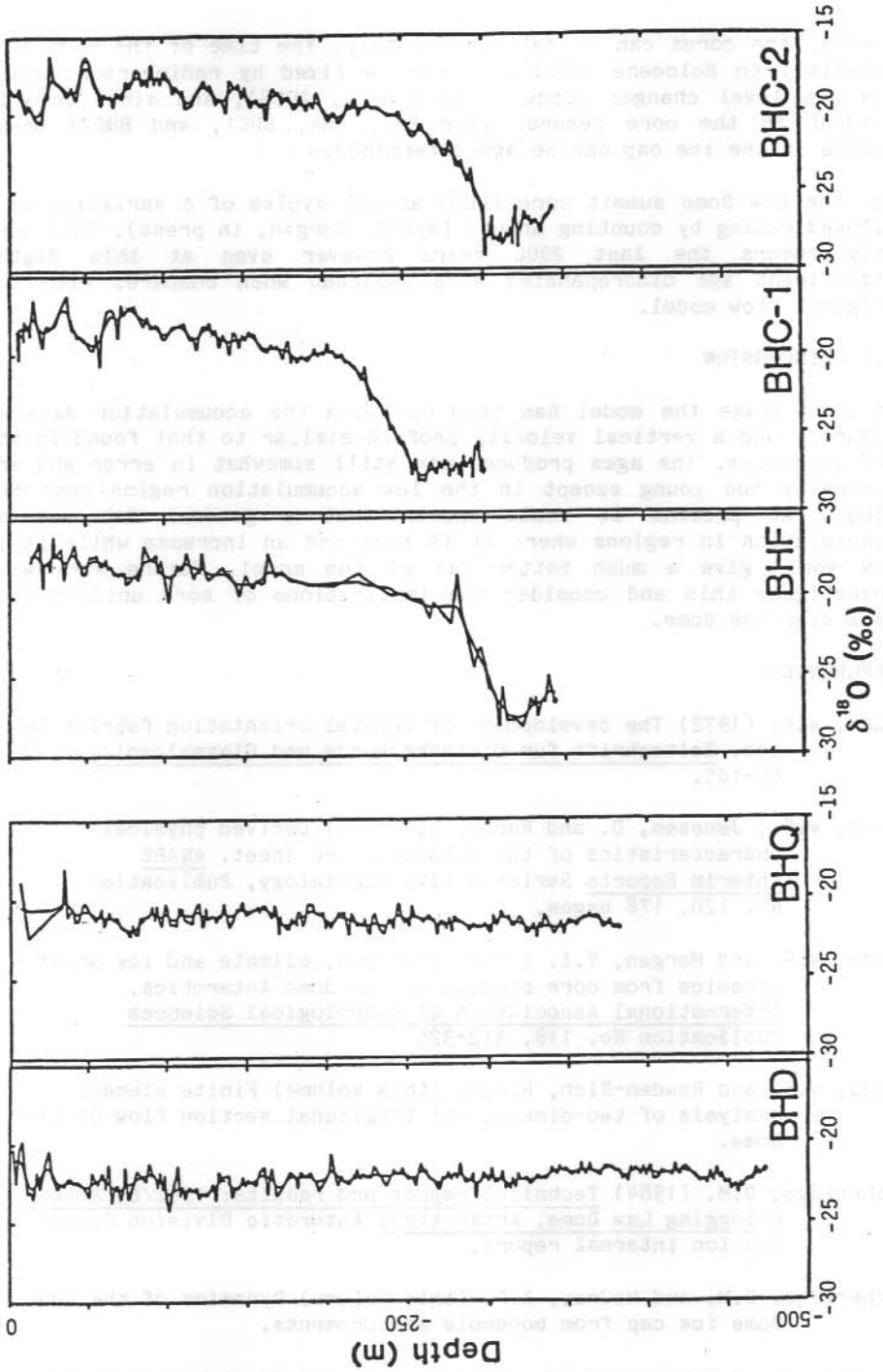

Figure 2. Oxygen isotope profiles. The raw data is shown together with a 9 point binominal weighted moving average.

events, the cores can be dated absolutely. The time of the Wisconsin (glacial) to Holocene transition can be fixed by radiocarbon dating via sea level changes (Godwin and others, 1958), and since this is evident in the core records (for BHF, BHA, BHC1, and BHC2) these levels in the ice cap can be age determined.

For the Law Dome summit core (BHD) annual cycles of δ variation have allowed dating by counting annual layers (Morgan, in press). This core only covers the last 2000 years however even at this depth, significant age discrepancies were apparent when compared with the original flow model.

1.5 DISCUSSION

At this stage the model has been run with the accumulation data of Figure 1 and a vertical velocity profile similar to that found in the BHC boreholes. The ages produced are still somewhat in error and are generally too young except in the low accumulation region near SGQ (BHQ). At present it would appear that a general decrease of accumulation in regions where it is high and an increase while it is low would give a much better fit of the model. Future work will investigate this and consider the implications of more uniform snow fall over the dome.

REFERENCES

Budd, W.F. (1972) The development of crystal orientation fabrics in ice. Zeitschrift fur Gletscherkunde und Glazealgeologie, 8, 65-105.

Budd, W.F., Jenssen, D. and Radok, U. (1971) Derived physical characteristics of the Antarctic ice sheet. ANARE Interim Reports Series A (IV) Glaciology, Publication No. 120, 178 pages.

Budd, W.F. and Morgan, V.I. (1977) Isotopes, climate and ice sheet dynamics from core studies on Law Dome Antarctica. International Association of Hydrological Sciences Publication No. 118, 312-325

Budd, W.F. and Rowden-Rich, R.J.M. (this volume) Finite element analysis of two-dimensional longitudal section flow on Law Dome.

Etheridge, D.M. (1984) Technical report and results: 1982/83 Borehole relogging Law Dome, Antarctica. Antarctic Division Glaciology Section internal report.

Etheridge, D.M. and McCray, A.P. (this volume) Dynamics of the Law Dome ice cap from borehole measurements.

Godwin, H., Suggate, P.P. and Willis, E.H. (1958) Radiocarbon dating of the estatic rise in ocean level. Nature, 181, 1518-1519.

McLaren, W.A. (1968) A study of the local ice cap near Wilkes, Antarctica. ANARE Scientific Reports, Series A(4), Glaciology Publication No. 103.

Morgan, V.I. (in press) An oxygen isotope - climate record from Law Dome, Antarctica. Climatic Change.

Nye, J.F. (1957) The distribution of stress and velocity in glaciers and ice sheets. Proceedings of the Royal Society, (A), 239, 113-133.

Pfitzner, M.L. (1980) The Wilkes Ice Cap project 1966. ANARE Scientific Reports, Series A(4) Glaciology, Publication No. 127, 133 pages.

Russell-Head, D.S. and Budd, W.F. (1979) Ice sheet flow properties derived from borehole shear measurements combined with ice core studies. Journal of Glaciology, 24, (90) 117-130.

2. DYNAMICS OF THE LAW DOME ICE CAP FROM BOREHOLE MEASUREMENTS

D.M. Etheridge and A.P. McCray
Antarctic Division, Department of Science
Kingston, Tasmania, 7150.

ABSTRACT

Boreholes BHC1 and BHC2 on Law Dome, Antarctica have been logged for orientation, diameter and temperature over a large enough time interval to allow the dynamics of the ice sheet to be determined. Orientation measurements are analysed to give the horizontal deformation profile. Borehole diameter records are used to give vertical strains. This data, together with temperature profiles, surface velocity data and bedrock relief, describe the flow regime of the ice sheet in the region.

2.1 INTRODUCTION

The internal dynamics of an ice sheet can most thoroughly be investigated by drilling through to bedrock and measuring the change in orientation and vertical length of the hole over a suitable time interval. This has been attempted for several boreholes on Law Dome in the past, but only recently has bedrock been reached and measurements made accurately enough to allow confident reduction of the data.

Boreholes BHC1 (300 m deep) and BHC2 (344 m), near Cape Folger, were both drilled to within metres of the bedrock during the 1981/82 austral summer (McCray, 1982). Their locations were chosen from ice radar sounding of the local area. BHC1 was positioned on a bedrock rise, and BHC2 in a trough 350 m downstream. Accurate logging of the holes was undertaken immediately after ice drilling, and during the following summer (Etheridge, 1983).

The equipment and techniques used for logging the boreholes were described in detail by Etheridge (1984). The resultant data set contained temperature values every 10 m, orientation (inclination and azimuth) every 2 m and continuous profiles of borehole diameter.

2.2 HORIZONTAL DEFORMATION

The orientation values were reduced to give a position profile of the borehole at the time of measurement. This consisted of a set of vectors giving the horizontal distance and azimuth of each measurement point in the hole from the vertical through the bottom of the hole. The position profile of the hole was vector subtracted from the position profile of the same hole some time later, to give the movement due to ice deformation through the ice sheet at the site. Division by the number of years between loggings then gives the velocity profile of the ice sheet, relative to the bottom of the hole.

The horizontal shear in the ice sheet is given by the vertical gradient of the horizontal velocity (also a vector) which is derived from vector differentiation of the velocity profile.

Figure 1 shows the magnitude of the horizontal velocity profile, V and horizontal velocity gradient, G for BHC1. Written alongside, are the azimuth, AZ of the velocity and the azimuth, AG of the velocity shear.

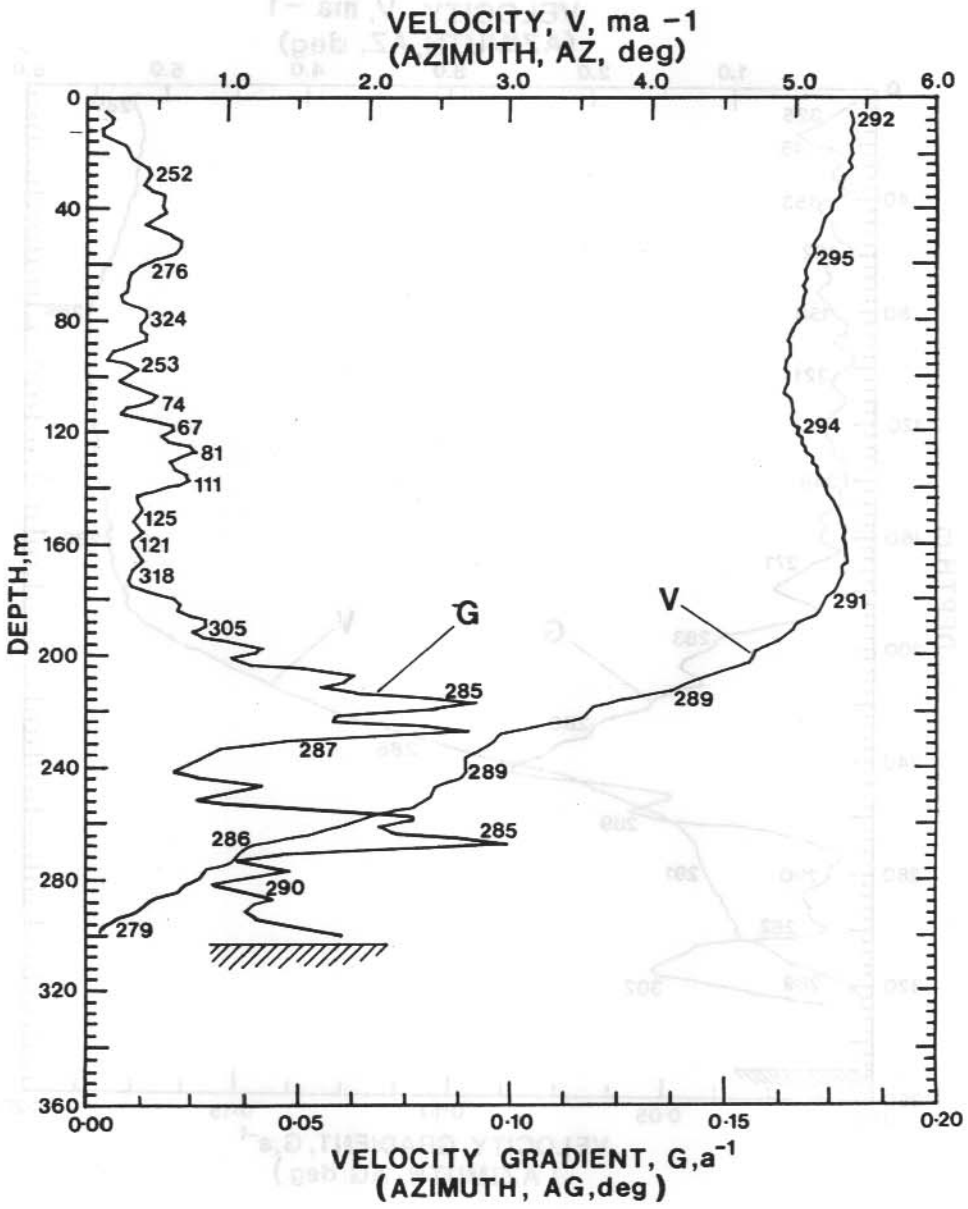

Figure 1. Velocity profile, V(V,AZ) relative to bottom of borehole and velocity gradient G(G,AG) for borehole BHC1.

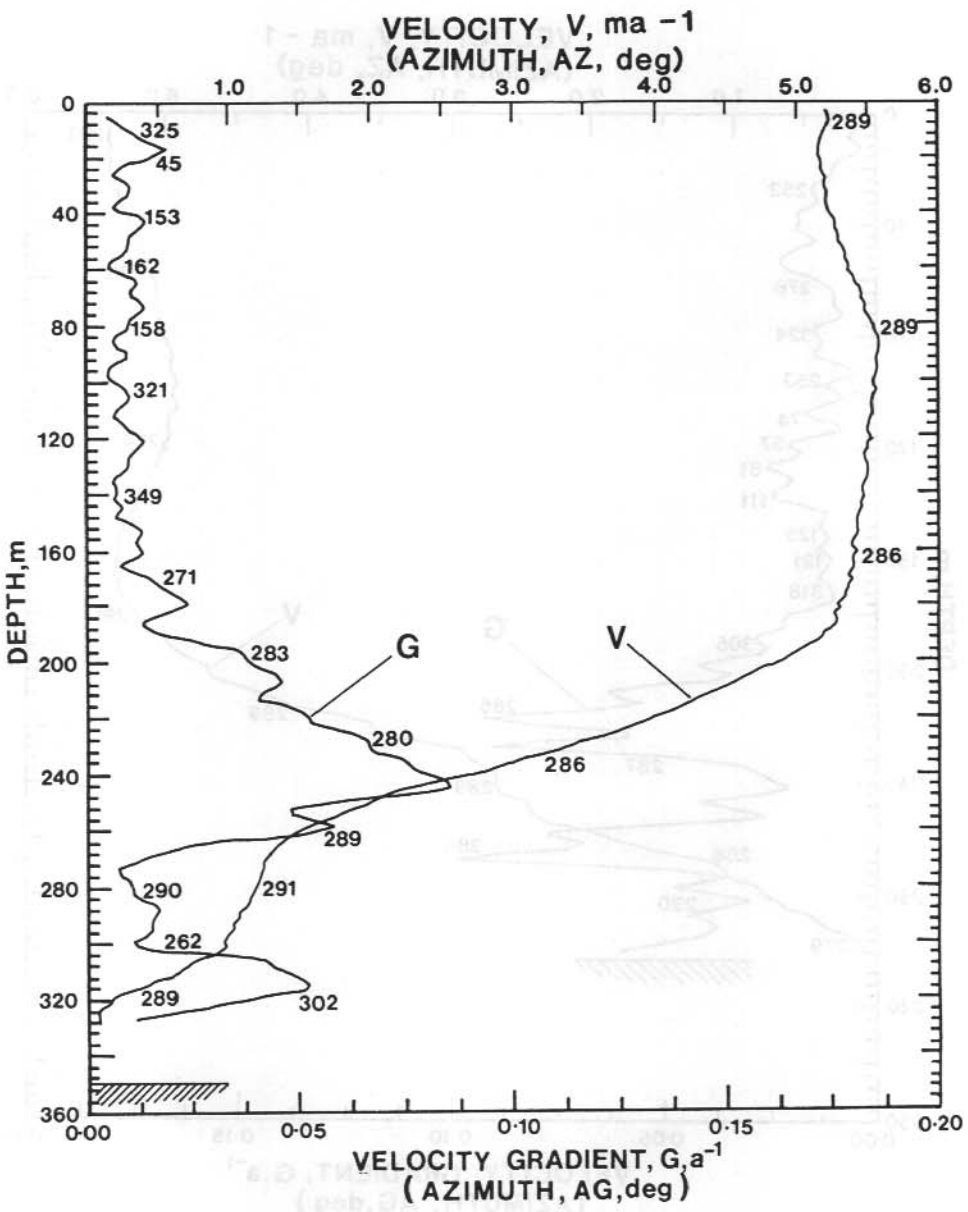

Figure 2. Velocity profile, V(V,AZ) relative to bottom of borehole and velocity gradient G(G,AG) for borehole BHC2.

The velocity profile was not smoothed and had an estimated accuracy at the surface of ± 0.4 ma^{-1} and $\pm 5^{o}$. This velocity profile deviates markedly from the typical case for an ice mass reported by Paterson (1981). Firstly, there are two main zones of velocity increase (centred at 215 and 270 m depth). Secondly, the velocity does not always increase towards the surface but decreases between 160 and 100 m. These aspects are more clearly identified in the velocity gradient profile. The shear in the two high shear zones is in the same direction as the surface flow (286^{o}). However, at 160 m the shear direction turns approximately 180^{o} to the general flow. This causes a velocity decrease of 0.50 ma^{-1} at the top of this layer. At 100 m the shear resumes its original direction. The velocity gradient, G shown in Figure 1 has been binomially smoothed over 5 data points (10 m). The estimated accuracy of G is 0.01 a^{-1}.

Similar features are seen in the BHC2 borehole (Figure 2). Two high shear zones are again apparent although at slightly different levels and with a smoother structure than in BHC1. The lower zone in BHC2 also has significantly lower shear than in BHC1, possibly because this part of the column is in a bedrock trough. The region where the velocity gradient reverses direction occurs between 90 and 30 m below the surface and causes a decrease of 0.45 ma^{-1} in the velocity at the top of the layer.

The observed increase of velocity with depth is an unexpected feature that is not explained by the classical theory of ice sheet dynamics. However, Savage and Paterson (1963) found a positive change of longitudinal velocity with depth in the upper 70 m of the 300 m thick Athabasca Glacier, and attributed the anomaly to variations in the glacier thickness in the longitudinal direction. Paterson (1983) found that velocities of the Byrd station borehole were greater between 600 and 800 m depth than at the surface but attributed this to measurement inaccuracies. The present analysis however uses measurements with sufficient coverage and accuracy to guarantee that the observed feature is real.

The shear zones discussed above can also be studied in relation to the crystal fabrics discussed by Xie and Young (in press). Further analysis will be reported in the near future.

2.3 BASAL SLIDING

Table 1 shows the measured absolute surface velocity and the ice deformation velocity integrated from bottom to top of the borehole. The difference represents the velocity that occurs between the bottom of the borehole and bedrock. Since BHC1 and BHC2 are within only a few metres of bedrock most of the velocity deficiency must be due to basal sliding. Further evidence for this is seen in the temperature profiles (Figure 3) which show that at the bedrock, the ice sheet is very close to the pressure melting point.

Table 1. Basal sliding velocities derived from absolute surface velocity and integrated ice deformation velocity.

Hole	Absolute surface velocity	Integrated deformation velocity	Basal sliding velocity
	$ma^{-1}(^{o}T)$	$ma^{-1}(^{o}T)$	$ma^{-1}(^{o}T)$
BHC1	9.6 (286)	5.4 (292)	4.5 (277)
BHC2	9.4 (285)	5.2 (289)	4.3 (278)

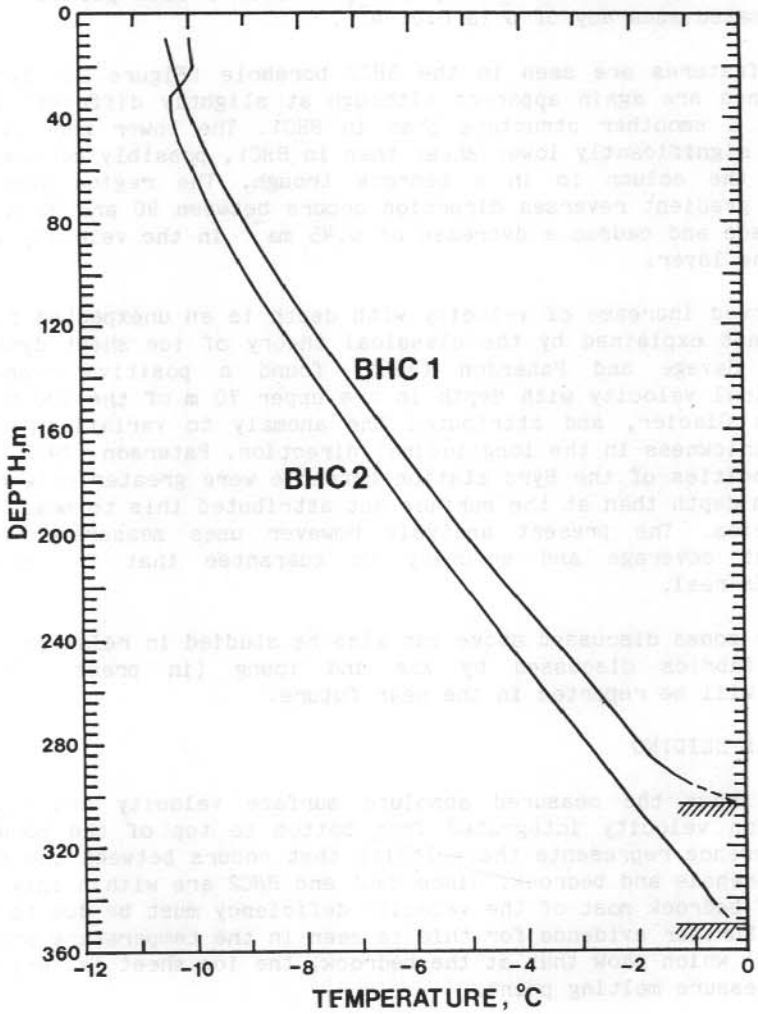

Figure 3. Temperature profiles of BHC1 and BHC2, extrapolated to bedrock.

2.4 VERTICAL DEFORMATION

Figures 4 and 5 show the vertical velocity of points in the two boreholes relative to the bottom of the hole. The points are recognisable features in the borehole that result from thermal drilling and appear on the initial and remeasured profiles. The difference in depth of these points (allowing for such factors as borehole inclination changes) over two loggings gives the vertical movement with an accuracy of 0.04 ma^{-1}. The results show that the ice sheet in the vicinity of both holes is contracting. There are two zones in BHC1 where the velocity is upwards and these correspond exactly with the high shear zones in Figure 1. Firn compaction accounts for the large velocity change in the top 25 m of each borehole. The ice/firn transition is complete by a depth of 32 m at both locations.

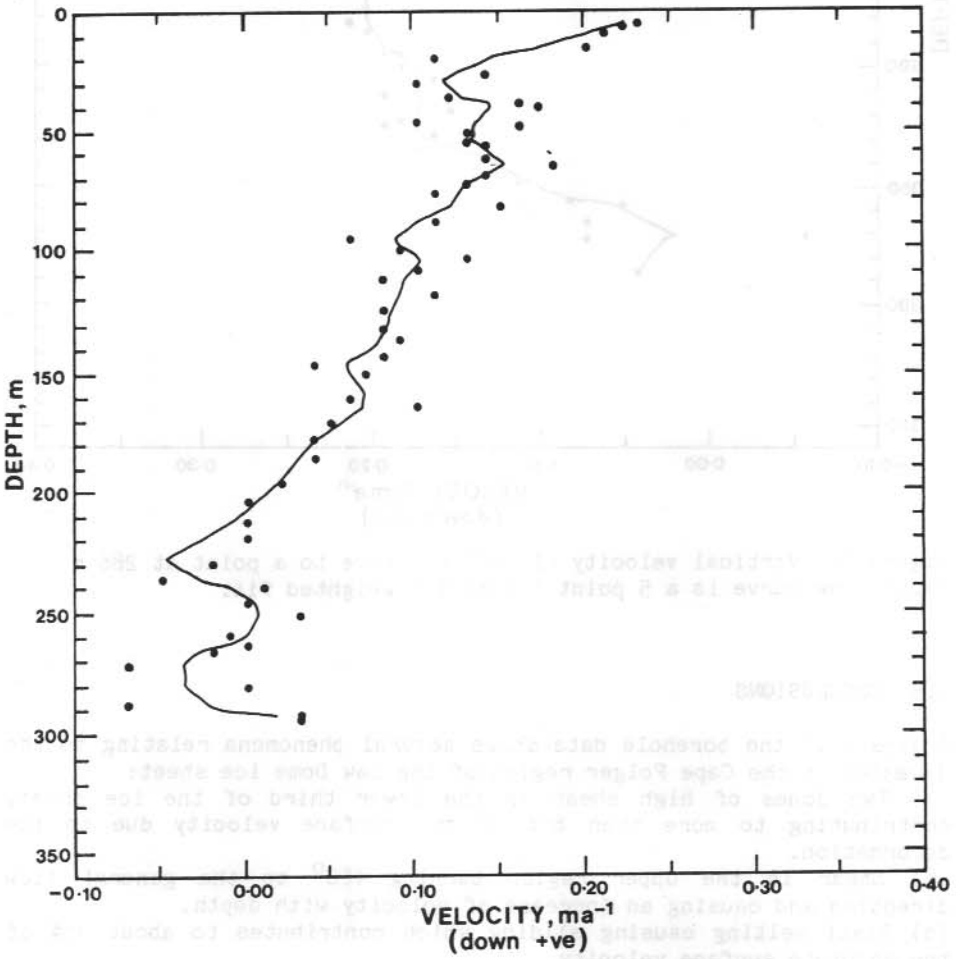

Figure 4. Vertical velocity of BHC1, relative to a point at 292 m depth. The curve is a 5 point binomially weighted fit.

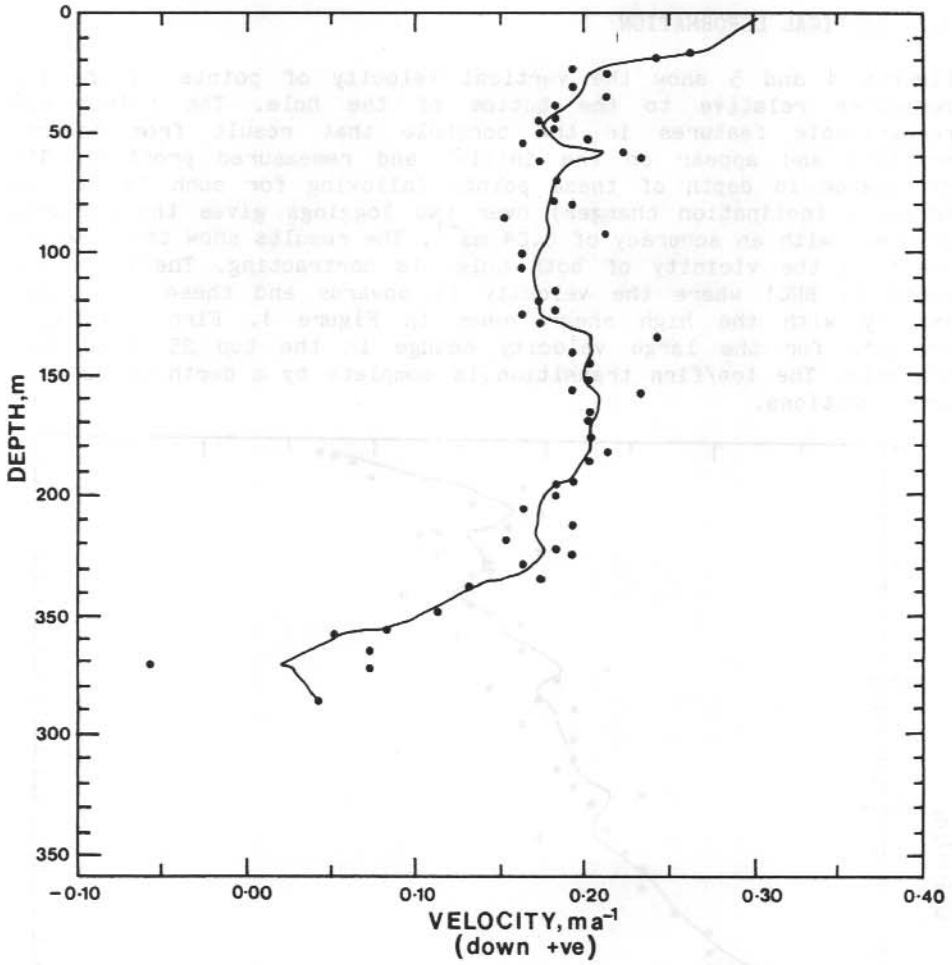

Figure 5. Vertical velocity of BHC2 relative to a point at 286 m depth. The curve is a 5 point binomially weighted fit.

2.5 CONCLUSIONS

Analysis of the borehole data shows several phenomena relating to the dynamics in the Cape Folger region of the Law Dome ice sheet:

(a) Two zones of high shear in the lower third of the ice sheet, contributing to more than 85% of the surface velocity due to ice deformation.

(b) Shear in the upper region turning 180° to the general flow direction and causing an increase of velocity with depth.

(c) Basal melting causing sliding which contributes to about 45% of the absolute surface velocity.

(d) Significant contraction and firn compaction of the ice sheet in the vicinity of the boreholes.

ACKNOWLEDGMENTS

We thank all the ANARE personnel who helped obtain this wealth of data, and Philip Catania for his computing dexterity.

REFERENCES

Etheridge, D.M. (1983) Operations report: 1982/83 Borehole relogging, Law Dome, Antarctica. Antarctic Division Glaciology Section internal report.

Etheridge, D.M. (1984) Technical report and results: 1982/83 Borehole Relogging, Law Dome, Antarctica. Antarctic Division Glaciology Section internal report.

McCray, A.P. (1982) BHC1 and BHC2 Ice drilling field log. Antarctic Division Glaciology Section internal report.

Paterson, W.S.B. (1981) The physics of glaciers. 2nd Edition. Pergamon Press.

Paterson, W.S.B. (1983) Deformation within polar ice sheets: An analysis of the Byrd station and Camp Century borehole-tilting measurements. Cold Regions Science and Technology, 8, 165-179.

Savage, J.L. and Paterson, W.S.B. (1963) Borehole measurements in the Athabasca glacier. Journal of Geophysical Research, 68, (15), 4521-4536.

Xie, Z. and Young, N.W. (in press) Ice crystallographic studies on Law Dome, Antarctica. ANARE Report.

3. MULTILAYER CRYSTALLOGRAPHIC STRUCTURE OF LAW DOME FROM ICE CORE ANALYSIS

N.W. Young
Antarctic Division, Department of Science
Kingston, Tasmania, 7150.

Xie Zichu and Qin Dahe
Lanzhou Institute of Glaciology and Geocryology, Academia Sinica
Peoples Republic of China.

ABSTRACT

An ice core from BHF (66°09'S, 111°00'E) on Law Dome, Antarctica has been analysed for crystal orientation fabric, crystal size and bubble elongation. Crystal size initially increases with depth then decreases to a minimum at about 60% depth in conjunction with the development of a strong vertical single-maximum fabric. In the remainder of the thickness there is an interleaving of coarse-grained multiple-maximum fabric ice with fine-grained single-maximum fabric ice. The initial single-maximum fabric develops under the influence of a shear stress increasing with depth. Closer to the bed there can be zones with a relative maximum in the shear stress some distance above the rough bed topography. It appears that single-maximum fabrics develop under the influence of the high shear stress where the trajectory of the ice intersects these zones. In the intervening zones the fabric may change to a multiple-maximum type and the crystals grow very large, where the stress is relaxed and the simple shear is small. The pattern of variation of the air bubbles in the ice confirms this general picture.

3.1 INTRODUCTION

The Law Dome is a small ice cap, approximately 200 km in diameter adjoining the main Antarctic ice sheet. Ice cores have been extracted from the Law Dome by thermal core drilling since 1969, mainly along a line between the summit (66°44'S, 112°50'E) and the coast near Cape Folger (Russell-Head and Budd, 1979). Crystal structure in the cores has been analysed by a number of workers and as each new analysis is made an increasingly complex picture emerges.

Twelve sections of an ice core from SGA (66°08'S, 110°57'E), about 5 km from the coast, were analysed for crystal c-axis orientation and crystal size (Wakahama, 1974; Budd, 1972). Budd (1972) described the main features of the spatial distribution of the crystal structure, as known then. In the upper part of the ice sheet there is a two-maximum (or girdle) fabric, changing to a strong, near-vertical, single-maximum fabric in the middle third of the thickness. Associated with this change in structure there is an increase in crystal size with depth. The basal layer consists of very large crystals with multiple-maximum c-axis concentrations.

Russell-Head (1979) analysed another core from BHF (3 km upstream of SGA) at depth intervals of 20 m for crystal size and orientation, and bubble size and orientation. The resulting hole was also logged to

determine the in situ shear deformation of the ice sheet. Russell-Head and Budd (1979) found a similar pattern of change in the crystal orientation fabrics between the surface of the ice sheet and the bottom of the hole. A strong vertical single-maximum fabric develops from the middle of the ice sheet downwards. Associated with the strong fabric is a decrease in mean crystal size, and a tendency for the bubbles trapped in the ice to be elongated. The lower quarter of the ice sheet is composed of very large crystals with multiple-maximum c-axis orientations. The layer of small crystal, strong vertical fabric, enlongate-bubble ice corresponds to the zone of high shear strain-rate found from the logging of the borehole. Neither of the holes at SGA or BHF reached bedrock.

Two further holes (BHC1 and BHC2, 350 m and 700 m respectively, downstream of SGA) were drilled to within a few metres of bedrock in 1981-82 (McCray, 1982). For those cores, Xie and Young (in press) found the same general trends in crystal and bubble size and orientation as in BHF but with a more complex detailed structure in the "active" layer of the ice sheet where much of the shear deformation occurs. They found an interleaving of layers of small crystal, strong single-maximum fabric ice with layers of large crystal, multiple-maximum fabric ice. The location of two layers of fine-grained ice with a strong single-maximum fabric corresponded generally with two separate layers with high shear strain-rate found from the logging of these holes (Etheridge and McCray, this volume).

Analysis of further samples from BHF revealed a similar interleaving in that core, not found in the first survey. This paper presents the collated measurements from BHF made by three different workers, D.S. Russell-Head, Xie Zichu and Qin Dahe.

3.2 MEASUREMENTS

The mean crystal area in a cross-section is calculated by counting the number of crystals within a specified area of a thin section. Some authors apply an adjustment to this measurement based on the assumption that the intersection with the crystal is random and will not necessarily represent its maximum cross-section. No such adjustment has been made here.

For bubble elongation, the breadth and length was measured for each of at least 100 bubbles in a test area in each thin section. The elongation ratio is then the ratio of the mean length to the mean breadth. Russell-Head (1979) noted that only about 60% of bubbles in a section were elongated. Xie and Young (in press) estimated an elongation ratio on the basis of the dimension of elongated bubbles which also happened to be in sections where a number of bubbles were very elongated. Russell-Head (1979) presented bubble measurements from individual sections as histograms. He found that bubble lengths were clumped into approximate multiples of the bubble breadth and therefore the elongation ratio of single bubbles took on approximately integer values and did not form a smooth continuous distribution. In one sample (241 m depth), some bubbles had ratios of up to ten but the

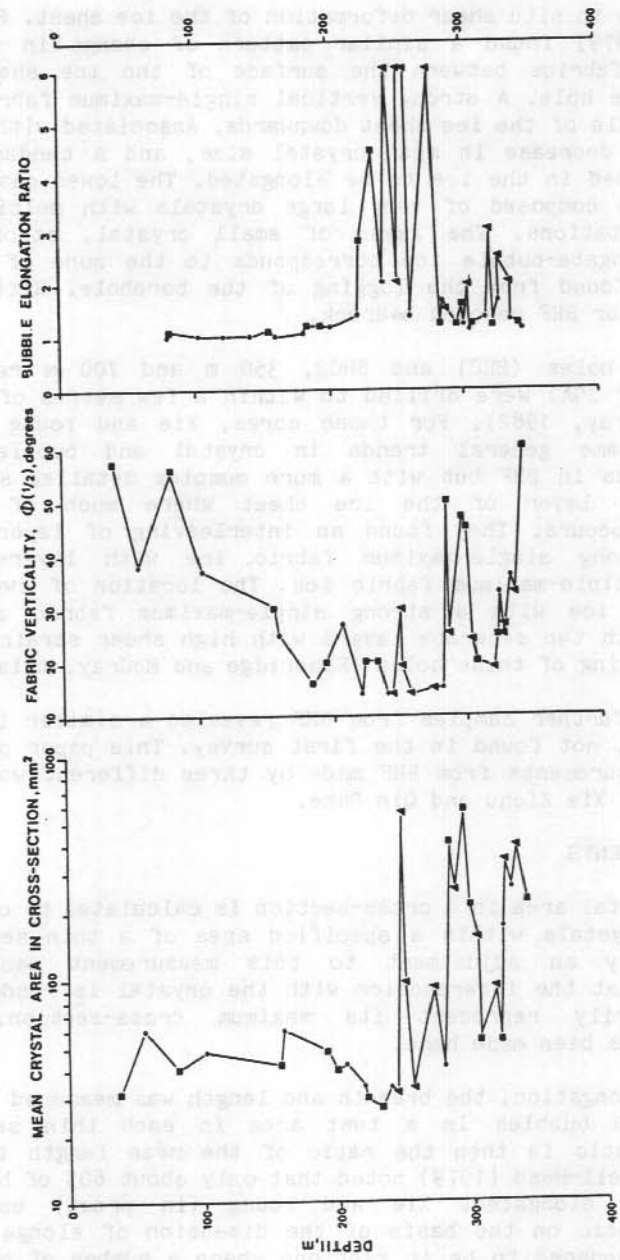

Figure 1. Measurements on the BHF ice core are taken from Russell-Head (1979)(dots), Xie and Young (in press) (triangles) and for this work (by Qin) (squares). The methods of measuring the mean crystal area in the cross-section, fabric verticality, and bubble elongation ratio are described in the text. Φ (1/2) = 60° for a uniform distribution.

mean for the section was only two. New measurements on other sections give mean values up to 4.5, averaged over 100 bubbles.

The c-axis orientations were measured on a Rigsby stage and plotted on a Schmidt equal-area net. The fabric verticality ϕ (1/2) is the half angle of the cone centred about the vertical which includes 50% of the c-axes in a section.

A total of 43 sections have been analysed. Not all measurements were made on all sections from the first survey by Russell-Head (1979). Measurements made by the different workers are represented by different symbols in Figure 1 to allow for any variation in technique.

3.3 RESULTS

The crystal size increases slightly in the upper 180 m of the ice sheet, and then decreases to a minimum at about 230 m depth. The fabric verticality strengthens from a uniform distribution near the surface to a strong vertical single-maximum at about 220 m depth. Between 243 and 251 m there is a sudden and very large increase in crystal size. The strong single-maximum fabric is replaced by a multiple-maximum fabric. The structure then reverts to the small crystal, strong single-maximium fabric over a depth interval of only 0.1 m (251.3 - 251.4 m). At 284 m depth there is a second sudden increase in crystal size and change of fabric to a multiple-maximum type, which extends to 306 m depth where it again reverts to the fine-grained ice. From 324 m to the bottom of the core at 342 m there is a third layer of very large crystal multiple-maximum fabric ice, which has been assumed to extend to the base of the ice sheet at 380 m depth. From 230 m depth there is a gradual increase with depth of the lower bound of crystal size, and a correlation between fabric verticality and crystal size.

The greatest bubble elongation occurs between 220 and 280 m where crystal size is smallest and fabric strongest. But the value of the elongation ratio is quite variable (between 1.5 and 4.5). Another zone of slightly elongated bubbles occurs between 305 and 335 m but is not as closely related to the crystal size and fabric strength.

3.4 DISCUSSION

The pattern of variation with depth of fabric type and crystal size in BHF is similar to that found by Gow and Williamson (1976) in the Byrd ice core. They found "interdigitations of coarse and fine-grained ice ... accompanied also by fabric reversals in which the strong single-maximum fabric of the fine-grained ice was replaced by a multiple-maximum fabric in the coarse-grained ice" commencing at a depth of 1670 m in a total depth of 2164 m (i.e. about 60% depth - similar to BHF). The bottom 20% of the thickness at BHF and Byrd is coarse-grained multiple-maximum fabric ice. At BHC1 and BHC2, nearer the coast of the Law Dome, the coarse-grained ice layers are confined to approximately the bottom 20-25% of the ice sheet.

Hooke and Hudleston (1980) found a comparable general pattern of fabrics in the Barnes Ice Cap, but no basal layer of very large

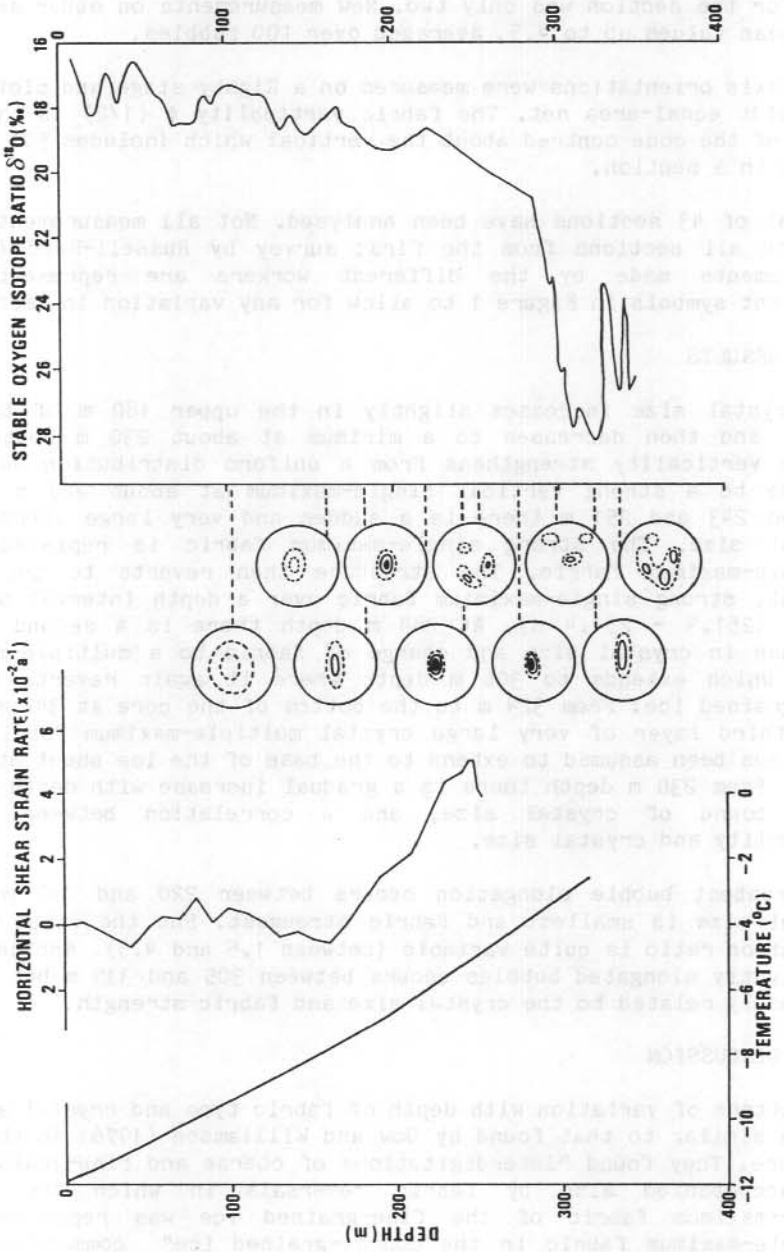

Figure 2. The measurements of borehole in situ temperature and horizontal shear strain rate and stable oxygen isotope ratio are taken from Russell-Head and Budd (1979) and Russell-Head (1979). Only the component of the strain rate in the direction of flow has been plotted. Some of the fabrics are taken from Russell-Head (1979) and Xie and Young (in press).

crystal multiple-maximum fabric ice. They found that "bands of ice with single-maximum fabric 2 to 5 m thick alternate with similar bands having multiple-maximum fabric in deformed superimposed ice" at the edge of the Barnes Ice Cap.

Herron (1982) also described the development of the single-maximum fabric with depth at Camp Century but made no mention of coarse-grained multiple-maximum fabric ice similar to that found at Byrd or Law Dome. Hooke and Hudleston (1980) constructed a "stability diagram for various fabrics developed in simple shear" to demonstrate the general relationship between the proposed independent variables of fabric, temperature, shear stress and cumulative strain. They noted that coarse-grained multiple-maximum fabric ice appeared to occur at temperatures above -10 ^{o}C while the temperature in the Camp Century borehole is everywhere below -13 ^{o}C.

Because of the close association of the boundary between Holocene and Wisconsin ice and the upper boundary of the small crystal strong single-maximum fabric ice at Camp Century, Byrd, Barnes Ice Cap and DYE3 (Herron, 1982), it has been suggested that some climatic effect has predisposed Wisconsin ice to shear strain and the development of the characteristic fabric and texture. On the Law Dome, however, strong single-maximum fabrics, minimum crystal size and measured maximum shear strain-rates (Figure 2) occur well above the upper boundary of the Wisconsin ice (Russell-Head and Budd, 1979; Xie and Young, in press; Etheridge and McCray, this volume; Morgan and McCray, this volume). Russell-Head and Budd (1979) inferred that a maximum in the shear stress occurred some 100 m above the bed at BHF as a result of the roughness of the bed topography. This could account for a broad band of ice with well developed single-maximum fabrics, but not the interleaved structure described. Budd and Rowden-Rich (this volume) calculated the shear stress field within a simple two-dimensional representation of the flowfield in the Law Dome about the BHC1 and BHC2 boreholes. They found that relative maxima in the shear stress could occur in layers at some distance (not constant) above the bedrock and that the layers could have limited horizontal extent. Further, the flow trajectory of the ice could pass through a number of these layers to give a varying stress history. The deformation of the ice changes in response to the varying stress along the trajectory, and this could give rise to changes in fabric type.

The strong single-maximum fabric therefore could develop in zones of simple shear with high shear stress, and the large crystal multiple-maximum fabric ice could result from a relaxation of the shear stress in the intervening zones. The small crystal size associated with the single-maximum fabric can be caused by the high shear strain-rate. The large crystals associated with the multiple-maximum fabric could then have grown in response to the warm temperatures, where there is little deformation by simple shear. Finally the boundary between the different ice types can be quite sharp (e.g. at 251 m depth in BHF), sometimes with interleaving layers only a few metres thick (Hooke and Hudleston, 1980; Gow and Williamson, 1976) or, with a large change over a depth interval of only a couple of metres (e.g. the DYE3 core; Herron, 1982).

REFERENCES

Budd, W.F. (1972) The development of crystal orientation fabrics in moving ice. Zeitschrift fur Gletscherkunde und Glazialgeologie, 8, (1-2), 65-105.

Budd, W.F. and Rowden-Rich, R.J.M. (this volume) Finite element analysis of two-dimensional longitudinal section flow on Law Dome.

Etheridge, D.M. and McCray, A.P. (this volume) Dynamics of the Law Dome from borehole measurements.

Gow, A.J. and Williamson, T. (1976) Rheological implications of the internal structure and crystal fabrics of the West Antarctic ice sheet as revealed by deep core drilling at Byrd station. Geological Society of America Bulletin, 87, (12), 1665-1677.

Herron, S.L. (1982) Physical properties of the deep ice core from Camp Century, Greenland. PhD Thesis, University of New York at Buffalo.

Hooke, R.L. and Hudleston, P.J. (1980) Ice fabrics in a vertical flow plane, Barnes Ice Cap, Canada. Journal of Glaciology, 25, (92), 195-214.

McCray, A. (1982) BHC1 and BHC2 Ice drilling field log. Antarctic Division Glaciology Section internal report.

Morgan, V.I. and McCray, A.P. (this volume). Enhanced shear zones in ice flow - implications for ice cap modelling and core dating.

Russell-Head, D.S. (1979) Ice sheet flow from borehole and laboratory studies. MSc Thesis, Meteorology Department, The University of Melbourne.

Russell-Head, D.S. and Budd, W.F. (1979) Ice sheet flow properties derived from bore-hole shear measurements combined with ice-core studies. Journal of Glaciology, 24, (90), 117-130.

Wakahama, G. (1974) Physical and Chemical studies on ice from glaciers and ice sheets. Report of the Japanese Science Foundation (In Japanese), 99-108.

Xie, Z. and Young, N.W. (in press) Ice crystallographic studies on Law Dome, Antarctica. ANARE Report.

4. SNOW ACCUMULATION AND OXYGEN ISOTOPE RECORDS IN TWO ADJACENT ICE CORES

V.I. Morgan
Antarctic Division, Department of Science
Kingston, Tasmania, 7150.

ABSTRACT

Detailed oxygen isotope analysis of two adjacent ice cores are compared and differences in the δ profiles are explained by the mechanisms of snow accumulation and redistribution by wind. Effects on different time scales are apparent and the significance of this is discussed in the context of using δ records as proxy climatic data.

4.1 INTRODUCTION

It is well established that climatic information can be obtained from oxygen isotope analysis of ice cores (Dansgaard and others, 1973; Robin, 1981) however it is not very well known how the vagaries of snow accumulation effect the record and hence limit its ultimate accuracy and its resolution in time.

In this study two shallow ice cores drilled 15 m apart, from the ice cap at the summit of Law Dome in East Antarctica have been measured in fine detail for oxygen isotope variations (hereafter called δ values following the common usage). The δ profiles obtained from what must be identical climates are compared both with each other and also with temperature records from Casey station some 100 km away on the edge of Law Dome.

4.2 ACCUMULATION AND δ PROFILES

For times longer than a few years the accumulation at two adjacent sites must be the same so as to maintain a level surface. On shorter time scales the existence of dunes and sastrugi causes the accumulation to have significant localised deviations from the mean value. Since, at this site the isotope profiles allow identification of seasonal layers, the accumulation for each year can be measured. Figure 1(a) shows the values obtained by analysis of both cores. The variability is large (0.45 in 0.9 m of ice equivalent) but the annual values are highly correlated between the two cores (Correlation coefficient, $r = 0.72$ for 25 data pairs).

The δ profiles for the two boreholes BHD and BHD-B are shown in Figure 2. Again the equality of the annual accumulation can be seen from the nearly parallel lines joining the summer peaks and there is obvious similarity between the curves. In contrast, the agreement between the δ values is relatively poor (Figure 1(b), (c), (d)). Not only is the correlation between annual mean δ values low ($r = 0.46$), but there are periods longer than one year (for instance between 1970 and 1975) where δ values in one core, although having similarly shaped annual cycles, have an offset of nearly 1‰ from values from the other core. There is obviously some mechanism which, while ensuring accumulation

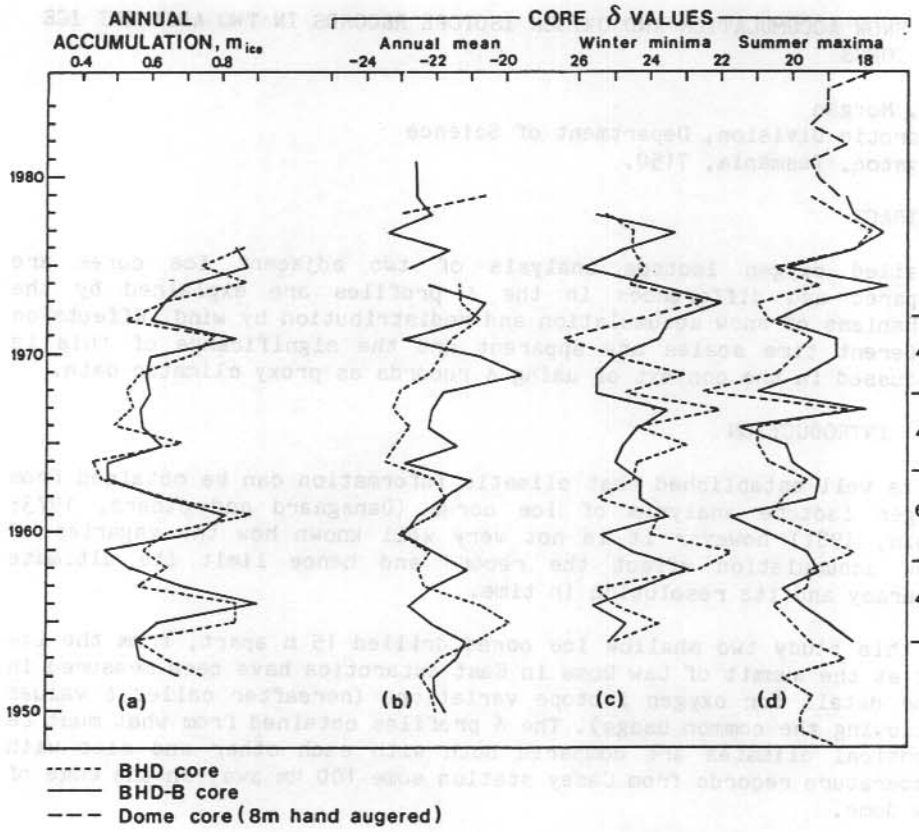

Figure 1. Core profile data. (a) Annual accumulation values determined in each core by the distance between successive "summer" $\delta^{18}O$ peaks. The values are converted from a thickness of firn to an equivalent of ice by multiplying by the measured density divided by 0.91. Values of $\delta^{18}O$ extracted from the profiles of Figure 2 are also plotted as (b) mean annual, (c) winter minima, and (d) summer maxima values.

is equalized annually, allows this to be achieved with snow of differing δ for the two borehole locations.

4.3 THE ACCUMULATION MECHANISM

Precipitation occurs very non uniformly throughout the year, primarily as a result of cyclonic activity, and generally, for the Law Dome region in Spring, Winter and Autumn (Budd, 1966).

Because of the action of strong winds, the fallen snow is well mixed and is formed into dunes which are the stable surface configuration under the prevailing conditions (Bagnold, 1941). Later in the season

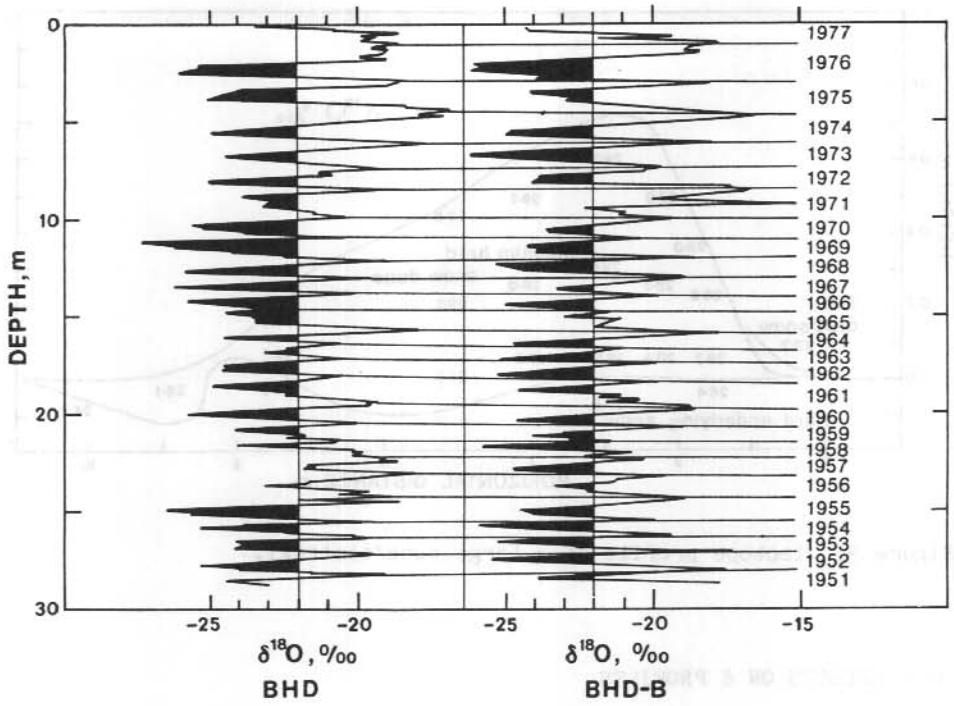

Figure 2. Isotope ratio profiles for the two cores. Depths are as measured so the upper layers are thicker because of the lower density of the firn. There are about ten δ values per year and the dating has been confirmed by identification of layers of radioactive fallout at known dates.

the dunes become eroded by wind and snow drift into the more sharply profiled sastrugi. Isotope measurements made on a large dune on the ice cap inland of Mirny Station show how the dune is composed of uniform, well mixed "winter" (low δ) snow while the harder underlying snow has a higher and more varied isotopic composition (Figure 3). Over the summer period, the effect of lighter winds, softening of the sastrugi by solar radiation and possibly some additional precipitation in calmer conditions lead to the disappearance of the rough surface. This process is described in detail by Gow (1965) for the South Pole where it accounts for the existence of seasonal strata in an annual accumulation which is usually smaller than the amplitude of the winter dunes and sastrugi. The same process appears to generally happen at the Law Dome summit and Figure 4 shows (a) the typical surface conditions in winter and (b) the very smooth and level surface in late summer.

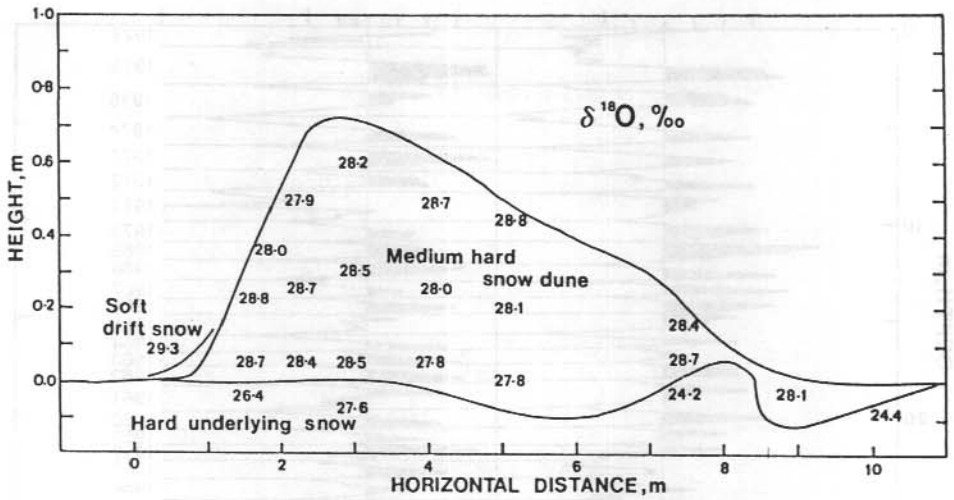

Figure 3. Isotope profile of a large dune/sastrugi.

4.4 EFFECTS ON δ PROFILES

The profiles of the cores are severely distorted by the accumulation process which, by modulating the amount of snow which is consolidated into accumulation effectively allows the two borehole sites to receive their average net accumulation from precipitation occuring at different times of the year. The effect is most pronounced for the "winter" layer (peak dune amplitude) and is a minimum in late summer when the surface has been smoothed over. The plots of Figure 1 show annual mean, winter minima and summer maximum δ values extracted from the profiles of Figure 2. The corresponding correlation coefficients are $r = 0.46$ (annual), $r = 0.26$ (winter) and $r = 0.67$ (summer) showing that, as expected, there is much better agreement using the summer values only.

4.5 COMPARISON OF δ AND TEMPERATURE DATA

Since the δ records from the cores show little agreement in winter or mean annual values, we can hardly expect any sensible correlation between these and regional temperature records. The "summer" δ value profiles however both suggest that a significant warming occurred between 1960 and 1980 and this is also observed in the mean annual temperature records from Casey Station as well as for the adjacent Antarctic stations, Mirny and Dumont d'Urville. Figure 5 shows the relevant temperature and δ profiles including curves smoothed by a Gaussian filter of half amplitude bandwidth approximately 3 years. (This smoothing reduces the large year to year variations which can be artificially introduced by the arbitrary January 1 to December 31 sampling period).

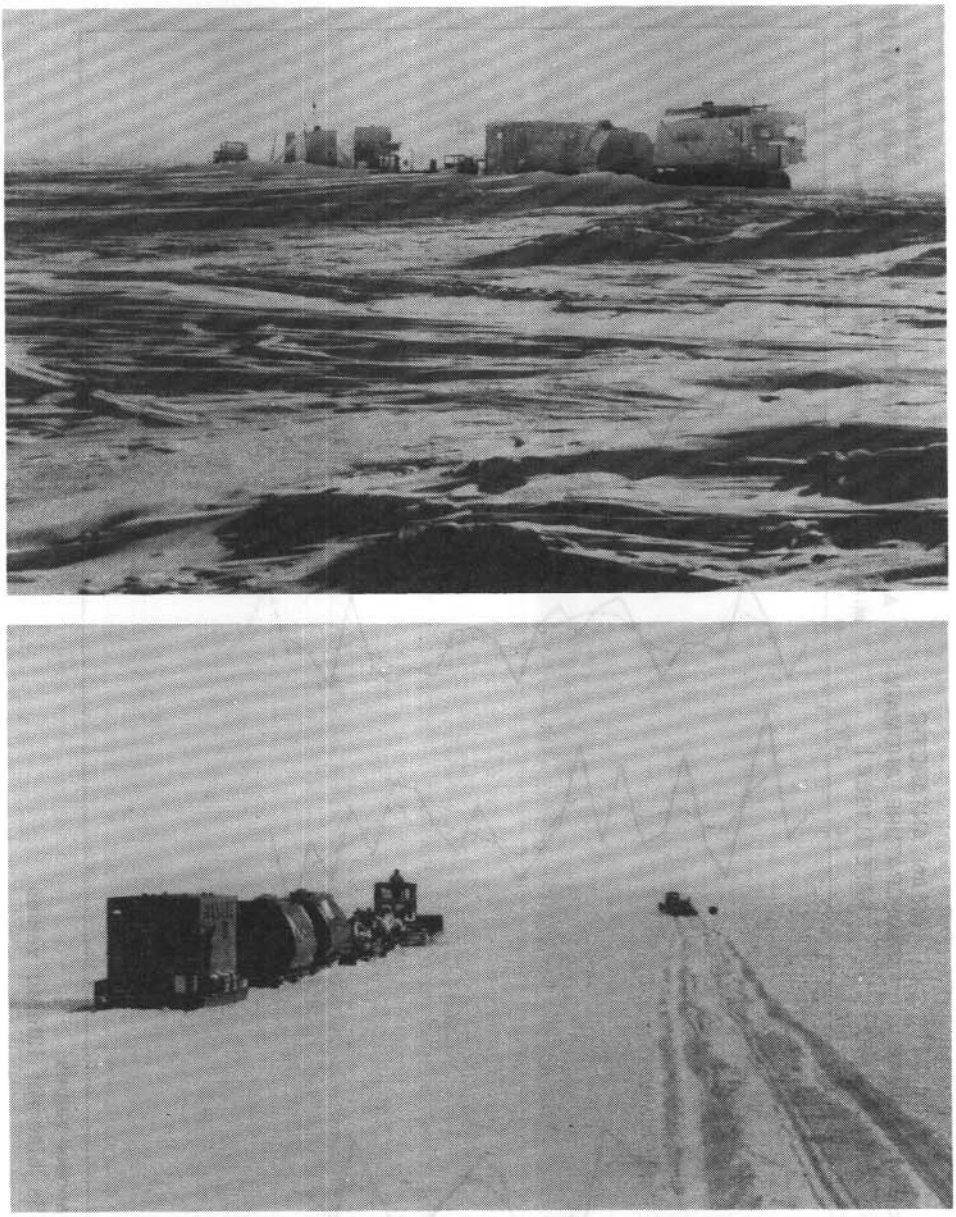

Figure 4. Photographs of the Law Dome summit area. (a) In late July when a considerable part of the annual precipitation has fallen and has been formed into irregular sastrugi, (b) In summer after light winds have rearranged unconsolidated precipitation and radiation softened sastrugi to form a level surface.

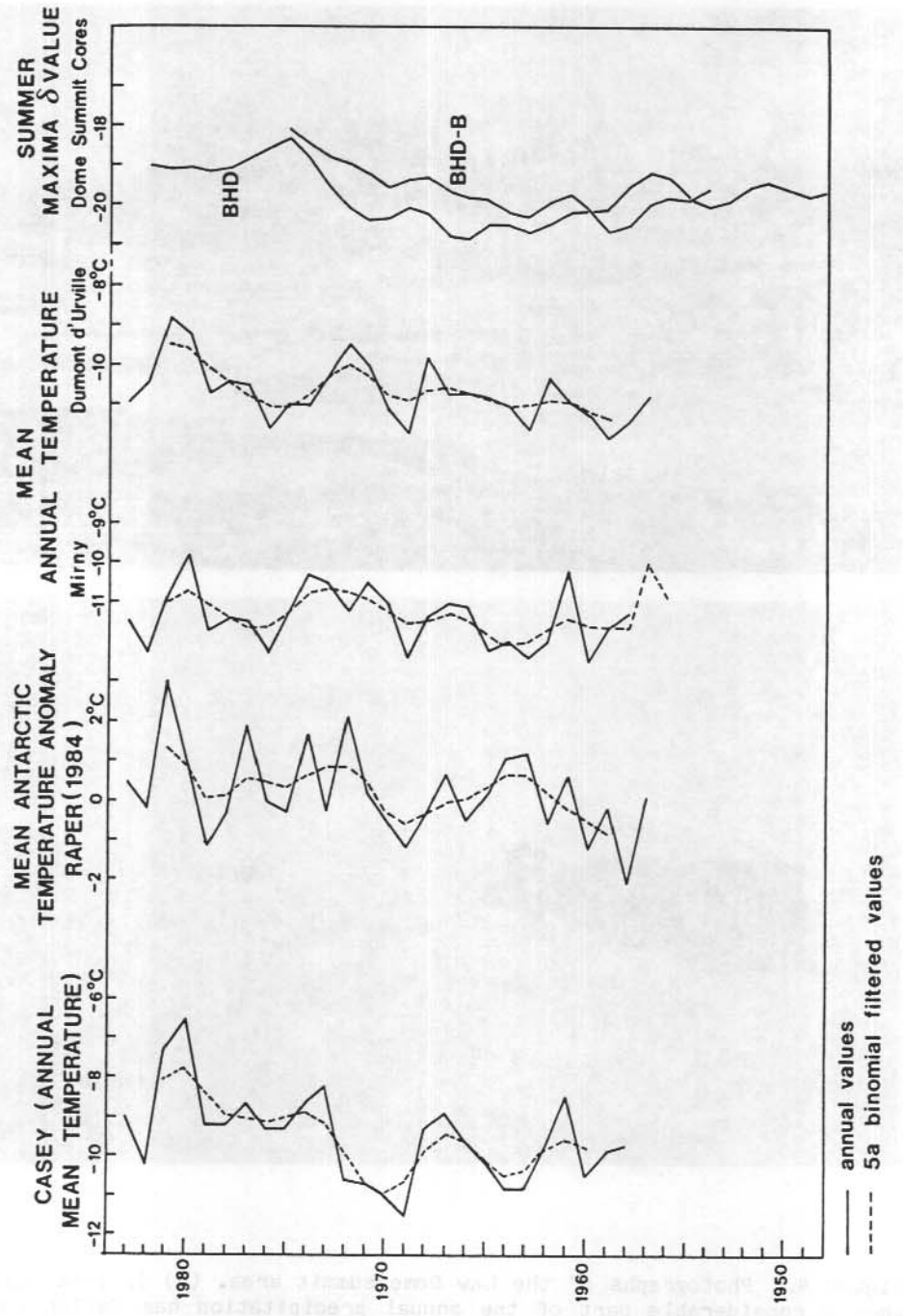

Figure 5. Comparisons between δ values from the Law Dome summit cores and temperature data from Casey and adjacent Antarctic stations.

4.6 LONGER TIME SCALES

For periods where the δ values in one core appear to be offset from those in the other for longer than one year, the explanation at present must be partly speculative. If the surface slope at one hole site is consistantly different than that at the other (i.e. over several years), it is likely that the net annual accumulation ratio of winter precipitation to summer in fill will also be different; even if the net annual accumulations are equalized over summer. Such conditions could be caused by dunes of large horizontal extent but small amplitude which migrate slowly at periods of several years. It is tempting to also attribute the apparent periodicity in the accumulation (Figure 1(a)) to such dune movements, but at present there are no reliable corroborative measurements.

4.7 DISCUSSION

The results presented here show that variations in accumulation patterns can alter core δ values independently of the δ value of the snow precipitation. In the short term this occurs as a result of dunes and sastrugi which are built up and filled in during one annual cycle but there also appears to be significant longer term effects which are attributed to longer period surface waves. These limit the accuracy of mean annual δ values, and averages over an arbitrary core length, unless the average covers several cycles of the longest period surface features. For the Law Dome summit this seems to be at least ten years from this set of data.

If the "summer" δ values can be selected by sufficient measurement detail they can be expected to have much less "accumulation noise" and are therefore much more suitable for comparisons of δ and temperature.

REFERENCES

Bagnold, R.A. (1941) The physics of blown sand and desert dunes. Chapman and Hall.

Budd, W.F. (1966) Glaciological studies in the region of Wilkes, Eastern Antarctica, 1961. ANARE Scientific Reports, A(IV) Glaciology. Publication No. 88.

Dansgaard, W., Johnssen, S., Clausen, H., and Gundestrup, N. (1983) Stable Isotope Glaciology. Meddeleser om Gronland, 197, (2) 53 pages.

Gow, A.J. (1965) On the accumulation and seasonal stratification of snow at the south pole. Journal of Glaciology, 25 (40) 467-477.

Robin, G de Q (1981) Climate into ice: The isotope record in polar ice sheets. In: Allison, I. (Ed.). Sea level, Ice and Climate Change. IAHS Publication No. 131, 207-216.

5. GAS EXTRACTION AND ANALYSIS FROM ANTARCTIC ICE CORES

D.M. Etheridge
Antarctic Division, Department of Science
Kingston, Tasmania, 7150

ABSTRACT

The significance of recently observed increases in atmospheric CO_2 concentration depends on what concentrations were in the past. It is now considered that air occluded as bubbles in polar ice represents the best available source for determining these past concentrations. The critical step in the reconstruction of past atmospheric composition is the extraction of these bubbles. The Antarctic Division Glaciology Section and the CSIRO Division of Atmospheric Research are currently involved in a program to extract and analyse the air from Antarctic ice cores. The techniques used and some preliminary results are discussed.

5.1 INTRODUCTION

The mean tropospheric concentration of CO_2 in the atmosphere has risen by 23 ppmv since accurate measurements commenced in 1958 (Keeling and others, 1982). Releases of carbon from fossil fuels and deforestation are now accepted as the main causes of this increase, and climatic effects of further increases have been predicted (Pearman, 1980).

Geochemical models of carbon exchanges between the biosphere, atmosphere and ocean have difficulty accounting for the more recent CO_2 concentration increase. This is primarily due to the lack of knowledge of the non-fossil biospheric carbon release and the pre-industrial CO_2 concentration. If the latter can be found accurately and be input as an initial condition, the models can be largely improved and then more emphasis placed on their predictions.

Ice core measurements should also reveal whether the present CO_2 concentration increase is typical of natural fluctuations in the past and confirm the suggested CO_2 increase toward the end of the last glaciation. The measurements are not only of scientific interest but are also important for future energy policies.

5.2 GAS IN POLAR ICE

It is important that the ice to be analysed for gas composition originates from a region where no melt occurs, so that the formation of the ice is purely by metamorphism and densification of firn to a point where the pores become isolated bubbles and cannot exchange with the surrounding firn or atmosphere. This "close off" occurs at a firn density of about 0.825 g cm^{-3} where the bubbles contribute about 10% to the total firn volume. Since gas diffusion through ice is extremely small (Hemmingsen, 1959) the composition of air occluded in these bubbles remains preserved. About 100 cm^3 of air at STP is contained as bubbles in each 1 kg of ice.

When studying CO_2 content however, it is important to note that polar ice also contains CO_2 other than that enclosed in the air bubbles. CO_2 dissolved in the snow particles during their formation and CO_2 evolved from dissolution of inorganic carbon dust can amount to as much as in the air bubbles themselves (Oeschger and others, 1982).

This means that procedures to extract the air from the bubbles in the ice must at no stage involve melting. Earlier extraction techniques which employed melt extraction gave anomalously high CO_2 concentrations (Stauffer and Berner, 1978). Two other groups have since devised dry extraction techniques which involve milling or crushing the ice at low temperatures (Raynaud and others, 1982; Neftel and others, 1982).

5.3 GAS EXTRACTION SYSTEM

The Melbourne system is based around a stainless steel milling flask which contains a cylindrical grater in which up to 1.5 kg of ice core can be placed. The flask is sealed at both ends with an indium metal ring and has a bellows valve outlet. The flask is evacuated, then shaken rapidly for several minutes and reattached to the vacuum system via a tube which passes through the cold room wall (Figure 1). All vacuum components inside the cold room must be able to perform at low temperatures, thus indium metal and ethylene propylene seals are used throughout.

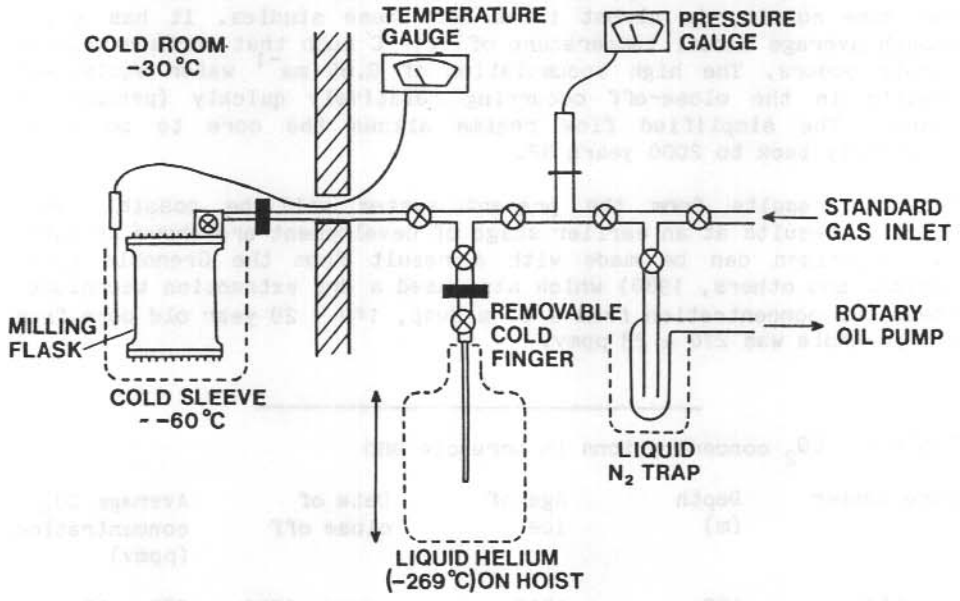

Figure 1. Vacuum extraction systems for ice core gas samples.

The vacuum system has a large internal diameter to enhance gas flow at molecular pressures. It is evacuated to about 10^{-4} Torr by a rotary oil vacuum pump and liquid N_2 trap combination. Pressure is monitored by a Pirani gauge. A standard gas mixture (e.g. CIG T58) can be injected to flush or calibrate the system.

As the extracted gas passes into the evacuated system it meets a cold finger at 4 ^{o}K. This is a 400 mm section of 5 mm diameter thin wall stainless steel tubing immersed in a sleeve of liquid helium. This acts as a trap for all atmospheric components and allows the gas sample from the 5 litre flask to be condensed to a useably high pressure sample. The cold trap is then closed, removed and mixed using an internal steel ball. Analysis is by the D.A.R. Carle gas chromatograph which gives CO_2 concentration to an accuracy of better than 1 ppmv. Other important trace gases such as CO, CH_4, NO_x and Freons can also be measured on D.A.R. equipment. The presence in the sample of Freons, which were only released in the past 40 years can be used as a dating system for close off, and as a leak detector.

Presently, efforts are being made to reduce the temperature of the flask and sample environment to around -60 ^{o}C. This will minimize the vapour pressure of the ice sample and reduce the amount of water entering the vacuum system and trap. Large CO_2 concentration variations are associated with the surface effects that water vapour causes in vacuum systems. Projected accuracy of the entire process from crushing to analysis is better than 1%.

The Melbourne program aims to measure ice cores thermally drilled from the Law Dome, near Casey, Antarctica. The site of borehole BHD, from the dome summit, is almost ideal for these studies. It has a low enough average annual temperature of -21 ^{o}C such that surface melting rarely occurs. The high accumulation of 0.65 ma^{-1} water equivalent results in the close-off occurring relatively quickly (perhaps 50 years). The simplified flow regime allows the core to be dated accurately back to 2000 years BP.

Accurate results from the present system will be possible very shortly. Results at an earlier stage of development are shown in Table 1. Comparison can be made with a result from the Grenoble group (Delmas and others, 1980) which also used a dry extraction technique. Their CO_2 concentration from a 61 m deep, 140 ± 20 year old core from D10 borehole was 270 ± 23 ppmv.

Table 1. CO_2 concentrations in borehole BHD

Core number	Depth (m)	Age of ice	Date of close off	Average CO_2 concentration (ppmv)
91D	159	1710	approx 1790	285 ± 10
68B	120	1800	approx 1880	265 ± 10

The Melbourne program, with its large extracted gas volume and accurately dated ice cores is now able to reconstruct recent CO_2 concentration history accurately. The large volume should also allow $^{13}C/^{12}C$ analysis in the near future. The next stage will be to look at cores of ages to 15 000 years BP.

ACKNOWLEDGMENTS

This program would not have been possible without the successful partnership with CSIRO Division of Atmospheric Research, and the scientific inspiration and technical prowess of Dr Graeme Pearman and Fred de Silva.

REFERENCES

Delmas, R., Ascencio, J.M. and Legrand, M. (1980) Polar ice evidence that atmospheric CO_2 20 BP was 50% of present. Nature, 284, 155-157.

Hemmingsen, E. (1959) Permeation of Gases through ice. Institute of Zoophysiology, University of Oslo. Tellus , XI, (3)

Keeling, C.D., Bacastow, R.B. and Worf, T.P. (1982) Measurements of the concentration of carbon dioxide at Mauna Loa, Hawaii, In: Carbon Dioxide Review 1982, W.C. Clarke (Ed.), Claredon Press, Oxford.

Neftel, A., Oeschger, H., Schwander, J., Stauffer, B. and Zumbrunn, R. (1982) Ice core sample measurements give atmospheric CO_2 content during the past 40 000 yr. Nature, 295, 220-223.

Oeschger, H., Stauffer, B., Neftel, A., Schwander, J. and Zumbrunn, R. (1982) Atmospheric CO_2 content in the past deduced from ice-core analysis. Annals of Glaciology, 3, 227-232.

Pearman, G.I. (Ed.) (1980) Carbon Dioxide and Climate: Australian Research, Australian Academy of Science, Canberra.

Raynaud, D., Delmas, R., Ascencio, J.M. and Legrand, M. (1982) Gas extraction from polar ice cores: a critical issue for studying the evolution of atmospheric CO_2 and ice-sheet surface elevation. Annals of Glaciology, 3, 265-268.

Stauffer, B. and Berner, W. (1978) CO_2 in natural ice. Journal of Glaciology, 21, (85), 291-300.

6. EVIDENCE OF SOUTHERN HEMISPHERE WARMING FROM OXYGEN ISOTOPE RECORDS OF ANTARCTIC ICE

E.R. Wishart
Meteorology Department, The University of Melbourne
Parkville, Victoria, 3052.

ABSTRACT

Comparison of a $\delta^{18}O$ record from Law Dome, Antarctica with mean annual temperature records from Casey, about 150 km west of Law Dome, over the period 1957 to 1977 gave no correlation. However when the $\delta^{18}O$ record was smoothed over long time scales, good qualitative agreement was made with New Zealand temperatures for the period 1853-1975, sea surface temperature data for 1880-1977 and a $\delta^{18}O$ record from Mizuho Station, Antarctica from about 1600 to 1900. On this basis the period around 1800 was the coldest period for over 2100 a BP with cooling around 1900 and fairly steady warming to at least 1977.

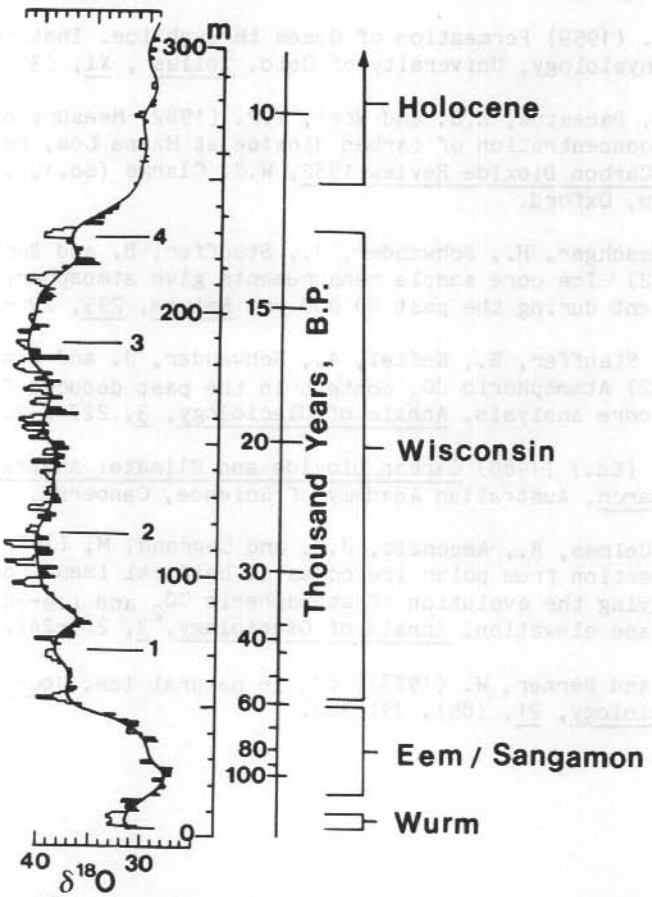

Figure 1. $\delta^{18}O$ record of ice core from Camp Century, Greenland (from Dansgaard, 1982)

6.1 INTRODUCTION

Figure 1 (from Dansgaard and others, 1982) showing a $\delta^{18}O$ record of an ice core from Camp Century, Greenland, illustrates in good detail, the four stages of the Winconsin Ice Age, the Eem/Sangamon Interglacial, etc. Figure 2 (from McCray, private communication) shows the $\delta^{18}O$ record of an ice core drilled from Cape Folger (66.1°S, 110.9°E). The last stage of the Winconsin and the warming at the beginning of the Holocene are evident.

While these results are qualitative, and there could be errors in dating, Dansgaard (1964) and Dansgaard and others (1973) have found a good correlation between mean annual surface air temperature and mean annual $\delta^{18}O$ of precipitation at Greenland, Iceland, and Northern Alaska, but poor correlation for inland Antarctica and no correlation for most coastal Antarctic stations. Nevertheless, in this study we first attempt to correlate with temperature, the $\delta^{18}O$ record of an ice core from the summit of Law Dome, Antarctica (66.7°S, 112.8°E). Reasons for choosing this location are given by Morgan (in press). As no meteorological station exists on Law Dome, temperature records were obtained from other areas.

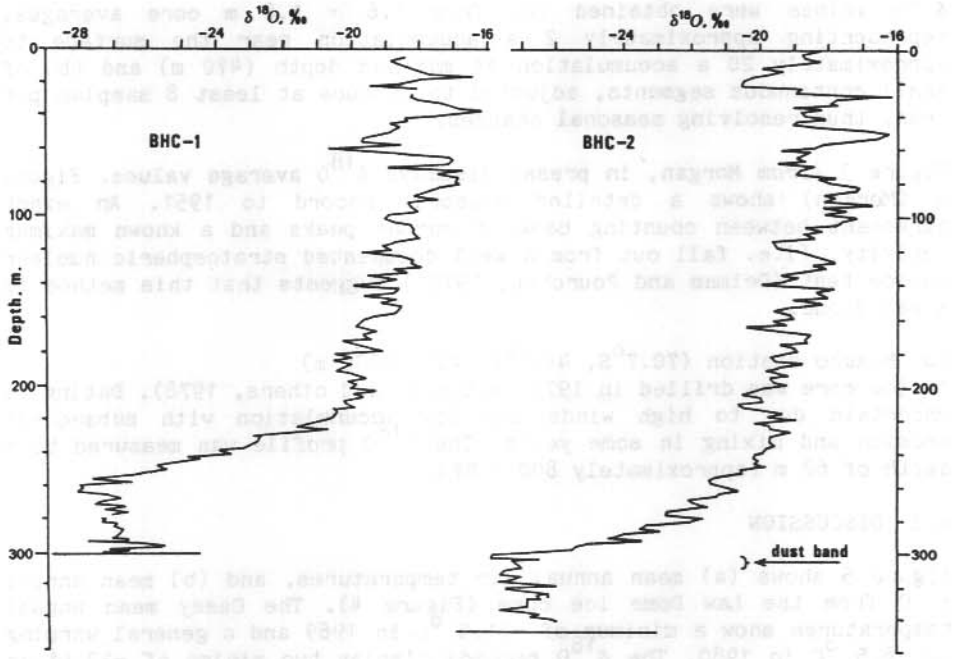

Figure 2. $\delta^{18}O$ record of two ice cores from Cape Folger, Antarctica. (from McCray, personal communications).

6.2 THE DATA SETS

6.2.1 Temperature

(a) Casey (66.3°S, 110.6°E)
A coastal Antarctic station, close to sea level at the edge of the continent, approximately 100 km west of Law Dome summit. Continuous weather observations have been kept since 1957. There was a site change in 1969, but no obvious discontinuity resulted.

(b) New Zealand (34 to 47°S, 168 to 179°E)
Salinger (1979) selected data from 77 New Zealand weather stations for the period 1853-1975. Similar trends were displayed for 5 and 17 a weighted moving average data of each of seasonal means, annual maximums, annual minimums, and annual means.

(c) Southern Hemisphere (30 to 50°S) Sea Surface Temperatures (SST)
Paltridge and Woodruff (1981) examined sea surface temperature records from 1880-1977 and taking 5 a averages were able to show SST versus time as a function of season and latitude zones.

6.2.2 $\delta^{18}O$

(a) Law Dome oxygen isotope record (66.7°S, 112.8°E, Alt. 1395 m)
(see Morgan, in press).
$\delta^{18}O$ values were obtained (a) from 1.6 - 1.8 m core averages, representing approximately 2 a accumulation near the surface to approximately 20 a accumulation at maximum depth (470 m) and (b) of small continuous segments, adjusted to produce at least 8 samples per year, thus resolving seasonal changes.

Figure 3 (from Morgan, in press) displays $\delta^{18}O$ average values. Figure 4 (Morgan) shows a detailed seasonal record to 1951. An exact agreement between counting back of summer peaks and a known maximum activity, (i.e. fall out from a well documented stratospheric nuclear device test (Delmas and Pourchet, 1977)) suggests that this method is a valid one.

(b) Mizuho station (70.7°S, 44.3°E, Alt. 2230 m)
An ice core was drilled in 1976 (Watanabe and others, 1978). Dating is uncertain due to high winds and low accumulation with subsequent erosion and mixing in some years. The $\delta^{18}O$ profile was measured to a depth of 62 m (approximately 800 a BP).

6.3 DISCUSSION

Figure 5 shows (a) mean annual air temperatures, and (b) mean annual $\delta^{18}O$ from the Law Dome ice core (Figure 4). The Casey mean annual temperatures show a minimum of -11.5 °C in 1969 and a general warming to -6.5 °C in 1980. The $\delta^{18}O$ records display two minima of -23.4‰ in 1966 and 1979 and a maximum of -20.8‰ in 1974.

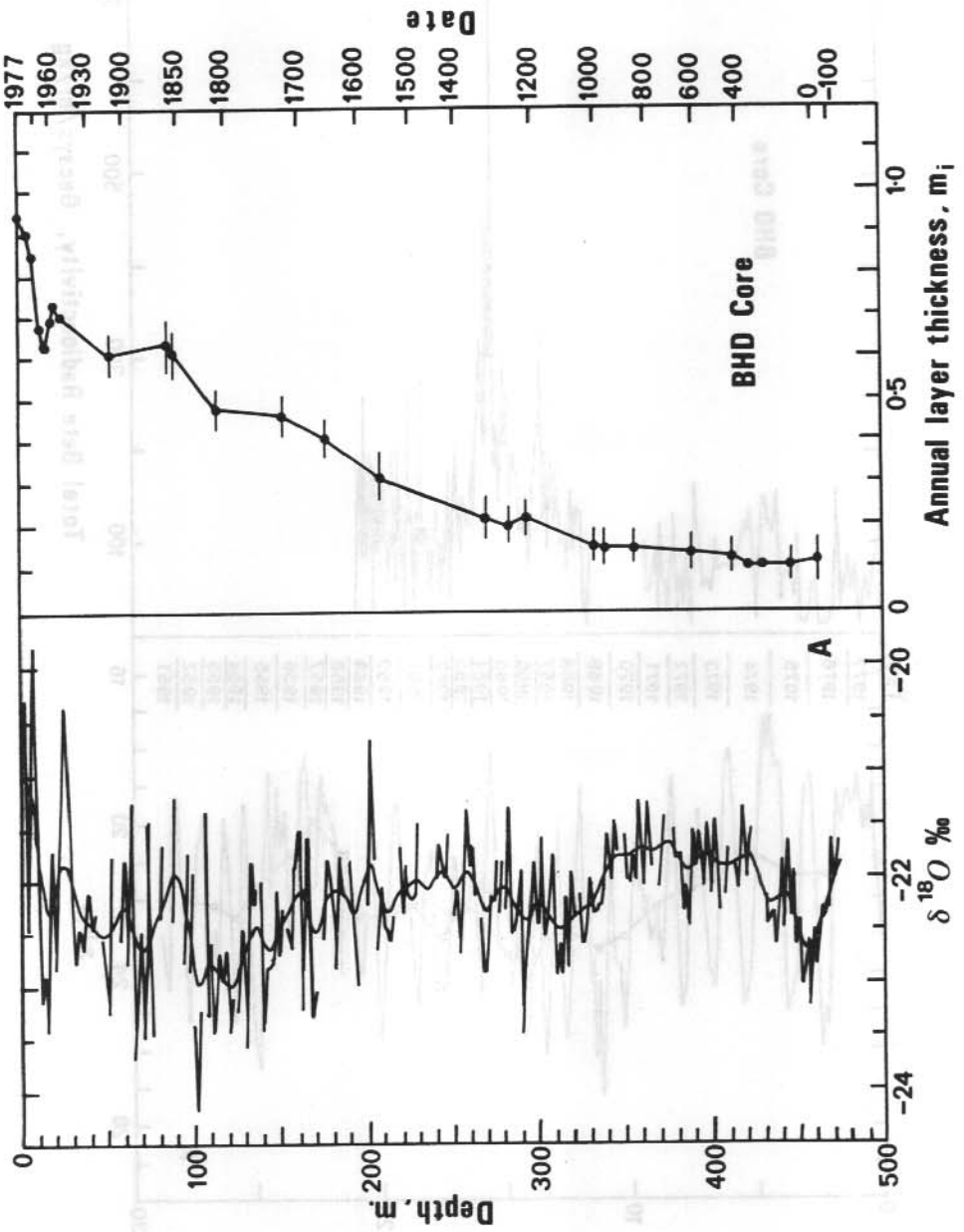

Figure 3. $\delta^{18}O$ record and estimated annual accumulation from an ice core from Law Dome summit, Antarctica (from Morgan, in press).

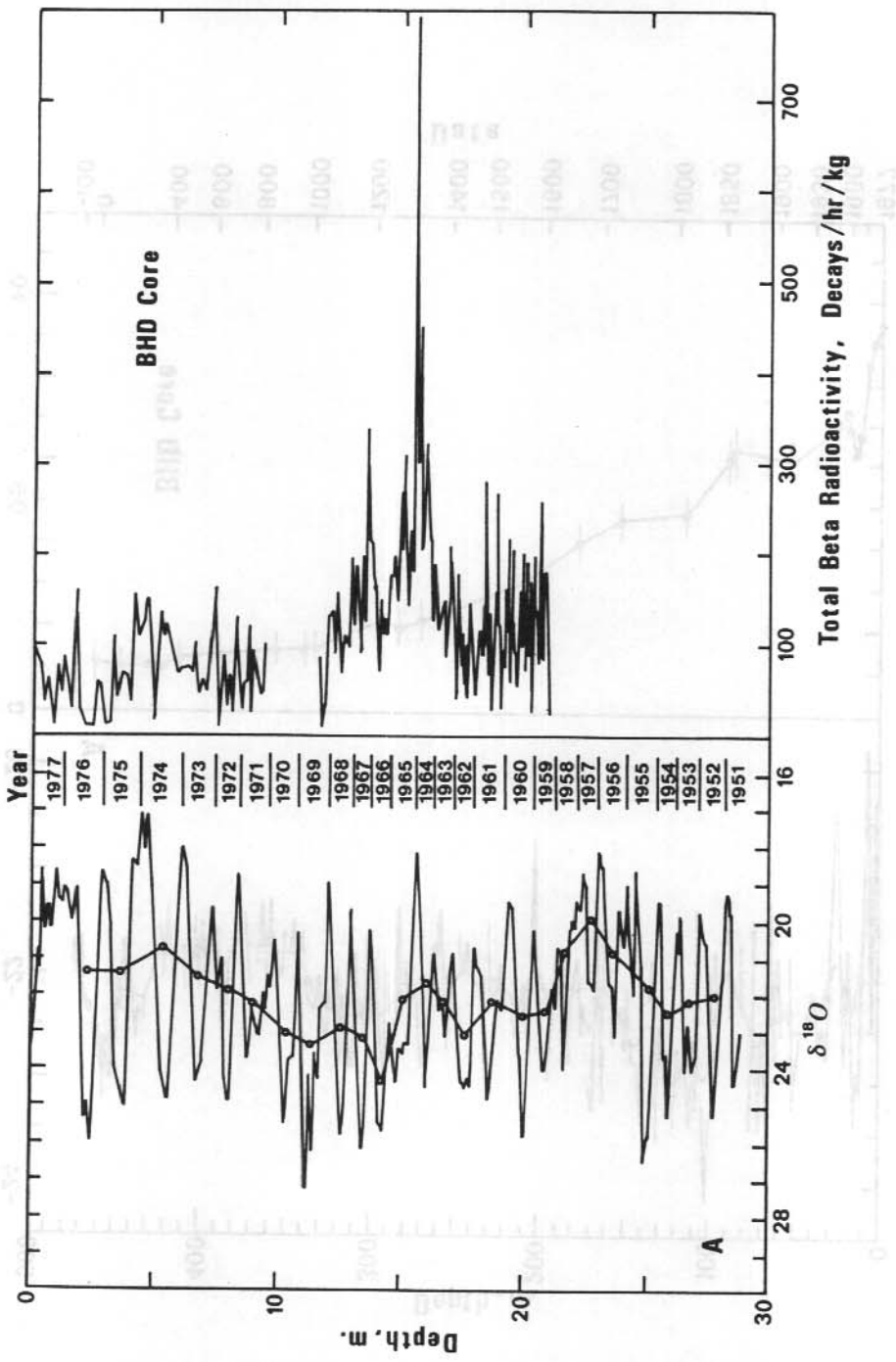

Figure 4. Detailed δ record and β decay from Law Dome summit ice core.

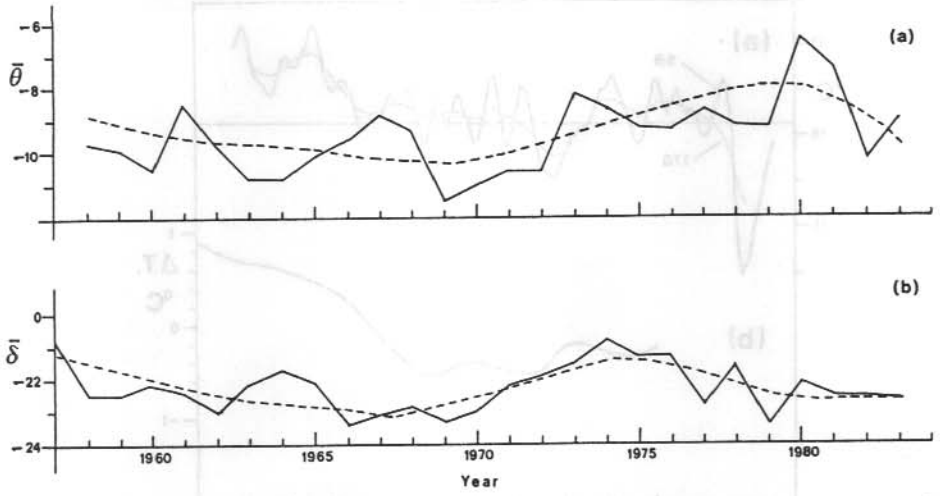

Figure 5. Annual mean of (a) Casey air temperature and (b) $\delta^{18}O$ record of Law Dome summit ice core.

Poor correlations of this nature are not surprising as, while Casey is only about 100 km to the west of the summit of Law Dome, the station is largely sheltered by the Law Dome massif, from the westerly to south-westerly snow bearing winds. At the height of summer, extensive melting occurs at Casey, however the temperature very rarely exceeds 0 ^{o}C due to the latent heat of melting.

Figure 6 displays: (a) New Zealand temperatures and 5 and 17 a moving averages (Salinger, 1979) illustrating a long term warming since the 1860s. There were two main cold periods, one in the early 1860s and the other, around 1900. Note the marked warming from 1945 to 1975. (b) Latitude 30 to 50 ^{o}S sea surface temperature measurements (Paltridge and Woodruff, 1981) showing a broad cool period from about 1905 to 1930, then steady warming to 1977. (c) Filtered $\delta^{18}O$ record for Law Dome summit showing a minimum about 1830, a secondary minimum around 1880, a general increase to 1965, then a dramatic rise to 1977. (d) Filtered $\delta^{18}O$ record from Mizuho station (Watanabe, 1978) which displays a marked minimum around 1800, a secondary minimum at about 1880 and then a general increase to around 1960.

With the assumption that the $\delta^{18}O$ records vary in the same direction as the temperature records (a), (c) and (d) of Figure 6, all display a very cold period about 1830. Note that the record (d) showing a strong minima around 1800, may be in error as discussed above. In fact this would have been the coldest period for at least 2000 a BP (Figure 3).

A secondary minima is shown in all four records from 1880 to 1930. A general warming is evident since 1930.

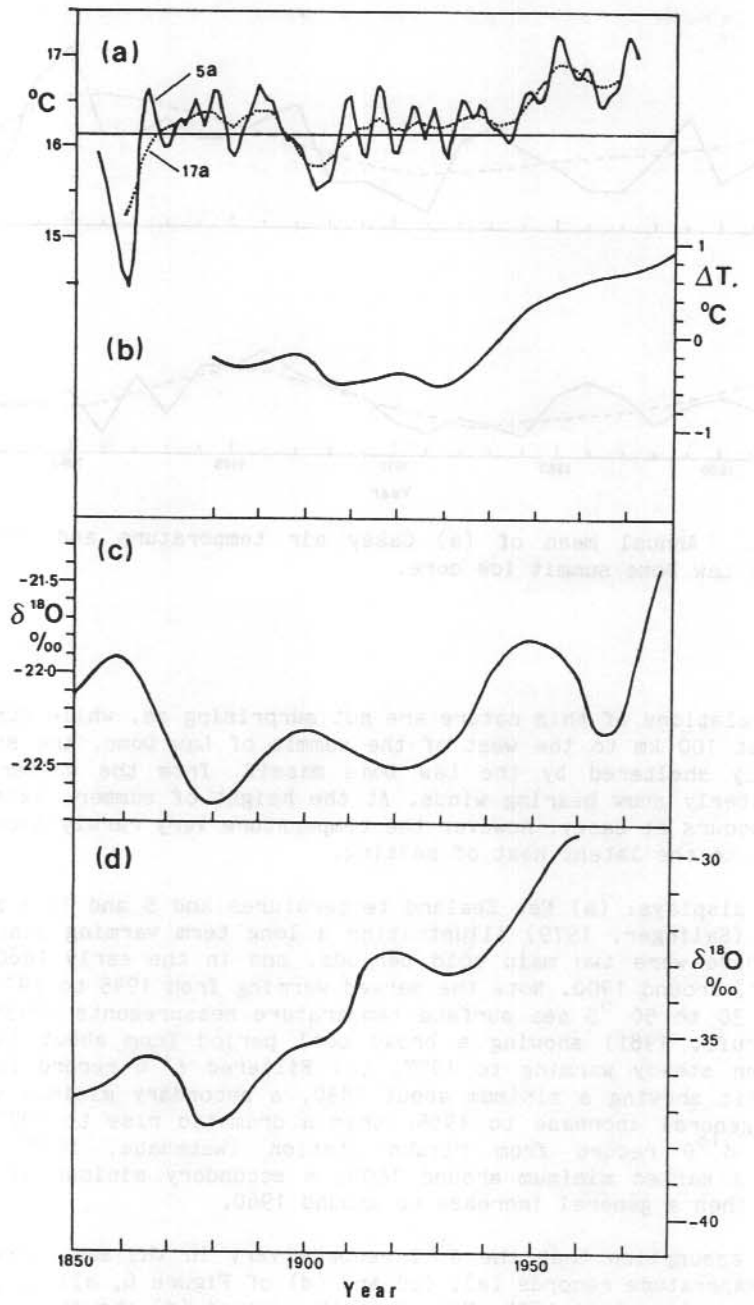

Figure 6. (a) New Zealand temperatures (Salinger, 1969); (b) Lat 30 - 50 ^{o}S sea surface temperatures (Paltridge and Woodruff, 1981); (c) filtered $\delta^{18}O$ (Morgan, in press); and (d) filtered $\delta^{18}O$ (Mizuho station)(Watanabe and others, 1978).

It is worth noting the very good agreement between the $\delta^{18}O$ records from Law Dome and from Mizuho, when consideration is given to the longitudinal difference of 68.5° between these two stations. On this basis the evidence presented supports the idea of a general atmospheric warming from about 1800 up to at least 1977 for the southern hemisphere mid-latitudes and extending to at least the coastal regions of Antarctica.

6.4 WORK IN PROGRESS AND FUTURE PLANS

Future plans include continuation of detailed $\delta^{18}O$ measurements to at least about 1830 (the minimum for the entire core). An automatic weather station is to be installed on Law Dome summit.

Snow samples need to be collected upwind and downwind (to near surface level) of Law Dome summit.

Precipitation samples are to be collected from Casey, Macquarie Island and Hobart, and from supply ships on route from Australia to Antarctica.

The continuation of sea surface temperature measurements is also needed. Static electrical conductivity measurements of ice cores (Hammer, 1980) will check $\delta^{18}O$ dating by detecting high seasonal changes of acidity (Bigg and others, 1984) and known major volcanic eruptions. Further ice core drilling is also required.

6.5 CONCLUSION

New Zealand temperatures, Southern Ocean sea surface temperatures, and $\delta^{18}O$ profiles of ice cores from Law Dome and Mizuho station, suggest that following an extremely cold period around 1830, a warming of ~1.2 °C occurred with a secondary minima at about 1900.

This warming would seem to extend from at least the mid latitudes to the coastal areas of Antarctica.

ACKNOWLEDGMENTS

Assistance with ice core sample preparation and sample filtering was given by B. Cook and L. Christou of The University of Melbourne. V.I. Morgan of Antarctic Division offered numerous constructive comments.

REFERENCES

Bigg, E.K., Gras, J.L. and Evans, C. (1984) Origin of Aitken particles in remote regions of the southern hemisphere. Journal of Atmospheric Chemistry, 1, 203-214.

Caig, H. (1961) Standard for reporting concentrations of deuterium and Oxygen-18 in Natural Waters. Science, 133 (3467) 1833-1834.

Dansgaard, W. (1964) Stable isotopes in precipitation. Tellus, 16(4), 436-468.

Dansgaard, W., Johnsen, S.J., Clausen, H.B. and Gundestrup, N. (1973) Stable isotope glaciology. Meddelelser on Gronland, 197 (2), 53 pp.

Dansgaard, W., Clausen, H.B., Gundestrup, N., Hammer, C.U., Johnsen, S.F., Kristinsdottir, P.M. and Reeh, N. (1982) A new Greenland Deep ice core. Science, 218 (4579), 1273-1277.

Delmas, R. and Pourchet, M. (1977) Utilisation de filtres e'changeurs dions pour le'Sude de l'activite' B globale d'un carottage glaciologique. In: Isotopes and Impurities in Snow and Ice. IAHS Publication No. 118, 159-163.

Hammer, C.U. (1980) Acidity of polar ice covers in relation to absolute dating, past volcanism and radio-echoes. Journal of Glaciology, 25 (93), 359-372.

Morgan, V.I. (1979) Oxygen isotope analysis of Antarctic snow and ice. Unpublished M.Sc. Thesis. Meteorology Department, The University of Melbourne.

Morgan, V.I. (in press) An oxygen isotope-climate record from the Law Dome, Antarctica. Climatic Change.

Paltridge, G. and Woodruff, S. (1981) Changes in global surface temperature from 1880 to 1977 dervied from historical records of sea surface temperature. Monthly Weather Review, 109, 2427-2434.

Salinger, M.J. (1979) New Zealand climate: The temperature record, historical data and some agricultural implications. Climate Change, 2, 109-126.

Watanabe, O., Kato, K., Satow, K., and Okuhina, F. (1978) Stratigraphic analyses of firn and ice at Mizuho station. Memoirs of the National Institute of Polar Research. Special Issue 10, 25-47.

B. ICE - ATMOSPHERE - OCEAN

One of the overall aims of the Australian glaciology program has long been to understand the interaction of ice in the Antarctic with the global environment, and particularly its role in the weather and climate system.

On the wider scale, the heat loss from the Antarctic atmosphere governs the main global north-south temperature contrast which drives the atmospheric and oceanic general circulations. The intensity of the Antarctic continental heat sink is determined by the regional surface energy balance, and factors which influence this include the surface characteristics and topography of the underlying ice sheet or sea ice. Micrometeorological and energy balance process studies of Antarctic snow and ice surfaces have been part of the Australian glaciology program since 1965 and are ongoing. Automatic weather stations to be deployed on glaciological traverses in the next few years will measure a range of surface energy budget parameters, including global radiation and snow and air temperature profiles.

Sea ice is the most dynamic of the Antarctic cryospheric elements, undergoing large and rapid fluctuations, and there is evidence that sea ice plays a significant role in climatic variations on both long and interannual time scales. The regional energy budget in the sea ice zone is determined not only by the characters of the ice but also by the dynamics which influence the nature of the surface (open water, thin ice, thick ice). There is also an active exchange of energy and salt between the ice and ocean: the movement of sea ice in the Antarctic produces a net equaterward transport at the sea surface of nearly fresh water and of negative thermal energy. Detailed Australian studies of sea ice have in the past concentrated on the narrow fringe of land fast sea ice. Little however is known about ice characteristics or processes within the extensive pack ice zone. Future programs, such as the deployment of drifting sea ice buoys and the measurement of pack ice characteristics during marine science voyages, will investigate larger scale processes. Compilation of ice extent and concentration data derived from satellite observations will continue to provide a data bank for statistical studies of sea ice/climate interaction.

The melt of icebergs is also important in determining the characteristics and circulation of the Southern Ocean; up to 1600 km^3 of fresh water ice are discharged annually from the Antarctic ice sheet. Further studies of iceberg - ocean and iceberg - atmosphere interaction are required as part of research into the overall ice - ocean system and for investigation of the feasibility of utilising icebergs as a freshwater resource.

The cryosphere also plays an important role in regional weather and climatic processes, a notable example of this being the katabatic winds which develop due to radiational cooling from the inclined ice sheet surface. Measurements of the atmospheric boundary layer will be made on traverses and by Antarctic weather stations to further study katabatic flow.

Regional weather forecasting for aircraft operations is becoming more important as intercontinental air transport to the Antarctic increases. Whilst not a glaciological problem per se, observations from both automatic weather stations and from parties occupying remote sites can provide data to aid the regional forecasting.

It is expected that studies of ice - atmosphere - ocean interaction will become increasingly important as activities within the World Climate Research Program (WCRP) increase. Many of the projects reported here, and planned future activities within the Australian glaciology program, contribute to the Antarctic research identified as a necessary contribution to the WCRP (Allison, 1983). On the shorter time scales of more immediate concern to the WCRP, sea ice is the most important of the Antarctic ice forms (WMO, 1982; WMO, 1983) but on the long time scales the ice sheet interaction is critical to both climate and sea level. The Antarctic ice sheet also contains a detailed and unique record of past climates and environments to more than 100 000 a BP (Section A). Ice cores provide numerous data on drastic past environment changes and interpretation of this record will help us understand the causes of climatic change.

Allison, I. (Ed.) (1983) Antarctic Climate Research; proposals for the implementation of a programme of Antarctic research contributing to the World Climate Research Programme. SCAR/ICSU.

WMO, (1982) Report of the WMO/CAS-JSC-CCCO meeting of experts on the role of sea ice in climatic variations. WCP-26.

WMO, (1983) Report of the meeting of experts on sea ice and climate modelling. WCP-77.

Ian Allison

7. CHARACTERISTICS OF SEA ICE IN THE CASEY REGION

Ian Allison
Antarctic Division, Department of Science
Kingston, Tasmania, 7150.

Qian Songlin
Lanzhou Institute of Glaciology and Geocryology, Academia Sinica
Peoples Republic of China.

ABSTRACT

Sea ice growth and characteristics were measured at a number of sites in Newcomb Bay near Casey, throughout 1983. The ice in this region is highly unstable, breaking out frequently in strong winds during winter months and then reforming. There appears to be little heat flux from the ocean to the underside of the ice at this site. The growth of the ice cover is controlled almost solely by conduction through the ice which is modified by a snow cover during the winter, although oceanic heat flux may be important when the ice starts to thin in summer.

Most of the ice growth is due to congelation, and the bulk of the ice is composed of columnar crystals with horizontal c-axes tnat show no preferred alignment. At one site however, there is a considerable proportion of frazil in the total ice column. This frazil accreted rapidly when there was open water less than 100 m away.

Multiyear ice from an almost enclosed bay to the south of Casey showed a very strong preferred alignment of the horizontal c-axes at almost all depths. It is suggested that these arise as a result of strong tidal currents that might be expected at this location.

7.1 INTRODUCTION

Regular measurement of shore fast sea ice formation and growth have been made near Mawson and Davis stations since the mid 1950s (Mellor, 1960) but systematic data for sea ice in the Casey region has only been available since the late 1970s. At Mawson and Davis the seasonal sea ice is usually stable from about May through until December or January, but in Newcomb Bay near Casey, the sea ice frequently breaks out and reforms during the winter months.

During 1983 regular measurements of ice thickness and physical characteristics were made at three sites in Newcomb Bay. The observation sites, shown in Figure 1, were:

A. "Kilby Strait", 450 m offshore and midway between Bailey Peninsula and Kilby Island, in an area of about 20 m water depth.
B. "Nicholson Strait", only 80 m offshore between Bailey Peninsula and a line of nearshore islands, in 6 m of water.
C. "Newcomb Bay", towards the centre of the Bay, where water depths are over 40 m.

The ice and snow thickness measurements were made at each site approximately weekly when ice conditions permitted. At the same time

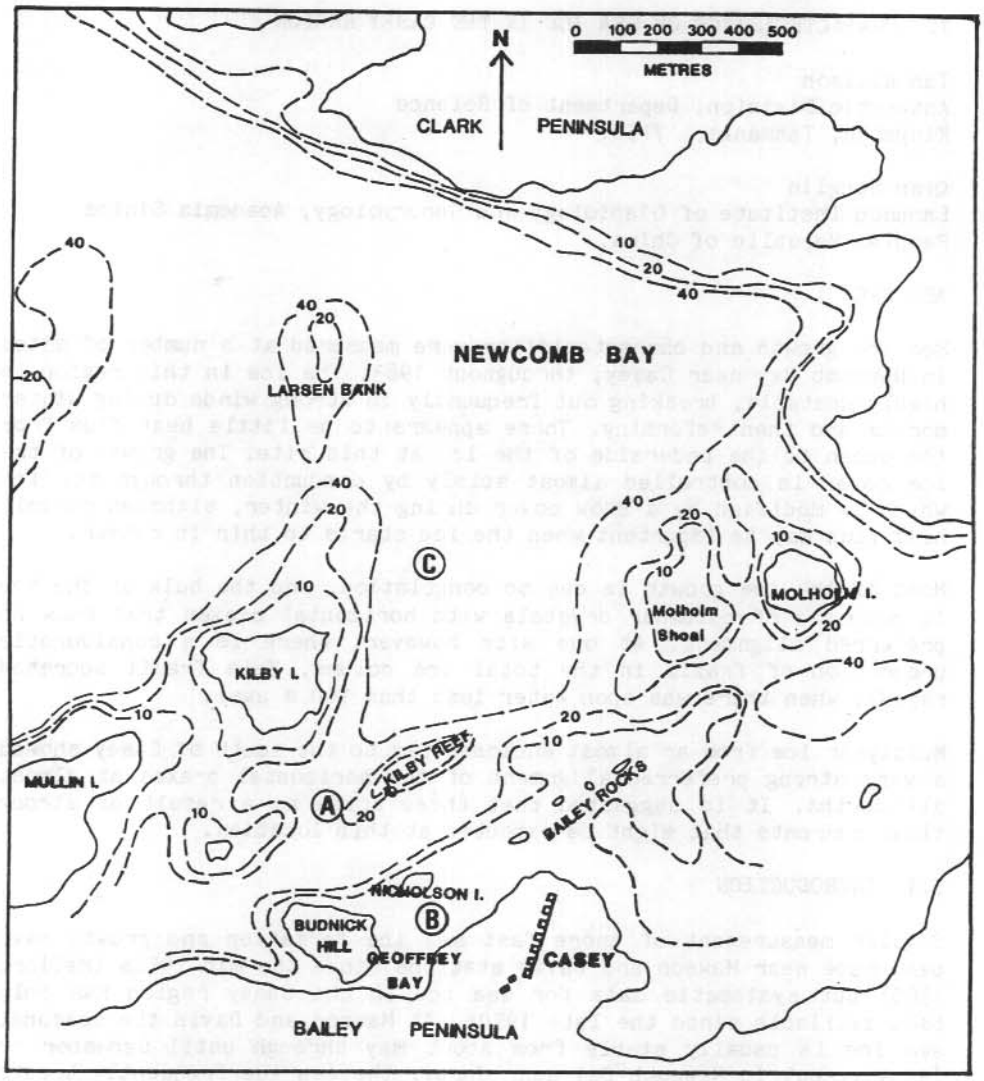

Figure 1. Newcomb Bay showing 1983 sea ice measurement sites and water depth in metres (dashed lines).

ice cores were taken for analysis of the salinity and the crystal structure of the ice. Other observations included measurements of ice temperature and of the salinity and temperature of the underlying water.

Overall the ice formation pattern in 1983 was similar to that observed in previous years, with frequent breakouts occurring during strong easterly blizzards, particularly in the central part of Newcomb Bay which is open to the east. The ice to the east and south of an arc

extending from Kilby Island east towards Molholm Island and then north to the Clark Penninsula (e.g. measurement sites A and B) is somewhat more protected than in the central bay, but even here numerous breakouts occured during the winter. In 1983 a fast ice cover first formed in the Casey region on March 17 and the last fast ice, apart from a few isolated patches between islands or in enclosed bays, disappeared by December 5. The history of ice at each of the three measurement sites is summarised in Table 1.

Table 1. Duration of ice cover, Newcomb Bay, 1983.

Site	Maximum ice thickness	Number of formation/ breakout events	Total number of days of fast ice cover
A	0.9 m	9	202
B	1.0 m	8	216
C	0.7 m	10	126

7.2 ICE GROWTH RATE

Figure 2 shows the sea ice growth at each of the three sites for two periods during which the ice remained fast for long enough to grow to a thickness of more than 0.5 m (July 10 to September 16 and September 18 to early December). Also shown are measurements taken at site B2 to the south of site B, where the ice did not breakout on September 16, but continued to grow to reach a thickness of 1.2 m.

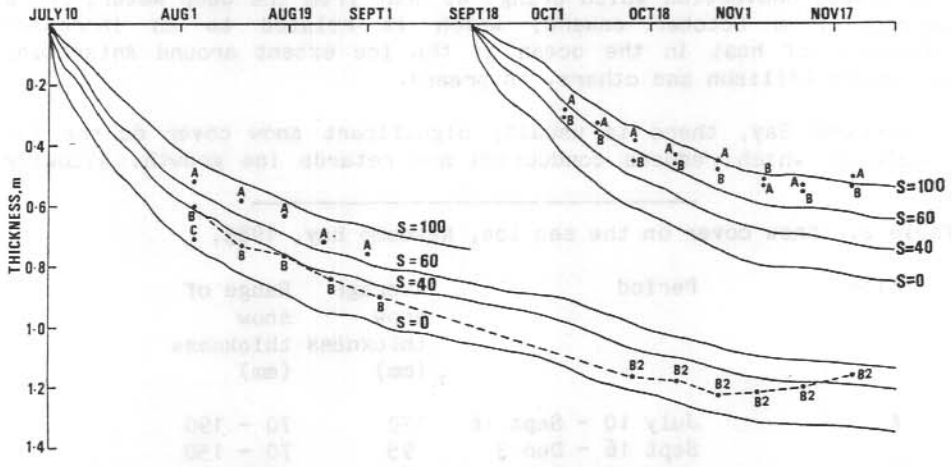

Figure 2. Measured and calculated thickness of sea ice. Measured thickness for the three sites are shown by a letter (A, B or C), while the continuous lines show thickness calculated from daily mean air temperature for different thicknesses of snow cover (mm)

The growth of the ice is controlled by the energy budget at the ice water interface. The classical Stefan relationship for ice growth assumes that at the lower boundary the only energy exchanges are the latent heat of ice growth and conduction through the ice. The heat conduction can be estimated from the temperature difference between the surface (the air temperature, T_a) and the lower boundary (the freezing point of seawater, -1.9 °C) to yield a relationship between ice thickness, z, after d days and the cumulative degree days below freezing:

$$z = \left[\frac{-2k}{\rho L \, d} \Sigma(T_a + 1.9) \right]^{1/2} \qquad \text{----------(1)}$$

where k is the thermal conductivity of the ice (1.93 $Wm^{-1} K^{-1}$)
ρ is the ice density and
L is the latent heat of fusion of sea ice.

The assumption of a linear temperature gradient within the ice, despite temperature change with time, implies that the ice has zero specific heat. Schwerdtfeger (1964) suggests correcting for changes in heat content of the ice by replacing the latent heat, L, with an effective latent heat, L_{eff}, which can be expressed as a function of ice salinity and ice temperature.

Allison (1981) shows that at Mawson, where the snow cover on the ice is negligible, heat conducted through the ice can be reasonably estimated from air temperatures but ice thicknesses are consistently less than estimated from Equation 1 because there is a considerable flux of heat from the ocean to the ice at the lower boundary. Oceanic heat flux can average as much as 20 Wm^{-2} and there are two periods of maxima; one during the early rapid growth when brine ejected from the ice causes convection which brings up heat from the deep water, and a second, from October onward, which is related to an increased advection of heat in the ocean as the ice extent around Antarctica decreases (Allison and others, in press).

In Newcomb Bay, there is usually significant snow cover on the ice (Table 2) which reduces conduction and retards ice growth. Allowing

Table 2. Snow cover on the sea ice, Newcome Bay, 1983.

Site	Period	Average snow thickness (mm)	Range of snow thickness (mm)
A	July 10 - Sept 16	130	70 - 190
	Sept 16 - Dec 3	95	70 - 150
B	July 10 - Sept 16	45	30 - 60
	Sept 18 - Dec 3	45	10 - 80
C	July 10 - Aug 6	50	40 - 50
	Sept 25 - Nov 17	20	10 - 40

for a snow cover thickness, S, the conducted flux, B, through the ice can be estimated by the solution of:

$$B = \frac{-k\,k_s}{k_s Z + kS}(T_A + 1.9) \qquad \text{----------(2)}$$

where k_s is the snow conductivity (0.5 $Wm^{-1}\,K^{-1}$ for windpacked snow) and for a constant thickness snow cover, the ice thickness, Z, after d days is then given by:

$$(\rho L_{eff}\,k_s)Z^2/2 + (\rho L_{eff}\,kS)Z - kk_s \Sigma_d(\theta + 1.9) = 0 \qquad \text{----------(3)}$$

Ice thicknesses estimated from daily mean temperatures at Casey by Equation 3 are shown in Figure 2 for different snow cover thicknesses. For most of the year these agree closely with the measured thickness if account is taken of the actual snow cover. This implies that there is probably a negligible oceanic heat flux to the underside of the sea ice in Newcomb Bay. Similar results were obtained from ice thickness measurements made in Newcomb Bay in 1979, 1980 and 1982. The difference between this and the situation at Mawson can be explained by the difference in water depth in the two regions. At Mawson the water is over 300 m deep and although the surface waters are cooled prior to ice formation, there is available heat at depth which is brought up by the haline convection. In Newcomb Bay the water depth is everywhere less than 50 m (Figure 1) and the entire water column is cooled to near the freezing point before ice formation. Measurements beneath the sea ice at site A on August 11 and August 29, 1983 showed the whole water column was isothermal at the freezing point (-1.86 ^{o}C) and isohaline with a salinity of 34.41‰ (on August 29).

From Figure 2, it can be seen that the ice at site B2, which did not break out on September 16, increased in thickness at a rate greater than that predicted. However analysis of ice cores showed that the ice cover did not grow simply by congelation in this period, but that frazil ice accumulated on the underside of the ice. This frazil is discussed further in Section 7.4.

Although the oceanic heat flux appears to be near zero in Newcomb Bay for the winter months, the ice cover starts to ablate from the lower boundary from November, when air temperatures are still below the freezing point of the seawater. Other energy fluxes such as short wave radiation penetration become important around this time but snow cover on the ice reduces this and even when it is important the main effect is observed to be the formation of a layer of melt at a depth of 0.1 to 0.2 m below the surface of the ice. This layer, at a temperature close to 0 ^{o}C, would cause heat to be conducted towards the lower boundary, but only at a rate sufficient to melt less than 0.04 m of sea ice per month. It is probable that, as at Mawson, the main source of heat for bottom melting in the summer months comes from the ocean, which is itself gaining radiant energy at this time from nearby ice free areas.

7.3 SEA ICE SALINITY

Most major physical properties of sea ice, including thermodynamic characteristics, are strongly dependent on the bulk salinity of the ice. Although brine is ejected from the crystal structure when the ice freezes, some brine cells remain at the platelet boundaries in the ice.

Figure 3 shows salinity profiles measured on ice cores from sites B and B2. The initial salinity of the ice is a function of the freezing rate and, if the high salinity frazil ice band between about 0.95 m and 1.15 m depth is excluded, the measurements from site B2 give an empirical relationship between salinity, s (‰), and growth rate, dz/dt (mm/day), of

$$s = 3.43 + 0.125\ dz/dt$$

with a correlation coefficient of 0.89. Since growth rate is dependent on ice thickness, the average salinity, s, can also be expressed as a function of ice thickness. The data from Newcomb Bay broadly fits the linear relationship

$$s = 7.88 - 1.59\ z$$

determined for Arctic sea ice greater than 0.5 m thick by Cox and Weeks (1974).

The salinity of the sea ice decreases during the growth season by the processes of brine migration and gravity drainage of the brine cells (Lake and Lewis, 1970). The average salinity of the top 0.8 m of ice at site B2 decreased from 5.8‰ on August 26 to 4.3‰ on November 19.

7.4 ICE STRUCTURE

The structure of the sea ice was examined from both horizontal and vertical thin sections made from the cores collected for salinity measurement.

In calm conditions a skim of sea ice may initially form with c-axes vertical, but the preferred growth direction is perpendicular to the c-axes and as the ice thickens geometric selection favours the downward growth of those crystals with c-axes off the vertical. A transition layer in the ice results, in which the c-axes become increasingly more horizontal until eventually all c-axes are oriented within a few degrees of the horizontal and the crystals are very long. This is analogous to the so called columnar zone in metal ingots. (Weeks and Ackley, 1982).

The majority of cores examined showed typical congelation ice. A transition zone could be identified above 0.1 m depth but beneath that the ice was columnar having horizontal c-axes with generally no preferred direction of alignment. The average crystal diameter in the horizontal section ($\sqrt{LW}$ where L is the length and W the width of the crystal) showed a linear increase from 6 mm at 0.1 m depth to 13 mm at

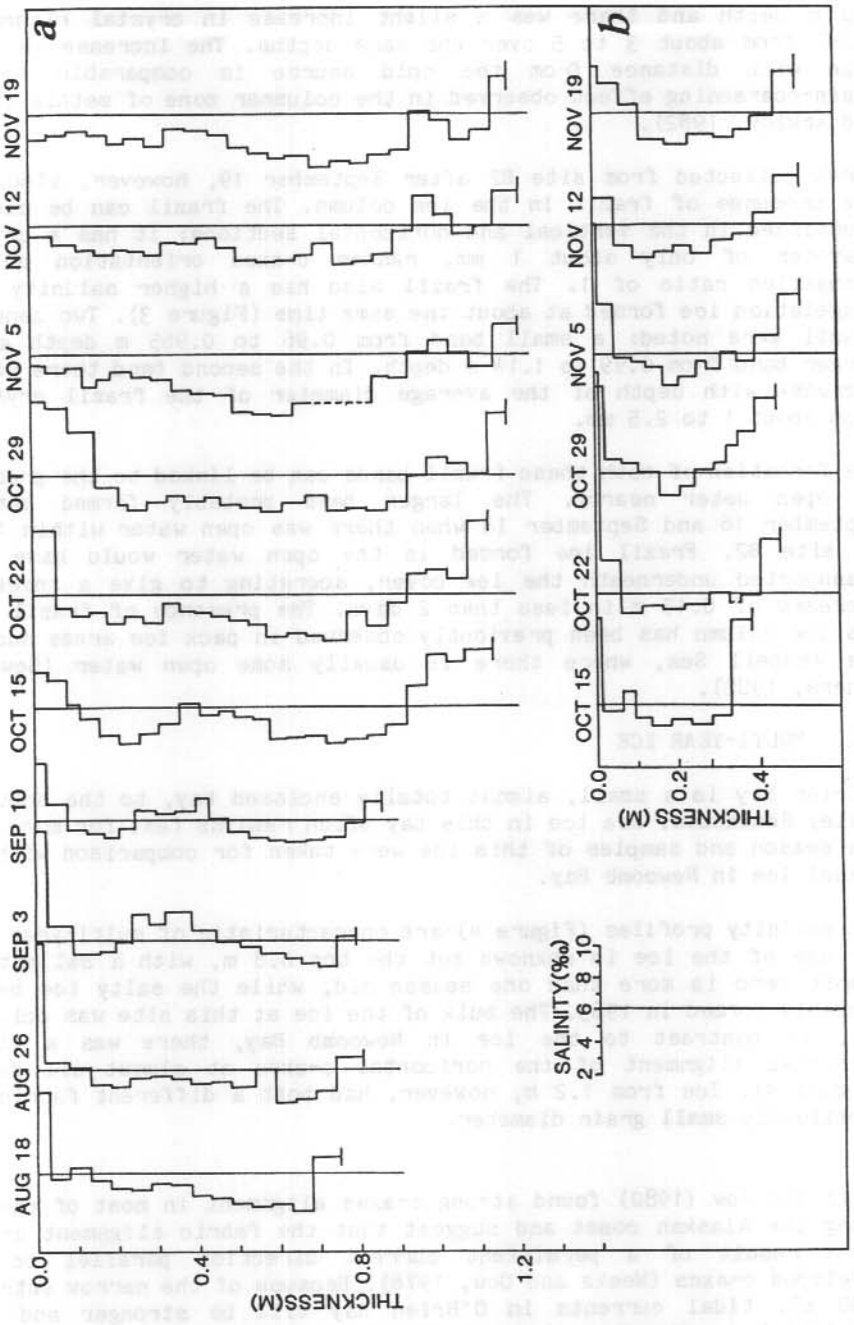

Figure 3. Measured salinity profiles of sea ice at site B2 (a), and site B (b).

0.8 m depth and there was a slight increase in crystal elongation (L/W) from about 3 to 5 over the same depths. The increase in grain size with distance from the cold source is comparable to the grain-coarsening effect observed in the columnar zone of metals (Weeks and Ackley, 1982).

Cores collected from site B2 after September 19, however, also show the presence of frazil in the ice column. The frazil can be clearly identified in the vertical and horizontal sections; it has a crystal diameter of only about 1 mm, random c-axes orientation and an elongation ratio of 1. The frazil also has a higher salinity than congelation ice formed at about the same time (Figure 3). Two zones of frazil were noted: a small band from 0.96 to 0.965 m depth and a larger band from 0.99 to 1.14 m depth. In the second band there was an increase with depth of the average diameter of the frazil crystals from about 1 to 2.5 mm.

The formation of both these frazil bands can be linked to the presence of open water nearby. The larger band probably formed between September 16 and September 18 when there was open water within 100 m of site B2. Frazil ice formed in the open water would have been transported underneath the ice cover, accreting to give a thickness increase of 0.15 m in less than 2 days. The presence of frazil in a sea ice column has been previously observed in pack ice areas such as the Weddell Sea, where there is usually some open water (Gow and others, 1982).

7.5 MULTI-YEAR ICE

O'Brien Bay is a small, almost totally enclosed bay, to the south of Bailey Peninsula. Sea ice in this bay often remains fast for more than one season and samples of this ice were taken for comparison with the annual ice in Newcomb Bay.

The salinity profiles (Figure 4) are characteristic of multi-year ice. The age of the ice is unknown but the top 0.8 m, with a salinity of almost zero is more than one season old, while the salty ice below, probably formed in 1983. The bulk of the ice at this site was columnar but, in contrast to the ice in Newcomb Bay, there was a strong preferred alignment of the horizontal c-axes at almost all depths (Figure 4). Ice from 1.2 m, however, had both a different fabric and anomalously small grain diameter.

Weeks and Gow (1980) found strong c-axes alignment in most of the ice along the Alaskan coast and suggest that the fabric alignment arises as a result of a persistent current direction parallel to the developed c-axes (Weeks and Gow, 1978). Because of the narrow entrance (300 m), tidal currents in O'Brien Bay will be stronger and more consistent in direction than at the Newcomb Bay sites. The absolute orientation of the measured fabrics (Figure 4) is not known, but the presence of a preferred c-axes alignment in the O'Brien Bay ice, and not elsewhere, is consistent with the hypothesis proposed by Weeks and Gow.

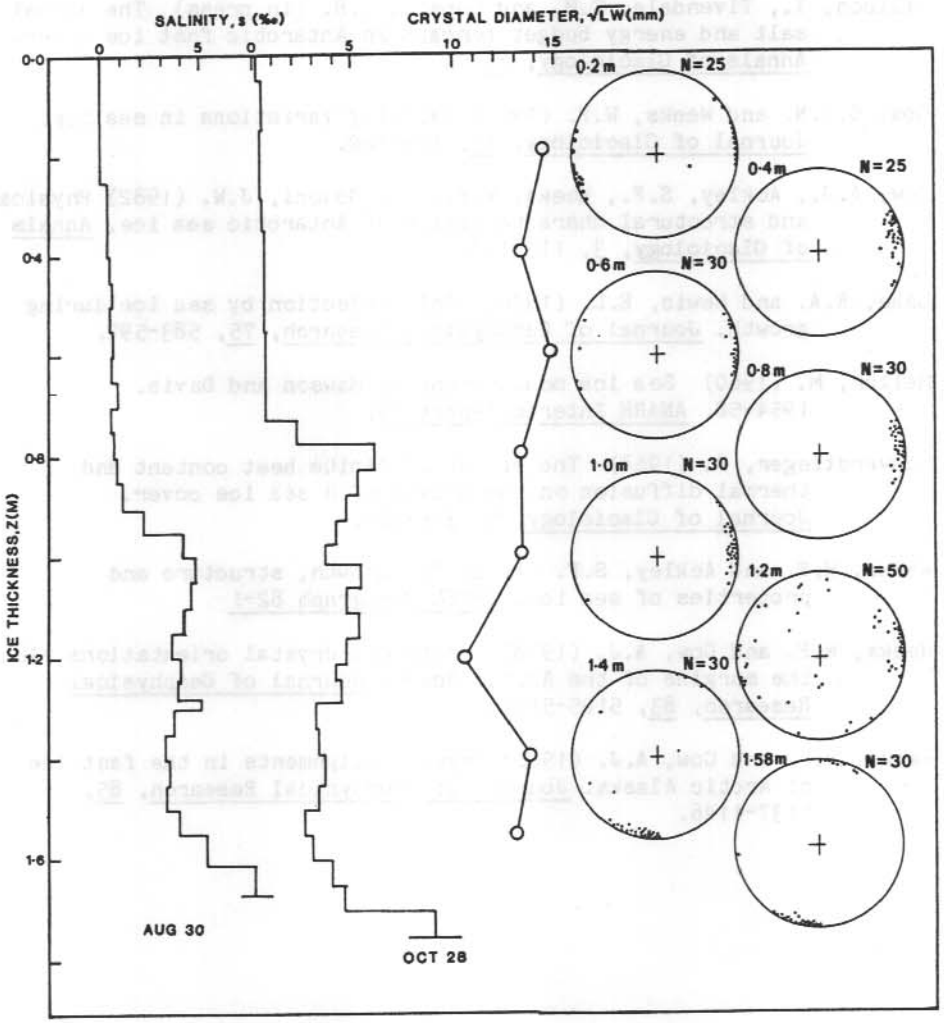

Figure 4. Characteristics of multiyear ice from O'Brien Bay. The c-axes fabric diagrams (right) show a strong preferred crystal alignment at most levels. The relative orientation of these fabric diagrams is random.

REFERENCES

Allison, I. (1981) Antarctic sea ice growth and oceanic heat flux. In: Allison, I. (Ed.). Sea level, Ice and Climate Change. IAHS Publication No. 131, 161-170.

Allison, I., Tivendale, C.M. and Copson, G.R. (in press) The annual salt and energy budget beneath an Antarctic fast ice cover. Annals of Glaciology, 6.

Cox, G.F.N. and Weeks, W.F. (1974) Salinity variations in sea ice. Journal of Glaciology, 13, 109-120.

Gow, A.J., Ackley, S.F., Weeks, W.F., and Govoni, J.W. (1982) Physical and structural characteristics of Antarctic sea ice. Annals of Glaciology, 3, 113-117.

Lake, R.A. and Lewis, E.L. (1970) Salt rejection by sea ice during growth. Journal of Geophysical Research, 75, 583-597.

Mellor, M. (1960) Sea ice measurement at Mawson and Davis. 1954-58. ANARE Interim Report 19.

Schwerdtfeger, P. (1964) The effect of finite heat content and thermal diffusion on the growth of a sea ice cover. Journal of Glaciology, 5, 315-324.

Weeks, W.F. and Ackley, S.F. (1982) The growth, structure and properties of sea ice. CRREL Monograph 82-1

Weeks, W.F. and Gow, A.J. (1978) Preferred crystal orientations along the margins of the Arctic Ocean. Journal of Geophysical Research, 83, 5105-5121.

Weeks, W.F. and Gow, A.J. (1980) Crystal alignments in the fast ice of Arctic Alaska. Journal of Geophysical Research, 85, 1137-1146.

8. SEA ICE OBSERVATIONS DURING ADBEX, 1982

N.A. Streten
Bureau of Meterology, Department of Science
Melbourne, Victoria, 3000.

D.J. Pike
Australian Numerical Meteorology Research Centre
Melbourne, Victoria, 3000.

ABSTRACT

During the ADBEX (Antarctic Division BIOMASS Experiment) cruise of November-December, 1982 a broadscale analysis of the extent and concentration of sea ice in the Prydz Bay region was made using shipboard and aerial observations in conjunction with USSR and US satellite data read out at Davis, Antarctica and on the relief vessel, Nella Dan. Further comparisons were made with coincident and longer term data derived from the NOAA-US Navy Joint Ice Centre (JIC) charts.

On the basis of the limited observations available for the expedition it appears that
(a) the "real" amount of ice is probably most accurately and confidently estimated by low level aerial observation;
(b) at high ice concentrations, shipboard observations may overestimate aerial observations by perhaps 1 to 2 tenths and satellite interpretation may further overestimate by up to 1 to 2 tenths;
(c) at low concentrations analyses of satellite imagery frequently do not accurately distinguish in the range from 0-2 tenths.
(d) there is probably less ice (or more open water) than is suggested by present long term satellite derived sea ice climatologies.

During the expedition period large Southern Ocean depressions moved in general, well to the north of the pack ice, but in the period from 19-26 November these lows approached and decayed just northward of the Prydz Bay region resulting in
(a) the compacting of ice in the region just west of the West Ice Shelf associated with N/NE winds on the eastern side of the lows; and
(b) weakened ice affected by the SW winds to the west of the depressions and observed on the southward approach by Nella Dan to Mawson.

Aerial photography from a fixed height of 300 m on 5 separate flights enabled a size distribution of floes to be determined showing over 40% to be less than 90 m^2 and approximately 15% greater than 360 m^2. Ice thickness and snow cover were roughly estimated by observation of floes upturned by the ship, the data indicating over 80% of floes were 1 m or less in thickness and that a similar percentage were covered with 0.2 m or less of snow. Wind and ice conditions apparently favourable for polynya formation were identified.

Satellite, aerial and shipboard observation of the sea ice for the period from 1 to 15 December enabled the mapping of sea ice

concentrations close to the continental edge and the identification of the shore polynya pattern. The pattern of four major polynyas in the region at that time was apparently related to
(a) the prevailing easterly winds in the region away from the immediate coast;
(b) the trend of the coastline;
(c) the location of the West and Amery Ice Shelves as a source of icebergs; and
(d) the location of the Fram, Storegg and other banks which act as filters on which icebergs are stranded to form an archipelago around which sea ice can form, be constrained, and often apparently survive for extended periods to form artificial coastlines.

An analysis was made of meteorological conditions encountered within the ice edge and a series of bucket derived sea surface temperature measurements within the Prydz Bay polynya indicated a "warm" core of water exceeding 2 ^{o}C, compared with water temperatures of less than 0 ^{o}C in the surrounding ice covered region.

9. UPDATING THE SEA ICE AND CLIMATE MONITORING PROGRAMS

T.H. Jacka
Antarctic Division, Department of Science
Kingston, Tasmania, 7150.

L. Christou and B.J. Cook
Meteorology Department, The University of Melbourne
Parkville, Victoria, 3052.

ABSTRACT

The 1983 Navy-NOAA Joint Ice Centre sea ice maps have been computer digitised. Sea ice extents are plotted along with data from previous years (Jacka, 1983), and anomalies noted.

Annual mean surface temperatures from most Antarctic and Southern Ocean stations have also been updated to 1983. These data are used to compile mean Southern Ocean and mean Antarctic temperature anomaly plots from which climatic trends are investigated.

9.1 THE 1983 SEA ICE ANALYSIS

Computer digitisation and analysis of the Joint Ice Centre Antarctic sea ice maps has been described by Jacka (1983), who also gave a description of mean sea ice distributions for the ten year period, 1973 to 1982.

Figure 1 shows the monthly ice limits for 1983 along with the 10 year mean curve. The 1983 sea ice extents were marginally lower than the mean, up until the maximum period. In November and December, 1983 there was marginally more sea ice than normal.

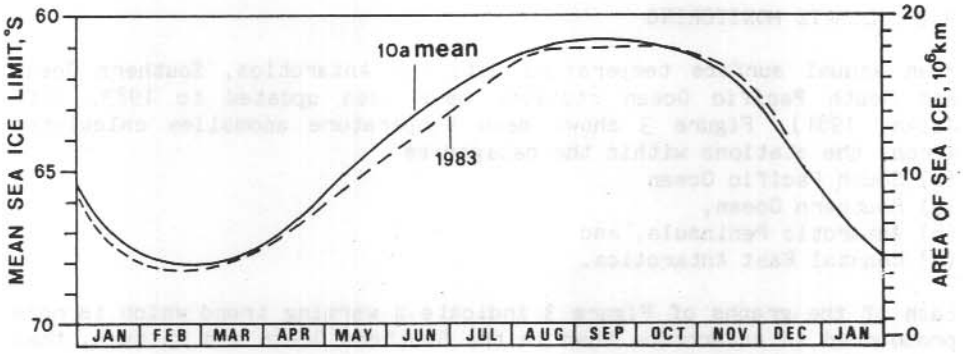

Figure 1. 10 a mean total sea ice extent (solid curve) and the 1983 ice extent (dashed curve).

The maximum ice extent was studied in further detail (Figure 2). The maximum occurred from late September to early October and in magnitude, was similar to the 10 year mean maximum extent.

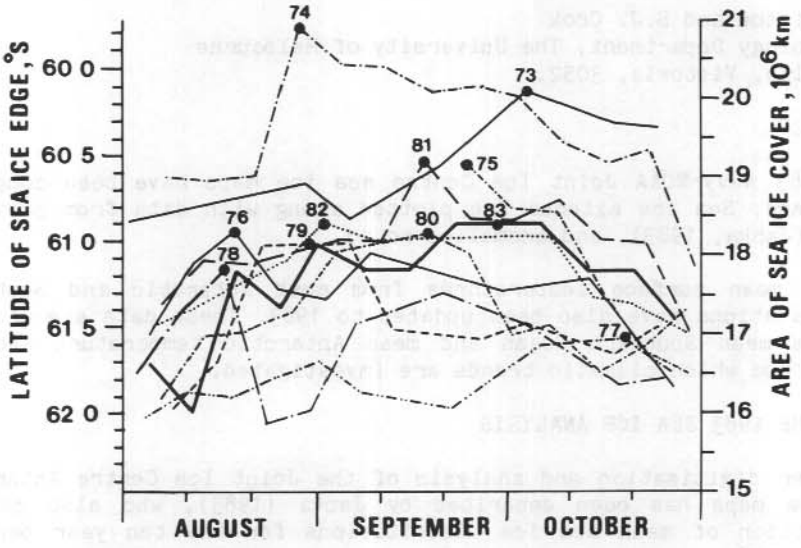

Figure 2. Total Antarctic sea ice extent for 1973-1983 for the period of maximum extent.

9.2 CLIMATE MONITORING

Mean annual surface temperature data for Antarctica, Southern Ocean and South Pacific Ocean stations have been updated to 1983. (cf: Jacka, 1981). Figure 3 shows mean temperature anomalies calculated across the stations within the catagories
(a) South Pacific Ocean
(b) Southern Ocean,
(c) Antarctic Peninsula, and
(d) Coastal East Antarctica.

Each of the graphs of Figure 3 indicate a warming trend which is more pronounced in Antarctica than in the Southern Ocean and in turn, than in the South Pacific Ocean.

On shorter time scales, it is seen that 1980 and 1981 were particularly warm years at coastal Antarctic stations, yet

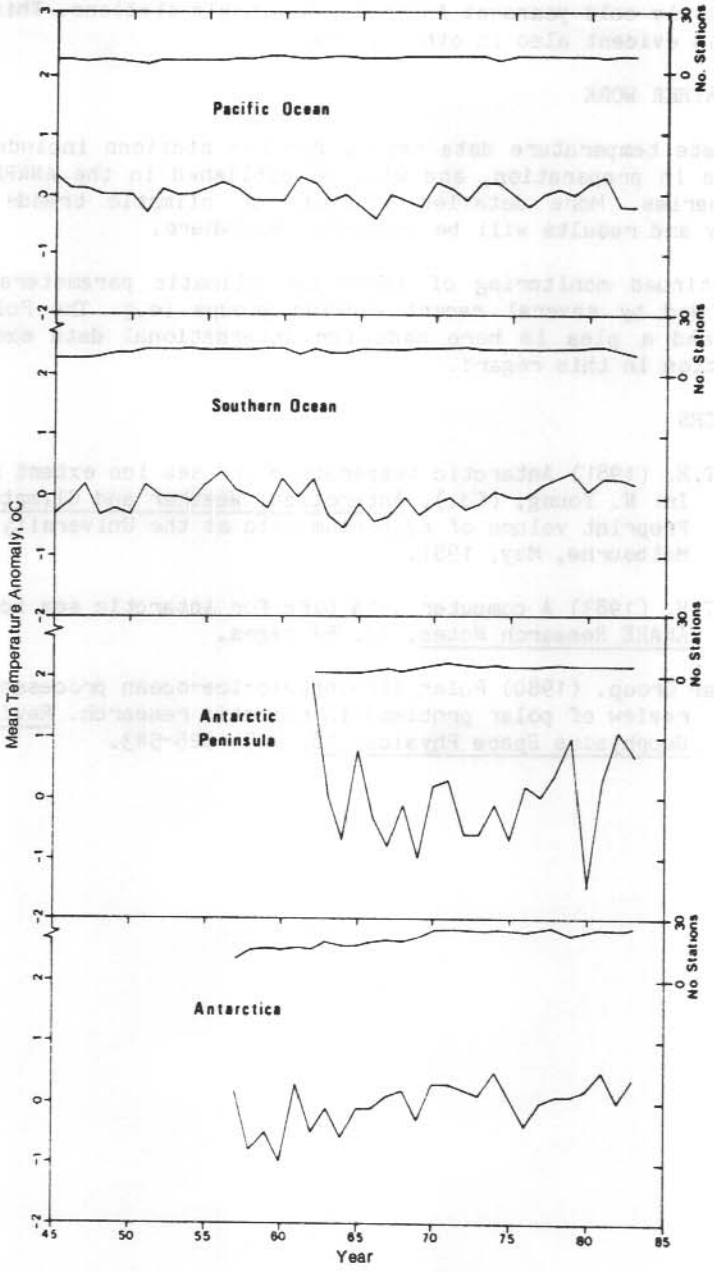

Figure 3. Temperature anomalies were calculated from full record means for each station, then averaged across the stations within the sectors (a) All Antarctica, (b) the Antarctic Peninsula (c) Southern Ocean, and (d) South Pacific Ocean. The number of stations used for each calculation is also shown.

particularly cold years at Antarctic Peninsula stations. This opposing effect is evident also in other years.

9.3 FURTHER WORK

A complete temperature data report for the stations included in this study is in preparation, and will be published in the ANARE Research Notes series. More detailed analysis of climatic trends are also underway and results will be presented elsewhere.

The continued monitoring of these two climatic parameters has been recommended by several recent working groups (e.g. The Polar Group, 1980), and a plea is here made for international data exchange and cooperation in this regard.

REFERENCES

Jacka, T.H. (1981) Antarctic temperature and sea ice extent studies. In: N. Young, (Ed.), Antarctica: Weather and Climate. Preprint volume of symposium held at the University of Melbourne, May, 1981.

Jacka, T.H. (1983) A computer data base for Antarctic sea ice extent. ANARE Research Notes, 13. 54 pages.

The Polar Group. (1980) Polar atmospheric-ice-ocean processes: A review of polar problems in climatic research. Reviews of Geophysics Space Physics, 18, (2), 525-543.

10. SEASONAL VARIATIONS IN WATER STRUCTURE UNDER ANTARCTIC SEA ICE

Ian Allison
Antarctic Division, Department of Science
Kingston, Tasmania, 7150.

ABSTRACT

Water salinity and temperature profiles, measured throughout the year under coast fast sea ice and in open water, are presented for a site near Mawson, Antarctica. These data are used to illustrate the role of sea ice in determining the structure of water on the Antarctic continental shelf. Not all features evident in the water structure at this site however are attributable to the cycle of ice growth and decay. Meltwater input from the continental ice sheet in summer, and ocean advection throughout the year are also important processes.

10.1 INTRODUCTION

The formation of a sea ice cover significantly changes the rate of turbulent and radiant energy exchange between the ocean and atmosphere, and hence influences the temperature structure in the water. During the growth of the ice cover brine is ejected from the ice and additional brine is added to the ocean as the ice salinity continues to decrease with time. This brine not only influences the structure of the near surface water but, because of its high density, causes instabilities which can result in deep haline convection, changing the structure of the whole water mass over the continental shelf.

Previous measurements of water temperature and salinity that have been made under a seasonal fast ice cover in the Antarctic have usually been limited to the winter period when the ice cover is stable (e.g. Bunt, 1960; Neal and Crew, 1976; Wakatsuchi, 1982). In this paper, data collected during the periods from October 1980 to February 1981 and from April 1982 to October 1982 are combined to show the development of the salinity and temperature structure over a full seasonal cycle. This includes a period of open water from the end of January to March as well as ice growth from March till October, and ice decay from November through to January.

10.2 OBSERVATIONAL SITE AND METHODS

The data presented were collected at a site in Kista Strait ($67^{o}36'S$, $63^{o}15'E$) about 1.5 km northwest of Mawson station. Water depths in the strait approach those found over the Antarctic continental shelf, generally being in excess of 350 m. However the Antarctic ice sheet terminates at ice cliffs 30 m above sea level only 1.5 km south of the hydrographic site and fresh water runoff from the ice sheet plays an important role in the hydrography of the region during summer.

In 1982 (when the measurements under a growing ice cover were made) the sea ice formed on March 23 and grew to a maximum thickness of 1.8 m at the end of October. During the 1980/81 sea ice season (when

the measurements were obtained under the decaying ice cover and in open water) the ice decreased in thickness from a maximum at the end of October to less than 0.7 m at the end of January when it was broken out by strong winds. The snow cover on the ice was generally less than 0.05 m thick during both years.

Water temperature and conductivity measurements were made with a thermistor (Seabird SBE-3) and conductivity cell (Seabird SBE-4) which were lowered either from a small vessel or through a hole in the ice. Digital signals from the sensors were fed sequentially up the hydrowire to a digital readout on the surface. Measurements could only be made at discrete depths: usually at every 5 to 10 m to a depth of 50 m and every 10 to 20 m interval from there to near the bottom. The measurements were made at periods ranging from every four days to once a month and the date of measurements is indicated on Figures 1 and 2.

Resolution of the sensors was better than 0.001 °C for temperature and 0.001‰ for salinity. Long term accuracy is however less than this,

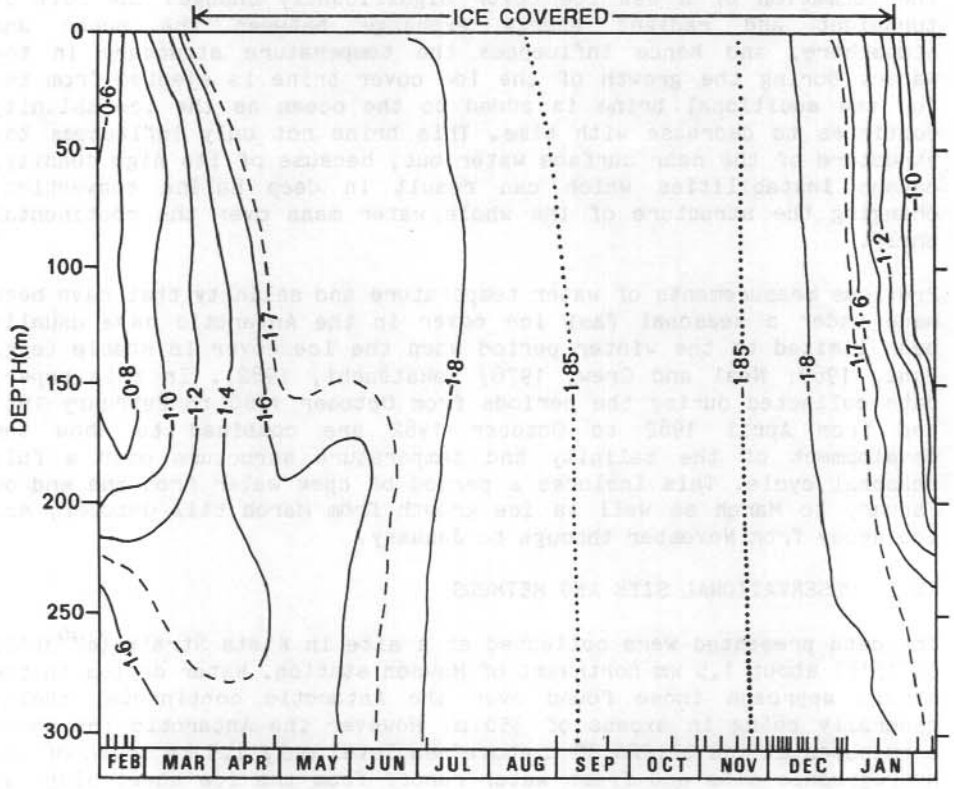

Figure 1. Isopleths of temperature (°C) at the Kista Strait site over a full season. The period of sea ice cover is indicated on the top of the graph, and the dates of measurements are indicated by tick marks along the lower axis.

although the thermistor calibration was regularly checked against an ice point and conductivity readings were compared against near-surface bottle samples measured in a laboratory salinometer. A number of comparative profiles were also measured in Kista Strait in February 1981 using a Neil Brown Mk III CTD system onboard Nella Dan. Overall the measurements are thought to be consistent to ±0.01 °C and ±0.02‰. Measured conductivities were converted to salinities using the method of Perkins and Lewis (1980).

Previous measurements of chlorinity and temperature were made at the Kista Strait site between July 1956 and January 1957 using reversing thermometers and Nansen bottle samples (Bunt, 1960). These were only made to 100 m depth and the reported results appear erroneous. Winter values of chlorinity as low as 9.00‰ (a salintiy of 16.3‰) are reported from 50 m depth, with much higher values at shallower depth which would give an unstable water column. The winter chlorinity values in general appear anomalously low probably due to nucleation of frazil ice in the sample by the cold metal bottle. The latent heat of

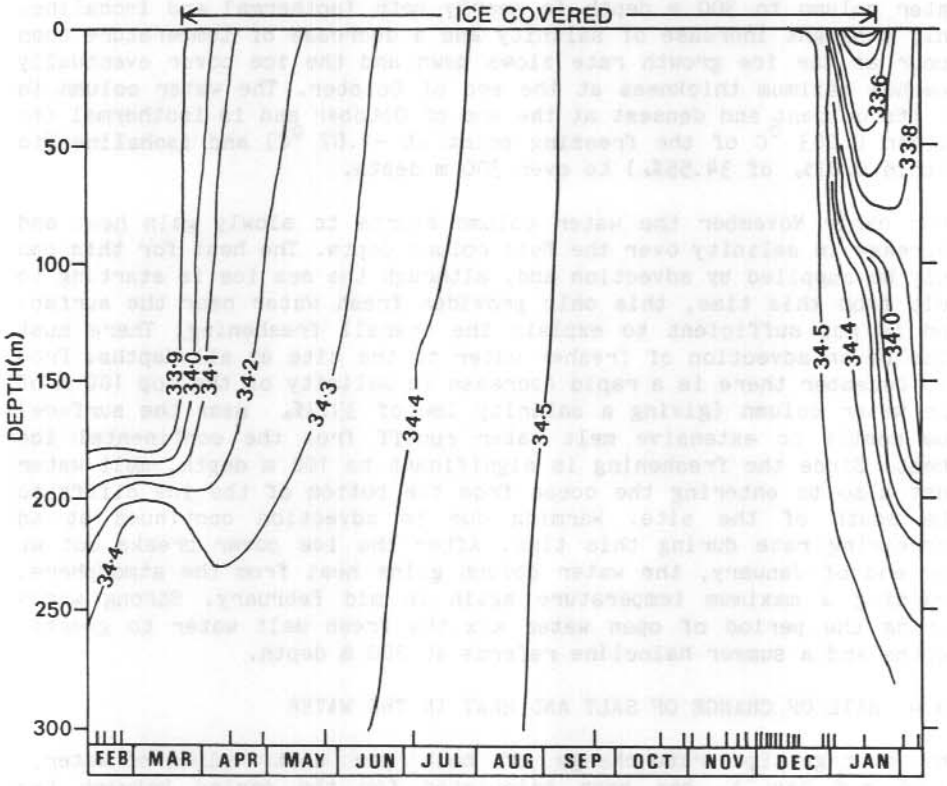

Figure 2. Isopleths of salinity (‰) at the Kista Strait site over a full season. The period of sea ice cover is indicated on the top of the graph, and the dates of measurements are indicated by tick marks along the lower axis.

formation of this frazil would also increase the measured temperature and none of the results of this earlier work are considered in this study.

10.3 SEASONAL VARIATIONS IN THE WATER TEMPERATURE

Profiles of salinity and temperature measured on 30 October 1980 and on 20 October 1982 were identical at all depths to better than 0.02‰ and 0.01 ^{o}C. Hence the data from the two years has been combined to give the variation over a full season. The seasonal variability of temperature and salinity are shown in the isopleths of Figure 1 and Figure 2 respectively.

In mid February the surface waters are at their warmest, with a strong halocline at about 200 m depth. This surface mixed layer cools rapidly in late February and March with little salinity change and a sea ice cover forms in late March. Brine ejected by the growing ice cover increases the overall salinity of the water and gradually deepens and weakens the halocline by convection so that by late June the whole water column to 300 m depth is nearly both isothermal and isohaline. Only a slight increase of salinity and a decrease of temperature then occur as the ice growth rate slows down and the ice cover eventually reaches maximum thickness at the end of October. The water column is at its coldest and densest at the end of October and is isothermal (to within 0.003 ^{o}C of the freezing point at -1.87 ^{o}C) and isohaline (to within 0.01‰ of 34.55‰) to over 300 m depth.

From early November the water column starts to slowly gain heat and decrease in salinity over the full column depth. The heat for this can only be supplied by advection and, although the sea ice is starting to melt from this time, this only provides fresh water near the surface and is not sufficient to explain the overall freshening. There must also be an advection of fresher water to the site at all depths. From mid December there is a rapid decrease in salinity of the top 100 m of the water column (giving a salinity low of 33.3‰ near the surface) due mostly to extensive melt water runoff from the continental ice sheet. Since the freshening is significant to 100 m depth, melt water must also be entering the ocean from the bottom of the ice cliffs to the south of the site. Warming due to advection continues at an increasing rate during this time. After the ice cover breaks out at the end of January, the water column gains heat from the atmosphere, reaching a maximum temperature again in mid February. Strong winds during the period of open water mix the fresh melt water to greater depths and a summer halocline reforms at 200 m depth.

10.4 RATE OF CHANGE OF SALT AND HEAT IN THE WATER

The average time rate change of heat per unit volume of water, H (J m^{-3} day^{-1}), has been calculated for the period between two measured temperature profiles as

$$H = (\rho Cp \int_{Z_1}^{Z_2} (T_b - T_a)\, dZ) / [(Z_2 - Z_1)(b-a)]$$

where ρ is the density of the water = 1027.6 kg m^{-3}, Cp is the specific heat (at -2°C, 35‰) = 3.984 kJ kg^{-1} $°C^{-1}$, Z_2 and Z_1, are the depths between which the heat change is averaged and T_a and T_b are the temperature profiles (°C) measured on days number b and a respectively.

Similarly the average time rate change of salt per unit volume, S (gm m^{-3} day^{-1}), is given by

$$S = \rho \int_{Z_1}^{Z_2} (S_b - S_a)\, dZ \;/\; [(Z_2 - Z_1)(b-a)]$$

where S_b and S_a are the salinity profiles (‰) measured on days number b and a respectively.

The rates of change of heat and salt per unit volume for two layers from 2 to 100 m depth, and from 100 to 250 m depth, are shown as functions of time in Figure 3 and further illustrate the seasonal changes under the ice cover.

From mid February until ice formation the uppermost layers (2 - 100 m) lose considerable heat to the atmosphere but there is little change in salt content. The lower layer (100 - 250 m) also loses heat as the total summer mixed layer extends to 200 m depth. As soon as the ice cover forms, the rate of heat loss drops significantly. Initially the upper layer is cooled more quickly by conduction through the ice cover, but as its temperature approaches the freezing point and as the haline convection extends more deeply, the lower layer loses heat more rapidly due to exchange with the upper layer. Salt ejected from the growing ice cover increases the salinity of both layers, although the increase is greatest at first near the top. The salinity changes in the two layers becomes nearly equal from July, as the convection extends to the bottom, and the rate of salinity change decreases as the ice growth slows. There is no change in either heat or salt near the time of maximum thickness.

From November there is a warming of both layers due to advection throughout the column. The warming at the top reaches a maximum immediately after ice breakout when the water gains heat from the atmosphere. The peak of meltwater input in the top 100 m is seen in late December to early January. Wind mixing of this fresh water after breakout shows as an effective salt increase in the upper layer and as a decrease between 100 and 250 m depth.

10.5 CONCLUSION

The role of winter sea ice growth in determining ocean salinity and temperature is clearly illustrated by the data presented. In particular, brine ejection from the ice causes haline convection which extends to 300 m depth, producing a homogeneous water mass by the time of maximum ice thickness. However not all features observed in the water structure are attributable to ice growth. Fresh water drainage from the continental ice sheet in summmer and ocean advection

throughout the year, are important processes at this site. The relative magnitude of these various processes in determining the salt and energy budget of the site are further discussed by Allison and others (in press).

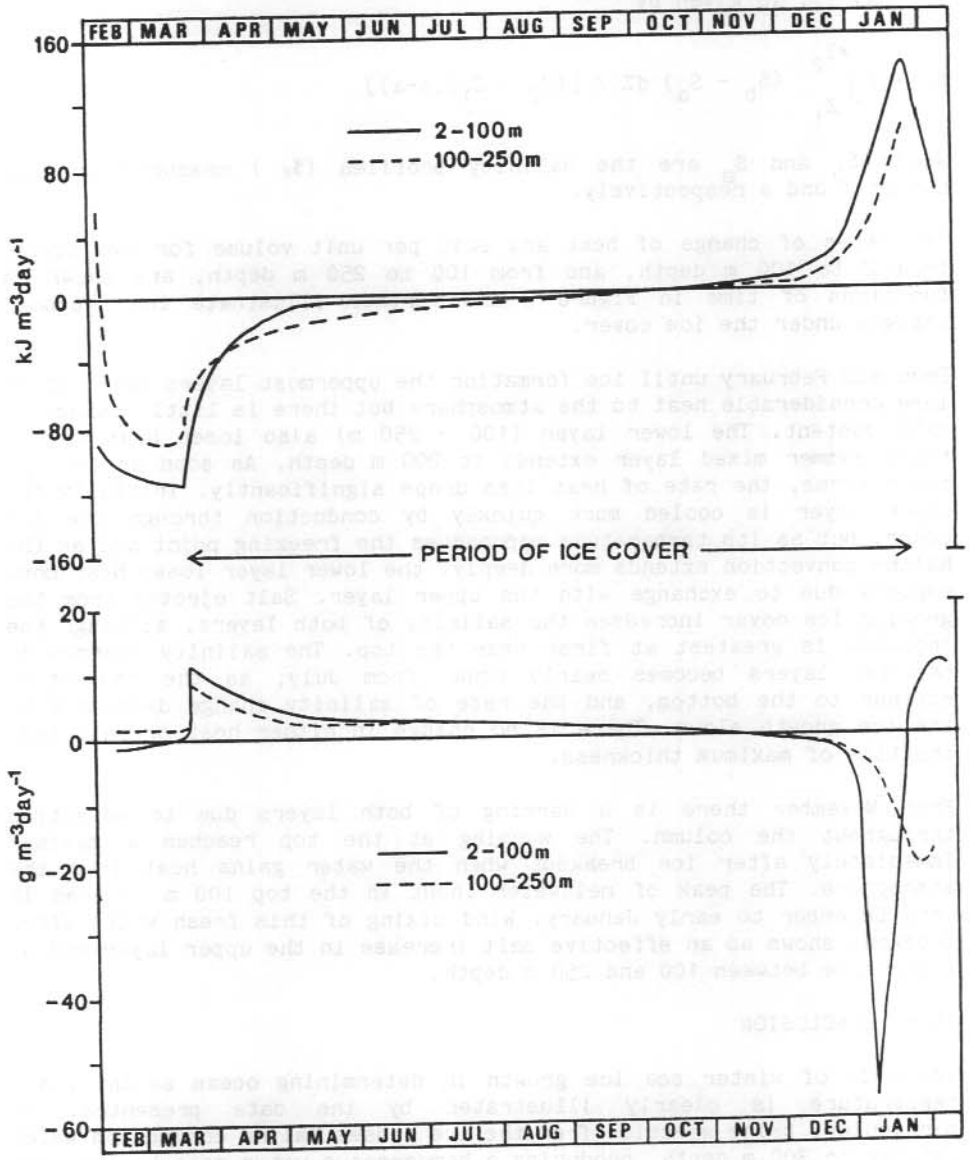

Figure 3. Rate of change of heat (top) and of salt (bottom) per cubic metre of water for two different depth intervals (2 to 100 m and 100 to 250 m) over a season.

It should be noted that the heat flux from the ocean to the ice has previously been observed to have a high value near this site (Allison, 1981). The oceanic flux varies with time, having one maximum when the ice growth rate (and hence haline convection) is greatest, and a second maximum after October when the present data indicates increased ocean advection of heat to the site.

ACKNOWLEDGMENTS

The raw data used in this study were collected in 1980/81 by Charles Tivendale and in 1982 by Geof Copson. Both are gratefully thanked for perservering in often very difficult field conditions.

REFERENCES

Allison, I. (1981) Antartic sea ice growth and oceanic heat flux. In: Allison, I. (Ed.). Sea level, Ice and Climate Change. IAHS Publication 131, 161-170.

Allison, I., Tivendale, C.M. and Copson, G.R. (in press) The annual salt and energy budget beneath an Antarctic fast ice cover. Annals of Glaciology, 6.

Bunt, J.S. (1960) Introductory studies: hydrology and plankton, Mawson, June, 1956 - February, 1957. ANARE Reports, Series B, 3, (56).

Neal, V.T. and Crew, H. (1976) Oceanographic measurements under winter sea ice in McMurdo Sound. Antarctic Journal of the United States, 11, 235-239.

Perkins, R.G. and Lewis, E.L. (1980) The practical salinity scale 1978; fitting the data. IEEE J. Oceanic Engineering, OE-5 (1), 9-16.

Wakatsuchi, M. (1982) Seasonal variations in water structure under fast ice near Syowa station, Antarctica, in 1976. Antarctic Record, 74, 85-108.

11. OBSERVATIONS OF WATER MASS MODIFICATION IN THE VICINITY OF AN ICEBERG

Ian Allison, Knowles Kerry and Simon Wright
Antarctic Division, Department of Science
Kingston, Tasmania, 7150.

ABSTRACT

Measurements of water salinity and temperature profiles to 500 m depth were made at various close distances around two icebergs during Antarctic Division marine science cruises in 1981/82 and 1982/83. Evidence of modification of the near surface water was found several hundreds of metres from both icebergs.

The T-S relationship of water around the first iceberg, which was in circumpolar deep water, suggests that convection alongside the iceberg is responsible for some of the observed changes, and that melt is occurring at considerable depth. The convection also decreases the depth of the pycnocline close to the iceberg.

In contrast, the second iceberg, which was in cold shelf water, was melting only at depths above the seasonal halocline. There was no deep convection alongside the iceberg and the T-S relationship of the near surface water around the iceberg can be explained simply in terms of mixing of the melt with the initial sea water above the halocline. In this case the pycnocline is deepened and strengthened by the addition of the iceberg melt.

Other water characteristics that appear to be associated with the iceberg were observed around the second iceberg. Water of a different characteristic than the bulk of the column is found at depths from 200 to 350 m around and behind the iceberg, but not in front. This may be associated with entrainment of a water mass by the iceberg. Close to the iceberg there is a layer with high acoustic reflectivity at about 50 m depth, which is not found away from the iceberg. This also suggests modification of the surface water around the iceberg.

11.1 INTRODUCTION

More than 10^{12} tonnes of fresh water, mostly in the form of icebergs, are discharged annually from the Antarctic ice sheet into the Southern ocean. A number of these icebergs may reach middle latitudes and melt in relatively warm waters, but the vast majority are trapped in the circumpolar current where they deteriorate and eventually melt at temperatures near the freezing point (e.g. Budd and others, 1980). Hence, while the melting of icebergs in warm water is relevant to studies of the feasibility of iceberg towing, the melt of ice in cold water, and the resultant modification of the water, is of more importance oceanographically.

When ice melts in sea water, it both cools the surrounding water (which increases its density) and freshens it (which decreases the density). Both laboratory and theoretical studies indicate that the

melt of the iceberg can drive vertical convection adjacent to the iceberg, and this results not only in modification of the water mass but can also cause upwelling of nutrient-rich deep water (Neshyba, 1977). Because of the opposing effects of cooling and dilution, the buoyancy processes are complex and highly dependent on the salinity and temperature structure of the ocean. Huppert and Josberger (1980) undertook laboratory studies of ice melting in cold water (+1.8 ^{o}C to 4.9 ^{o}C) which was highly stratified (a salinity gradient of 10‰ m^{-1}), and showed that under these circumstances the melt resulted in convection in a series of small scale horizontal cells which gave a step-like vertical density structure. However the scaling of these laboratory experiments to the open ocean is contentious because of the widely different salinity gradient and stability found there.

Field observations around icebergs are scarce. Josberger and Neshyba (1981) measured temperature profiles around a grounded iceberg off Newfoundland. The water at a distance from this iceberg, was isothermal at -1 ^{o}C below the pycnocline (40 m depth) and increased to +6 ^{o}C at the surface. Closer to the iceberg the water above the pycnocline depth showed an overall cooling of 1 ^{o}C. This large cooling was interpreted as being in part due to advection of cold deep water by convection resulting from melt of the iceberg. Jacobs and others (1981) measured salinity and temperature profiles close to the floating Erebus Glacier tongue and observed a step-like structure with a vertical scale of 30 m in both the temperature and salinity. While analogous to the structure suggested by the laboratory results of Huppert and Josberger (1980) the vertical scale was approximately double that predicted.

The data presented in this paper were collected during marine science cruises conducted by the Antarctic Division in 1980/81 and 1982/83. The iceberg observed during the 1980/81 First International BIOMASS Experiment will be referred to here as the FIBEX iceberg, and that observed during the 1982/83 Antarctic Division BIOMASS Experiment, as the ADBEX iceberg. All temperature and salinity measurements were made with a Neil Brown Mark III CTD system onboard MV Nella Dan. The size of the ship and the fact that the icebergs were free floating limited the closeness of approach to the icebergs.

11.2 THE FIBEX ICEBERG

Observations around this iceberg, at 65^{o}18.3'S, 81^{o}29.8'E were made on 22 January 1981. The iceberg was relatively small (about 280 m long), and irregularly shaped, with a freeboard of 25 m and estimated draft of about 200 m. The pycnocline in the surrounding water was at about 40 m depth and the temperature above this increased from about +0.5 ^{o}C to +0.9 ^{o}C. Below the pycnocline the temperature decreased to about -1.5 ^{o}C between 50 and 100 m and then increased to +1.7 ^{o}C at 200 m (see inset to Figure 1). The deep water had the typical temperature and salinity characteristics of Circumpolar Deep Water (CDW), which originates as warm salty subantarctic abyssal water.

Four CTD casts were made on the lee side of the iceberg at distances from the iceberg of 50 m (cast 6B), 100 m (6A), 250 m (6C) and 1000 m

(7). Casts 6A to 6C were made to 400 m depth, and cast 7 to 1000 m. The observed profiles of salinity and temperature in the upper 100 m are shown in Figure 1.

Above the pycnocline the water close to the iceberg is cooled by generally less than 0.2 °C and shows a slight decrease of salinity. Both these effects are consistent with melting. There is also a systematic decrease in pycnocline depth from about 40 to 30 m as the iceberg is approached. This raising of the pycnocline further reduces the total heat content of the surface water adjacent to the iceberg,

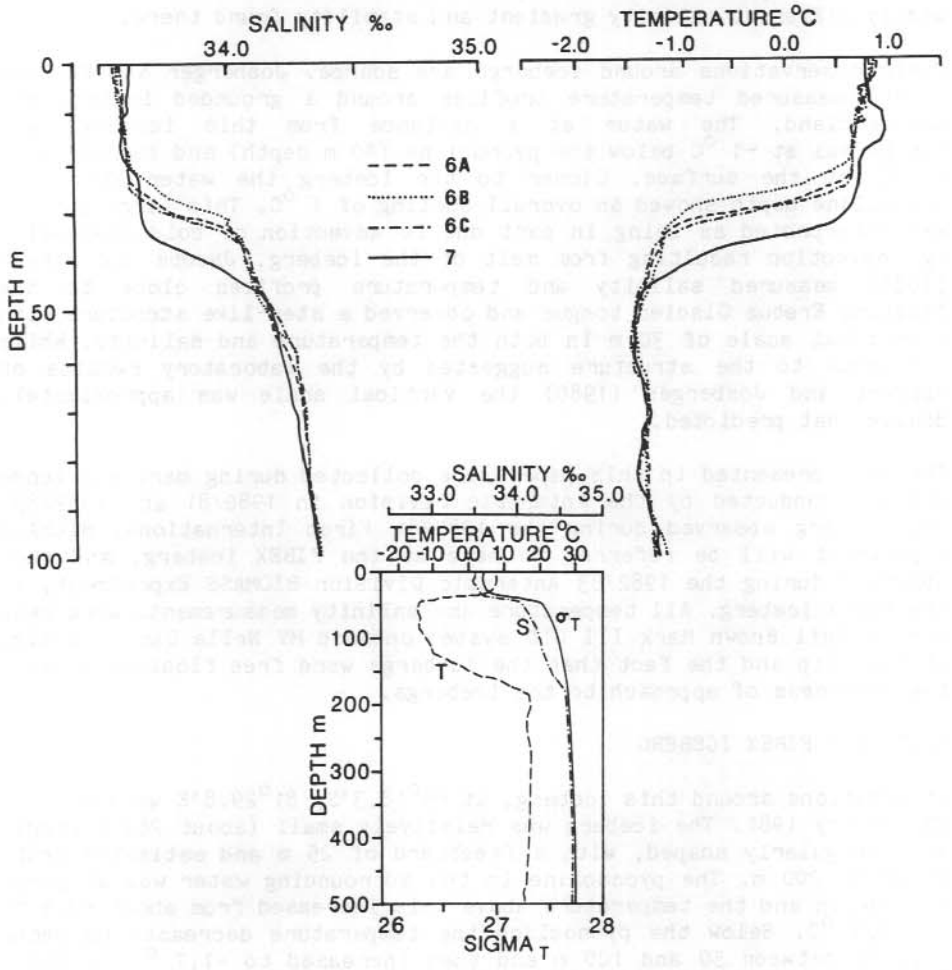

Figure 1. Ocean salinity and temperature profiles of the surface 100 m of water near the FIBEX iceberg. Cast 6B is 50 m from the iceberg, 6A is 100 m, 6C is 250 m and 7 is more than 1000 m away. The inset (bottom right) shows the water characteristics to 500 m depth at station 7.

and increases the salt content. There is no significant difference in the four profiles between 50 and 100 m depth. There is some slight suggestion of a layered structure, with a vertical scale less than 10 m, in the top of cast 6C, but not in the closer profiles.

11.3 THE ADBEX ICEBERG

Observations around this iceberg, initially at $67^{o}32.5'S$, $74^{o}40.2'E$, were made on 16 December 1982. The iceberg, which was tilted and rounded, was about 320 m long, 140 m wide, had a freeboard of 23 m and an estimated draft of about 180 m. The iceberg drifted a total distance of 6.8 km towards the south-west in 27 hours (0.07 ms^{-1}). Windspeeds during this time were 3 ms^{-1} or less from the south-east. The iceberg was over the continental shelf in Prydz Bay and the surrounding water showed a strong halocline and thermocline at less than 20 m depth (inset to Figure 3). The water above the pycnocline depth had a temperature of +1.5 ^{o}C while below it was generally isothermal and at the freezing point (-1.87 ^{o}C). The relatively fresh layer over a strong seasonal halocline is typical of the summer surface water (AASW) found over the continental shelf.

Ten CTD casts (number 66 to 75) were made around the iceberg, generally to a depth of 500 m. The location of the casts relative to the iceberg is shown in Figure 2. The profiles of salinity and temperature in the top 100 m are shown in Figure 3. Figure 3(a) shows data from a number of casts along a line approximately following the iceberg movement while Figure 3(b) shows select casts across the iceberg in the wind direction.

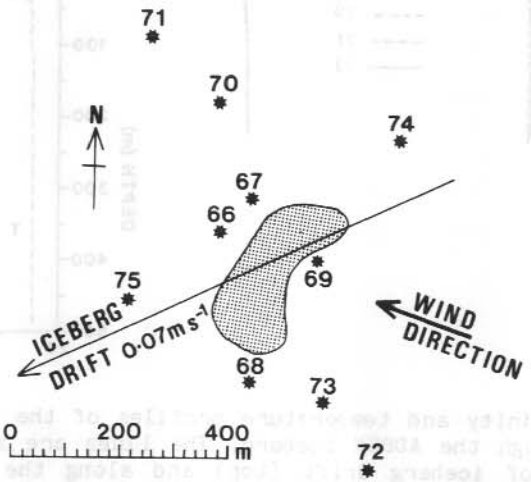

Figure 2. Location of casts around the ADBEX iceberg.

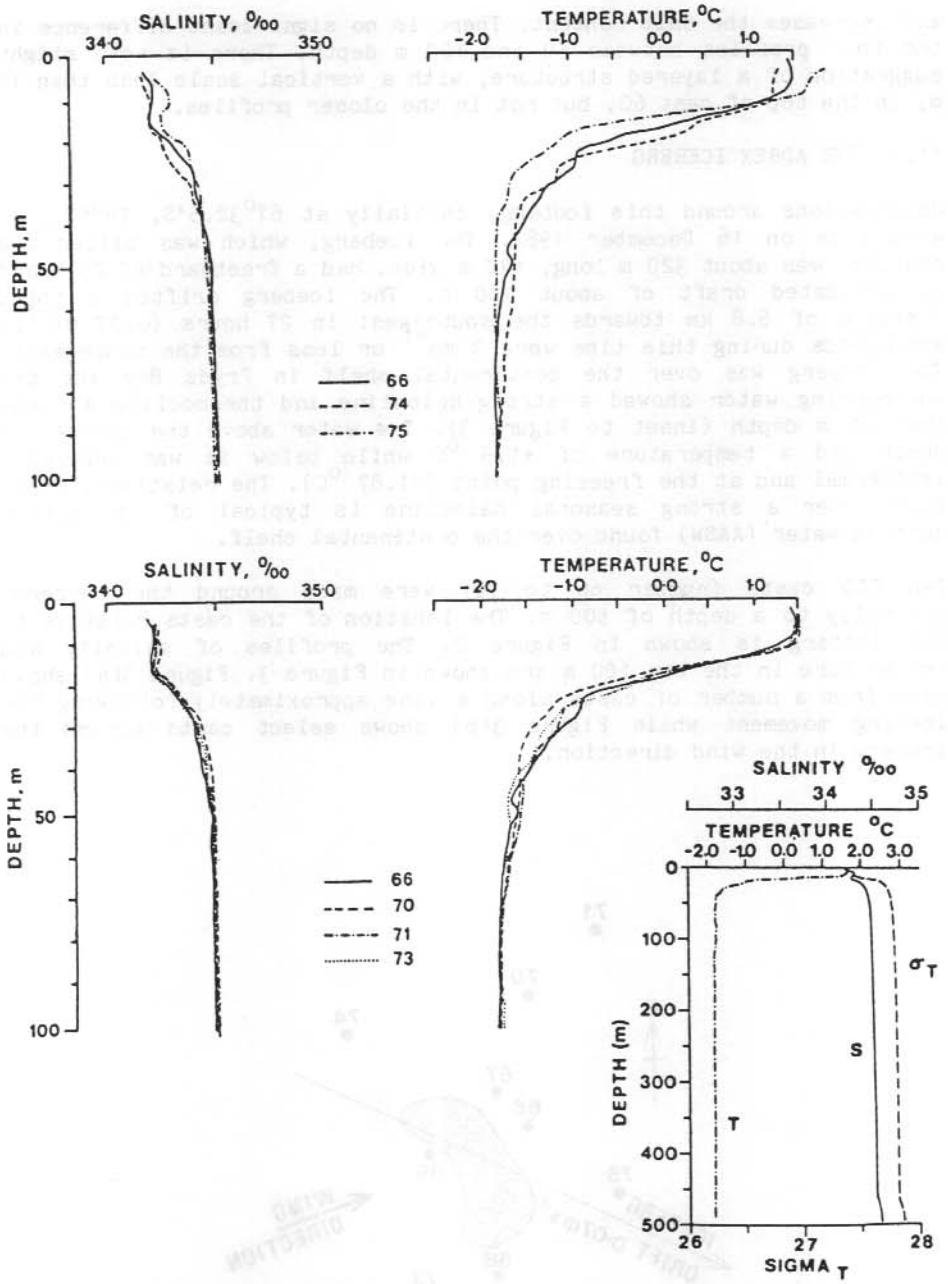

Figure 3. Salinity and temperature profiles of the top 100 m along two lines through the ADBEX iceberg. The lines are approximately in the direction of iceberg drift (top) and along the wind direction (bottom). See Figure 2 for the location of the casts. The inset (bottom right) shows water characteristics to 500 m depth at station 75.

From Figure 3(a) the temperature of the surface water decreases and the salinity increases systematically from a point downstream (cast 75, where the iceberg has not yet passed), to a point alongside the iceberg (cast 66), and then to a point upstream (cast 74, where the iceberg passed by a few hours earlier). The iceberg appears to be moving relative to the instantaneous surface current. At the same time the pycnocline depth is deepened (by about 5 m) as the iceberg passes. This contrasts with the situation found around the FIBEX iceberg, where the pycnocline sloped upwards towards the iceberg. There are no significant changes from below the pycnocline to 100 m depth.

The observations along the wind direction show no significant change with distance from the iceberg. The casts show progress from 250 m on the windward side to 320 m on the lee side of the iceberg.

There is no evidence of a layered structure in the upper parts of any profile.

11.4 DISCUSSION

Gade (1979) has shown that there is a linear relationship between salinity and temperature change when ice melts in sea water. For ice at an internal temperature T_i melting in sea water of temperature T_w and salinity S,

$$\delta T/\delta S = [T_w - T_f + (T_f - T_i)\, C_i/C_w + L/C_w\,]/S$$

where T_f is the freezing point of seawater of salinity S,
C_i is the thermal conductivity of the ice,
C_w is the thermal conductivity of the water and
L_w is the latent heat of ice at T_f.

While we do not know the internal temperatures of the icebergs we can expect them to be well below zero. The mean annual temperature at both sites is below zero, there is little heating from the surface, and heating from the ocean produces melt, rather than warming the iceberg. Hence icebergs remaining in Antarctic waters can be expected to maintain cold core temperatures for decades. Orheim (1980) estimates the core temperature of an iceberg in the Weddell Sea from near surface temperature measurements as about -17 ^{o}C.

In Figure 4 we show the T-S relationship at 10 m depth for casts at varying distances from the FIBEX and ADBEX icebergs. Also shown are the T-S relationships for the melt/sea water mix as derived by Gade (1979). For an iceberg at -10 ^{o}C and at -20 ^{o}C, we have used values of C_i = 2.09 kJ kg^{-1} ^{o}C^{-1}, C_w = 3.99 kJ kg^{-1} ^{o}C^{-1}, L = 330 kJ kg^{-1}, T_f = - 1.83 ^{o}C for the FIBEX iceberg, and T_f = -1.87 ^{o}C for the ADBEX iceberg. At an ice temperature of -20 ^{o}C, $\delta T/\delta S$ = 2.83 for the FIBEX iceberg and 2.79 for the ADBEX iceberg.

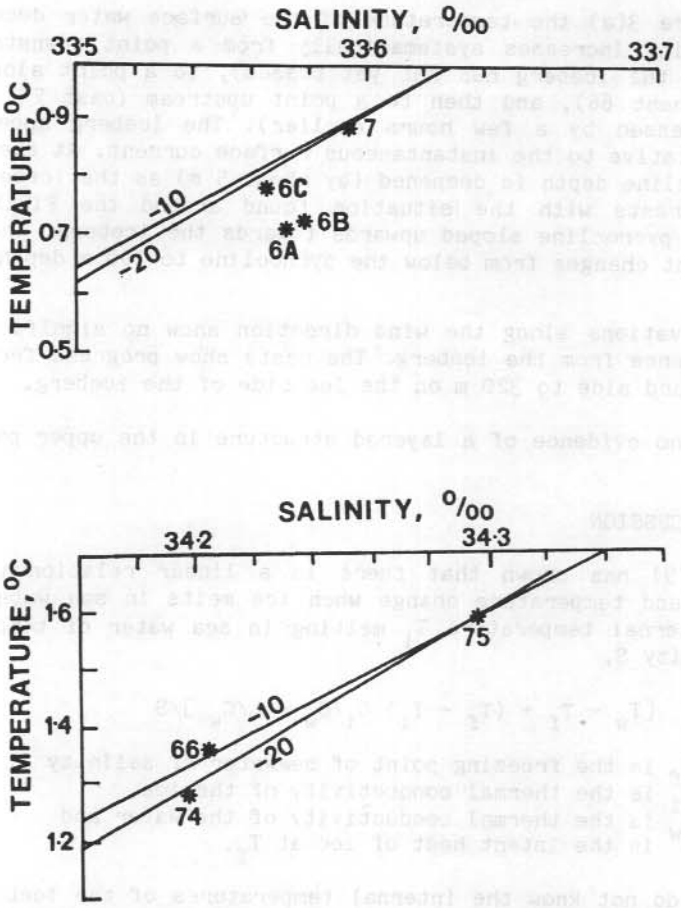

Figure 4. Temperature-salinity relationships for water at 10 m depth from selected casts around the FIBEX (top) and ADBEX (bottom) icebergs. The continuous lines are the predicted T-S relationships for melt from an iceberg at -10 °C and -20 °C.

For the FIBEX iceberg, the near surface water 250 m from the iceberg (cast 6C) has characteristics approximating those expected for simple melt. The closer casts however show water that is saltier than would be expected from a mix of melt and sea water at this level. We interpret this difference as being due to convection near the sides of the iceberg which is bringing saltier water from depth to the surface. This convection would also lead to the observed decrease in the pycnocline depth near the iceberg. In contrast, the water at 10 m depth around the ADBEX iceberg fits the predicted T-S relationship and is therefore derived solely from melt of the iceberg near the surface, with no contribution due to convection from the deeper water. This addition of melt at the surface strengthens and deepens the pycnocline, as was observed.

The difference between the two icebergs is a result of the different water masses they are in. The water temperature around the FIBEX iceberg is always greater than -1.5 ^{o}C and increases to +1.7 ^{o}C near the base of the iceberg. Hence we can expect significant melt at all depths. Around the ADBEX iceberg, however, the water temperature below the pycnocline is close to melting point. There will be negligible ice melt at depth, and no convection.

11.5 OTHER OBSERVED PHENOMENA ASSOCIATED WITH THE ADBEX ICEBERG

Two other phenomena, possibly associated with the ADBEX iceberg were observed. The first of these was the variation in salinity and temperature noted at a depth between 200 and 350 m. Cast 75, downstream of the iceberg, does not show this but cast 66, only 60 m from the iceberg shows a significant change at these levels (Figure 5). All casts upstream of the iceberg show a similar change, with a magnitude roughly proportional to the distance from the iceberg. For example, cast 74 (180 m from the iceberg) shows a much smaller change in salinity and temperature between 200 and 350 m than cast 66. This modified water, which is at a depth below the iceberg, cannot be derived from ice melt, and the T-S relationship for these casts shows that it has characteristics very similar to those of circumpolar deep water (Figure 6). As a preliminary hypothesis we suggest that this water may be a column of CDW entrained by and moving with, the iceberg. No mechanism for this process is suggested.

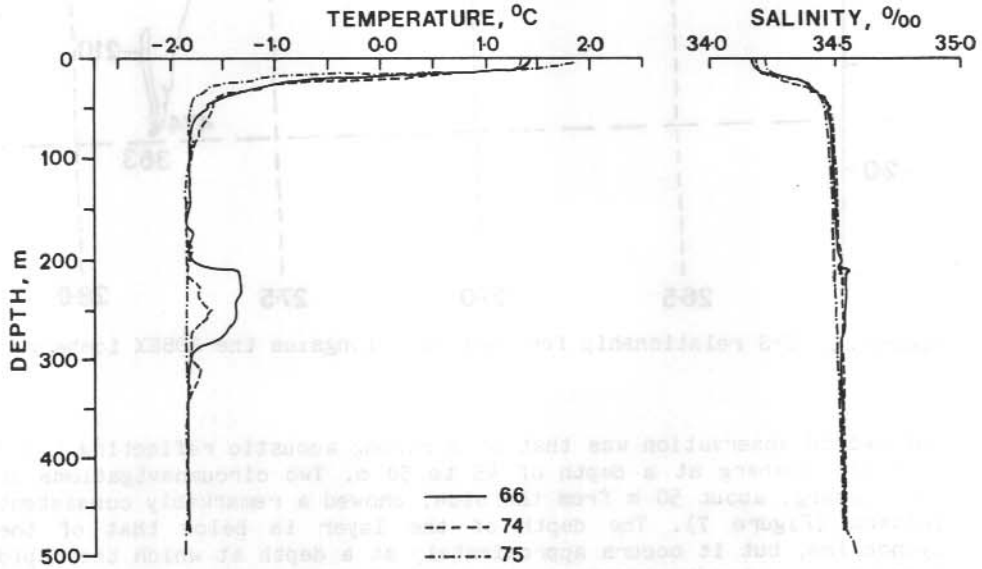

Figure 5. Salinity and temperature profiles to 500 m for casts around the ADBEX iceberg. Cast 66 is 50 m from the side of the iceberg, 74 is 160 m behind, and 75 is 200 m in front.

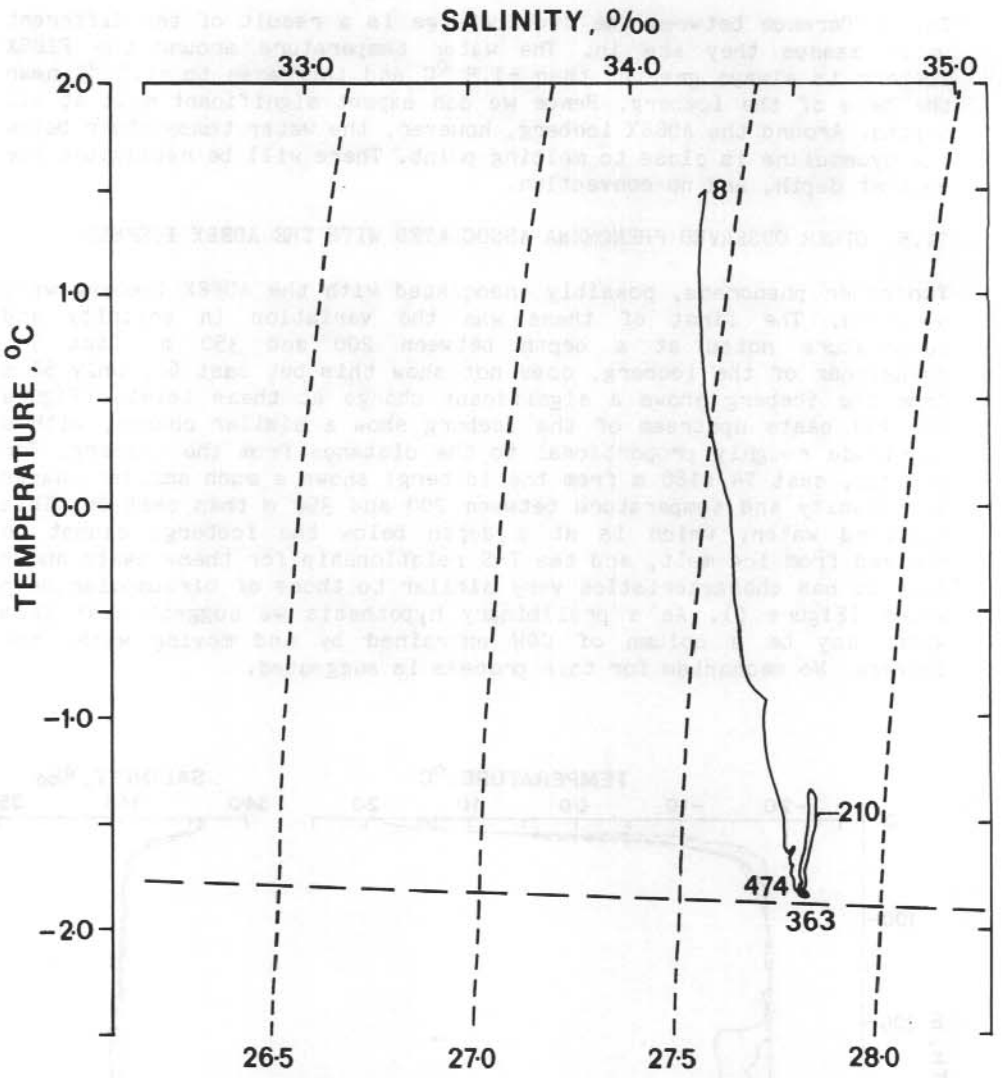

Figure 6. T-S relationship for cast 66, alongside the ADBEX iceberg.

The second observation was that of a strong acoustic reflecting layer near the iceberg at a depth of 45 to 50 m. Two circumnavigations of the iceberg, about 50 m from the side, showed a remarkably consistent pattern (Figure 7). The depth of the layer is below that of the pycnocline, but it occurs approximately at a depth at which the rapid decrease in water temperature with depth finishes, at which point the water is within 0.2 °C of the freezing point. The strong acoustic reflecting layer is not found further from the iceberg and is probably also a result of the ice melt. One possible, but unconfirmed cause, is the presence of frazil ice in the water at this depth.

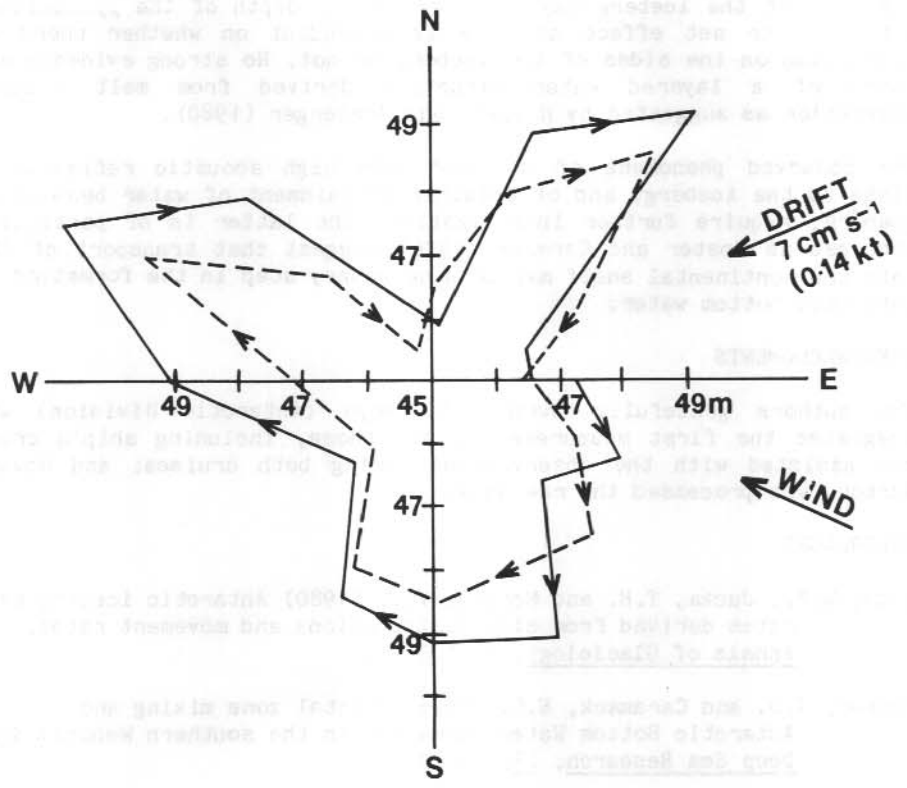

Figure 7. Depth of the layer with high acoustic reflectivity measured on two passes around the ADBEX iceberg at a distance of about 50 m from the walls.

11.6 CONCLUSIONS

The reported observations show that the effect of melting icebergs, even in cold water, can be detected in the salinity and temperature profiles at distances of several hundred metres from the iceberg. Icebergs over the continental shelf will only melt significantly during the summer months and only to a depth of the seasonal thermocline. However icebergs further north, in circumpolar deep water, can melt on the sides at all depths and their modification of the surface ocean water is partly determined by melt induced convection.

The melt of the iceberg may also modify the depth of the pycnocline, although the net effect of this is dependent on whether there is convection on the sides of the iceberg or not. No strong evidence was found of a layered water structure derived from melt induced convection as suggested by Huppert and Josberger (1980).

The observed phenomena of a layer with high acoustic reflectivity close to the iceberg, and of possible entrainment of water beneath an iceberg, require further investigation. The latter is of particular interest as Foster and Carmack (1976) suggest that transport of CDW onto the continental shelf may be a necessary step in the formation of Antarctic bottom water.

ACKNOWLEDGMENTS

The authors gratefully thank J.S. Boyd (Antarctic Division) who suggested the first measurements; all those, including ship's crew, who assisted with the observations during both cruises; and Howard Burton, who processed the raw data.

REFERENCES

Budd, W.F., Jacka, T.H. and Morgan, V.I. (1980) Antarctic iceberg melt rates derived from size distributions and movement rates. Annals of Glaciology, 1, 103-112.

Foster, T.D. and Caramack, E.C. (1976) Frontal zone mixing and Antarctic Bottom Water formation in the southern Weddell Sea. Deep Sea Research, 23, 301-317.

Gade, H.G. (1979) Melting of ice in sea water: a primitive model with application to the Antarctic ice shelf and icebergs. Journal of Physical Oceanography, 9, 189-198.

Huppert, H.E. and Josberger, E.G. (1980) The melting of ice in cold stratified water. Journal of Physical Oceanography, 10, 953-960.

Jacobs, S.S., Huppert, H.E., Holdsworth, H. and Drewry, D.J. (1981) Thermohaline step induced by melting of the Erebus Glacier tongue. Journal of Geophysical Research, 86, 6547-6555.

Josberger, E.G. and Neshyba, S. (1981) Iceberg melt driven convection inferred from field measurements of temperature. Annals of Glaciology, 1, 113-117.

Neshyba, S. (1977) Upwelling by icebergs. Nature, 267, 507-508.

Orheim, O. (1980) Physical characteristics and life expectancy of tabular Antarctic icebergs. Annals of Glaciology, 1, 11-18.

12. DIURNAL VARIABILITY OF THE SURFACE WIND AND AIR TEMPERATURE AT AN INLAND ANTARCTIC SITE: 2 YEARS OF AWS DATA

Ian Allison
Antarctic Division, Department of Science
Kingston, Tasmania, 7150.

ABSTRACT

Two years of data from an automatic weather station (AWS) have been analysed to show diurnal variability of surface air temperature, temperature gradient (1 to 2 m and 2 to 4 m above the surface), wind speed and wind direction. All elements show a large diurnal variability in summer, no variability in winter, and an identical transition situation for autumn and spring.

In summer a wind speed minimum occurs at approximately 2000 hour local solar time, considerably after the maximum temperature, minimum inversion strength, and most easterly wind direction at 1400-1600 LST. The phase difference between the wind speed and wind direction variations gives an anticlockwise cyclic variation in the total wind vector (as shown by the diurnal hodograph). There is also some evidence for a similar variation in the mean seasonal wind vector.

During winter there is a constant temperature inversion and near logarithmic potential temperature profile (about 0.15 ^{o}C temperature difference from 1 to 2 m and from 2 to 4 m). During the nocturnal hours in summer, the temperature profile shows a much stronger inversion from 1 to 2 m (0.35 ^{o}C mean temperature difference) than from 2 to 4 m, but this breaks down during daytime and the profile becomes logarithmic and near neutral. In spring and autumn, which show identical profiles, the temperature structure is initially difficult to explain: the diurnal variation in the temperature profile is of opposite phase to that observed in summer and is most non-logarithmic around midday. It is suggested that this is due to airborne drift snow at the site which absorbs short wave radiation and results in relatively greater heating of the atmosphere at some distance above the surface.

12.1 INTRODUCTION

An automatic weather station operated continuously at a remote site on the East Antarctic ice sheet from January 1982 to May 1984. The station was located at 68^{o}39'S, 60^{o}33'E (about 130 km inland from the coast near Mawson station) at an elevation of 1850 m on the relatively steep slope of the ice sheet where katabatic wind flow is dominant. Data from the station was obtained via the ARGOS data system on TIROS-N satellites. Details of the station design and construction are given by Allison and Morrissy (1983).

Parameters measured by the station included air pressure, wind speed and direction 4 m above the surface, air temperatures at 1, 2 and 4 m above the surface, and snow temperature. The air temperature sensors were shielded, ventilated naturally, and had a resolution and relative

accuracy of better than 0.03 ^{o}C so that accurate temperature profiles could be obtained. The station is in a region of relatively low snow accumulation and the relative height of the sensors above the snow surface changed by less than 0.1 m over two years.

Because of the near polar orbit of the TIROS-N satellites, an average of 28 transmissions a day were recieved from the station, although the orbit geometry results in fewer transmissions being received around local noon than at other times. The station itself takes readings every 54 minutes.

Two years of data from this station have been analysed to show the diurnal variation of wind and temperature at the site. Preliminary results of this analysis are presented.

12.2 DATA ANALYSIS

Magnetic tapes of data from the station were received monthly from service Argos. The data was first edited automatically to exclude any transmissions for which null sensors included in the station were non zero, and was then edited manually to eliminate obviously faulty transmissions. Data were then assigned to one hour periods (0000-0100, 0100-0200 LST, etc) and group means taken of the various parameters every 2 months (January/February, March/April, etc). All valid data was included in these means and no attempt has been made to eliminate periods during which specific synoptic events (e.g. blizzards) occurred.

These means showed almost identical diurnal variations for November/December as for January/February and for May/June as for July/August. Similarly the diurnal variability of each of the parameters had both the same phase and amplitude in 1982 as in 1983, although there was some difference in the mean values (especially wind speed) between the two years. Additional data from a solar cell on the station indicated that the year could be conveniently divided into four seasons (on the basis of the duration and intensity of solar radiation) of "summer" (November to February), "autumn" (March to April), "winter" (May to August) and "spring" (September to October). This is similar to the division of the year into periods of sunlight, dark and transition used by Lettau and others (1977) at Plateau station. All data from the station have been combined to show the mean diurnal variability for each season over two years.

The diurnal variation of wind direction, wind speed, 2 m air temperature, and the air temperature differences between 4 and 2 m and between 2 and 1 m are shown as a function of local solar time for each season in Figures 1 to 4. The atmospheric pressure showed no systematic diurnal variation. Also shown are the number of temperature measurements analysed for each group. Because of some problems with the wind sensors there were fewer wind measurements but most failures occurred only when temperatures were below -40 ^{o}C; in the winter months when there is no diurnal variability.

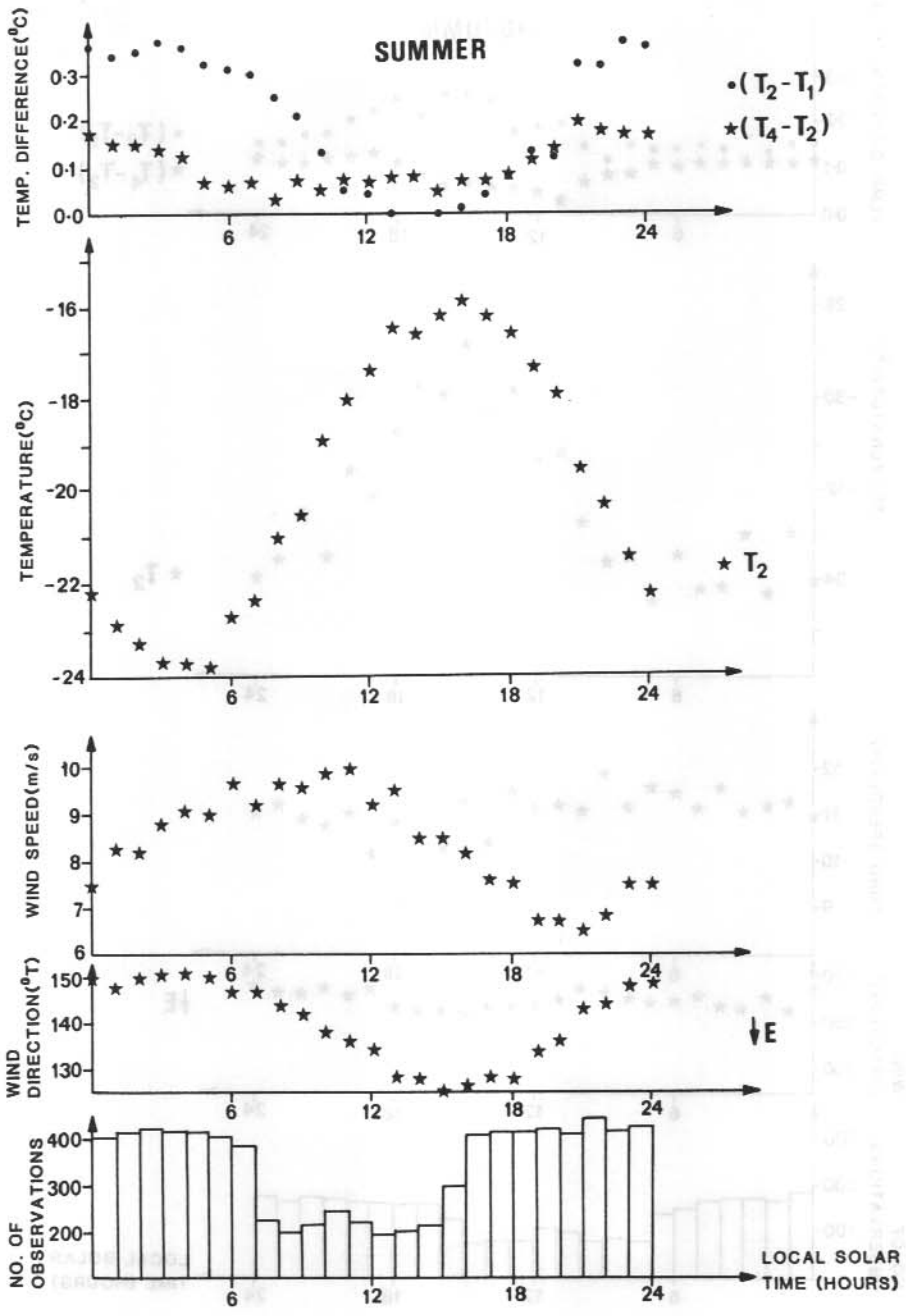

Figure 1. Mean diurnal variation of surface air temperature differences, 2 m air temperature, wind speed, and wind direction for the period November to February.

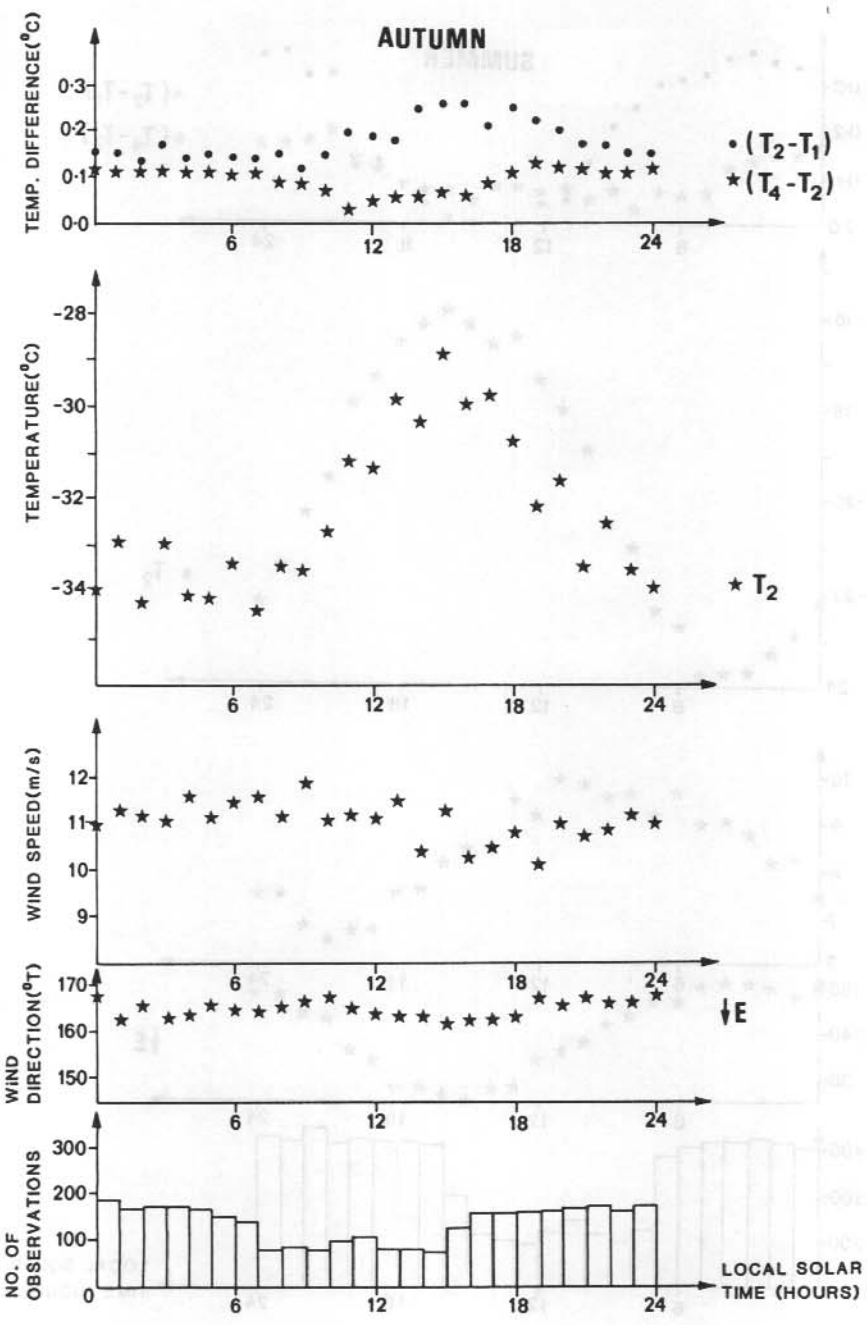

Figure 2. Mean diurnal variation of surface air temperature differences, 2 m air temperature, wind speed, and wind direction for the period March to April.

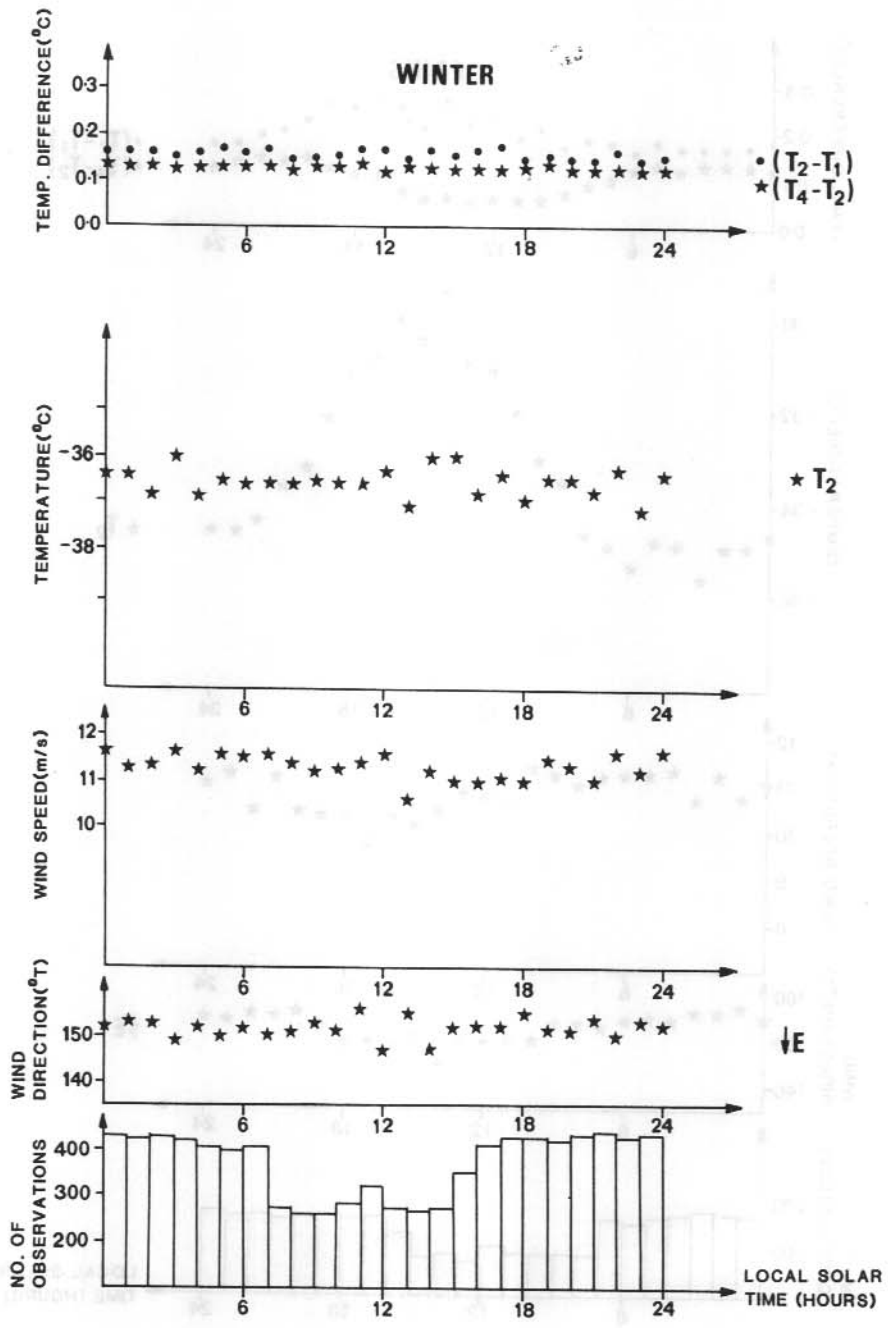

Figure 3. Mean diurnal variation of surface air temperature differences, 2 m air temperature, wind speed, and wind direction for the period May to August.

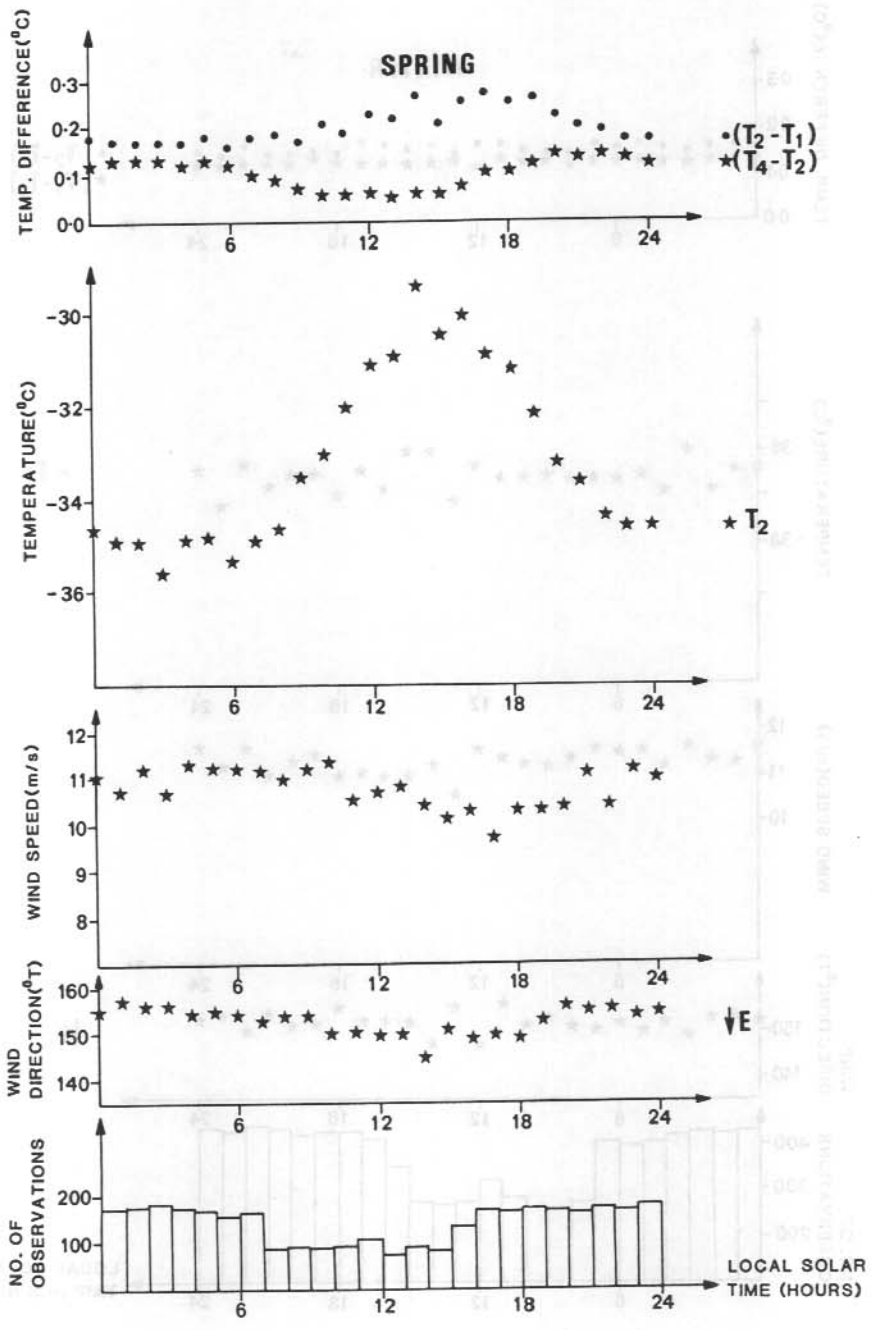

Figure 4. Mean diurnal variation of surface air temperature differences, 2 m air temperature, wind speed, and wind direction for the period September to October.

12.3 DIURNAL VARIATION OF WIND

During the summer months (Figure 1) there is a very pronounced oscillation in the 4 m wind speed, (a mean amplitude of 4 ms^{-1}) and in the wind direction (a 25^{o} amplitude), but these oscillations are not in phase. The wind direction starts to turn easterly at about 0500 LST when the air temperature starts to increase and the inversion strength decrease. The wind is most easterly about 3 hours after solar noon. The wind speed however does not start to decrease until about noon, reaching a minimum at about 2000. Maximum surface windspeeds around midday are a common feature in the interior of ice sheets and numerous examples for Antarctica are documented by Mather and Miller (1967). This contrasts with the situation at Antarctic coastal stations where typically the wind speed is at maximum during the coldest part of the day, and minimum after noon. Loewe (1974) ascribes the maximum wind speed at noon to energy transfer from the upper wind to the surface layer, which is facilitated by the smaller inversion strength at this time. The combination of the upper geostrophic wind and of the thermal wind in the inclined inversion layer can lead to a stronger surface wind during the midday hours.

The phase difference between the wind speed and wind direction oscillation arises as a result of an anticlockwise cyclic variation in the wind vector as shown in Figure 5. A similar oscillation in Antarctic surface wind has been observed at Plateau station (Riordan, 1977) where it is primarily attributed to the inclination of the surface and the pressure gradient variation which results from the diurnal cycle of temperature (Dabberdt, 1970). If the sloping snow surface has a uniform surface temperature and if at all times isothermal surfaces are parallel with the snowfield, then the resultant diurnally varying horizontal gradient in the temperature field leads to an oscillating thermal wind which blows perpendicular to the flow line, with cold air on the right (in the southern hemisphere).

An alternative explanation for the cyclic wind oscillation is suggested by the results of Wallace and Hartranft (1969) who reported a diurnal counterclockwise oscillation over the Antarctic at levels between the surface and 10 mb, which they ascribe to solar tides, a result of the global solar heating pattern (Lindzen, 1967). However such tidal variations are both of inadequate magnitude (a measured diurnal range of less than 0.3 ms^{-1} at 800 mb) and of the wrong phase (maximum southerly component at local noon) to explain the oscillation in Figure 5.

Diurnal oscillation of the wind is also present during autumn and spring, although with a reduced amplitude (Figure 5), but no regular variation is apparent during the sunless months. Both these observations are compatible with Dabberdt's proposal of a diurnally varying surface thermal wind.

There is also some suggestion from Figure 5 that the mean seasonal wind vectors show a similar cyclic variation, which might arise from thermal wind variation with the annual temperature cycle.

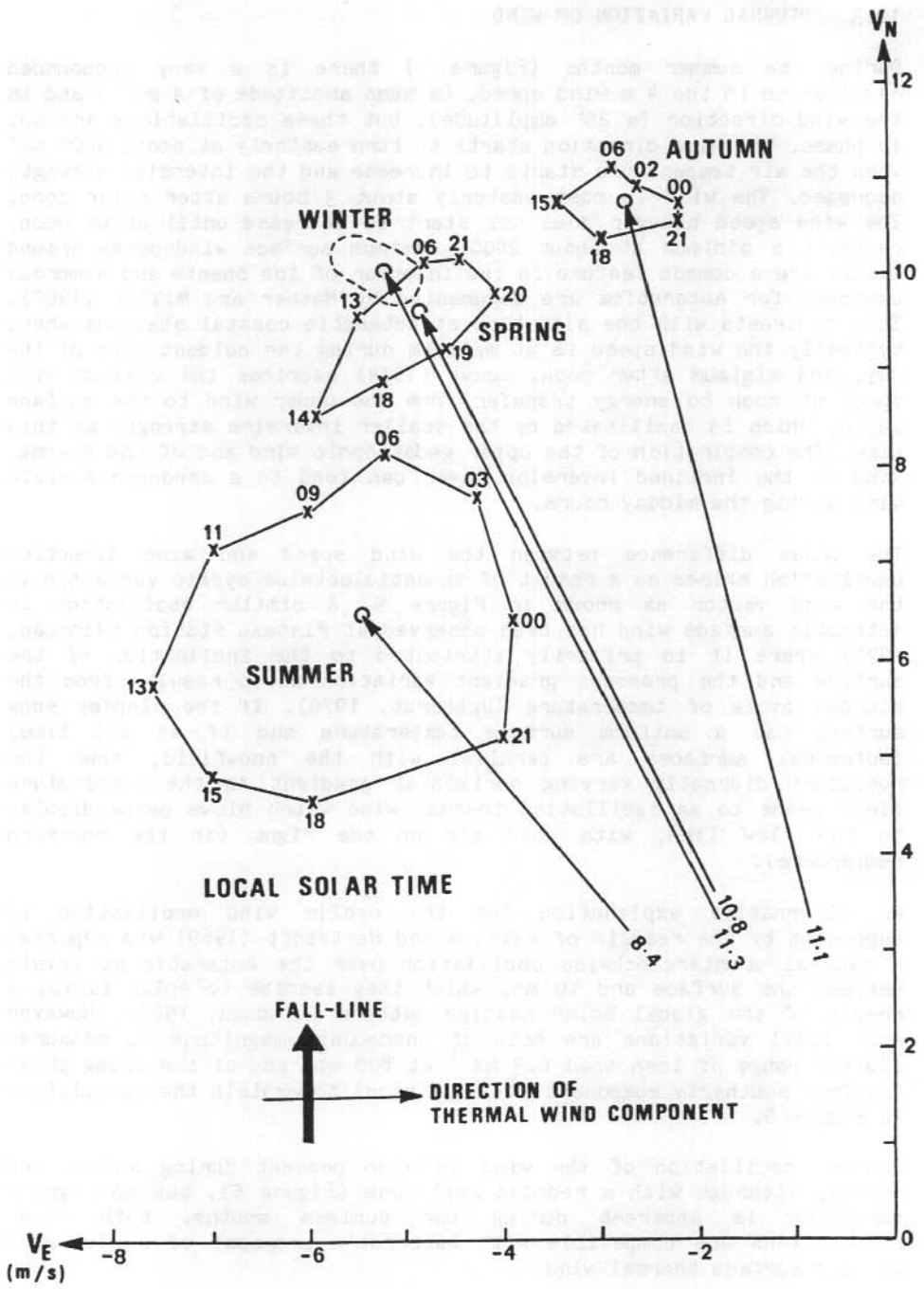

Figure 5. Hodographs of 3-hourly (local solar time) positions of the seasonal mean 4 m wind vectors for 1982-1983. The surface slope direction is also shown.

12.4 DIURNAL VARIATION OF TEMPERATURE AND TEMPERATURE GRADIENT

The air temperature at 2 m shows a mean diurnal range of about 9 ^{o}C in summer, 5 to 6 ^{o}C in autumn and spring and is constant throughout the day in the winter months when there is no short wave radiation. Maximum temperatures occur about 3 to 4 hours after solar noon.

Mean profiles of potential temperature are shown schematically in Figure 6 for 4 times of day. During the winter months the net radiation at the site will be always outgoing and relatively constant. A near logarithmic temperature inversion develops, which also remains constant throughout the day, with a mean temperature difference of 0.15 ^{o}C between 1 and 2 m. Winter surface inversion strengths of equal magnitude have been observed at Mizuho, a similar site on the Antarctic coastal slope (Sasaki, 1979).

In contrast, the inversion strength during summer varies both with height and with time. The inversion is strongest at the lower level during the night but decreases during the day, as the surface is heated by solar radiation. Although the inversion strength is weakened greatly, a mean inversion down to 1 m is maintained throughout the day. Despite this, the atmosphere above the surface is heated considerably during the day and as at Plateau Station (Riordan, 1977) eddy transfer must play a role in this vertical heat transport. On some individual days surface heating may lead to a reversal of the temperature gradient and to occurence of a minimum temperature at 2 m. Lapse conditions however are only ever observed in the lower layer and are always weak. Observations of an elevated temperature minima have previously been reported from Little America V and Plateau (Riordan, 1977).

Initially one could expect the temperatures and temperature profiles in autumn and spring to be transitional between those in summer and winter. The diurnal temperature range is only about half of that during the summer but the temperature profiles in Figure 5 show a surprising diurnal variation. The nocturnal profiles are similar to those observed during the winter and, while the inversion strength between 2 and 4 m is weakened (in phase with the solar heating), the inversion between 1 and 2 m is strengthened during the day. Instrumental error is discounted as the cause of this observation since both the summer and winter patterns are similar to those observed elsewhere in Antarctica and because the spring and autumn observations are consistent from month to month, between the two seasons and from year to year.

Strengthening of the lower level inversion during daytime occurs because the air at 2 m is warmed at a greater rate than that nearer the surface. One possible mechanism that might cause this would be for the drift snow, which is present at similar sites up to 80% of the time during autumn and spring (D. Jones, T. Medhurst personal communications), to act as an effective absorber of short wave radiation at a height between 1 and 2 m. The mean wind speed between March and October at the site is about 11 ms^{-1}. Drift snow densities

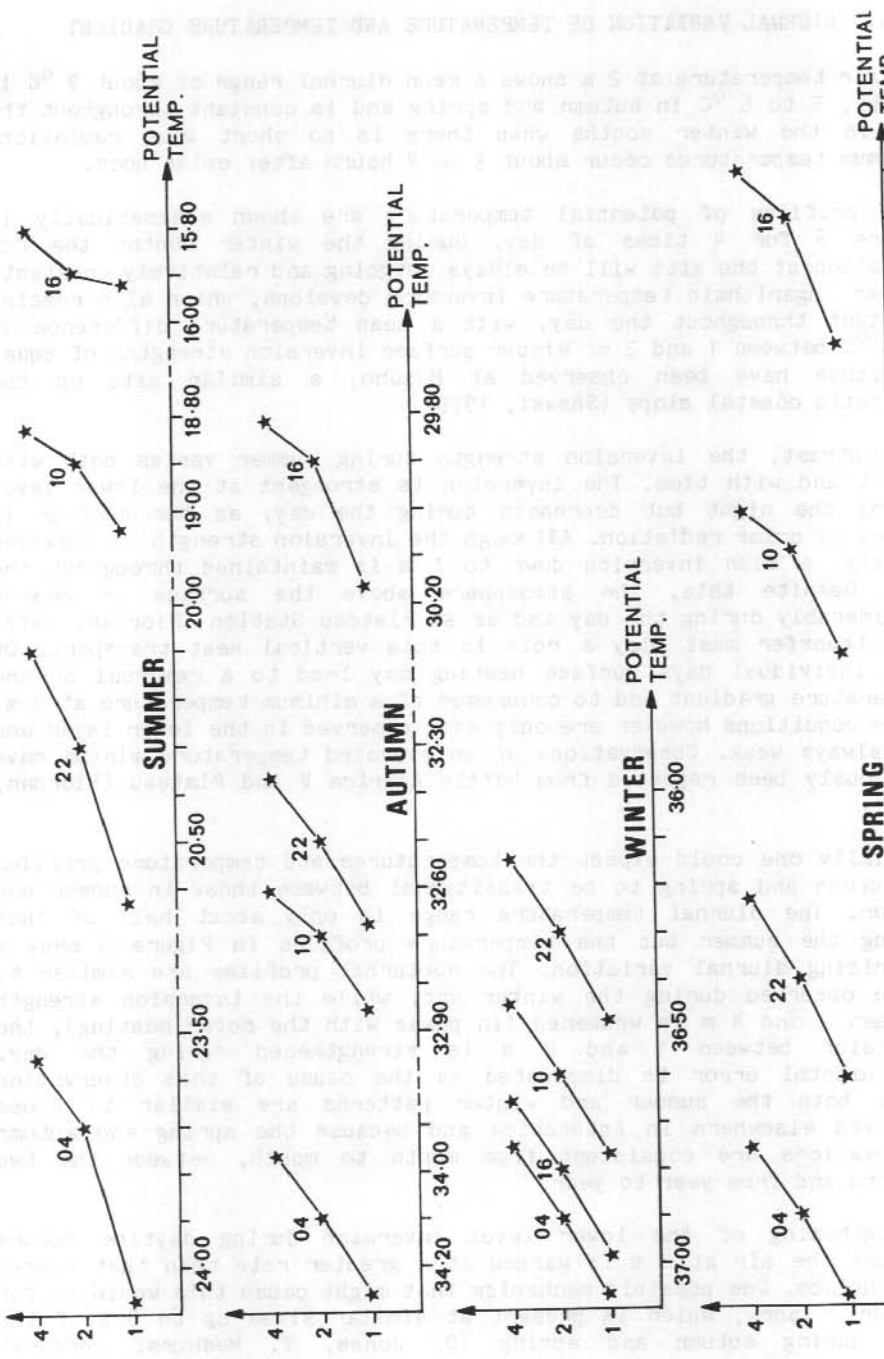

Figure 6. Near surface potential temperature profile variation with season and time of day (hours LST).

at Byrd at these wind speeds were measured to be about 0.4 gm/m^3 at 1 m above the surface, 0.2 gm/m^3 at 2 m and 0.1 gm/m^3 at 4 m (Budd and others, 1966). During summer months at the AWS site the mean wind drops to 8.5 ms^{-1}, surface snow grains are larger, and often a glaze forms on the surface (Jones, 1983). Under these conditions there is little drift snow.

Yamanouchi and Kawaguchi (in press) have measured the radiation budget at 30 m and 1.5 m above surface at Mizuho and relate radiation differences at the two levels to wind speed, and hence indirectly to drift snow. They suggest that the incoming longwave radiation is increased by about 2 Wm^{-2}/ms^{-1} for the component of wind speed in excess of 13 ms^{-1}. The incoming direct shortwave radiation is decreased markedly, but the scattered radiation is increased and overall the net short wave flux is decreased by only about 1% $/ms^{-1}$ for the wind in excess of 13 ms^{-1}. Hence, unless the net short wave flux is greater than 200 Wm^{-2}, the net effect of the drift is to supress the surface radiative cooling.

Because of the high albedo at the AWS site, the net short wave flux will be less than 200 Wm^{-2} at all times and the results of Yamanouchi and Kawaguchi would suggest that the presence of drift snow might not explain the more rapid daytime rise of the air temperature at 2 m than at 1 m. However differences in surface snow structure may result in different drift densities at the AWS site than at Mizuho. Further field investigation of both the observed phenomena and the proposed hypothesis is required.

Finally it should be noted that the observation by Yamanouchi and Kawaguchi that the incoming longwave radiation at the surface is increased during drift snow, can explain why the night time temperature inversion at the lowest level during summer (no drift) is greater than during the rest of the year.

REFERENCES

Allison, I. and Morrissy, J.V. (1983) Automatic weather stations in the Antarctic. Australian Meteorological Magazine, 31, 71-76.

Budd, W.F., Dingle, R. and Radok, U. (1966) The Byrd snow drift project: outline and basic results. In: Rubin M.J. (Ed.), Studies in Antarctic Meteorology, AGU Antarctic Research Series, 9, 71-134.

Dabberdt, W.F. (1970) A selective climatology of Plateau Station, Antarctica. Journal of Applied Meteorology, 9, 311-315.

Jones, D. (1983) Snow stratigraphy observations in the katabtic wind regions of eastern Wilkes Land, Antarctica. ANARE Research Note, 17.

Lettau, H., Riordan, A.J. and Kuhn, M. (1977) Air temperature and two-dimensional wind profiles in the lowest 32 metres as a function of bulk stability. In: Businger, J.A. (Ed.), Meteorological Studies at Plateau Station Antarctica, AGU Antarctic Research Series, 25, 77-91.

Lindzen, R.S. (1967) Thermally driven diurnal tide in the atmosphere. Quarterly Journal of the Royal Meteorology Society, 93, 18-42.

Loewe, F. (1974) Die tagliche Windschwankung uber dem Innern von Inlandeisen in Sommer. Archiv fur Meteorologie, Geophysik und Bioklimatologie, B, 22, 219-232.

Mather, K.B. and Miller, G.S. (1967) Notes on topographic factors affecting the surface wind in Antarctica, with special reference to katabatic winds: and bibliography. Technical Report Grant No. G.A.-900, Geophysical Institute, University of Alaska.

Riordan, A.J. (1977) Variations of temperature and air motion in the 0- to 32- meter layer at Plateau Station, Antarctica. In: Businger, J.A. (Ed.), Meteorological Studies at Plateau Station Antarctica, AGU Antarctic Research Series, 25, 113-127.

Sasaki, H. (1979) Preliminary study on the structure of the atmospheric surface layer in Mizuho Plateau, East Antarctica. Antarctic Record, 67, 86-100.

Wallace, J.M. and Hartranft, F.R. (1969) Diurnal wind variations, surface to 30 kilometres. Monthly Weather Review, 97, No. 6, 446-455.

Yamanouchi, T. and Kawaguchi, S. (in press) Effects of drifting snow on the surface radiation budget in the katabatic wind zone, Antarctica. Annals of Glaciology, 6.

13. THE UTILITY OF METEOROLOGICAL OBSERVATIONS MADE AT THE S2 GLACIOLOGICAL STATION, ANTARCTICA IN 1957

H.R. Phillpot
Meteorology Department, The University of Melbourne
Parkville, Victoria, 3052.

ABSTRACT

The problems posed by the poor understanding of the weather and climate of the Antarctic continent, particularly in the short-term variations of the surface wind behaviour on the coastline of East Antarctica, are discussed. In 1957, very soon after Wilkes station was set up at 66° 15.5'S, 110° 31.2'E, altitude 12 m, a field station designated S2 was established at 66.5°S, 112.2°E, altitude 1139 m, for glaciological purposes, and additionally a quite extensive program of surface meteorological observations was maintained until January 1958.

An examination of the S2 data, comparison with the corresponding surface observations in conjunction with the extensive upper air observations from Wilkes, plus the surface and 500 mb charts for the International Geophysical Year (1957-58) published by the South African Weather Bureau, have thrown new light on the surface wind behaviour in the coastal sector. Unfortunately no specific conclusions can be drawn; nor is it believed, will any be possible until the availability of satellite cloud imagery permits the centres of action to be identified and tracked near the station, but the value of meteorological observations from a site such as S2 is demonstrated.

13.1 INTRODUCTION

For some time investigations have been directed to the problem of forecasting surface weather conditions on the Antarctic continent, particularly at places on the coast. Emphasis has been given mostly to strong wind events because of their importance, but unfortunately little real progress has been achieved. The katabatic wind is a complex phenomenon which has not been completely resolved, because of the problem of separating the katabatic effect from that due to the prevailing pressure gradient.

The forecasting problem is difficult because the available data base is inadequate. Considerable attention has been given to the International Geophysical Year (IGY) period (1957-58) because of the continental observing network, and because the data have been carefully analysed, with a series of daily charts, and grid-point data published by the South African Weather Bureau. This chart series though, is confined to the surface (mean sea level) pressure field, and the 500 mb contour (constant pressure topography) field.

Setting aside satellite-derived products - particularly the cloud imagery fields observed by the geostationary satellites - the most important single aid for surface weather forecasting is the mean sea level (MSL) pressure field with its associated frontal systems. Unfortunately the great height of the Antarctic ice mass precludes the

construction of such a pressure field on and south of the continental coastline, and, in this area, frontal systems are very difficult to identify for various reasons. Close attention must therefore be paid to the circulation processes shown at the 500 mb level - the first standard pressure level which does not intersect the Antarctic ice mass, and for which data are always reported on the upper air flights. The problems here are that 500 mb data are only available from stations where upper air soundings are made, and perhaps more importantly, little experience has been gained on preparing surface weather forecasts from 500 mb contour fields.

13.2 OBSERVATIONAL DATA

Early in February 1957, Wilkes station, with a full meteorological observational program, was established on Clark Peninsula in 66°15.5'S, 110°31.2'E, altitude 12 m. A set of surface observations every 6 hours (00, 06, 12, 18 GMT), and upper air observations (rawinsondes) every 12 hours (00, 12 GMT, except in adverse weather) has been published on microcards for the IGY period (1 July 1957 to 31 December 1958) by the World Meteorological Organisation (WMO).

In March 1957, a glaciological program was commenced at a site, designated S2, near 66.5°S, 112.3°E, altitude 1139 m about 80 km inland from Wilkes. From March 1957 to January 1958 meteorological observations were made at S2 (Cameron and others, 1959). Whilst those for March and April 1957 are incomplete because the station was not then occupied full time, from May 1957 to January 1958 a reasonably extensive surface meteorological program was maintained every three hours, excluding 0400 local time (21 GMT) and some other hours which were missed due to the demands of the glaciological program.

13.3 DATA TREATMENT

Some comparisons have been made of the two sets of data for the July - December 1957 period. The six months have been grouped into two periods July - September (called "winter") and October - December ("spring").

The following assessments and comparisons have been made:
(a) the surface katabatic wind at S2
(b) the variation of snow behaviour with surface wind speed at S2
(c) a comparison of Wilkes upper winds with S2 surface winds
(d) a classification of the surface wind regimes at Wilkes and S2.

Considering each of these:

(a) The surface katabatic wind at S2.

This was assessed by the single-station "effective pure katabatic wind" technique (Phillpot, 1968). The Wilkes upper winds were assumed to be representative of the S2 site, and the (Wilkes) 850 mb wind components correlated with the corresponding, near simultaneous, surface wind components observed at S2. The "effective pure katabatic

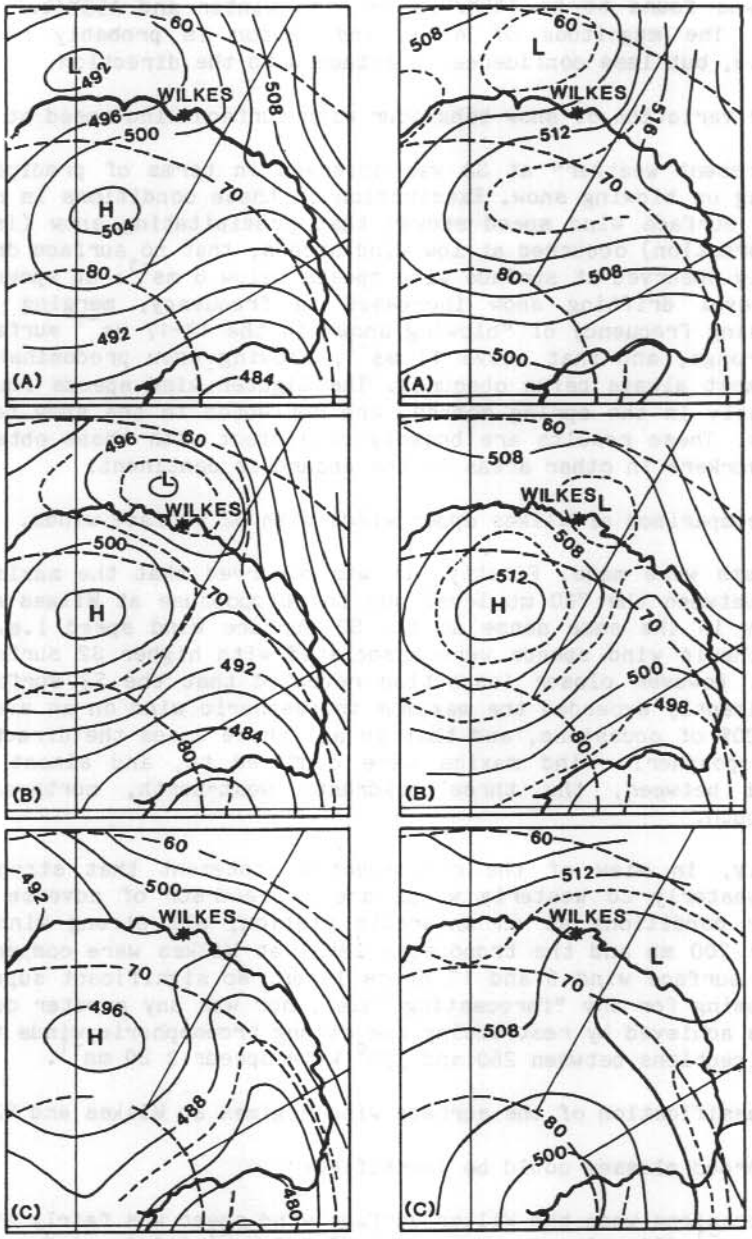

Figure 1. Mean 500 mb contour charts for the occasions in winter (July - September, left hand side) and spring (October - December, right hand side) corresponding to three broad classes:
(A) When the Wilkes surface wind speed $\geq$ 10.3 ms^{-1} (S2 wind strong)
(B) When the S2 surface wind speed $\geq$ 17 ms^{-1} (Wilkes surface wind speed < 10.3 ms^{-1})
(C) When the S2 surface wind speed $\leq$ 4.5 ms^{-1}.

wind" was found to be 145°/9.1 ms^{-1} in winter and 155°/6.1 ms^{-1} in spring. The magnitude of each wind vector is probably reasonably accurate, but less confidence is attached to the direction.

(b) The variation of snow behaviour with surface wind speed at S2.

The "present weather" at S2 was observed in terms of precipitating, drifting or blowing snow. Examination of these conditions in relation to the surface wind speed showed that precipitating snow (including rime formation) occurred at low wind speeds; that no surface drift was commonly observed at surface wind speeds below 8 ms^{-1}; at speeds above this level drifting snow increased in frequency, merging with an increasing frequency of "blowing snow" in the 14-17 ms^{-1} surface wind speed range, and that above 17 ms^{-1}, blowing snow predominated, the sky almost always being obscured. The lighter wind speeds found more frequently in the spring months, are reflected in the snow behaviour pattern. These results are broadly consistent with those obtained by other workers in other areas on the Antarctic continent.

(c) A comparison of Wilkes upper winds with S2 surface winds.

Two tests were made. Firstly, it was observed that the maximum wind speed between the 700 mb level and the tropopause at Wilkes appeared to vary in the same sense as the S2 surface wind speed i.e. higher tropospheric wind speeds were associated with higher S2 surface wind speeds. However closer inspection revealed that the S2 surface wind significantly exceeded the maximum tropospheric wind on an average of about 20% of occasions, and that in all these cases the directions of the tropospheric wind maxima were confined to, and almost equally divided between, the three quadrants west-north, north-east and east-south.

Secondly, in view of the often-quoted statement that strong upper north-westerly to westerly winds are a precursor of adverse surface weather conditions at an Antarctic station, all strong wind events between 700 mb and the tropopause level at Wilkes were compared with the S2 surface wind 6 and 12 hours later. No significant support was forthcoming for any "forecasting rule", nor was any greater degree of success achieved by restricting the strong tropospheric winds to those from directions between 260 and 330° with speeds $\geq$ 20 ms^{-1}.

(d) Classification of the surface wind regimes at Wilkes and S2.

Three broad classes could be identified:

(1) occasions when the Wilkes surface wind speed was fairly strong, $\geq$ 10.3 ms^{-1} (20 kn), cf: an average of 5.3 ms^{-1} (10.3 kn) for the July - December period. On these occasions the S2 surface wind was strong;
(2) occasions when the S2 surface wind $\geq$ 17 ms^{-1} (33 kn), corresponding to Beaufort Force 8, Fresh Gale) and the Wilkes surface wind speed was < 10.3 ms^{-1}.
(3) occasions when the S2 surface wind was light $\leq$ 4.5 ms^{-1} (8.7 kn). cf: the average of 11.2 ms^{-1} (21.8 kn) observed through the period the site was occupied.

The days meeting these criteria at 12 GMT were identified and grouped for each class, for the winter and spring seasons separately. The number of days in each class and season was: (1) 22 and 12; (2) 15 and 14, and (3) 17 and 18 respectively. Mean 500 mb charts (for each class and season) derived from the 12 GMT grid-point data published by the South African Weather Bureau (Figure 1) show that in the mean:

(1) surface winds ($\geq$ 10.3 ms^{-1}) are experienced at Wilkes when there is a 500 mb trough lying parallel to, but seaward of the coastline in this coastal sector, with a 500 mb contour gradient producing an E/NE air-stream;

(2) gale force winds ($\geq$ 17 ms^{-1}) are experienced at S2, but the winds at Wilkes will be < 10.3 ms^{-1} when there is a 500 mb low off the coast near Wilkes, a trough extending across the Antarctic continent towards the Ross Sea/Ice Shelf and a high over the continental plateau, so that the resultant contour gradient in the Wilkes-S2 area produces an E/SE airstream;

(3) the S2 surface winds fall to 4.5 ms^{-1} or less when the pressure trough across the Antarctic continent, towards the Ross Sea/Ice Shelf area, either alone or in association with a low pressure centre between Wilkes and Dumont d'Urville produces a contour gradient appropriate to a SW airstream.

13.4 CONCLUSION

All results are interesting, but most particularly are those classifying the S2 and Wilkes surface winds in terms of the 500 mb contour fields.

Zimmerman (1960) and Budd (1966) drew attention to the difference between the Wilkes surface wind speed and that experienced on the ice cap. Zimmerman commented..."one can look up to the ice cap before a storm and see streamers of snow blown into the air, while at the base the air is quiet...". Additionally he noted the effects of the local terrain, particularly the influence of the Vanderford Glacier in producing a southerly wind - which he regarded as being a true gravity wind - at Wilkes. Budd expressed the view that the lower surface wind speed at Wilkes was due in part to the "channelling of the wind ... north over the region of Cape Folger and south over the low region of the Vanderford Glacier". It now appears that in addition to these influences near the station, the Law Dome itself plays a major role in the Casey area surface wind field.

The value of these S2 observations is therefore clear. They have made a significant impact on understanding the surface wind behaviour in the area around Casey, and suggest that field observations in other areas might make possible the development of reasonably reliable relationships between 500 mb contour fields and associated surface weather at Antarctic continental coastal stations.

Further work on the S2 records is continuing, to relate weather conditions there with those observed simultaneously at Wilkes. This

would greatly help in assessing the expected weather conditions at an airstrip planned for construction a few miles from Casey at an altitude of about 500 m above MSL.

REFERENCES

Budd, W.F. (1966) Glaciological studies in the region of Wilkes, Eastern Antarctica, 1961 ANARE Scientific Reports, Series A, (IV) Glaciology, Publication No. 88, 152 pages.

Cameron, R.L., Loken, O.H., and Molholm, J.R.T. (1959) Wilkes Station Glaciological Data 1957-1958. Report by the Ohio State University Research Foundation, RF Project 825, Report No. 1, Part III.

Phillpot, H.R. (1968) A study of the synoptic climatology of the Antarctic. International Antarctic Meteorological Research Centre, Technical Report No. 12, 139 pages.

Weather Bureau, South Africa. (1959) Tables, diagrams and charts for the southern hemisphere for the first half of the International Geophysical Year (July 1957 - March 1958 Notos, 8, (1/4)

Weather Bureau, South Africa. (1960) International Geophysical Year (1957-58). World weather maps part III Southern Hemisphere south of 20 S.

Zimmerman, J.R. (1960) Wilkes climatology. In: Antarctic Meteorology. Proceedings of the symposium held in Melbourne, February 1959 Pergamon press. 415-422.

14. VOLCANIC CLOUD DETECTION FROM AEROSOL OPTICAL DEPTHS OVER LAW DOME, ANTARCTICA

D.M. Etheridge
Antarctic Division, Department of Science
Kingston, Tasmania, 7150.

ABSTRACT

Measurements of the aerosol optical depth of the atmosphere were taken at 3 sites near Law Dome during the summer of 1982/83. They were used to determine the type and amount of particulate matter in the atmospheric column. The results were significantly higher than expected for a remote location and it is shown that this was due to the El Chichon volcanic eruption cloud having reached Antarctic latitudes.

14.1 INTRODUCTION

Particulate matter in the atmosphere acts as a scattering and absorbing medium for solar radiation and is thus an important factor in the global radiative energy balance. It is this same quality that allows the measurement of the amount of particulates (or aerosols) via measurement of the attenuation of the direct solar beam after passing through the atmosphere. The aerosol optical depth is the index of attenuation due to aerosols and is related to the amount and size distribution of the aerosols. Note that it refers to the total aerosol loading integrated through the vertical atmospheric column, although it is normally the lower troposphere where most aerosols reside.

Aerosol optical depth is now being measured at a network of remote locations. The data are used to monitor the background aerosol level as changes in this level, whether from natural causes (usually volcanic) or resulting from human activity can be climatically significant. However measurements at some of these locations (such as the Department of Science's Cape Grim Baseline Air Pollution Station) are susceptible to domination by local sources such as sea spray or high humidity (Etheridge and others, 1984). Inland Antarctica thus offers an ideal site for measurement of global background aerosol optical depths.

14.2 OBSERVATIONS

The measurements were part of a summer program at Casey, Antarctica and nearby Law Dome. It was of interest to see whether the aerosol optical depths, which during certain conditions in Antarctica can be regarded as global background amounts, were influenced by the dispersed volcanic cloud resulting from the eruption of the Mexican volcano, El Chichon. In March 1982, El Chichon erupted causing a huge injection of particulates, mostly sulphuric acid droplets, into the stratosphere. It caused a record stratospheric warming of 4 ^{o}C and confused satellite temperature and water vapour soundings. The resulting climatic perturbation is expected to be the largest this

century (Mitchell, 1982; Hofmann and Rosen, 1983). Little information however has thus far been published on its extent in the southern hemisphere.

Depletion of the direct solar beam through the atmosphere is given by the Bouguer-Lambert law:

$$E(\lambda) = E_o(\lambda)\, e^{-\tau(\lambda)m} \qquad \text{----------(1)}$$

where $E(\lambda)$ is the observed irradiance of the beam at wavelength λ, $E_o(\lambda)$ is the extra-terrestrial irradiance, $\tau(\lambda)$ is the total optical depth of the atmosphere, and m is the optical path length, a function of time and location.

The total optical depth is due to Rayleigh (molecular) scattering, molecular absorption and scattering and absorption by aerosols, respectively:

$$\tau(\lambda) = \tau_R(\lambda) + \tau_M(\lambda) + \tau_A(\lambda) \qquad \text{----------(2)}$$

All three components are strongly wavelength dependent. $\tau_R(\lambda)$ is a known function (Frohlich and Shaw, 1980) so measurements of $E(\lambda)$ outside of absorption bands will give $\tau_A(\lambda)$.

Measurements were carried out using a sun photometer provided by Flinders Institute for Atmospheric and Marine Science. The photometer consists of a number of narrow bandpass filters in a wheel, a columnator and a silicon photodiode sensor with operational amplifier. Irradiance, $E(\lambda)$ is then ouput as a voltage. $E_o(\lambda)$ is the calibration coefficient for each wavelength, and is obtained by extrapolating the plot of photometer output for a wide range of m values. This was possible for each Law Dome measurement day. The results are summarised in Table 1.

Two items are of special interest. Firstly, the aerosol optical depth at a wavelength of 500 nm, $\tau_A(500)$, is the directly comparable international standard. Secondly, the dependence of aerosol optical depth on wavelength between 300 and 1000 nm gives information on the amount and size distribution of the aerosol.

14.3 DISCUSSION

The Law Dome aerosol optical depths were the first to be measured in this region, so no comparison with earlier results can be made. However, in the period of 1980/1981 measurements were made at Japan's Syowa station which is similar in location and geography to Law Dome. It is thus expected that aerosol optical depths should be very similar at both locations. We can then see from Figure 1 that $\tau_A(500)$ over Law Dome experienced an increase of about 0.06 after the El Chichon eruption. This increase is similar to that found in the stratosphere at 55°S during NASA aircraft flights in April, 1983. (Dutton and DeLuisi, 1983), also shown in Figure 1. It seems that the large aerosol optical depths over Law Dome were a result of mainly stratospheric particles. The only other Antarctic station for which

Table 1. Aerosol optical depths for 3 locations near Law Dome, Antarctica.

BHC1 (CAPE FOLGER)

66° 7'S 110° 53'E 210 m
31 December 1982 P =968 mb
Cloud: 1/8 Wind: Calm Temp: 1°C

14 Measurements 1533 → 1951 HRS LOCAL TIME

WAVELENGTH, nm	420	500	680	870
MEAN AEROSOL OPTICAL DEPTH	0.105	0.092	0.059	0.040

BHQ (LAW DOME)

66° 25'S 110° 50'E 915 m
10 January 1983 P = 893 mb
Cloud: 0/8 Wind: Light, variable Temp: -8°C

37 Measurements 1200 → 1956 HRS LOCAL TIME

WAVELENGTH, nm	420	500	680	870
MEAN AEROSOL OPTICAL DEPTH	0.086	0.076	0.049	0.031

CASEY STATION

66° 18'S 110° 33'E 20 m
31 January 1983 P = 997 mb
Cloud: 0/8 Wind: Light NW Temp: 2°C

14 Measurements 1600 → 1844 HRS LOCAL TIME

WAVELENGTH, nm	420	500	680	870
MEAN AEROSOL OPTICAL DEPTH	0.087	0.075	0.051	0.038
ERROR AT m = 2 FOR ALL ABOVE	0.008	0.006	0.005	0.004

measurements are presently available for both before and after the eruption is South Pole, which showed a rise of 0.025 in $\tau_A(500)$.

The spectral dependence of aerosol optical depth is shown in Figure 2. Curve 1 is the average of the Law Dome results. Curve 2 is the Syowa average (for the same time of year and same meteorological conditions as the Law Dome results) and can be regarded as a typical background curve for Law Dome before the El Chichon eruption. The difference (curve 1 minus curve 2) is the apparent increase in the aerosol

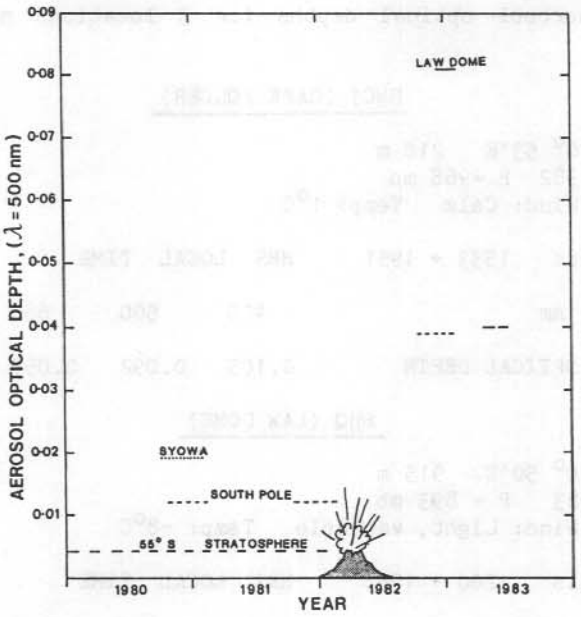

Figure 1. Aerosol optical depth at 500 nm for several Antarctic locations, before and after eruption of El Chichon.

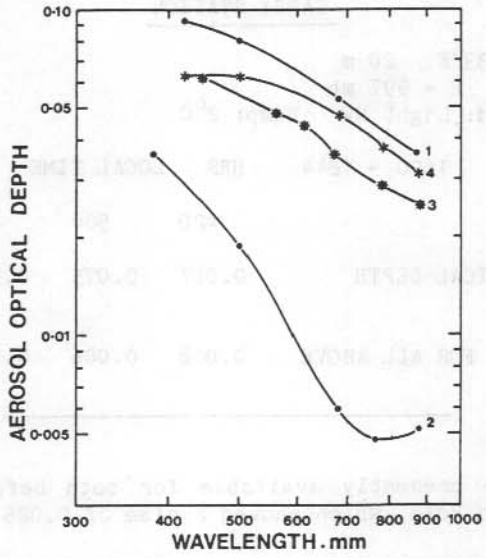

Figure 2. Spectral aerosol optical depths for several Antarctic locations. Curve 1: Law Dome average, summer 1982/83; Curve 2: Syowa summer average, 1980/81 (Matsubara and Kawaguchi, 1983); Curve 3: Statosphere 36^{o}S, October 1982 (Spinhurne, 1983); Curve 4: Curve 1 minus Curve 2.

optical depths over Law Dome, shown as Curve 4. Curve 3 shows the spectral aerosol optical depths of the 36°S stratosphere from NASA flights (Spinhurne, 1983) 6 months after the eruption. Normally, stratospheric aerosol optical depths are immeasurably small. The closeness of Curves 3 and 4 again shows that the increase in aerosols over Law Dome occurred mainly in the stratosphere.

Another feature of interest is the unusual flatness of Curves 3 and 4, indicating an aerosol size distribution with significantly more large particles (about 1 μm diameter) than normally occurs in a background aerosol. This is a characteristic of the El Chichon cloud of sulphuric acid droplets, as reported by many sources. (e.g. Dutton and DeLuisi, 1983).

14.4 CONCLUSIONS

The aerosol optical depth of the atmosphere over Law Dome in 1982/83 was significantly greater than expected for a background level. The aerosols responsible for the increase resided mostly in the stratosphere and had a size distribution biased towards larger particles. This indicates that the source was the El Chichon eruption plume that had dispersed through the stratosphere to the latitudes of Antarctica. Subsequent measurements would monitor further dispersal of the plume and show whether or not the aerosol optical depth returned to its background level.

ACKNOWLEDGMENTS

Many thanks to Dr Bruce Forgan for useful discussions on the data analysis.

REFERENCES

Dutton, E., and DeLuisi, J. (1983) Optical thickness features of the El Chichon stratospheric debris cloud. Proceedings 5th. AMS Conference on Atmospheric Radiation, Baltimore.

Etheridge, D.M., Patterson, G.R. and Platt, C.M.R. (1984) Solar Radiation - research. In R.J. Francey (Ed.). Baseline 1981-82. Department of Science and Technology, Canberra.

Frohlich, C. and Shaw, G.E. (1980) New determination of Rayleigh scattering in the terrestrial atmosphere. Applied Optics 19, (11).

Hofmann, D.J. and Rosen, J.M. (1983) Sulphuric acid droplet formation and growth in the stratosphere after the 1982 eruption of El Chichon. Science, 222, 325 -327.

Matsubara, K. and Kawaguchi, S. (1983) Spectral extinction measurement by sunphotometer at Syowa station, Antarctica. Memoirs of National Polar Research Institute Spec. Issue, 29 [Japan].

Mitchell, J.M. (1982) El Chichon, weather maker of the century? Weatherwise, 35, (6)

Shaw, G.E. (1982) Atmospheric turbidity in polar regions. Journal of Applied Meteorology, 21, (8) 1080-1088.

Spinhurne, J.D. (1983) El Chichon eruption cloud: latitudinal variation of the spectral optical thickness for October 1982. Geophysical Research Letters, 10, (9), 881-884.

C. MECHANICAL PROPERTIES OF SNOW AND ICE

The study of the physical and mechanical properties of ice is fundamental for an improved understanding of dynamics of large ice masses. The effect of temperature, stress, crystal size and crystal orientation on the flow of ice needs to be studied in various stress configurations, for comparison with Antarctic field data.

Recent Australian studies have examined ice deformation in compression and in simple shear, and several papers recently published have examined the minimum and tertiary creep rates of ice at various stresses and temperatures, and the effect on these creep rates of crystal size and orientation.

It has been found however that to attain strain rates for the low stresses and temperatures typical of the Antarctic ice sheet, laboratory experiments need to run for several decades. Thus alternative techniques are being devised to measure strain rates at these conditions. Further studies in the laboratory aim at investigating crystal structure in ice sheets. This is being done by carrying out tests which simulate the deformation in the ice sheet, and also by studying the micro-structure of recrystallizing grains within deforming samples.

Future plans include estimation of strain rates at low stresses and temperatures, studies of the effect of ice sample-platten bonding, comparison of various stress configurations, and comparison of laboratory results, including crystal size, with those from Antarctic ice cores and borehole studies.

Australian studies of snow mechanics have resulted as a consequence of recent recommendations for a snow runway capable of use by wheeled inter-continental aircraft.

Further on-site and laboratory experimentation on the engineering properties of snow is plannned.

T.H. Jacka

15. ENGINEERING PROPERTIES OF SNOW

D.S. Russell-Head
Faculty of Engineering, The University of Melbourne
Parkville, Victoria, 3052.

ABSTRACT

An important engineering property of Antarctic snow is its ability to resist surface penetration. Wheel loadings on laboratory-made snow and Antarctic snow have been assessed by bearing tests. The prospects for constructing a compressed snow runway near Casey for use by heavy aircraft are discussed.

15.1 INTRODUCTION

Recent Australian interest in developing a direct Australia-Antarctica air link has promoted a study of the mechanical properties of compressed snow. The main requirements of a compressed snow runway for use by wheeled aircraft are:
(a) a sufficiently high bearing capacity to prevent bogging of wheels
(b) a sufficiently high tyre/surface friction for safe handling of the aircraft, and
(c) sufficiently long and wide runway for safe take-off and landing.
This brief paper outlines the results of laboratory and field work on the first of these requirements.

15.2 LABORATORY TESTS

The laboratory work on compressed snow by Russell-Head and others (1982) focussed on the compressibility of disaggregated snow and the bearing strength of compacted snow as measured by the California Bearing Ratio test (Standards Association of Australia, 1977). The general outcomes of the testing program were:
(a) compaction of disaggregated snow is more easily achieved by static loading than by impact loading, and
(b) the California Bearing Ratio (CBR) strength increases rapidly with density.

An analysis of previously published data for processed Greenland snow (Abele, 1963) in conjuction with the laboratory data suggested the existence of power law relationships connecting snow density, CBR strength and rammsonde hardness. The snow type, temperature, and age determine the exponent in the power relationships. As an example, for aged snow at -5 ^{o}C, the CBR increases approximately with the fifth power of the density, and the rammsonde hardness value increases approximately with the square of the CBR.

15.3 FIELD TESTS

Field construction tests were undertaken at Lanyon Junction near Casey in the 1983-84 summer. The main results from the equipment trials showed that:

(a) snow is very easily compacted to high densities when moisture is present.
(b) disaggregation of the in situ material by a Schmidt snow miller increases the average density of the snow from 0.48 to 0.61 Mg m^{-3}. The density increase is due to a broadening of the distribution of snow grain sizes.
(c) a laser controlled grader can readily level-off processed snow to produce a pavement surface to a specified grade.

A snow pavement some 250 mm thick produced with the construction equipment was tested for density, CBR and plate bearing capacity and creep. The density averaged 0.69 Mg m^{-3}, and the average CBR was 40%. The average CBR of the in situ material under the pavement was about 10%. A circular steel plate was loaded to the wheel load of a nearly fully laden C-130H (Hercules) aircraft. The diameter of the plate was 600 mm, which is about 2% less than the tyre contact diameter at maximum aircraft mass and for tyre pressures of 586 kPa (85 psi).

The short term penetration (after a few second's loading) of the plate into the pavement was less than 3 mm. The settlement after some 2.5 hour's loading was less than 14 mm. The creep settlement is plotted on logarithmic scales in Figure 1.

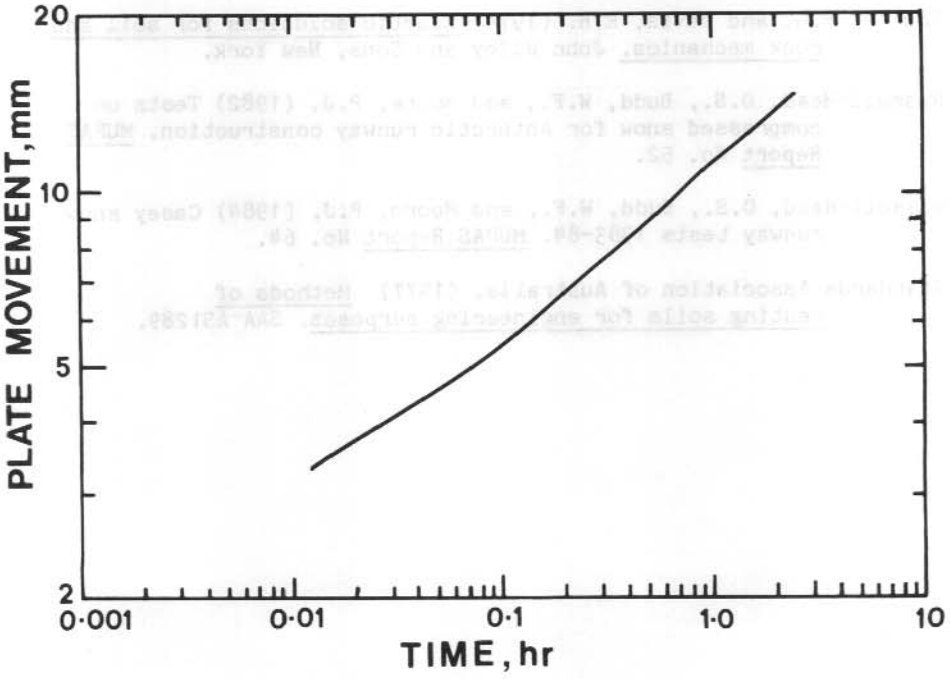

Figure 1. Plate bearing data plotted on logarithmic scales. (Plate diameter = 600 mm, static load = 16.2 Mg, pressure = 562 kPa)

The settlement calculated by a two-layer elastic model (Poulos and Davis, 1974) of the pavement and subgrade is about 3 mm. This value is compatible with the observed settlement at a few minute's loading when the effects of the test pavement surface roughness are taken into account (Russell-Head and others, 1984). The elastic constants used in the analysis were derived from the CBR load/displacement curves (Russell-Head and others, 1982). This outcome confirms the utility of the CBR method for predicting the bearing capacity of snow, and also supports the use of the two-layer method for predicting the performance of a compacted snow pavement.

15.4 CONCLUSIONS

The prospects for contructing a compacted snow runway at Lanyon Junction are excellent from the snow mechanics point of view. The optimization of techniques for producing a pavement of full runway dimensions (50 m by 3000 m) needs to evolve from on site experimentation with the selected construction equipment.

REFERENCES

Abele, G. (1963) A correlation of unconfined compressive strength and ram hardness of processed snow. U.S.A. CRREL Technical Report 85.

Poulos, H.G. and Davis, E.H. (1974) Elastic solutions for soil and rock mechanics. John Wiley and Sons, New York.

Russell-Head, D.S., Budd, W.F., and Moore, P.J. (1982) Tests on compressed snow for Antarctic runway construction. MUPAS Report No. 52.

Russell-Head, D.S., Budd, W.F., and Moore, P.J. (1984) Casey snow runway tests 1983-84. MUPAS Report No. 64.

Standards Association of Australia. (1977) Methods of testing soils for engineering purposes. SAA AS1289.

16. THE EFFECT OF SAMPLE LENGTH AND DIAMETER ON ICE MINIMUM CREEP RATES IN COMPRESSION

S.A. Williams
Meteorology Department, The University of Melbourne
Parkville, Victoria, 3052.

T.H. Jacka
Antarctic Division, Department of Science
Kingston, Tasmania, 7150.

ABSTRACT

Uniaxial compression tests were performed on cylindrical ice samples of various lengths and diameters. All tests were carried out at -5.0 ± 0.2 ^{o}C and under an octahedral shear stress of 0.25 MPa. Sample diameters ranged from 16.2 to 64.9 mm while lengths were 17.4 to 132.3 mm. It was found that minimum flow rate was dependent on sample diameter, yet independent of length. The studies also revealed no crystal size dependence on flow rate, and infact no sample size/crystal size ratio dependence.

16.1 INTRODUCTION

Most laboratory studies of the uniaxial compressive deformation of cylindrical ice samples have assumed no dependence of sample size or shape on flow rates. Recommendations to constrain sample length, L, to diameter, D, ratios to within the range 3 ± 1 in order to avoid end effects and geometric instabilities have been made by several researchers (Mellor and Cole, 1982; Jones and Chew, 1983; Jacka, 1984). To these authors knowledge, no systematic study of the effect of sample shape or size on ice deformation exists, although similar studies have been carried out on other solids (Hawkes and Mellor, 1970).

Typically, uniaxial compression is applied through a platen or plunger such that a bond is created between the platen and the test material. This radially constrains the sample at the end planes, producing a non uniform stress field within the sample. A uniform stress field, compatible with the applied load will only exist if the sample is completely unrestrained along its entire length.

This study investigates whether or not the degree of non uniformity of the stress field created by end bonding is affected by sample shape and/or size. Apparent minimum ice strain rates are examined at a fixed stress and temperature and with end constraint, using samples of various shapes and sizes.

16.2 EXPERIMENTAL TECHNIQUE

Polycrystalline ice samples were prepared by the method described by Jacka and Lile (1984). Moulds of 25.4 mm and 100 mm diameter were used and the samples were turned down to the required diameter on a lathe. The compression apparatus used was the direct load apparatus described

by Jacka and Lile. An octahedral shear stress of 0.25 MPa was applied to all samples and the temperature was held constant at -5.0 ± 0.2 °C throughout the tests. Bakelite platens of greater diameter than the test samples were used, and the samples bonded to the platens.

Two separate grain sizes were chosen to study the effect of this parameter, and of sample size to grain size ratio on the deformation rate. Grain diameter was determined by counting the number of grains per unit area and assuming circular cross sections. This procedure was chosen for comparison with that of Jones and Chew (1981, 1983). Universal stage measurement showed that crystal c-axis orientations were approximately random for all test samples.

A total of twenty-five samples were tested, of which fifteen had lengths of approximately 65 mm and diameters varying from 16.2 to 64.9 mm. Twelve samples having diameters of 25.4 mm, had lengths varying between 17.4 mm and 132.3 mm. Some sample sizes were duplicated to allow the effect of sample diameter to grain size to be examined by using two different grain sizes. The effect on the flow rate of sample diameter, of length and of sample diameter to grain size ratio were each able to be assessed independently.

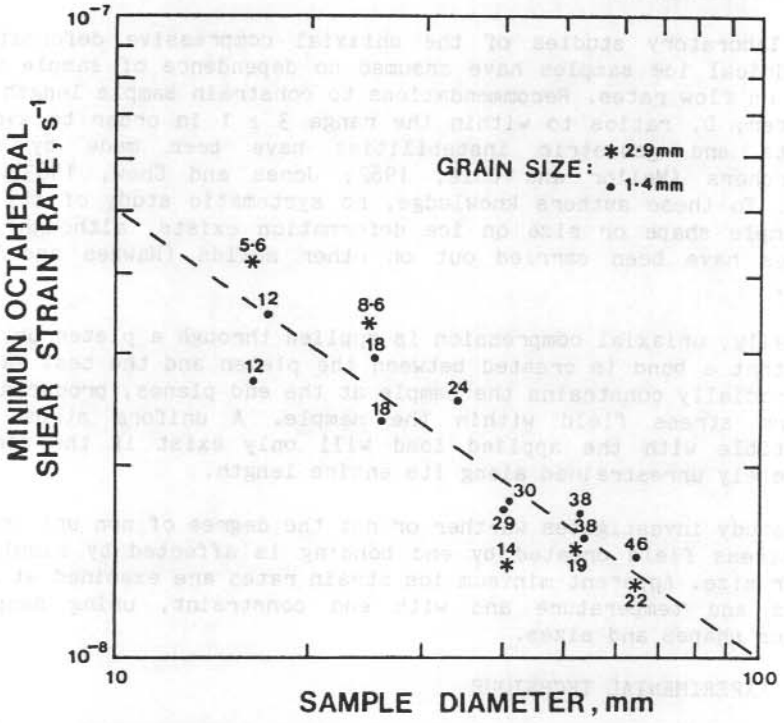

Figure 1. Minimum octahedral shear strain rate plotted as a function of sample diameter on log scales. The numbers beside each point indicate the sample size to crystal size ratio.

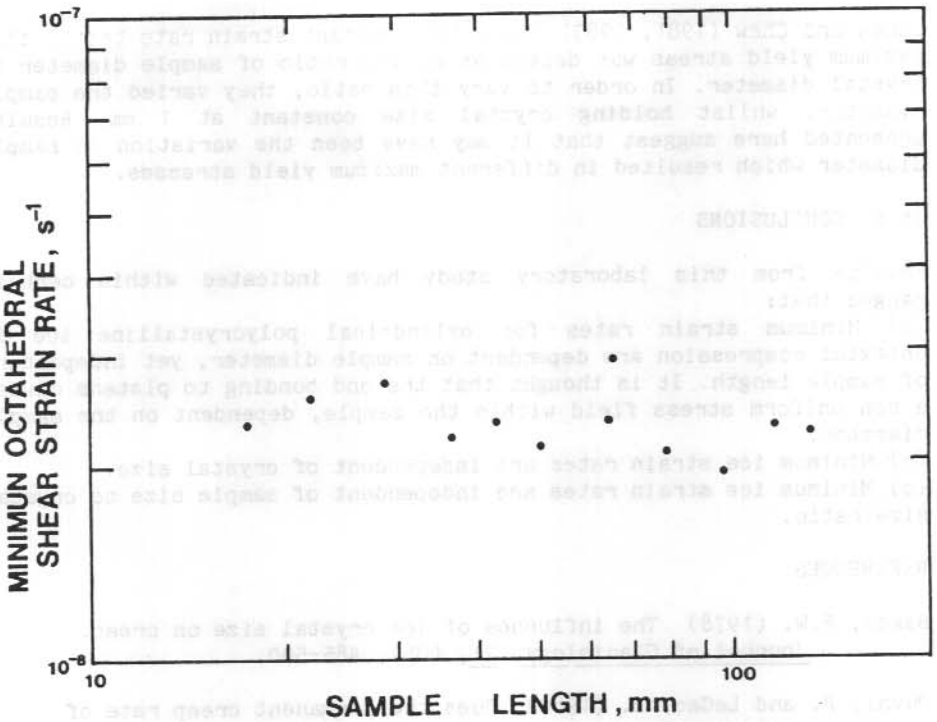

Figure 2. Minimum octahedral shear strain rate plotted as a function of sample length (for constant diameter) on log scales.

16.3 RESULTS

Figure 1 is a plot of log minimum octahedral shear strain rate as a function of log sample diameter, for the constant length tests. It is apparent that the larger the sample diameter, the smaller the minimum strain rate. Linear regression analysis of the plotted points on log scales gives a correlation coefficient, $r = 0.91$, suggesting that over the range of diameters examined,

$$\dot{\varepsilon}_{o_{min}} = f\,(D^{-0.7}).$$

The numbers with each data point represent the ratio of sample diameter to grain diameter. There is no indication of this parameter affecting the minimum strain rate.

Figure 2 is a plot of log minimum octahedral shear strain rate as a function of log sample length for tests on ice with constant diameter (25.4 mm). No dependence of minimum strain rate on sample length is revealed.

Jones and Chew (1981, 1983) found for constant strain rate tests, that maximum yield stress was dependent on the ratio of sample diameter to crystal diameter. In order to vary this ratio, they varied the sample diameter, whilst holding crystal size constant at 1 mm. Results presented here suggest that it may have been the variation in sample diameter which resulted in different maximum yield stresses.

16.5 CONCLUSIONS

Results from this laboratory study have indicated within certain ranges that:

(a) Minimum strain rates for cylindrical polycrystalline ice in uniaxial compression are dependent on sample diameter, yet independent of sample length. It is thought that the end bonding to platens causes a non uniform stress field within the sample, dependent on the sample diameter.

(b) Minimum ice strain rates are independent of crystal size.

(c) Minimum ice strain rates are independent of sample size to crystal size ratio.

REFERENCES

Baker, R.W. (1978) The influence of ice crystal size on creep. Journal of Glaciology, 21, (85), 485-500.

Duval, P. and LeGac, H. (1980) Does the permanent creep rate of polycrystalline ice increase with crystal size? Journal of Glaciology, 25, (91), 151-157.

Hawkes, I. and Mellor, M. (1970) Uniaxial testing in rock mechanics laboratories. Engineering Geology, 4, 179-285.

Jacka, T.H. (1984) The strain and time required for development of minimum ice strain rates. Cold Regions Science and Technology, 8, (3), 261-268.

Jacka, T.H. and Lile, R.C. (1984) Sample preparation techniques and compression apparatus for ice flow studies. Cold Regions Science and Technology, 8, (3), 235-240.

Jones, S.J. and Chew, H.A.M. (1981) On the grain size dependence of secondary creep. Journal of Glaciology, 27, (27), 517-518.

Jones, S.J. and Chew, H.A.M. (1983) Effect of sample and grain size on the compressive strength of ice. Annals of Glaciology, 4, 129-132.

Mellor, M, and Cole, D. (1982) Deformation and failure of ice under constant strain-rate. Cold Regions Science and Technology, 5, (3), 201-219

Jones, S.J. and Chew, H.A.M. (1983) Effect of sample and grain size on the compressive strength of ice. Annals of Glaciology, 4, 129-132.

Mellor, M, and Cole, D. (1982) Deformation and failure of ice under constant strain-rate. Cold Regions Science and Technology, 5, (3), 201-219

17. STUDIES OF THE EFFECT OF STRESS AND TEMPERATURE ON THE SHAPE OF ICE CREEP CURVES

T.H. Jacka
Antarctic Division, Department of Science
Kingston, Tasmania, 7150.

ABSTRACT

It has been established elsewhere (Mellor and Cole, 1982; Jacka, 1984) that plots relating time, strain and strain rate for ice deformation exhibit similar curves.

In this paper, strain curves reported by Jacka (1984) are normalised such that the minimum strain rate, and the strain to minimum strain rate are forced to values of 1.

These normalised raw data exhibit a scatter of points which are discussed in terms of test temperature and stress.

17.1 INTRODUCTION

Mellor and Cole (1982) and Jacka (1984) have demonstrated over a large temperature (-5.0 to -32.5 ^{o}C) and stress (0.1 to 3.0 MPa) range, that log-log plots of strain or of time against strain rate for isotropic ice in uniaxial compression, exhibit families of similar curves. Similar curves also result from laboratory experiments in uniaxial extension (Jacka and Maccagnan, 1984) and in simple shear (Russell-Head and Budd, 1979).

Laboratory measurements have not been accurate enough to clearly ascertain whether the curves within each family have been identical in shape. Here the raw strain vs. strain rate data for the suite of results are studied, and indications of possible effects of stress and temperature are examined.

17.2 NORMALISATION

For each data set, the strain rates throughout the experiment were divided by the minimum strain rate, along with division of the strains by the strain at minimum. Various techniques may be devised for estimating the minimum of a set of data points exhibiting experimental scatter. For this exercise, the minimum strain rate was taken as the minimum of a 5 point binomially weighted running mean through the raw data. The above process (eqivalent to linearly shifting the data sets on log-log scales) forces curves through the data to pass through the point (1, 1) on arbitrary scales to which each experiment can be fitted independently.

17.3 THE EFFECT OF STRESS AND TEMPERATURE

Figures 1-4 show the normalised data sets for experiments at (1) -5.0, (2) -10.6, (3) -17.8 and (4) -32.5 ^{o}C for, in each case, a range of stresses. It is apparent that stress does not significantly affect the

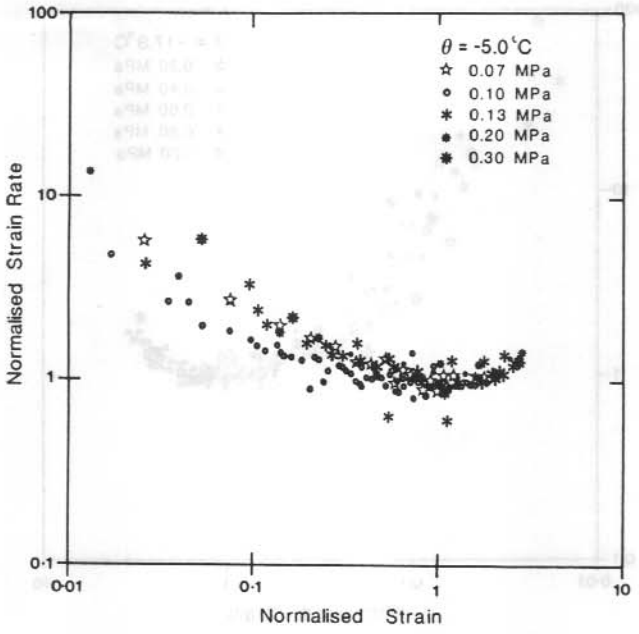

Figure 1. Raw data plots of minimum strain rate as a function of strain on log scales for data at -5.0 ^{o}C. Data has been normalised to a smoothed minimum strain rate of 1.

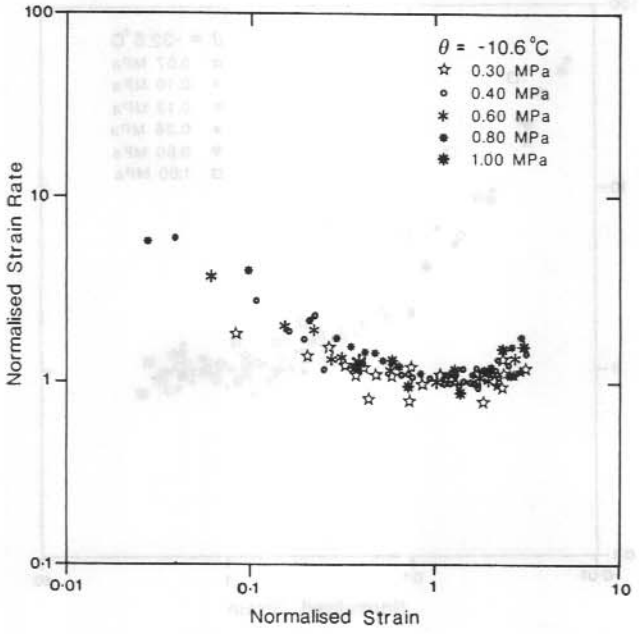

Figure 2. Normalised data at -10.6 ^{o}C

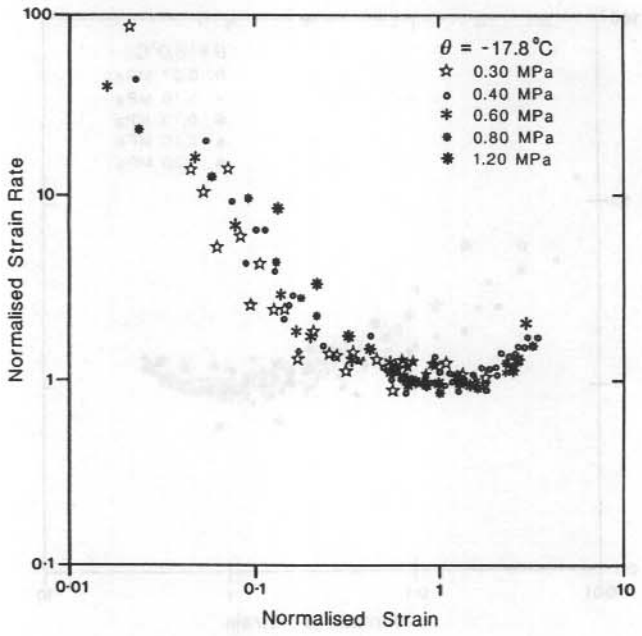

Figure 3. Normalised data at -17.8 °C

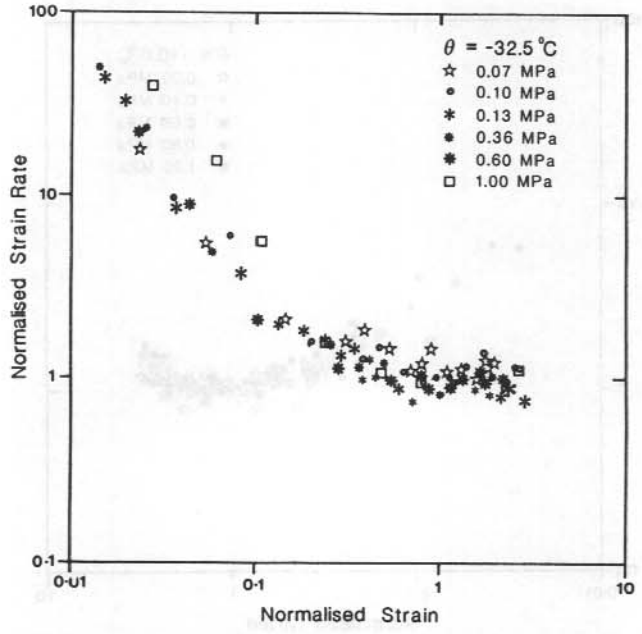

Figure 4. Normalised data at -32.5 °C

shape of the strain curve, there being little variation within each temperature data set. The shape of the transient section of the ice deformation curve however, appears to be temperature dependent, with a relatively slower approach to minimum strain rate at warm temperatures. Characteristic creep curves, independent of stress, may then be constructed for the data, however their detailed dependence on temperature remains unknown until further, more accurate measurements are made.

Further comparisons of these characteristic curves with experiments at lower temperatures and stresses are required. In particular, the transient flow which occurs prior to minimum creep rate, needs careful, accurate measurement in order to ascertain the exact nature of the ice creep curve.

REFERENCES

Jacka, T.H. (1984) The time and strain required for development of minimum strain rates in ice. Cold Regions Science and Technology, 8, (3), 261-268.

Jacka, T.H. and Maccagnan, M. (1984) Ice crystallographic and strain rate changes with strain in compression and extension. Cold Regions Science and Technology. 8, (3), 269-286.

Mellor, M. and Cole, D. (1982) Deformation and failure of ice under constant stress or constant strain-rate. Cold Regions Science and Technolgy, 5, 201-219.

Russell-Head, D.S. and Budd, W.F. (1979) Ice-sheet flow properties derived from bore-hole shear measurements combined with ice-core studies. Journal of Glaciology, 24, 117-130.

creep rate versus strain curves.

The fabric diagram in Figure 2 is typical of the four fabrics at 40% octahedral shear strain (100% simple shear strain). The minimum strain rate occured at about 1% octahedral strain, and the maximum was at about 8%. The ratio between minimum and maximum strain rates was about 7.

The type of fabric developed for this fairly large shear strain (Figure 2) is not compatible with the fabrics observed in the shear zones in ice sheets (Russell-Head, 1979) and the question of the appropriateness of the apparatus to adequately mimic the shear zone deformation needs to be raised. The apparatus (Figure 3) consists of two stiff plates separated with bearing balls. The top plate is constrained to move parallel to the bottom one and the distance between them is constant. This arrangement induces a constant volume deformation.

The geometry of the ice sample alters during the deformation and gives rise to an imbalance of the volume of ice essentially in compression and that which is essentially in tension. Additionally, the constraint of the plates to move at a constant separation distance may induce secondary (and unknown) forces at the boundary of the ice sample.

A new arrangement of the shear plates is shown in Figure 4. The plates are cranked so that the external loads are applied collinearly. The absence of the load induced torque avoids the necessity of any external constraint to maintain parallelism of the plates, and therefore imposes no constraint on the thickness of the ice sample. However, the altered geometry (and therefore altered stress distribution) at large deformations is still present with the proposed apparatus.

18.3 CONTINUING STUDIES

A series of experiments needs to be performed to define the role of boundary geometry in the deformation sequence. Once this effect is quantified, the simple shear flow law for ice can be formulated. Comparisons can then be made with the compression and tension flow laws, when boundary effects in those experiments are taken into account.

ACKNOWLEDGMENTS

I am grateful to T. Jacka and M. Maccagnan for providing the randomly oriented polycrystalline ice for the tests. M. Maccagnan also contributed significantly to the preparation of the experiments. R. Thwaites measured orientation data for a number of the deformed samples.

REFERENCES

Glen, J.W. (1955) The creep of polycrystalline ice. Proceedings of the Royal Society, Series A, 228, (1175), 519-538.

Jacka, T.H. and Maccagnan, M. (1984) Ice crystallographic and strain rate changes with strain in compression and extension. Cold Regions Science and Technology, 8, (3), 269-286.

Russell-Head, D.S. (1979) Ice sheet flow from borehole and laboratory studies. M.Sc Thesis, Meteorology Department, The University of Melbourne.

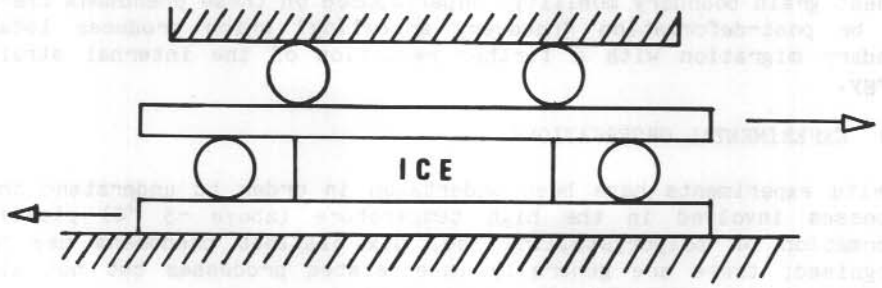

Figure 3. Outline sketch of a constant thickness simple shear apparatus.

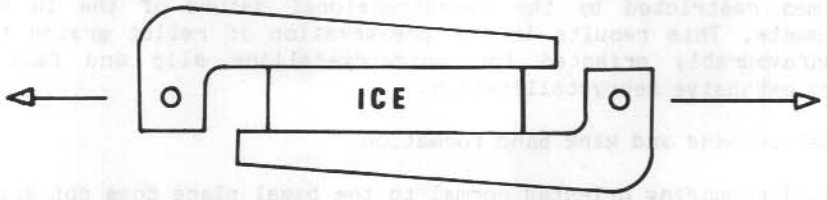

Figure 4. Outline sketch of a torque balanced variable thickness shear apparatus.

19. IN SITU RECRYSTALLIZATION OF POLYCRYSTALLINE ICE

C.J.L. Wilson, J.C. Mitchell and J.P. Burg
Geology Department, The University of Melbourne
Parkville, Victoria, 3052.

ABSTRACT

Experimental deformation of ice above -5 °C produces dynamic recrystallization by rotation of subgrains and/or bulging of new high angle or pre-existing boundaries, through a process of migration recrystallization. Recrystallized grains in the boundary of an old grain undergo the greatest degree of rotation and also show the highest grain boundary mobility. Superimposed on these phenomena there may be post-deformation "recovery annealing" which produces local boundary migration with a further reduction of the internal strain energy.

19.1 EXPERIMENTAL OBSERVATIONS

In situ experiments have been undertaken in order to understand the processes involved in the high temperature (above -5 °C) plastic deformation of polycrystalline ice. Six distinct phenomena may be recognised; these are generally interrelated processes but not all occurring in any one grain at any given time.

Initial grain boundary adjustments

Contemporaneous with the occurrence of intracrystalline slip on (0001), pre-existing boundaries may become serrated prior to any marked c-axis orientation change within a grain. These boundary adjustments are particularly obvious below -5 °C.

Slip band formation and grain rotations

Slip lamellae develop in favourably oriented grains in the first 1% of shortening and these grains undergo a substantial grain rotation. Glide within individual crystals is not uniform across the entire grain. This is strongly suggested by the development of undulose extinction of small steps on grain boundaries. Grain rotation is sometimes restricted by the two-dimensional nature of the in situ experiments. This results in the preservation of relict grains that are unfavourably oriented for intracrystalline slip and fail to undergo extensive recrystallization.

Deformation band and kink band formation

Deformation banding oriented normal to the basal plane does not appear in every grain. Kink bands occur only in highly anisotropic shaped grains after there has been extensive intracrystalline glide or in strongly oriented grain aggregates.

Grain nucleation

New grain nucleation, between adjacent highly misoriented grains, appears to occur at intergranular sites and not within grain interiors. Nucleation of such grains is preceeded by appreciable lattice bending adjacent to the grain boundary and involves progressive subgrain rotation.

Dynamic grain boundary migration

After a new grain has been nucleated it is capable of undergoing rapid grain growth consuming both the old grains and other newly nucleated grains. Boundaries that have undergone early migration may continue to undergo adjustments. A bulge forms as a lobe that migrates into the neighbouring grain. The bulge migration cuts across the (0001) basal lamellae of the invaded grain and it does not appear to be an orientation controlled migration.

Annealing recrystallization

All the changes described above involve dynamic recrystallization processes with the nucleation and growth of strain free grains at the expense of neighbouring plastically strained grains. However, "recovery annealing" is grain growth that follows deformation and occurs after the deformed sample has been unloaded, with the maintenance of the deformation temperature.

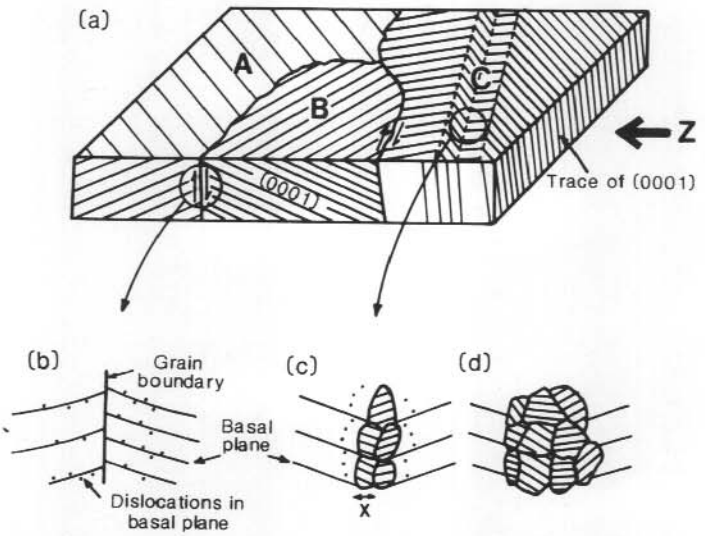

Figure 1. Schematic illustration to explain the origin of the dynamic recrystallization features during the in situ deformation. (a) shows the general relationship between the three grains A, B and C to the shortening direction, Z. (b - d) is a general sequence of recrystallisation events that may be observed at a grain boundary or kink band boundary.

19.2 DISCUSSION AND CONCLUSIONS

Recrystallization features are concentrated along pre-existing anisotropies or in grain boundary regions, and can take the form of grain boundary bulging, intragranular nucleation or dynamic recrystallization by rotation. For ice deformed at temperatures above -5 ^{o}C no clear distinction can be made as to whether migration recrystallization versus dynamic recrystallization by rotation is the dominant process. The model in Figure 1 accounts qualitatively for the behaviour of the ice. The dynamic recrystallization is achieved principally via progressive subgrain rotation where nuclei are able to grow provided their misorientation with respect to the neighbours becomes high enough. There is no clear evidence nor reason to invoke the classical heterogeneous nucleation processes to explain the nuclei in deformed ice aggregates.

D. NUMERICAL MODELLING OF ICE MASSES

New Developments

The application of computer modelling to studies of the Antarctic Ice Sheet has been greatly advanced in recent years by new data from field observations and laboratory studies of ice as well as new computer techniques. The coarse "whole Antarctic" derived characteristics survey for the present regime by Budd and others (1971) is being recomputed with higher resolution (20 km compared to the earlier 200 km) using the recent data from the new SPRI maps by Drewry (1983) as well as the new Australian data. A regional component of this study for a part of West Antarctica is addressed by Jenssen and Budd (this volume) and Budd and others (this volume). The new approach is extensively automated using large digitising pads with comprehensive computer data analysis programs and plotting routines. A comparison of the application of the new techniques with the older manual methods has been provided for Greenland by Radok and others (1982) and Budd and others (1982).

The initial approach of starting from a steady state analysis in absence of measured velocities and past time changes, although still useful, has been greatly extended. The analysis of individual borehole and flowline data including non-steady state changes has become routine along the lines indicated by Budd and Young (1983).

The deep ice core data and numerical modelling have provided information on the past changes of the climate and the ice sheets to allow testing of non-steady state dynamic modelling of the interaction of the ice sheets with the global climate. The three dimensional modelling studies of the paleo- North American Ice Sheet and the Antarctic Ice Sheet by Budd and Smith (1981, 1982) indicated how the climate, the ice sheets and sea level may have changed since the last interglacial (about 120 ka BP), and provided strong support for the Earth's orbital radiation changes as the major cause of the ice ages' initiation and demise. The more recent work presented here extends this study back to 500 000 years BP and shows close agreement between the model results and the ocean sediment isotope record. This now presents a challenge to find more clear confirmation of these past changes from the deep Antarctic ice cores.

Current activities

The large scale modelling has highlighted the importance of the major ice streams and outlet glaciers in controlling the ice cap balance and response to change. The deep ice stream basins of West Antarctica, found to be most sensitive in this regard are therefore a key to the response of the Antarctic to future climatic change. For these fast flowing ice streams and glaciers, basal sliding is dominant and needs to be appropriately modelled. The papers by Budd and others (1984, this volume) and by Jenssen and Budd (this volume) attempt to model the present flow with sliding in West Antarctica and to address the question of the present state of balance. At this stage observed velocities for the ice streams are still not available. The new

measurements of surface velocity of the ice sheet from the traverses (Budd and Young, 1979; Young, 1979; Jones and Davis, this volume; Jones and Hendy, this volume; Medhurst, this volume; Hamley, this volume) plus the measurements of ice flow properties in the laboratory (Russell-Head and Budd, 1979; Jacka, 1984; Jacka and Maccagnan, 1984; Williams and Jacka, this volume; Jacka, this volume; Russell-Head, this volume) are providing a wide range of data to check the computation of the ice sheet velocities from the flow law relations together with the stress and temperature of the ice. It is now recognised that anisotropy and tertiary flow are more relevant to ice sheet flow than minimum creep rates for isotropic ice. The numerical modelling needs to take this into account and also needs to address the question of the development of the crystal anisotropy in the ice sheet.

The series of boreholes along the Law Dome flowline provide a unique data set for determining the way in which the crystal structure develops and the influence of that structure on the ice flow. The ice core and borehole studies of Russell-Head and Budd (1979), Young and others (this volume), Morgan and McCray (this volume) and Etheridge and McCray (this volume) show the existing in situ crystal structure with the strong single maximum vertical c-axis crystal orientations well above the base corresponding to the high horizontal shear rates in the boreholes.

The finite element numerical modelling technique used by Budd and Rowden-Rich (this volume) provides a first attempt at understanding the complex stress distribution in the flow of ice over a rough bed. The resulting stress distribution can be considered as the primary cause of the development of the anisotropic crystal structure. Then, through the feedback of the crystal structure on the ice flow and the time dependent Langrangian flow of the ice through the stress field, an interactive finite element model with crystal development may be devised and coupled with a flowline model to trace particle paths through the ice sheet. Such detailed calculations are needed to help interpret the basal layer isotope profiles now determined in the several boreholes near Cape Folger as given by Budd and Morgan (1977) and Morgan (this volume).

Future activities

The extensive amount of new data collected in recent years makes it now timely to use the various new modelling techniques for a number of specific applications.

(a) Law Dome summit to Cape Folger flowline

The new borehole data for isotopes, deformation and crystal fabrics make it ideal for a new detailed flowline study to derive more accurate particle paths and ages.

(b) Law Dome 3D model

The Law Dome data now collected have become sufficiently comprehensive

to construct a 3D model with resolution down to about 5 km. An initial balanced state could be examined and there is sufficient surface velocity data to check the balance and the computations for dynamics velocity.

(c) Vanderford Glacier 2D and 3D models

The new data of surface, bedrock and ice velocities are ideal for use in constructing a model to examine the transition from slow ice sheet flow, where internal deformation dominates, to fast outlet glacier flow, dominated by basal sliding.

The large variations in bedrock topography over the region suggest that a large scale 3D model is needed together with a number of more detailed flowline studies along the major ice streams.

(d) Inland ice sheet - primary IAGP region

The large region of East Antarctica between Dumont d'Urville, Dome C, Vostok, Dome B, and Mirny is now well covered for the basic data required for modelling, and to assess the current state of balance and dynamics. A 3D model of the whole region and a number of detailed flowlines would be appropriate. Of the flowlines the one inland of Casey currently has the most comprehensive data. Other primary flowlines include those inland of Mirny, Dumont d'Urville and the Denman Glacier.

(e) Finite element analysis

There are a number of important problems for which finite element analysis can provide a valuable insight into the features of the ice sheet by the delineation of the stress and strain rate distribution in complex situations. Much can be learned from the use of the two-dimensional vertical section model along a flowline.

Several areas of current interest include:
(i) The Law Dome for the flow of the ice sheet over rough bedrock, e.g. Dome Summit to Cape Folger and on the smaller scale the region of the 4 boreholes near strain grid A.
(ii) The interior ice sheet inland of Casey (where on the large scale, bedrock variations exceed 2 km) offers an important application to see how the ice flows over such topograpy.
(iii) The detailed flowline undulation study. One part of the flowline inland of Casey has a series of prominent bedrock and surface undulations. The ice flow over these undulations has been studied in detail. This provides a particularly valuable data set for use with finite element analysis to study how ice flows over a rough bed.

Budd, W.F., Jacka, T.H., Jenssen, D., Radok, U. and Young, N.W. (1982) Derived physical characteristics of the Greenland Ice Sheet. Publication No. 23. Meteorology Department, The University of Melbourne.

Budd, W.F., Jenssen, D. and McInnes, B.J. (this volume) Numerical modelling of ice stream flow with sliding.

Budd, W.F., Jenssen, D. and Radok, U. (1971) Derived physical characteristics of the Antarctic ice sheet. ANARE Interim Reports Series A (IV) Glaciology, Publication No. 120.

Budd, W.F., Jenssen, D. and Smith, I.N. (1984) A three-dimensional time-dependent model of the West Antarctic ice sheet. Annals of Galciology, 5, 29-36

Budd, W.F. and Morgan, V.I. (1977) Isotopes, climate, and ice sheet dynamics from core studies on Law Dome, Antarctica. IASH Publication No. 118, 312-321.

Budd, W.F. and Rowden-Rich, R.J.M. (this volume) Finite element analysis of two-dimensional longitudinal section flow on Law Dome.

Budd, W.F. and Smith, I.N. (1981) The growth and retreat of ice sheets in response to orbital radiation changes. In: Allison, I. (Ed.), Sea Level, Ice and Climate Change. IASH Publication No. 131, 369-409.

Budd, W.F. and Smith, I.N. (1982) Large scale numerical modelling of the Antarctic Ice Sheet. Annals of Glaciology, 3, 42-49.

Budd, W.F. and Young, N.W. (1979) Results from the IAGP flow-line study inland of Casey, Wilkes Land, Antarctica. Journal of Glaciology, 24, (99), 89-101.

Drewry, D.J. (ed.) (1983) Antarctica: Glaciological and Geophysical Folio. Scott Polar Research Institute, Cambridge.

Etheridge, D.M. and McCray, A.P. (this volume) Dynamics of the Law Dome ice cap from borehole measurements.

Hamley, T. (this volume) Glaciological measurements on the 1983-84 Soviet traverse from Mirny to Dome C.

Jacka, T.H. (1984) The time and strain required for development of minimum strain rates in ice. Cold Regions Science and Technology, 8, (3), 261-268.

Jacka, T.H. (this volume) The effect of the stress and temperature on the shape of ice creep curves.

Jacka, T.H. and Maccagnan, M. (1984) Ice crystallographic and strain rate changes with strain in compression and tension. Cold Regions Science and Technology, 8, (3), 269-286.

Jenssen, D. and Budd, W.F. (this volume) Three-dimensional modelling of ice dynamics in West Antarctica.

Jones, D.J. and Davis, E. (this volume) The Vanderford Glacier topographic survey.

Jones, D.J. and Hendy, M. (this volume) Glaciological measurements in Eastern Wilkes Land, Antarctica.

Medhurst, T.G. (this volume) Glaciological measurements in Western Wilkes Land, Antarctica.

Morgan, V.I. (this volume) Snow accumulation and oxygen isotope records in two adjacent ice cores.

Morgan, V.I. and McCray, A.P. (this volume) Enhanced shear zones in ice flow-implication for ice cap modelling and core dating.

Radok, U., Barry, R.G., Jenssen, D., Keen, R.A., Kiladis, G.N. and McInnes, B. (1982) Climatic and physical characteristics of the Greenland ice sheet. Cooperative Institute for Research in Environment Sciences, University of Colorado, Boulder, Colorado.

Russell-Head, D.S. (this volume) Shear deformation of ice to large strains.

Russell-Head, D.S and Budd, W.F. (1979) Ice-sheet flow properties derived from bore-hole shear measurements combined with ice-core studies. Journal of Glaciology, 24, (90), 117-130.

Williams, S.A. and Jacka, T.H. (this volume) The effect of sample length and diameter on ice minimum creep rates in compression.

Young, N.W. (1979) Measured velocities of interior East Antarctica and the state of mass balance within the I.A.G.P. area. Journal of Glaciology, 24, (90), 77-87.

Young, N.W., Xie Zichu and Qin Dahe (this volume) Multilayer crystallographic structure of Law Dome from ice core analysis.

W.F. Budd

20. NUMERICAL MODELLING OF ICE STREAM FLOW WITH SLIDING

W.F. Budd, D. Jenssen and B.J. McInnes
Meteorology Department, The University of Melbourne
Parkville, Victoria, 3052.

ABSTRACT

Many outlet glaciers and icestreams of Antarctica have basal shear stresses which increase from the interior to a maximum at some considerable distance inland of the grounding line then decrease to near zero at the grounding line. At the same time the velocity continues to increase and in some cases reaches relatively high values while the ice is still grounded. Although transverse and longitudinal stresses need also to be considered, the main control of the flow is the down slope driving stress which is approximately in equilibrium with the basal shear stress. Empirical sliding studies show that the sliding velocities increase also with decreasing normal stress which also occurs in the ice streams as they approach the grounding line. In addition, the basal temperature distribution can strongly influence the sliding. Two-dimensional and three-dimensional modelling of ice stream flow has been used to derive the effective sliding parameters and explain the broadscale dynamics and flow regime of ice streams in West Antarctica and other regions.

20.1 INTRODUCTION

A large part of the ice flux from the Antarctic continent is concentrated into a number of large ice streams. These ice streams are typically associated with deep bedrock depressions connecting to the sea at the coast. In many cases the ice streams are characterised by a basal shear stress maximum at a considerable distance inland of the grounding line. The zone between the decreasing basal shear stress and the grounding line is typically accompanied by a rapidly increasing ice flow velocity. Before the ice streams can be successfully modelled, it is necessary to understand the basis of the dynamics of the high speed ice flow with low basal shear stress and low downslope gravitational driving stress.

One of the most prominent regions of ice stream flow is the West Antarctic Ross Ice Shelf drainage basin. A large amount of basic geophysical data is now available for the region (Jankowski and Drewry, 1981; Drewry, 1983; Budd and others, 1984). This extensive data set makes the region valuable for an analysis of the dynamics of the flow regime even though little data on observed flow velocities over the ice stream region is yet available.

A preliminary analysis of the dynamics of the region by numerical modelling was given by Budd and others (1984). In that analysis it was shown that, as the grounding line was approached, an important factor involved in the increasing velocities, V with decreasing shear stress, τ was likely to be the decreasing normal stress, N. It was also indicated that the basal thermal regime may play an important role in determining the velocity of the ice in the ice streams relative to the

velocity of the surrounding ice. This paper explores that concept further by considering the dependence of ice sliding on the basal temperature.

20.2 MAJOR FEATURES OF THE ROSS ICE SHELF BASIN

The elevation contours shown in Figure 1 with some representative flowlines illustrate chanelling of the ice over the greater part of the basin into 5 major ice streams (A, B, C, D, E) near the grounding

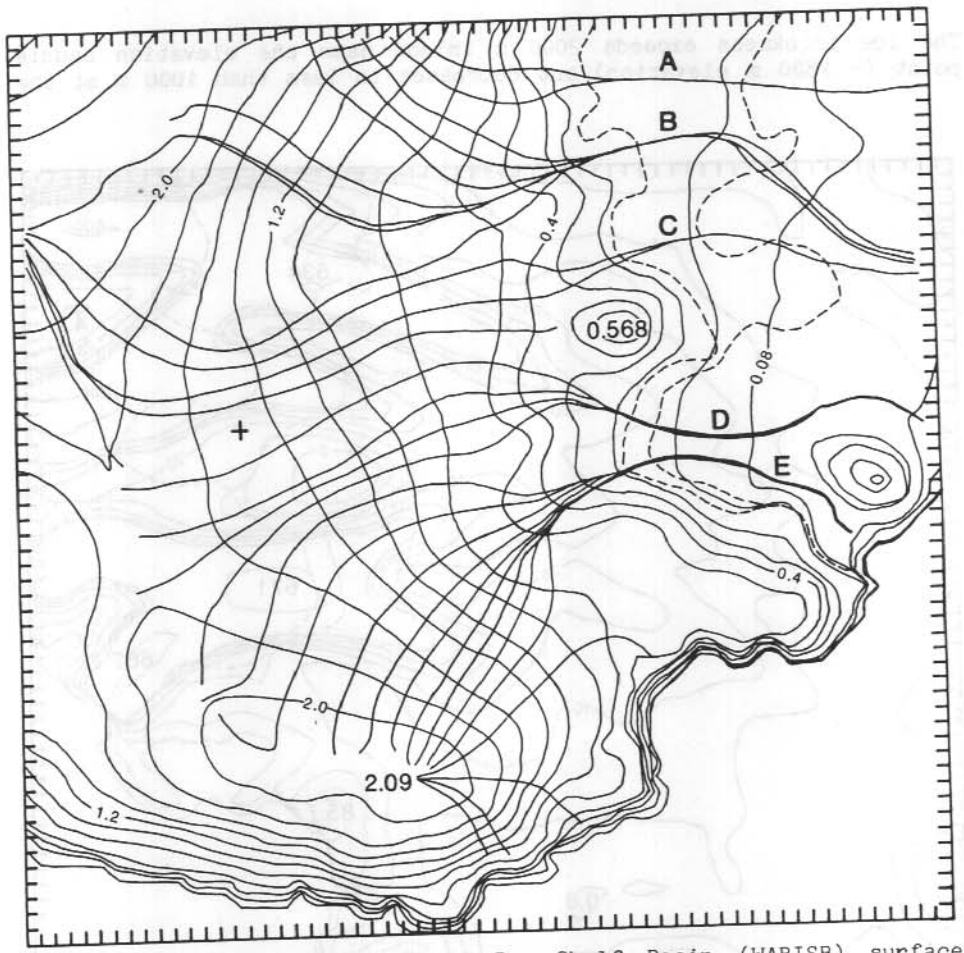

Figure 1. West Antarctic Ross Ice Shelf Basin (WARISB) surface elevation and representative flowlines.
Elevation contours: 20 m intervals to 100 m,
100 m intervals to 500 m,
250 m intervals to 1000 m
then 200 m intervals to 2000 m.
The major ice streams are indicated as A, B, C, D, E. The approximate grounding zone is indicated by the dashed lines.

zone, indicated by the dashed lines. It is also apparent from the elevation contours that there is a region of higher slope along the flowlines located in the vicinity of the 1000 m elevation contour. This corresponds to the region of maximum basal shear stress, τ_b ~ 0.5 to 0.8 bars, which then decreases to ~ 0.1 bars near the grounding line. It is shown by Budd and others (1984) that this zone of decreasing shear stress is also characterised by the basal normal stress (above buoyancy), N decreasing, from the equivalent ice thickness over-burden of Z* ~ 1000 m to ~ 20 m near the grounding line, and with lower values being reached sooner along the ice stream valleys.

The ice thickness exceeds 2000 m inland near the elevation saddle point (~ 1800 m elevation) but decreases to less than 1000 m at the

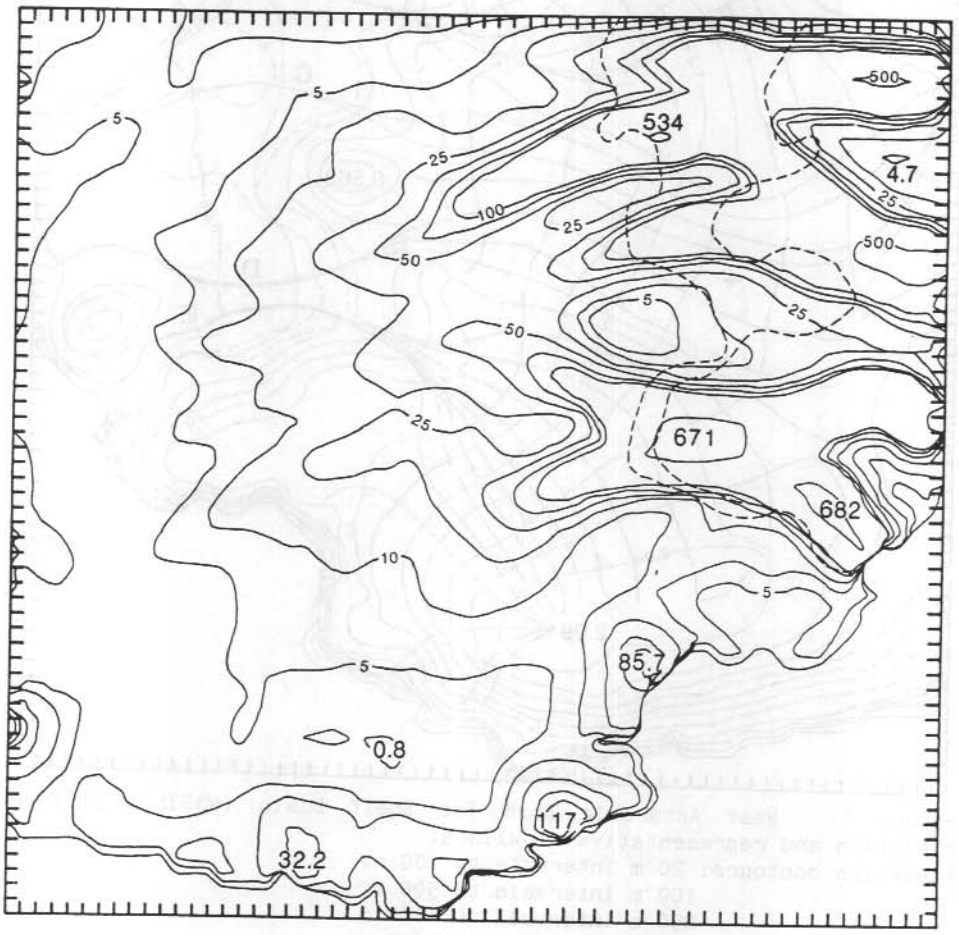

Figure 2. WARISB computed balance velocities (ma^{-1}).

grounding line (~ 100 m elevation). The major ice streams tend to be situated over slight bedrock depressions with slightly thicker ice.

These are the major features relevant to the ice dynamics.

20.3 STATE OF BALANCE OF THE BASIN

The accumulation over the basin tends to increase from 0.15 ma^{-1} (ice) near the centre to greater than 0.3 ma^{-1} near the coast, but tends to decrease towards the Ross Ice Shelf grounding line reaching about 0.1 ma^{-1} on the shelf. The pattern of "balance velocities" computed from the accumulation and flow pattern is shown in Figure 2. Within the ice streams, values in excess of 100 ma^{-1} are reached well inland of the grounding line. Values of 400 to 500 ma^{-1} on the ice shelf where the

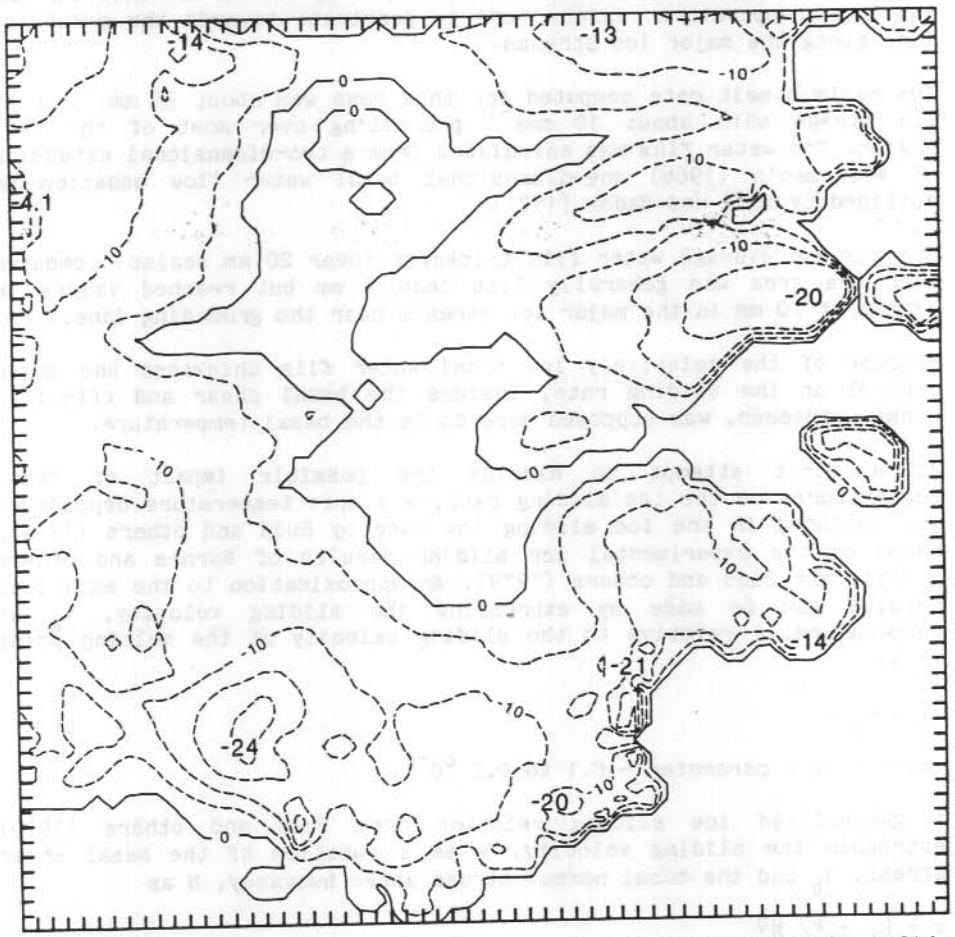

Figure 3. WARISB computed basal temperatures below pressure melting point (^{o}C), using a geothermal gradient of 3.0 $^{o}C/10^{2}m$ and the balance velocities.

ice streams enter are quite compatible with velocities observed on the ice shelf (cf: Thomas and MacAyeal, 1982). This suggests that the present basin regime may be close enough to balance to allow the balance velocities to be used as a useful guide to the pattern of actual velocities.

20.4 THERMODYNAMICS AND ICE SLIDING VELOCITY

Assuming steady state balance, the temperature distribution throughout the ice sheet has been computed as described by Budd and others (1982, 1984). The most important unknown parameter which is required is the geothermal heat flux gradient, γ_G which has a large effect on the basal temperature distribution. The basal temperature distribution calculated with $\gamma_G = 3.0\ ^{o}C/10^{2}$ m is shown in Figure 3.

There is a large melt zone under the very deep ice in the interior and the high temperature regions tend to penetrate towards the grounding line along the major ice streams.

The maximum melt rate computed for this case was about 36 mma^{-1} in an ice stream with about 10 mma^{-1} prevailing over most of the melt region. The water flux was calculated from a two-dimensional extension of Weertman's (1966) one-dimensional basal water flow equation as outlined by Budd and Radok (1971).

The maximum average water film thickness (over 20 km scales) computed over the area was generally less than 5 mm but reached values in excess of 10 mm in the major ice streams near the grounding line.

Because of the relatively low basal water film thickness the major control on the sliding rate, besides the basal shear and effective normal stresses, was supposed here to be the basal temperature.

At a first attempt to examine the possible impact of basal temperatures on the ice sliding rate, a simple temperature dependence was included in the ice sliding law used by Budd and others (1984), based on the experimental ice sliding results of Barnes and others (1971), and Budd and others (1979). An approximation to the empirical results can be made by expressing the sliding velocity, v_θ at temperature, θ relative to the sliding velocity at the melting point v_o as

$$v_\theta = v_o\, e^{\nu\theta}$$

where ν is a parameter ~ 0.1 to 0.2 $^{o}C^{-1}$.

A generalised ice sliding relation from Budd and others (1979) expresses the sliding velocity, v as a function of the basal shear stress, τ_b and the basal normal stress above buoyancy, N as

$$v = k_s\, \tau_b^{p} / N^{q}$$

where p and q are exponents which may vary with stress, and k_s is a parameter which depends mainly on bed roughness. For the Ross Ice

Shelf basin, Budd and others (1984) found that a general trend of computed dynamics velocity which combined ice sliding and internal deformation was found to have a broad similarity with the trend of balance velocities for

$$v = k_s \tau_b / Z^{*2}$$

where $k_s = 5 \times 10^3$ m^3 bar^{-1} a^{-1} and Z* is the effective ice thickness overburden.

Although more general relations were found by McInnes and Budd (1984) to give somewhat better fits to the balance velocity, equation (3) was chosen here because of its simplicity. This relation was therefore combined with the temperature dependence above to give

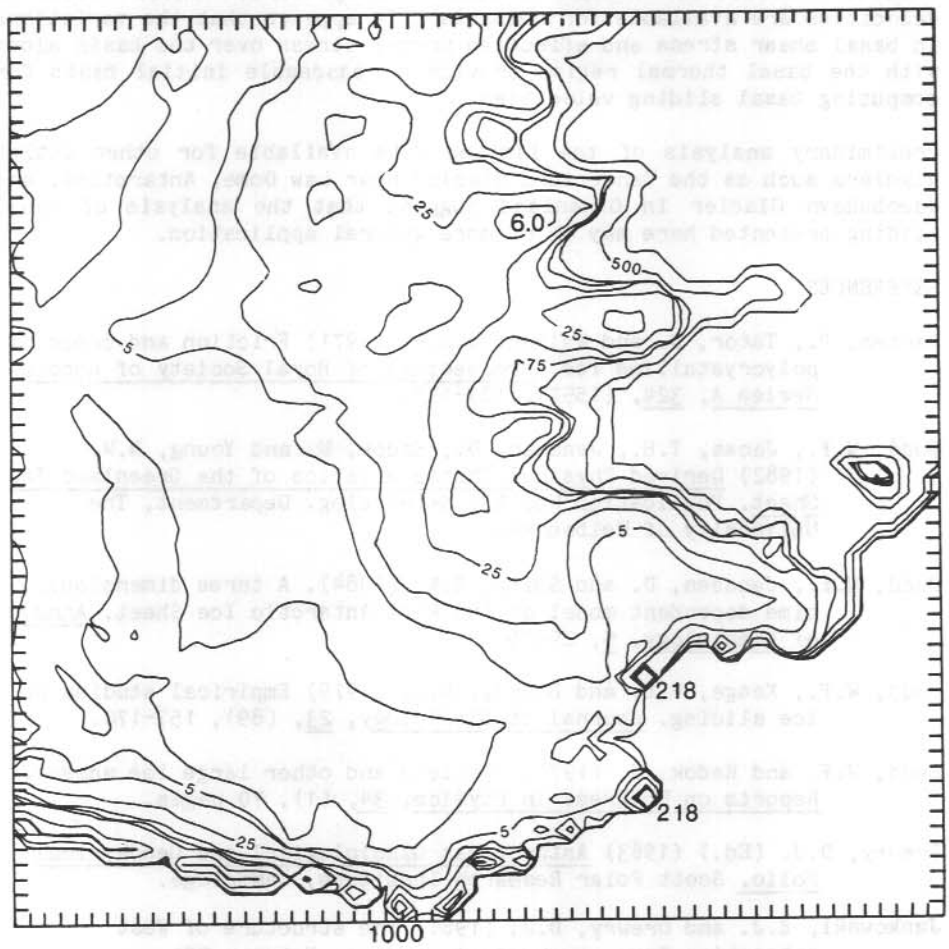

Figure 4. WARISB computed sliding velocities (ma^{-1}), using a temperature dependent sliding relation.

$$v = k_s (\tau_b / Z^{*2}) e^{\nu\theta}.$$

The relation was used with $k_s = 2 \times 10^6$ m^3 bar^{-1} a^{-1}, and $\nu = 0.1$ $^oC^{-1}$, to recompute the sliding velocities over the basin resulting from the temperature distribution shown in Figure 3.

The results are illustrated in Figure 4 which shows a clear enhancement of the sliding velocities within the major ice streams compared to the velocities of the neighbouring ice. The magnitudes of the velocities reached values typically of several hundred ma^{-1} by the grounding zone and are also in broad agreement with the pattern given by the balance velocities.

Further work is still needed to study the feedback between the sliding velocities and the thermal regime. Nevertheless, even though the balance velocities remain somewhat conjectural until observed velocities are available for comparison it appears that the variations in basal shear stress and effective normal stress over the basin along with the basal thermal regime provide a reasonable initial basis for computing basal sliding velocities.

Preliminary analysis of the limited data available for other outlet glaciers such as the Vanderford Glacier near Law Dome, Antarctica, and Jacobshavn Glacier in Greenland suggest that the analysis of basal sliding presented here may be of more general application.

REFERENCES

Barnes, P., Tabor, D. and Walker, J.C.W. (1971) Friction and creep of polycrystalline ice. Proceedings of Royal Society of London Series A, 324, (1557), 127-155.

Budd, W.F., Jacka, T.H., Jenssen, D., Radok, U. and Young, N.W. (1982) Derived Physical Characteristics of the Greenland Ice Sheet. Publication No. 23, Meteorology Department, The University of Melbourne.

Budd, W.F., Jenssen, D. and Smith, I.N. (1984). A three dimensional, time dependent model of the West Antarctic Ice Sheet. Annals of Glaciology, 5, 29-36.

Budd, W.F., Keage, P.L. and Blundy, N.A. (1979) Empirical studies of ice sliding. Journal of Glaciology, 23, (89), 157-170.

Budd, W.F. and Radok, U. (1971) Glaciers and other large ice masses. Reports on Progress in Physics. 34, (1), 70 pages.

Drewry, D.J. (Ed.) (1983) Antarctica: Glaciological and Geophysical Folio. Scott Polar Research Institute, Cambridge.

Jankowski, E.J. and Drewry, D.J. (1981) The structure of West Antarctica from geophysical studies. Nature, 291, (5810), 17-21.

McInnes, B.J. and Budd, W.F. (1984) A cross-sectional model for West Antarctica. Annals of Glaciology, 5, 95-99.

Thomas, R.H. and MacAyeal, D.R. (1982) Derived characteristics of the Ross Ice Shelf, Antarctica. Journal of Glaciology, 28, (100), 397-412.

Weertman, J. (1966) Effect of a basal water layer on the dimensions of ice sheets. Appendix: Water flow at the bottom of an ice mass. Journal of Glaciology, 6, (44), 191-207.

21. THREE-DIMENSIONAL MODELLING OF ICE DYNAMICS IN WEST ANTARCTICA

D. Jenssen and W.F. Budd
Meteorology Department, The University of Melbourne
Parkville, Victoria 3052.

ABSTRACT

A simple method of computing flowlines objectively for any large ice mass is described. By integrating the accumulation along any one flowline, and assuming no change in the ice shape with time, balance velocity along the line is determined. By treating many such lines, the full balance velocity field may be found. The scheme is checked on mathematically prescribed fields for which the analytic velocity is known. The method is then applied to the West Antarctic and the results critically discussed.

21.1 INTRODUCTION

In this short paper a brief outline will be given of how balance velocities may be computed for any glacial ice mass. The theory will be applied first to mathematically specified data, and then to the 'real' data of West Antarctica.

It will be assumed that the basic data sets available are those of surface elevation, E, bedrock elevation, B, and surface accumulation or ablation, A. This information is given for each point of a rectangular grid, which, for convenience, will be assumed to be of equal spacing in both dimensions.

21.2 THE BALANCE EQUATION

The continuity equation for any vertical in the ice mass is:

$$\partial D/\partial t + \nabla \cdot DV = A \qquad \text{---------- (1)}$$

where D is the ice thickness (= E - B) and V is the average horizontal velocity in the column. For steady-state conditions, D is constant in time. Hence

$$\nabla \cdot DV = A \qquad \text{---------- (2)}$$

If now a 'natural coordinate' system is chosen where the X-axis is down the flow, and the Y-axis is orthogonal to this and to the left, then it is easy to show that equation (2) becomes

$$\partial DV/\partial X + DV\ \partial \sin\psi/\partial Y = A \qquad \text{---------- (3)}$$

This is the equation which will be used to determine the balance flow, V.

21.3 DETERMINATION OF FLOWLINES

Since equation (3) applies along flowlines, it becomes necessary to compute the location of these flowlines over the grid area. It is assumed that the flow is down the elevation gradient, so that the flow direction, ψ measured in cartesian coordinates, will be given by

$$\psi = \text{artan}\,[(-\partial E/\partial x)/(-\partial E/\partial y)] \qquad \text{---------} \quad (4)$$

where x and y are the grid (cartesian) axes. With the angles computable in this fashion, the determination of flowlines, through every point of the data grid, proceeds as in Table 1.

21.4 DETERMINATION OF BALANCE VELOCITIES

Now equation (3) is used. Since the flowlines just produced pass through the grid points, only the data there are required, and there is now no need for the time-consuming interpolation between grid points which is necessary when using the exact flowlines. This use of approximate flowlines clearly may be a source of error. In order to gauge how good or bad this scheme may be, analytic data are used as a check on the theory. Section 21.5 addresses this problem.

Table 1. Computation of Flowlines

1. From elevations compute ψ at each grid point.

2. Scan the grid: get the next point which does not have a flowline through it.

3. Using the value of ψ move down the flowline a distance, $\Delta G/10$. (ΔG is the grid spacing).

4. Interpolate to ψ at this new point.

5. Continue until the end of the flowline is reached.

6. Find the first point again and repeat 3 to 5, but this time go up the flowline.

7. Scan the flowline and convert it to a line which passes through the nearest grid points. The flowline is now defined only at these grid points.

8. Continue until all grid points have at least one flowline through them.

9. Put the flowlines in order of length. Discard any/all flowlines which are composed only of grid points which already have a flowline through them.

Consider two points along the flowline: k and k+1, spaced a distance L apart. Now apply equation (3) halfway between these two points, and approximate the derivatives therein by centred finite differences. It follows immediately that:

$$(A + A_{k+1})/2 = (D_{k+1}V_{k+1} - D_kV_k)/L + \delta(D_{k+1}V_{k+1} + D_kV_k)$$

where

$$\delta = [(\partial \sin\psi/\partial Y)_{k+1} + (\partial \sin\psi/\partial Y)_k]/2$$

And so the following recurrence relation will hold:

$$V_{k+1} = [(A_k + A_{k+1})/2 + D_kV_k(1-L\delta)]/[D_{k+1}(1+L\delta)] \qquad \text{--------- (5)}$$

Where, of course, $V_1 = 0$.

Table 2. Analytic expressions and values for the test case.

$$E = ay + c(e-y)\{1 + (x/g)^h\}\cos(bx + f)$$

$$\partial E/\partial x = c(e-y)[(h/g)(x/g)^{h-1}\cos(bx + f) - b\{1 + (x/g)^h\}\sin(bx + f)]$$

$$\partial E/\partial y = a - c\{1 + (x/g)^h\}\cos(bx + f)$$

$$H = [(\partial E/\partial x)^2 + (\partial E/\partial y)^2]^{1/2}$$

$$\psi = \arctan[(-\partial E/\partial y)/(-\partial E/\partial x)]$$

$$V = d(e-y)H/E$$

$$A = d[a + c\cos(bx + f)\langle(e-y)^2[b^2\{1 + (x/g)^h\} - \{h(h-1)/g^2\}(x/g)^{f-2}] - \{1 + (x/g)^h\}\rangle + \{2bch(e-y)^2/g\}(x/g)^{h-1}\sin(bx + f)]$$

where:

$a = 2 \times 10^{-3}$ $\qquad$ $b = 3/e$, $\quad m^{-1}$

$c = 5 \times 10^{-4}$, $\quad m$ $\qquad$ $d = 50$, $\quad ma^{-1}$

$e = 1.2 \times 10^6$, $\quad m$ $\qquad$ $f = -\pi/2$

$g = e$, $\quad m$ $\qquad$ $h = 2.5$

Hence selecting the first flowline, moving down it, and applying equation (5) from point to point, will allow the balance velocities along that line to be computed. If all flowlines are followed in this manner then some grid points - in particular those in regions of convergence - will have more than one flowline through them. The various estimates of the balance flow are then averaged together to produce the final value. Note that the stronger the convergence, the greater will be the number of estimates for the velocity.

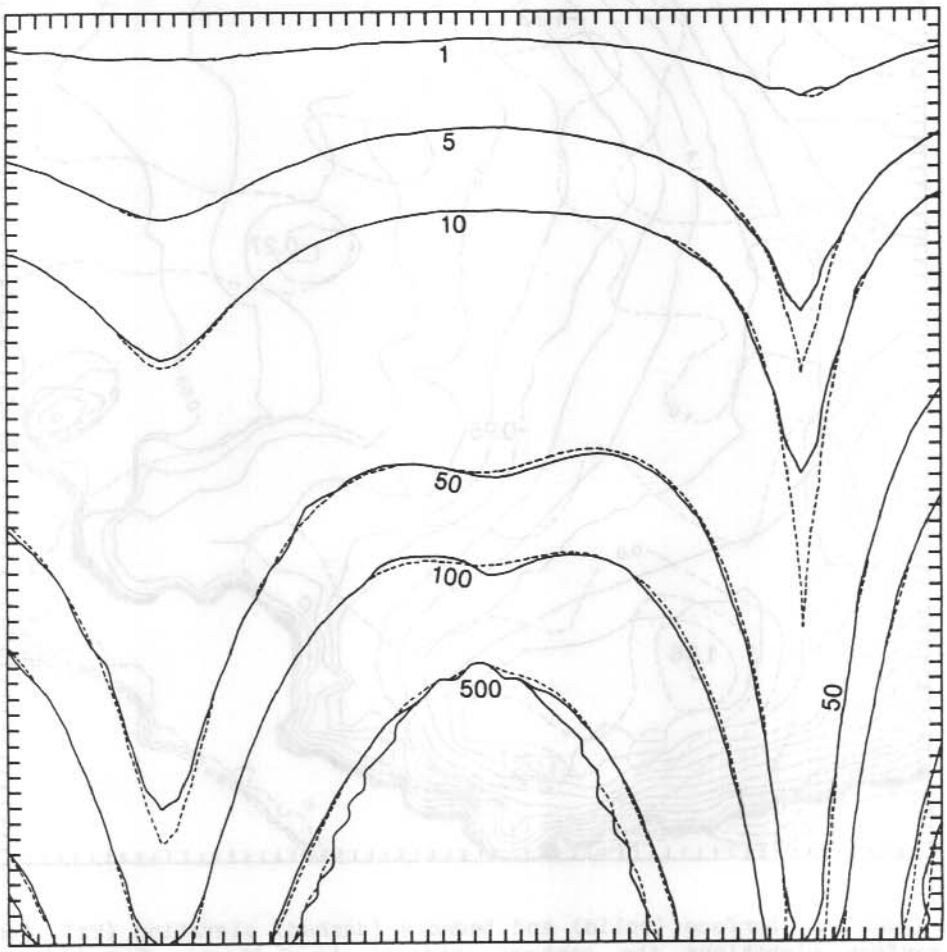

Figure 1. Analytic and computed balance velocities for the functions of Table 2. The dashed lines are the analytic velocities, and the solid lines those computed by the method of this paper.

The lateral divergence, $\partial(\sin\psi)/\partial Y$ is found by moving one twentieth of a grid space to the left (and right) of the current point, and interpolating to the flow directions there. The sines are found, and a standard centred finite difference will give the derivative.

21.5 APPLICATION: ANALYTIC DATA

To test the accuracy of the above scheme, the model was applied to analytic functions of A and E for which the balance velocity can be found analytically, when a flat bedrock is assumed. Table 2 gives the

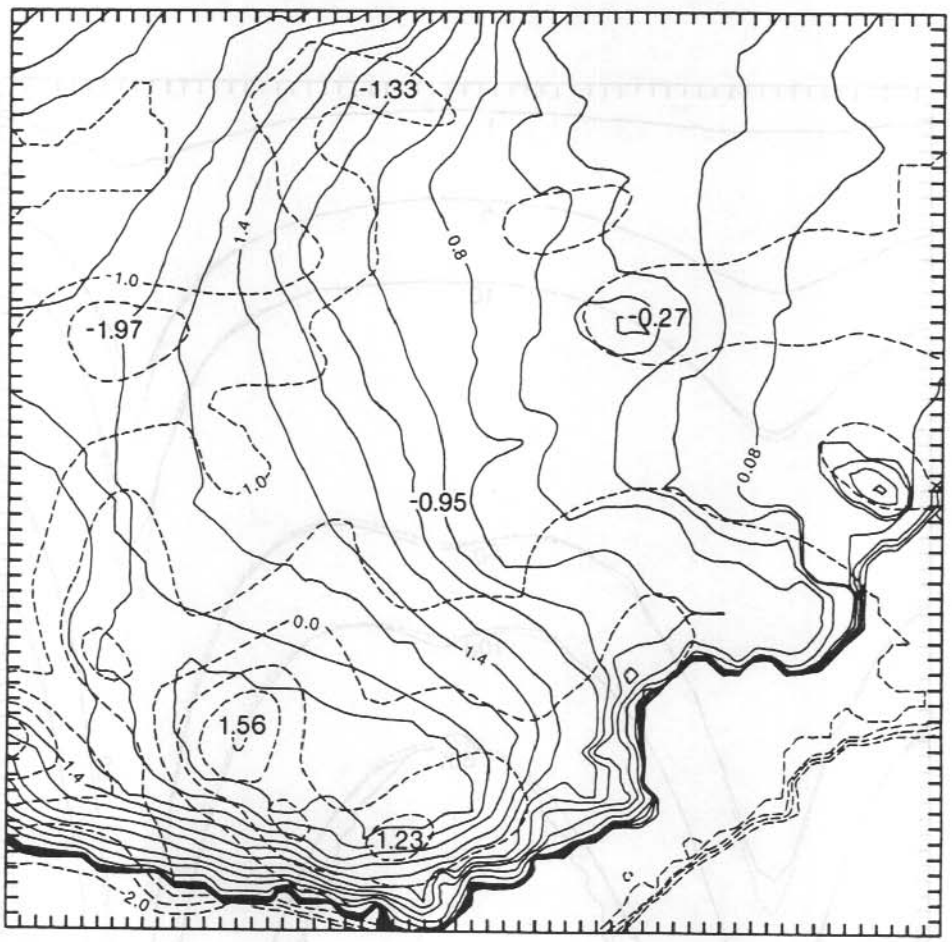

Figure 2. Surface (solid) and bedrock (dashed) elevation (km). For surface elevations the contour interval is 0.02 km. For bedrock elevations the spacing is every 0.5 km from -2.0 to 1.5 km. The location of the grid is such that the top left corner is at 82.5°S, 86°00; the top right is at 83.4°S, 172.8°S; the lower left is at 73.4°S, 118.5°W; and the lower right is at 73.9°S, 157.5°W.

form of A and E, from which the slope, H, flow angle, ψ and velocity can be determined.

Figure 1 shows the analytic (dashed lines) and modelled (solid lines) balance velocities. The agreement between these two sets is excellent, especially in view of the extreme nature of this test case. There should be no qualms in applying the scheme to reality.

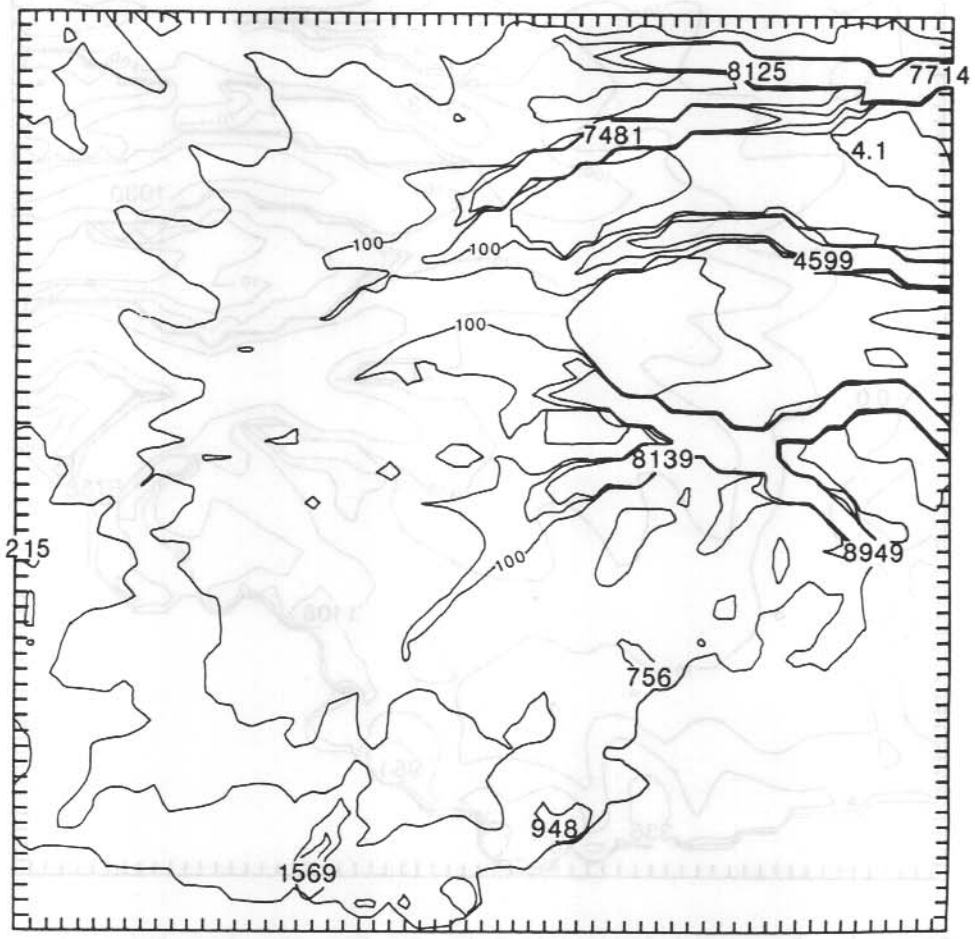

Figure 3. Computed balance velocities (ma^{-1}). The contours are 10, 100, 500 and 1000 ma^{-1}.

21.6 APPLICATION: WEST ANTARCTICA

The model was then applied to West Antarctica. Figure 2 shows the surface and bedrock elevations. The upper left corner is at 82.5°S, 86°W; the upper right is at 83.4°S, 172.8°W; the lower left is at 73.4°S, 118.5°W: and the lower right is at 73.9°S, 157.5°W. Figure 3 gives the computed balance velocities. Note that the ice streams are very cleary delineated. In fact, the velocities are, in some regions, too high, reaching such unrealistically high values of 8000 ma^{-1} or more.

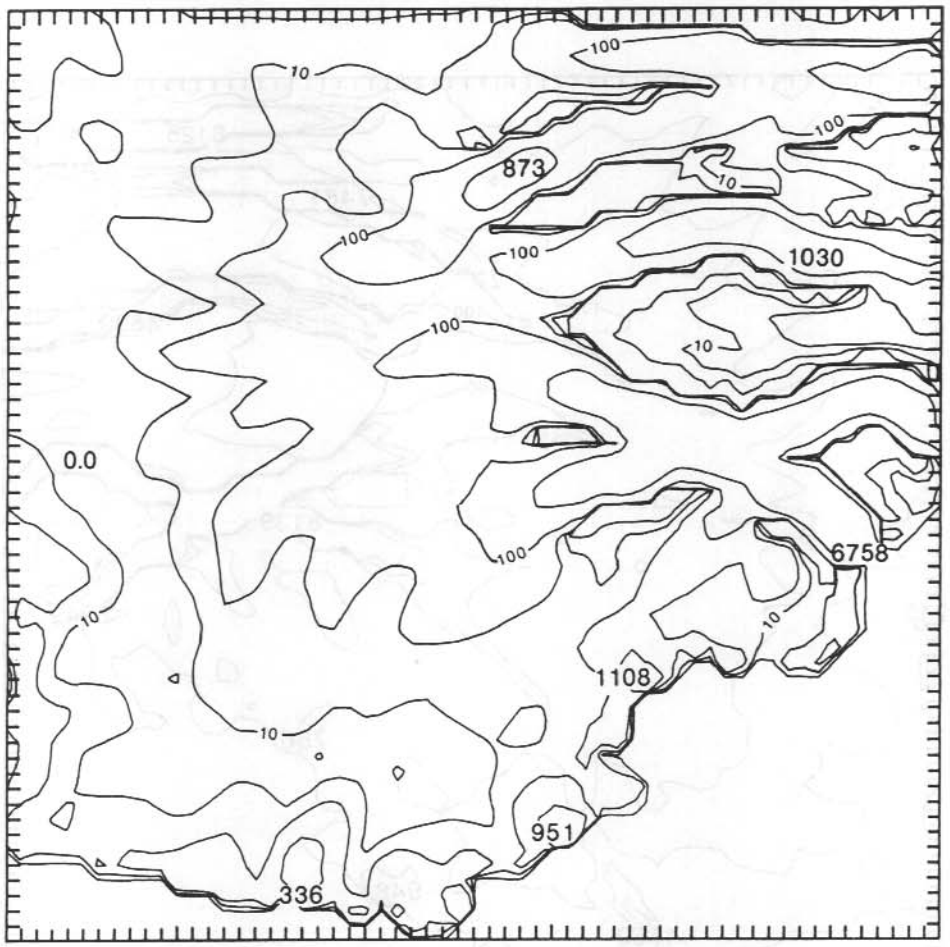

Figure 4. Computed balance velocities for the case where the mass flux has been smoothed in high velocity regions. The smoothing preserves mass, and the velocities have been computed from the smoothed flux field. The contours are 10, 50, 100 and 500 ma^{-1}.

This may be due to the possible incorrectness of the assumption of steady state conditions, but is far more likely due to the model's inadequacy in handling ice streams. While in the analytic data, the flowlines do converge very strongly, so that the ice streams have an exceedingly narrow width, in reality they do not. However, there is nothing in the model which will force the streams to have a minimum width. The streams computed in fact, have widths of 2 km or less. With a large flux forced into such a confine, the velocity becomes very large.

Here, then is the most pressing problem: to incorporate into the model some means of preventing too narrow an ice stream. One method immediately suggests itself: that is to smooth the mass flux uniformly across the high flow areas. When this is done, the velocity pattern becomes as in Figure 4. Although the flow is still too high, the change is in the right direction. Further work on the smoothing process is required.

22. A 500 000 YEAR SIMULATION OF THE NORTH AMERICAN ICE SHEET AND CLIMATE

W.F. Budd and I.N. Smith
Meteorology Department, The University of Melbourne
Parkville, Victoria, 3052.

ABSTRACT

The three-dimensional ice sheet model used by Budd and Smith (1981) to study the reaction of the North American ice sheet and climate to the earth's orbital radiation changes over the last 120 ka has been used to extend the study back to 500 ka BP. The earlier work was refined to define more clearly the values of the radiation-temperature parameter and the ice sheet albedo-temperature parameter to give good fit simulations for the last 120 ka as judged from the available proxy evidence. The orbital radiation changes over the last 500 ka were then used, with a range of the parameters around the best fit values, for the longer term simulations. The results for ice volume changes show close similarity to $\delta^{18}O$ records from sea sediments and in particular indicate clear and robust major interglacial periods which are little effected by small changes to the albedo feedback parameter.

22.1 BACKGROUND AND MAIN FEATURES OF THE MODEL

The three-dimensional ice sheet model used by Budd and Smith (1981) for a simulation of changes in the North American Ice Sheet over the last 120 ka has since been used to extend the ice sheet simulation, in response to the earth's orbital radiation changes, back to 500 ka BP. The details of the model are given in Budd and Smith (1981). The main features of the model are:

(a) Bedrock topography is specified over the North American region at a 200 km horizontal resolution on a 31 x 31 point grid.
(b) Precipitation is prescribed over the area based on the present precipitation distribution but decreasing with elevation over the ice sheet as the ice sheet grows.
(c) Ablation rates are prescribed as a function of latitude and elevation and varying with the orbital radiation changes and ice sheet albedo feedback. These ablation rate changes can be interpreted as effective summer temperature changes or as elevation changes of the ablation level using a constant temperature lapse rate of $-6.5\ ^{o}C\ km^{-1}$.
(d) A time dependant formulation of isostatic bedrock response to the ice load is used with the major delay centred on about 5 ka and a maximum response equal to 25% of ice thickness.
(e) The earth's radiation variations from the orbital changes, R have been taken from Vernekar (1972). The summer half year changes have been prescribed as a function of latitude in the model from $80^{o}N$ to $40^{o}N$. The changes in the ablation levels have been taken as proportional to the summer radiation levels, plus the effect of the ice sheet albedo feedback, as mentioned in (c) above and (f) below. The radiation component of the total change can also be interpreted as an equivalent change in summer temperatures through the lapse rate.

The large number of simulations carried out so far suggest that the best fit value of the radiation-ablation elevation factor is

δ = 30 m ly^{-1} day, (1 ly day^{-1} = 0.486 Wm^{-2})

= 1.95 ^{o}C ly^{-1} day, for the lapse of -6.5 ^{o}C km^{-1}

This gives for the most recent radiation minimum, at about 26 ka BP, with a reduction of summer radiation for 70^{o}N of

ΔR = 23 ly day^{-1}, a summer temperature drop of

$\Delta\theta$ = 4.5 ^{o}C,

or ΔE = 690 m for the elevation decrease of the ablation level.

This value of δ = 30 has been used for the current simulations along with various values of the albedo feedback parameter, f as described below.

(f) The ice sheet albedo feedback takes account of the effect on the climate, and in particular the summer temperatures, of the presence of the ice sheet. Again the ablation elevation levels change with the ice sheet area through a factor f such that for f = 1 the elevation lowering is 400 m when the ice cover area equals that of the last ice age maximum. With a lapse rate of -6.5 ^{o}C km^{-1}, f = 1 corresponds to a 2.6 ^{o}C summer temperature change, $\Delta\theta$. The range of values required for close matches of the proxy evidence for the last ice age using δ = 30 is from f = 1.8 to 2.0 or ΔE = 720 to 800 m, or with a lapse rate of -6.5 ^{o}C km^{-1}, $\Delta\theta$ = 4.7 to 5.2 ^{o}C.

This magnitude of summer temperature change for the last ice age maximum is also quite compatible with the atmospheric modelling results of Gates (1976) and Manabe and Hahn (1977) (cf: Budd, 1981).

22.2 TUNING OF THE MODEL FOR THE LAST 120 000 YEARS

Only slight changes have been made to the model as described by Budd and Smith (1981). The initial heights of the 1 ma^{-1} ablation level have been adjusted to give a better representation of present mean values as shown in Table 1.

No adjustment to the initial precipitation was made. When the precipitation exceeded the ablation rate, snow accumulated, and as the ice built up, its flow was determined from the model as described by Budd and Smith (1981, 1982).

Table 1. Elevation, E_o of the 1 ma^{-1} ablation rate.

Latitude (^{o}N)	30	40	50	60	70	80
E_o (m)	5100	4200	2600	1700	900	500

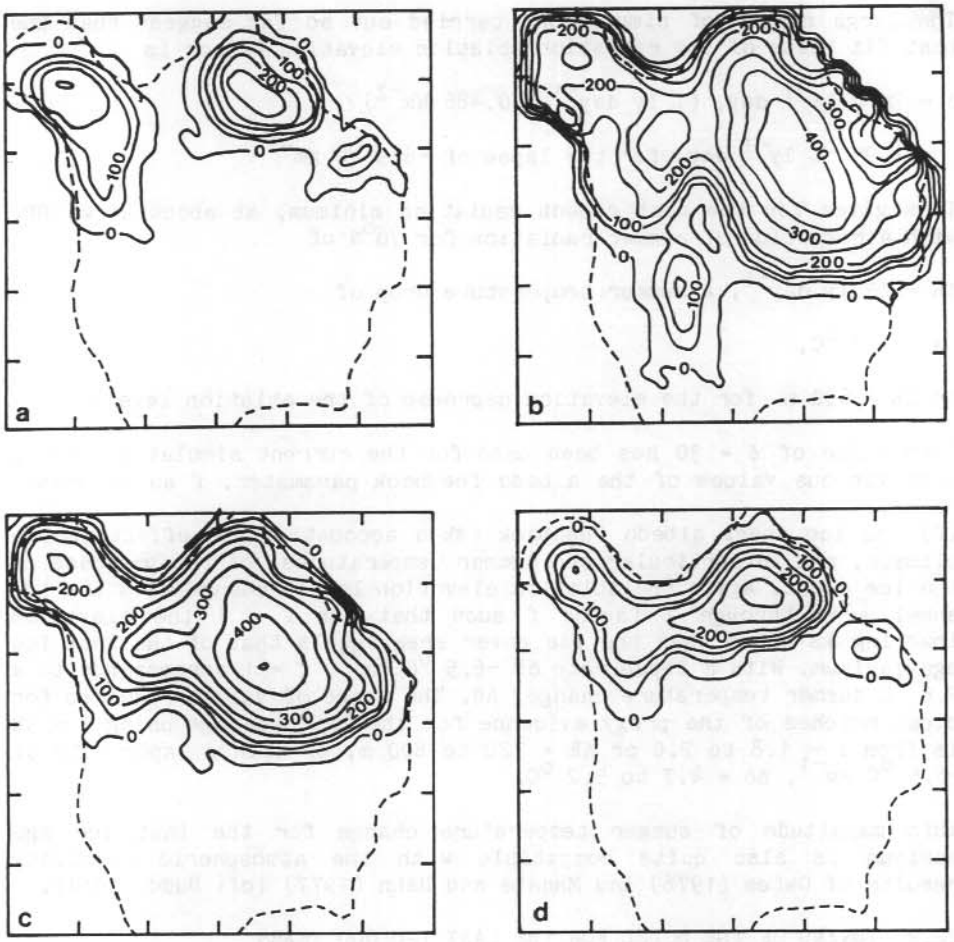

Figure 1. Ice sheet surface elevation from the model simulation for the last major advance and retreat at times BP. (a) 36 ka (b) 18 ka (c) 12 ka (d) 8 ka. (units of 10 m).

The model as outlined was found to give a reasonable simulation of the ice sheet, as inferred from proxy data, for the period since 120 ka BP. The main uncertainties seem to be with regard to the amount of ice remaining at the interstadial periods around 80 and 40 ka BP. The values of f = 1.8 to 2.0 seemed to cover a reasonable range for matching the proxy evidence. The pattern of ice thickness from the model for the last major advance and retreat is shown in Figure 1. The ice volume changes for the last 140 ka BP are shown in Figure 2.

22.3 DISCUSSION OF 500 000 YEAR SIMULATION

Using the same values of the parameters as required to match the last 120 ka BP the model was then used to simulate the changes since 500 ka

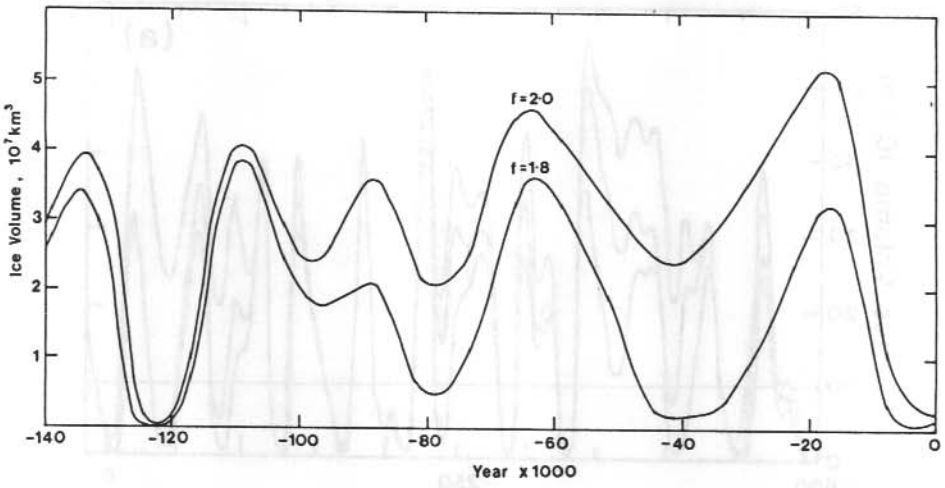

Figure 2. Ice volumes for the North American ice sheet model from 140 ka BP with δ = 30 (m ly^{-1} day) no precipitation change (ΔP = 0) and two different values of albedo feedback, f = 1.8 and 2.0. (1 ly day^{-1} = 0.486 Wm^{-2}).

BP. The results for the ice volume changes are shown in Figure 3(a) for three different values of f, (1.6, 1.8, 2.0), and for

δ = 30 m ly^{-1} day.

Although the different f values strongly effect the amount of ice growth for many of the glacials, it appears that the major interglacials are quite robust and well defined. A comparison with the sea sediment $\delta^{18}O$ record from Broeker and van Donk (1970) is shown in Figure 3(b).

It should be remembered that the different sediment cores around the world show somewhat different records but with often similar major features. Also, more detailed records tend to show more clearly the evidence of the more minor stadial episodes, as shown for example by Shackleton and others (1983).

It is therefore notable that the major interglacials of the model show a clear correspondence with the sea sediment inferred interglacials. The major glacials also correspond, but the minor variations may be obscured to some extent by the coarse resolution of the sea sediments, and also need to be considered with the effect of the Antarctic ice sheet on the ocean isotope changes as indicated by Budd (1981) and Budd and Smith (1982).

An examination of the summer radiation variations in the northern hemisphere for latitudes 40 to 80 ^{o}N over the 500 ka period reveals that the major interglacials follow coincident high summer radiation

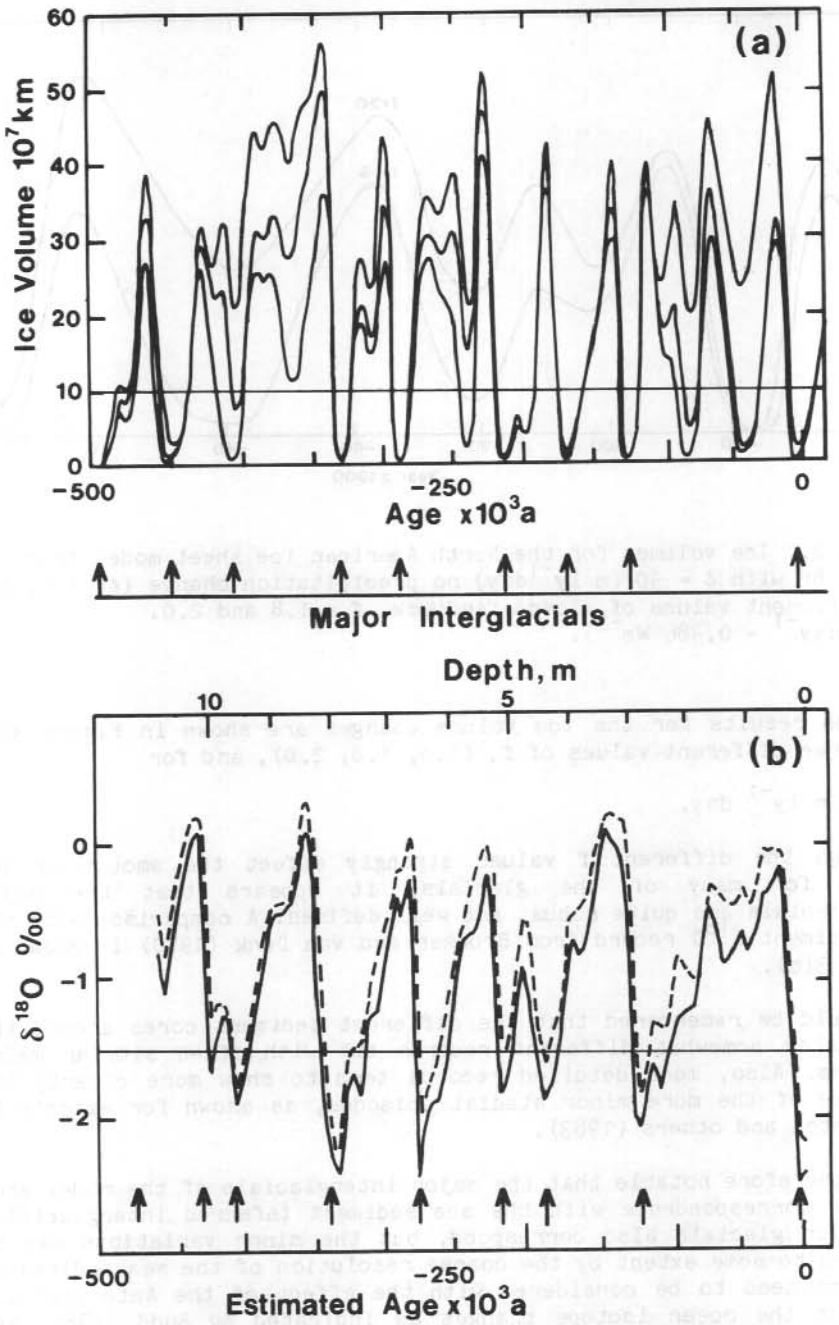

Figure 3. (a) Ice volume curves computed for the North American ice sheet model for three different values of the albedo feedback factor f = 1.6, 1.8, 2.0, from -500 ka to + 20 ka. (b) Oxygen isotope data on two species of foraminifera from Carribbean core V12-122 from Broeker and van Donk (1970).

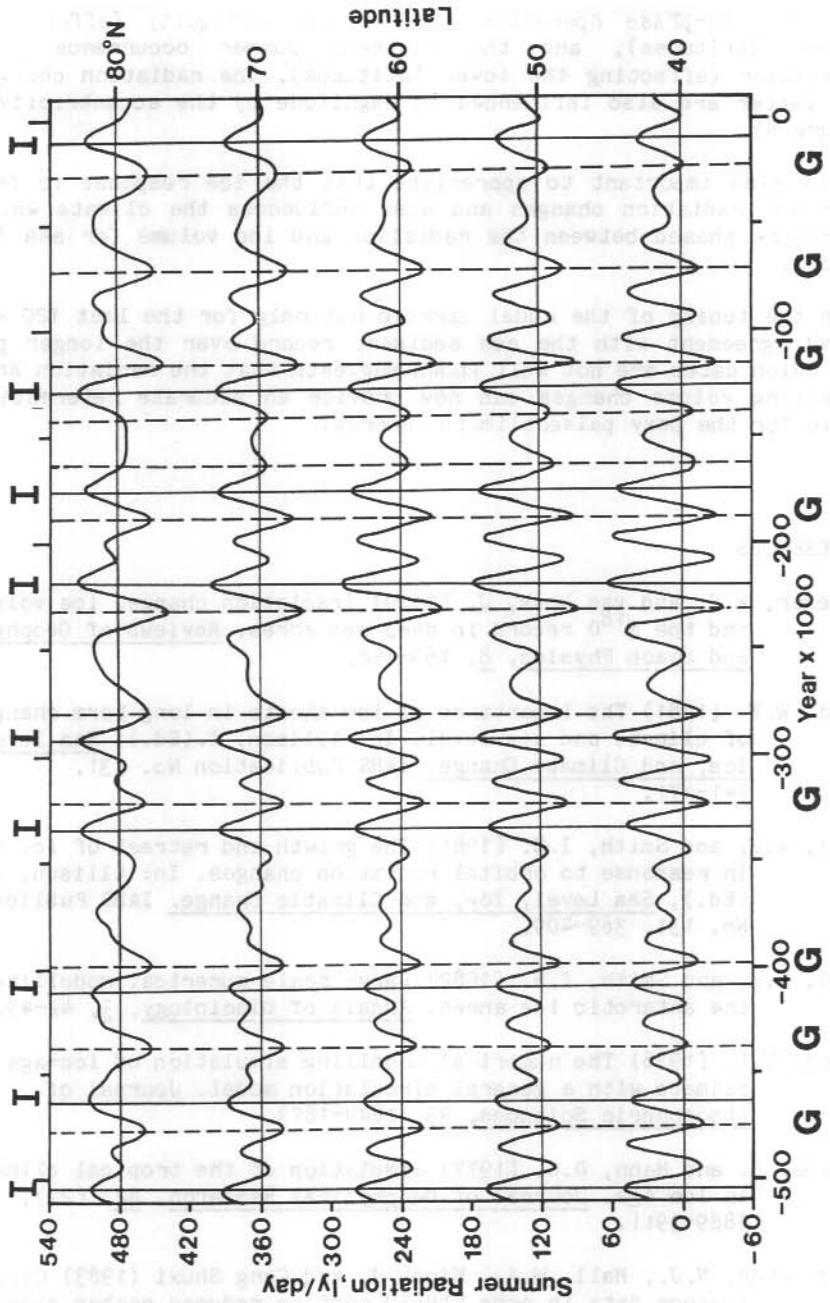

Figure 4. Changes in summer radiation for latitudes 40^{o} - 80^{o}N from -500 ka to + 20 ka, from Vernekar (1972). The major glacials (G) and interglacials (I) tend to follow large radiation deviations which are synchronous over a wide range.

from the in-phase operation of the high obliquity (effecting the higher latitudes), and the northern summer occurrence of the perihelion (effecting the lower latitudes). The radiation changes of the latter are also influenced in magnitude by the eccentricity (cf: Figure 4).

It is also important to appreciate that the ice response is delayed from the radiation changes and also influences the climate which is therefore phased between the radiation and ice volume (or sea level) record.

With the tuning of the model carried out only for the last 120 ka the broad agreement with the sea sediment record over the longer period for which dates are not well known suggests that the radiation and ice modelling volume changes can now provide an accurate reference time scale for the poxy palaeoclimate records.

REFERENCES

Broeker, W.S. and van Donk, J. (1970) Insolation change, ice volumes and the $\delta^{18}O$ record in deep sea cores. Reviews of Geophysics and Space Physics, 8, 169-198.

Budd, W.F. (1981) The importance of ice sheets in long term changes of climate and sea level. In: Allison, I.(Ed.), Sea level, Ice, and Climate Change. IAHS Publication No. 131. 441-471.

Budd, W.F. and Smith, I.N. (1981) The growth and retreat of ice sheets in response to orbital radiation changes. In: Allison, I. (Ed.), Sea Level, Ice, and Climatic Change. IAHS Publication No. 131, 369-409.

Budd, W.F. and Smith, I.N. (1982) Large scale numerical modelling of the antarctic ice sheet. Annals of Glaciology, 3, 42-49.

Gates, W.L. (1976) The numerical modelling simulation of ice-age climate with a general circulation model. Journal of Atmospheric Sciences, 33, 1844-1873.

Manabe, S. and Hahn, D.G. (1977) Simulation of the tropical climate of an Ice Age. Journal of Geophysical Research, 82, (27), 3889-3911.

Shackleton, N.J., Hall, M.A., Kine, J. and Cang Shuxi (1983) Carbon isotope data in core V19-30 confirm reduced carbon dioxide concentration in the ice age atmosphere. Nature, 306, 319-322.

Vernekar, A.D. (1972) Long-period global variations of incoming solar radiation. Meteorology Monographs, 12, (34).

23. FINITE ELEMENT ANALYSIS OF TWO-DIMENSIONAL LONGITUDINAL SECTION FLOW ON LAW DOME

W.F. Budd and R.J.M. Rowden-Rich
Meteorology Department, The University of Melbourne
Parkville, Victoria, 3052.

ABSTRACT

Ice flow over irregular bedrock can be very complex and involves a feedback whereby the stress and flow regime strongly influence the flow properties of the ice through the development of strong anisotropy in the ice crystal alignments. The pattern of crystal orientation then in turn influences the ice flow.

Finite element analysis provides a powerful technique for studying the variation of stress and strain rates for ice flow over irregular beds. A 15 km longitudinal section of Law Dome approximately along a flow line for which data from 4 deep boreholes is available was chosen for a detailed study. In the first instance ice flow was taken to depend only on stress and temperature, to derive the stress and strain rate fields which give rise to the development of the anisotropy. The added dependence of the ice flow on the anistropy can then be used to recompute the flow regime.

23.1 INTRODUCTION

The detailed measurements available of the ice flow in a region of Law Dome near Cape Folger make it ideally suitable for an analysis by finite element techniques.

The ice thickness from radio echo sounding was determined by Carter (1976). Ice movement and strain rates were measured by McLaren (1968) and Pfitzner (1980). A number of borehole measurements have been made along the line from the Dome summit to Cape Folger. A summary of those cored up to 1977 was given by Russell-Head and Budd (1979). Since that time two further holes, BHC1 and BHC2 have been cored to bed about 0.6 and 1.0 km approximately downstream of borehole A respectively (Morgan and McCray, this volume; Etheridge and McCray, this volume). Crystallographic data from borehole A has been discussed by Budd (1972), Matsuda and others (1976) and Matsuda and Wakahama (1978).

From borehole F, ice core data and borehole shear were presented by Russell-Head (1979) and Russell-Head and Budd (1979). Isotope data was presented by Budd and Morgan (1977). More recent data for the boreholes BHC1 and BHC2 are given by Morgan and McCray (this volume), Etheridge and McCray (this volume) and McCray (unpublished).

The temperature regime of the region has been discussed by Budd and others (1976). Further data is also available from BHC1 and BHC2.

From the deliniation of the ice surface and bed obtained by Carter (1976) from optical levelling and radio echo sounding, as shown in Figure 1, it is apparent that variations greater than 20% of the ice

thickness occur over distances of less than 20 ice thicknesses. The measurements of ice surface velocity obtained by Pfitzner (1980) showed variations proportionally much less than that of the ice thickness. The borehole shear at F presented by Russell-Head and Budd (1979) indicated that the maximum shear layer occurred about 100 m above the bed where there was also a strong concentration of vertical c-axes in the ice crystals. The crystallographic distribution throughout the ice mass strongly influences the ice flow. At the same time the stress distribution and pattern of ice flow effects the crystal structure. Finite element analysis provides a powerful technique to determine the stress and strain rate distribution for the complex flow over irregular bedrock and can thereby provide further understanding of the development of the crystal structure.

23.2 METHODOLOGY OF A SERIES OF FINITE ELEMENT ANALYSES

The basic principles of the application of finite element analysis to two-dimensional longitudinal section ice flow have been given elsewhere (Hooke and others, 1979; Iken 1977, 1981).

The particular technique used here is a slightly modified version of a program developed by Coulthard (1982).

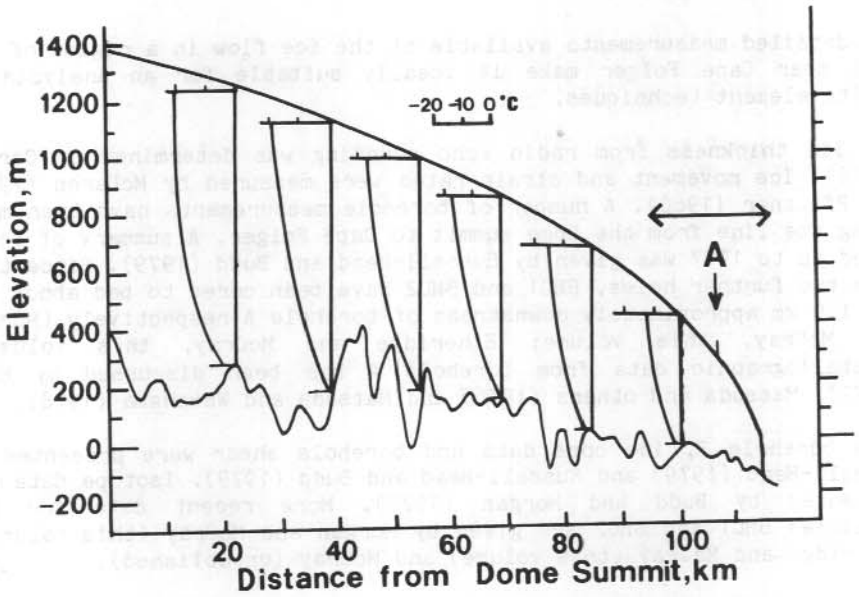

Figure 1. Section of Law Dome from the summit to Cape Folger showing the surface and bedrock profiles given by D. Carter. The echo sounding data is plotted at a coarse 1.6 km spacing. A more detailed plot of the last 20 km section is shown in Figure 2. Temperature profiles computed by Budd and others (1976) are also shown.

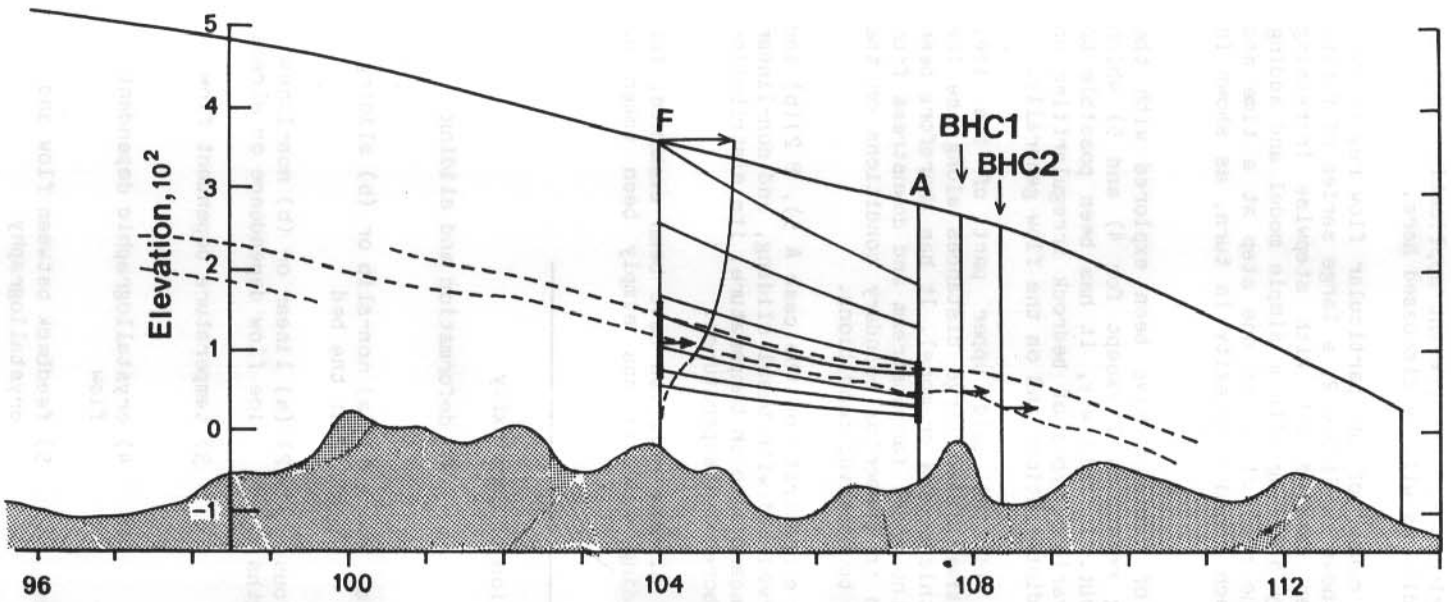

Figure 2. Surface and bedrock elevation of the coastal end of the Dome-Folger line from Carter's approximately 0.25 km spacing data. The section is in the general direction of the flow and the approximate position of the boreholes on the line are shown: F, A, BHC1, BHC2. The dashed lines indicate the subsurface echoes observed by Carter. At F a velocity profile is shown from Russell-Head and Budd (1979). Lines are shown joining similar $\delta^{18}O$ isotope ratios at F and A. The thicker parts of the vertical lines in A and F indicate the zone of strong vertical c-axis concentrations.

Only the specific points relevant to the present application such as the prescribed boundary conditions will be discussed here.

In order to understand the causes of the particular flow regime over the irregular section, as shown in Figure 2, a large series of finite element analyses have been carried out with stepwise increasing complexity. This is done by starting with a simple model and adding complexities approaching the real situation one step at a time and exploring the impact of each added complexity in turn, as shown in Table 1.

Each of the slab shapes of Table 1 have been explored with the different flow and sliding relations B except for 4) and 5) which still have to be carried out. In this way, it has been possible to study the effects of the various types of bedrock irregularities on the stress and strain rate distributions and on the flow generally.

Because of the stiffness of the cold upper part of the ice, longitudinal stresses are transmitted large distances along the ice mass (the order of 20 ice thicknesses or more). It has therefore been found necessary to extend the model far upstream and downstream from the region of interest and to prescribe boundary conditions on the ends as near as practicable to observed conditions.

For the present context we concentrate on the case A 5), B 2)(b) and 3), that is using the observed bed with basal sliding, and non-linear stress dependent flow, dependent also on temperature, its distribution controlled by the observed borehole temperatures.

Several different types of sliding relation have been examined. For the present case the sliding velocity has simply been taken as

---

Table 1. Stepwise Progression of Complexity

A boundary shape properties	B deformation and sliding
1) uniform slab on inclined plane	1) (a) non-slip or (b) sliding at the bed
2) sinusoidal beds of various amplitudes and wavelengths	2) (a) linear or (b) non-linear ice flow dependence on stress
3) curved surface with decreasing thickness	3) temperature dependent flow
4) combination of above model forms	4) crystallographic dependent flow
5) observed surface and bed	5) feedback between flow and crystallography

proportional to the basal shear stress and inversely proportional to the normal stress.

Studies have also been carried out on the effects of variations in the model grid element sizes. It is important to have at least sufficient resolution to cover the major features needed to be studied. Higher resolutions should then be shown to converge with the coarser resolution and not add much further information for greatly increased computation time.

In the model it is possible to vary the element size as required. This has been done to provide more detail where the variations are largest as shown in the section of Figure 3.

The full length of the section modelled was 20 km. Here we examine only the region around the 3 boreholes A, BHC1 and BHC2.

23.3 RESULTS OF SHEAR STRESS DISTRIBUTION

It needs to be remembered when comparing the results with the real situation on Law Dome that the model flow is strictly two-dimensional. In practice the bed irregularities are more complex and a certain amount of three-dimensional flow can be expected. Furthermore, smaller scale irregularities are not resolved in the model but can influence the observed ice flow, particularly near the bed.

Table 2. Average horizontal shear stress in the calculation elements.

column	50	51	52	53	54	55	56	57	58
level	shear stress (bars)								
1	.27	-.03	-.48	.21	.24	.23	.19	.13	.13
2	.53	.26	-.14	.39	.44	.37	.31	.28	.30
3	.74	.66	.38	.65	.59	.48	.42	.42	.49
4	.90	.97	.82	.88	.69	.54	.49	.52	.64
5	1.00	1.20	1.15	1.05	.74	.57	.54	.58	.73
6	.99	1.46	1.54	1.06	.75	.60	.56	.63	.78
7	.97	1.34	1.37	.97	.71	.59	.58	.65	.80
8	.89	1.21	1.30	.94	.66	.59	.60	.67	.80
9	.73	1.05	1.22	.78	.58	.62	.64	.67	.77
10	.46	.68	.92	.49	.51	.68	.71	.64	.67

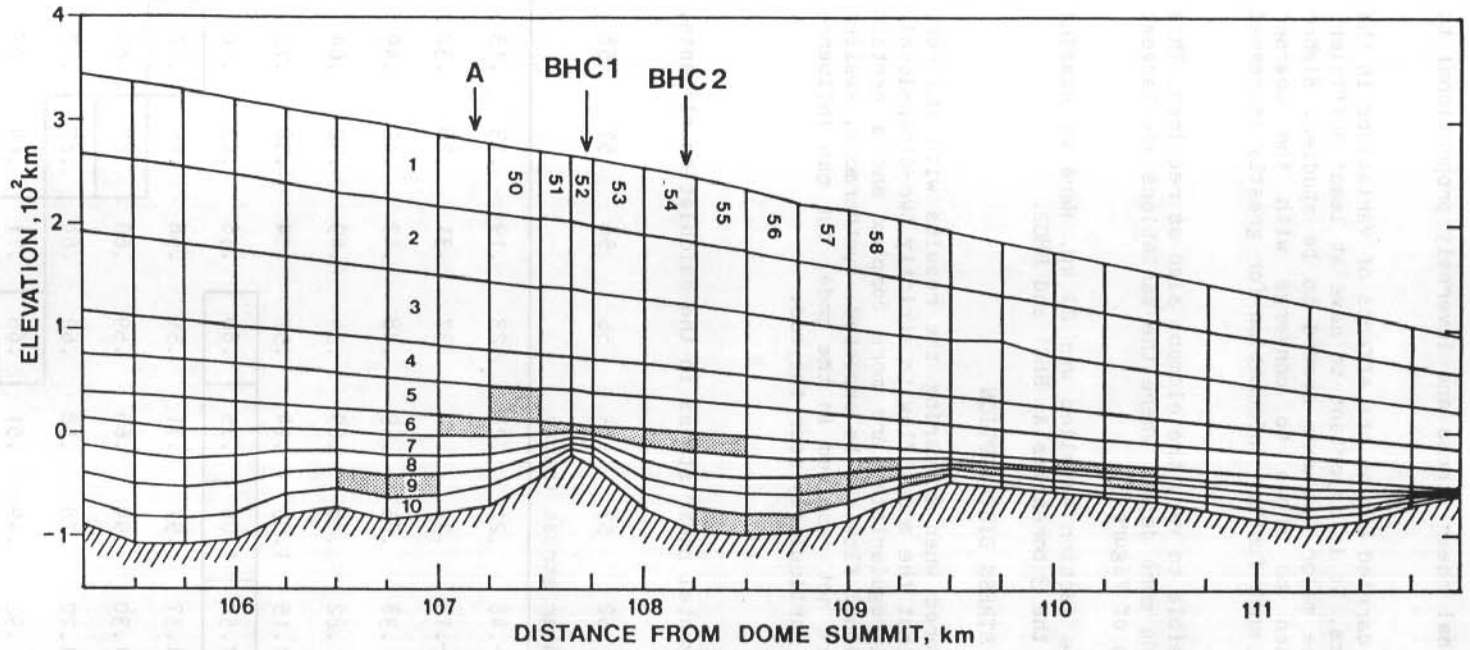

Figure 3. The section of the finite element analysis region around boreholes A, BHC1 and BHC2 is shown with the element net indicated. The average horizontal shear stress in the elements at levels 1 to 10 for columns 50 to 58 is shown as indicated in Table 2. The location of the maximum shear stress in the column is shown shaded.

Table 2 shows a printout for the average shear stress from the model for each of the elements of the vertical columns 50 to 58 as shown in Figure 3 around the region corresponding to the boreholes A, BHC1 and BHC2.

Since at this stage there is no crystal anisotropy in the model a certain lack of simulation can be expected. Nevertheless the stress pattern as computed can be considered in the context of a cause of the development of the crystal distribution.

The vertical resolution is still too coarse to delineate the finer features of the vertical profiles but even so the following points are worth noting.

(a) The maximum shear stress is well above the bed (approximately 100 m) near borehole A (columns 49-50). This compares favourably with the high shear zone inferred from the fabrics and bubbles in the A core.
(b) By column 52 over the bump summit corresponding to BHC1 the maximum shear stress occurs about 50 m above the bed. This also corresponds with a shear maximum in the BHC1 hole. A higher maximum at BHC1 may correspond to a continuation of the upstream shear maximum and crystal fabrics to further downstream.
(c) By columns 55-56, over the hollow, corresponding to BHC2, the maximum shear stress is developing at the base although for column 55 there is still a secondary maximum about 100 m above the bed. Two similarly located maxima are observed in the BHC2 shear profile.
(c) It also should be noted that the shear stress generally increases greatly over the bump and decreases over the hollow. This implies that for ice flow over rough terrain the local shear stress may be greatly disturbed. Such large disturbances need to be taken into account in the analysis of the ice flow relationship from borehole deformation studies.

In conclusion, although the present work is very preliminary, needing higher resolution, and incorporation of anisotropic ice flow properties, it nevertheless gives some insight into the complex disturbances to the stress field for ice flow over an irregular bed. The variation in the stress field also provides a basis for the variation in the ice crystallography, with high horizontal shear giving rise to high concentrations of verical c-axis, while stress relaxation, especially with higher temperatures, gives rise to larger crystal growth. The interesting feedback with coupled ice crystallography and flow has still to be explored.

ACKNOWLEDGMENTS:

The authors are indebted to M.A. Coulthard of the CSIRO Divison of Applied Geomechanics for providing the basic finite element analysis computer program and for extensive advice on its use. We alsc appreciate the cooperation of the ANARE expeditioners for discussion on the results of their recent work; in particular, Tony McCray and David Etheridge from the Antarctic Division Glaciology Section and Professor Xie Zichu from the Lanzhou Institute of Glaciology and Geocryology, Peoples Republic of China.

REFERENCES

Budd, W.F. (1972) The development of crystal orientation fabrics in moving ice. Zeitschrift fur Gletscherkunde und Glazialgeologie, 8, (1-2), 65-105.

Budd, W.F. and Morgan, V.I. (1977) Isotopes climate and ice sheet dynamics from ice core studies on Law Dome, Antarctica. IAHS Publication No. 118, 312-321.

Budd, W.F., Young, N.W. and Austin, C.R. (1976) Measured and computed temperature distributions in the Law Come Ice Cap, Antarctica. Journal of Glaciology, 16, (74), 99-110.

Carter, D. (1976) Wilkes ice cap project 1967. M.Sc. Thesis, Department of Meteorology, The University of Melbourne.

Coulthard, M.A. (1982) Plane strain nonlinear finite element program NTJEP2 - modifications and corrections for use in mining geomechanics. Technical Report No. 129. CSIRO, Division of Applied Geomechanics, 57 pages.

Etheridge, D.M. and McCray, A.P. (this volume) Dynamics of the Law Dome Ice Sheet from borehole measurements.

Hooke, R.Le B., Raymond, C.F., Hotchkiss, R.L. and Gustafson, R.J. (1979) Calculations of velocity and temperature in a polar glacier using finite element analysis. Journal of Glaciology, 24, (90), 131-146.

Iken, A. (1977) Movement of large ice mass before breaking off. Journal of Glaciology, 19, (81), 595-605.

Iken, A. (1981) The effect of the subglacial water pressure on the sliding velocity of a glacier in an idealised numerical model. Journal of Glaciology, 27, (97), 407-421.

McCray, A. (unpublished). Ice coring and borehole studies near Cape Folger, Law Dome, Antarctica. Antarctic Division Glaciology Section Internal Report.

McLaren, W.A. (1968) A study of the local ice cap near Wilkes, Antarctica. ANARE Scientific Reports, Publication No. 103, 82 pages.

Matsuda, M., Wakahama, G. and Budd, W.F. (1976) Twinning of ice from Antarctic ice sheet. Observation of a-axis orientation associated with diamond c-axis orientation faric. (in Japanese). Low Temperature Science, Series A. 34, 163-71.

Morgan, V.I. and McCray, A.P. (this volume) Enhanced shear zones in ice flow-implications for ice cap modelling and core dating.

Russell-Head, D.S. (1979) Ice sheet flow from borehole and laboratory studies. M.Sc. Thesis, Meteorology Department, The University of Melbourne.

Russell-Head, D.S. and Budd, W.F. (1979) Ice-sheet flow properties derived from borehole shear measurements combined with ice core studies. Journal of Glaciology, 24, (90), 117-130.

E. RESULTS FROM ANTARCTIC GLACIOLOGICAL FIELD SURVEYS

One of the major goals of the Australian glaciology program is to reach an understanding of the dynamics and characteristics of the Antarctic ice sheet including its history, mass budget and probable response to a changing environment. Field activities comprise traverses, aerial surveys and ice core drilling on the ice sheet, its outlet glaciers and ice shelves. Much of the work forms a major Australian contribution to the I.A.G.P. (International Antarctic Glaciology Project), which links institutes and expeditions from six nations (Australia, France, Japan, U.K., U.S.A., U.S.S.R.) in a cooperative study of the East Antarctic ice sheet. The overall aims of the I.A.G.P. are given by Bentley and others (1972). They include surveys along three flowlines inland of Dumont d'Urville, Casey and Mirny, to study the dynamics, and along fluxlines, principally the 2000 m elevation contour but including other inland routes, to study the mass budget of the ice sheet.

Current Australian activities are concentrated on traverse routes to the south, east and west of Casey, between Mirny and Dome C in cooperation with the Soviet Antarctic Expeditions, on the Law Dome and neighbouring outlet glaciers. The Law Dome is a medium sized ice cap, about 200 km in diameter, adjoining the main ice sheet. It is large enough to have the features of a large ice sheet but small enough to be studied in detail as a model of the Antarctic ice sheet.

Results from the field surveys make up a basic data set on the physical attributes of the Antarctic snow and ice cover. Measurements along oversnow traverse routes and from aerial surveys over the ice sheet and its outlet glaciers include ice surface and bedrock topography, ice movement, snow accumulation rate and surface temperature. Additional data collected on the surveys include gravity and magnetic measurements for geophysical studies of bedrock, surface meteorological observations, snow structure and snow samples for a variety of studies.

The data set provides the boundary conditions for numerical modelling studies of the ice sheet and its interaction with the environment. In addition it provides the information essential for the interpretation of ice core data in terms of paleorecords of temperature and other climatic changes.

The Antarctic ice sheet is a significant component in the world's water budget, and its development with time has important implications for sea level changes. Studies of outlet glaciers are important in this context since they together drain a major portion of the ice sheet and will react first to a change in sea level.

Preliminary results from several field studies are presented in this report. A significant product of this work is the extensive and unique set of velocity measurements of the inland ice sheet that are now becoming available. Surveys in 1984, 1985 and 1986 will complete the measurements on the southern, eastern and western routes respectively, covering Wilkes Land. The mass budget of the ice sheet can be analysed

in detail by studying separately each of the sectors delineated by the network of surveys. The surveys of the southern route will provide reconnaissance data for selection of a potential future deep drilling site.

These studies are complemented by the earlier work in Enderby Land on the mass budget and outlet glaciers, and on the Lambert Glacier/Amery Ice Shelf system. Work of other nations adds further information: surveys and icecore drilling between Mirny and Vostok by the Soviet Antarctic Expeditions, French activities inland of Dumont d'Urville and at Dome C, Scott Polar Research Institute and the U.S. National Science Foundation cooperative echo sounding of eastern Wilkes Land and the interior, and Japanese surveys between Enderby Land and Queen Maud Land.

The largest remaining unsurveyed sector is the interior of the Lambert Glacier basin. It is prosposed to cover this area by Australian traverses operating out of Mawson, south of the Prince Charles Mountains as far as Grove Mountains and Davis. The sector between Mirny and Davis will be closed by a planned extension of the western route out of Casey to produce a linked set of surveys. Surveys of glaciers in the Northern Prince Charles Mountains and large glaciers along the coast will complete the program.

Bentley C.R., Budd, W.F., Kotlyakov, V.M., Lorius, C. and Robin, G de Q (1972) The International Antarctic Glaciological Project standardisation document. Polar Record, 16, (101), 349-364.

N.W. Young

24. GLACIOLOGICAL MEASUREMENTS IN EASTERN WILKES LAND, ANTARCTICA

D. Jones and Martin Hendy
Antarctic Division, Department of Science
Kingston, Tasmania, 7150.

ABSTRACT

Data on ice surface and bedrock topography, ice surface velocity and snow accumulation rate are presented from a traverse route in eastern Wilkes Land, Antarctica, approximately along the 69°S parallel of latitude between 112°E and 131°E longitude. These data are used to calculate the mass outflux through this sector near the edge of the ice sheet. Comparison of the outflux with the estimated mass influx suggests that, within the limits of accuracy, this area of Antarctica is not significantly out of balance.

24.1 INTRODUCTION

From 1980 to 1982 ANARE glaciological traverses from Casey traversed a route on the Antarctic ice sheet, following the 69°S parallel of latitude in eastern Wilkes Land. These traverses were part of the Australian contribution to the International Antarctic Glaciological Project (SCAR, 1971). In 1980 a route was pioneered to 123°E and accumulation markers established along the track, although because of problems with the satellite doppler surveying equipment, the position of ice movement stations were not accurately determined. The route was extended as far as 127°E in 1981, and the initial survey of ice movement every 50 km (GD01 to GD12) was made. In 1982 these movement markers were resurveyed, ice radar data on ice thickness was obtained along the route, and the line was extended again to 131°E.

The 1982 route to GD15 (Figure 1), was from Casey to A028 via the Law Dome summit (A001), along a rhumb line to GD03 and then east along 69°S latitude to the end of the line at 131°E. The return route to GD03 followed a line 28 km (15' of latitude) due south of the outward route to obtain additional surface and bedrock data. The return to Casey was made via GC17 and A022.

24.2 SUMMARY OF RESULTS

Surface and bedrock profiles were successfully obtained on all lines. An ANARE 100 MHz Ice Radar (Morgan, unpublished, Smith, unpublished) was used to carry out ice thickness measurements, and a "Setra-quartz" based electronic barometer (Morgan and Davis, unpublished) was used to measure atmospheric pressure from which elevations could be calculated. Absolute elevation control was obtained from doppler satellite positioning measurements at GD01,....GD15, GC16, GC17, GC19 and A022. The profiles are shown in Figures 2.

Ice velocities were derived from successive annual doppler satellite position measurements at all sites except for GD13, GD14 and GD15. The computed ice surface velocities are shown in Table 1.

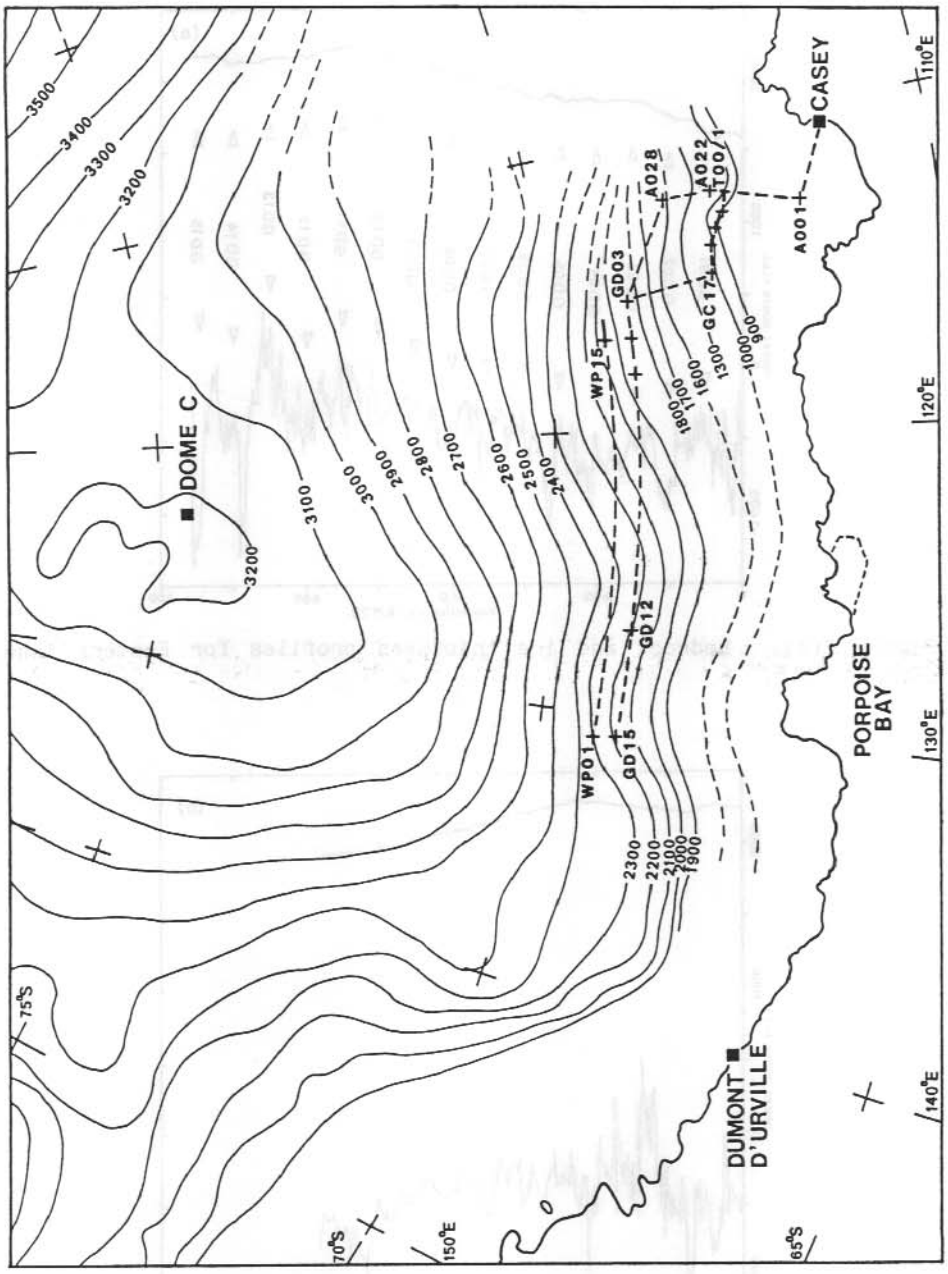

Figure 1. Surface elevation contours (m) and 1982 traverse routes, Eastern Wilkes Land.

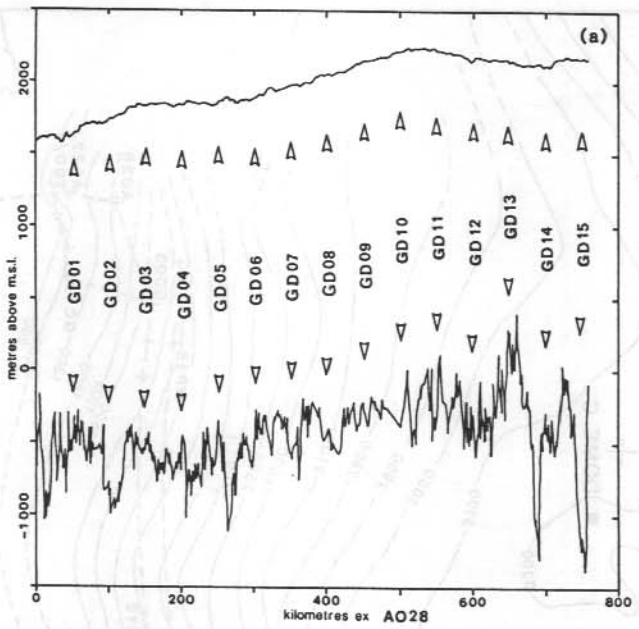

Figure 2(a). Bedrock and ice thickness profiles for Eastern line, GD01 to GD15.

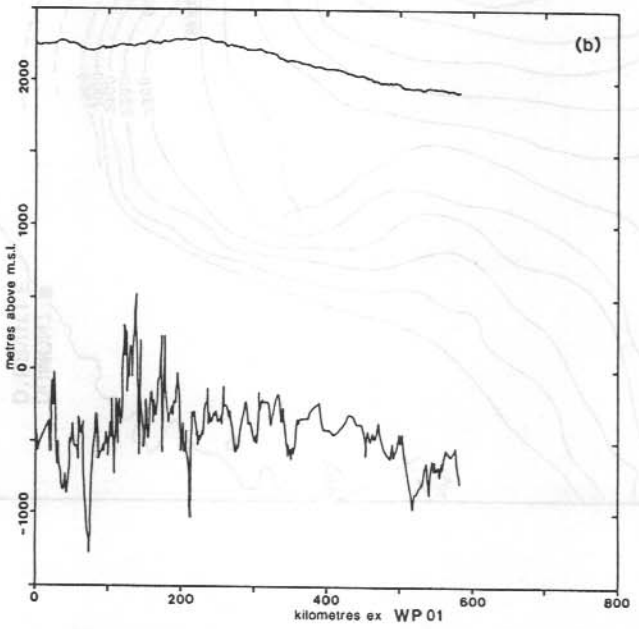

Figure 2(b). Bedrock and ice thickness profiles for 69°15'S parallel line, WP01 to WP15.

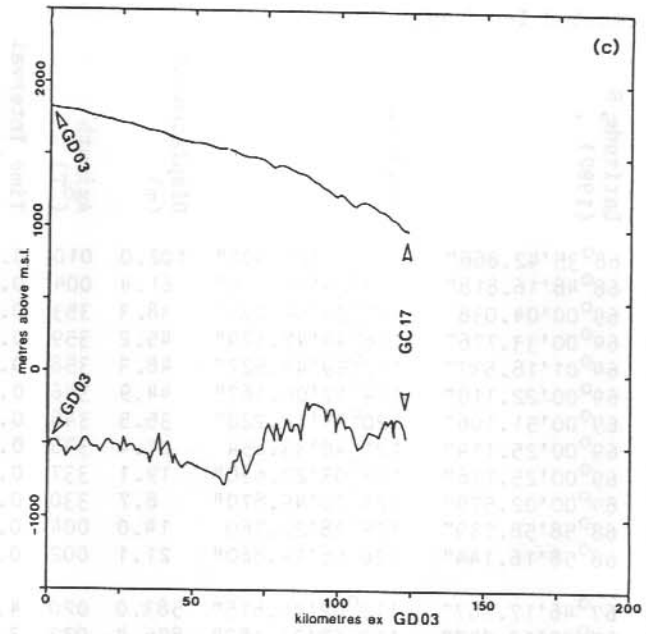

Figure 2(c). Bedrock and ice thickness profiles for Upper Totten line, GD03 to GC17.

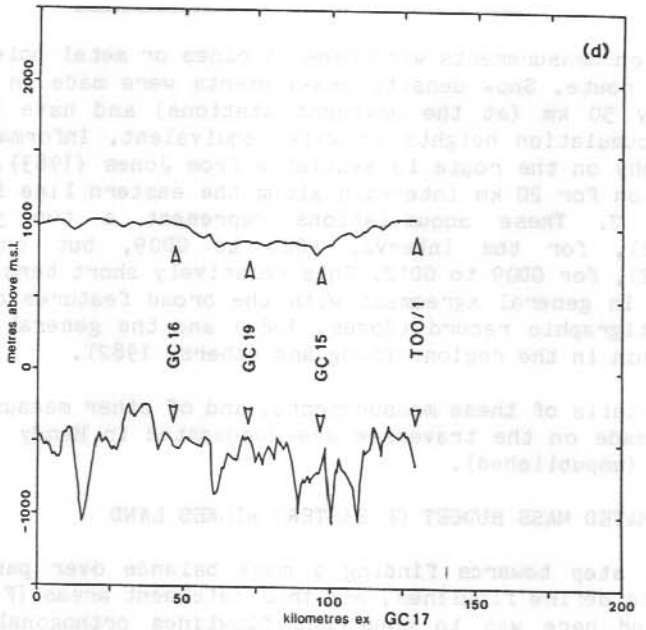

Figure 2(d). Bedrock and ice thickness profiles for Totten offset line, GC17 to TOO/1.

Table 1. Computed Ice Surface Velocities

Station	Year of last fix	Latitude, S (1982)	Longitude	Displacement (m)	Azimuth ($^{o}_{T}$)	Time Interval (yrs)	Velocity (ma^{-1})
GD01	1981	68°35'42.866"	113°19'25.302"	102.0	010	0.94	108.9
GD02	1981	68°48'16.818"	114°24'51.158"	61.4	004	0.80	76.5
GD03	1981	69°00'04.038"	115°29'44.092"	38.3	353	0.94	40.6
GD04	1981	69°00'33.776"	116°44'47.529"	45.2	359	0.83	54.2
GD05	1981	69°01'18.537"	117°59'43.827"	48.3	358	0.95	51.1
GD06	1981	69°00'22.118"	119°17'06.167"	44.9	346	0.94	47.7
GD07	1981	69°00'51.106"	120°33'14.228"	35.5	346	0.94	37.9
GD08	1981	69°00'25.114"	121°48'33.854"	27.4	336	0.95	29.0
GD09	1981	69°00'25.776"	123°03'27.690"	19.1	337	0.92	20.7
GD10	1981	69°00'02.579"	124°20'49.870"	8.7	330	0.92	9.5
GD11	1981	68°58'58.739"	125°38'22.760"	14.0	004	0.93	15.1
GD12	1981	68°58'16.144"	126°56'14.860"	21.1	002	0.95	22.2
A022	1978	67°46'17.167"	112°02'46.615"	583.0	020	4.23	137.8
GC15	1979	67°40'13.042"	112°52'32.183"	876.4	032	3.02	290.0
GC16	1979	67°53'34.960"	113°52'30.078"	806.0	002	3.00	268.4
GC17	1981	67°54'52.640"	114°56'00.198"	95.1	011	0.98	96.7
GC19	1981	67°46'36.882"	113°22'41.295"	327.6	022	0.98	333.1

Accumulation measurements were made at canes or metal poles every 2 km along the route. Snow density measurements were made in stratigraphy pits every 50 km (at the movement stations) and have been used to reduce accumulation heights to water equivalent. Information on snow stratigraphy on the route is available from Jones (1983). The average accumulation for 20 km intervals along the eastern line is summarised in Table 2. These accumulations represent a two year average (1980-1982), for the interval A028 to GD09, but only one year (1981-1982), for GD09 to GD12. This relatively short term accumulation record is in general agreement with the broad features of the longer term stratigraphic record (Jones, 1983) and the general accumulation distribution in the region (Young and others, 1982).

Further details of these measurements, and of other measurements (e.g. gravity) made on the traverses are documented in Hendy (unpublished) and Jones (unpublished).

24.3 ESTIMATED MASS BUDGET OF EASTERN WILKES LAND

The first step towards finding a mass balance over part of an ice sheet is to define flowlines, and thus catchment areas (Figure 3). The method used here was to construct flowlines orthogonal to the ice surface contours, working backwards from known points, on a polar stereographic map (Drewry, 1983; Figure 2). The surface elevation

Table 2. Average Accumulation (water equivalent) - Eastern Line

Mark	Distance from A028 (km)	Average Elevation (m)	Density ($kg\ m^{-3}$)	Average Accumulation ($k\ gm^{-2}\ a^{-1}$)
A028	0			
		1622		512
	20			
		1608		463
	40			
GD01	50	1637	400	411
	60			
		1700		268
	80			
		1713		313
GD02	100		360	
		1756		331
	120			
		1814		281
	140			
GD03	148	1833	300	276
	160			
		1838		314
	180			
		1828		379
GD04	198		370	
		1847		367
	220			
		1844		408
	240			
GD05	248	1846	350	396
	260			
		1869		388
	280			
		1871		369
GD06	299		350	

Mark	Distance from A028 (km)	Average Elevation (m)	Density ($kg\ m^{-3}$)	Average Accumulation ($Kg\ m^{-2}\ a^{-1}$)
GD06	299		350	
		1911		0.319
	320			
		1978		0.371
	340			
GD07	350	1970	410	0.350
	360			
		1985		0.300
	380			
		2037		0.285
GD08	400		340	
		2056		0.242
	420			
		2089		0.372
	440			
GD09	449	2134	-	0.339
	460			
		2161		0.334
	480			
		2192		0.274
GD10	501		400	
		2221		0.247
	520			
		2227		0.389
	540			
GD11	552	2212	400	0.301
	560			
		2193		0.342
	580			
		2216		0.337
GD12	604		360	

contours in the region of the traverse routes have been adjusted slightly to conform with the collected data (Figure 1).

The accumulation rate within the catchment was measured by overlaying a map of accumulation isopleths (Figure 4) based on the most recent data (Young, 1979; Young and others, 1982) and graphically measuring the enclosed areas. Table 3 contains the derived input mass flux.

The ice volume outflux through the sector between GD03 and GD12 (areas A and B in Figure 3) was determined, for each 50 km interval between ice movement stations, as a product of the orthogonal ice surface

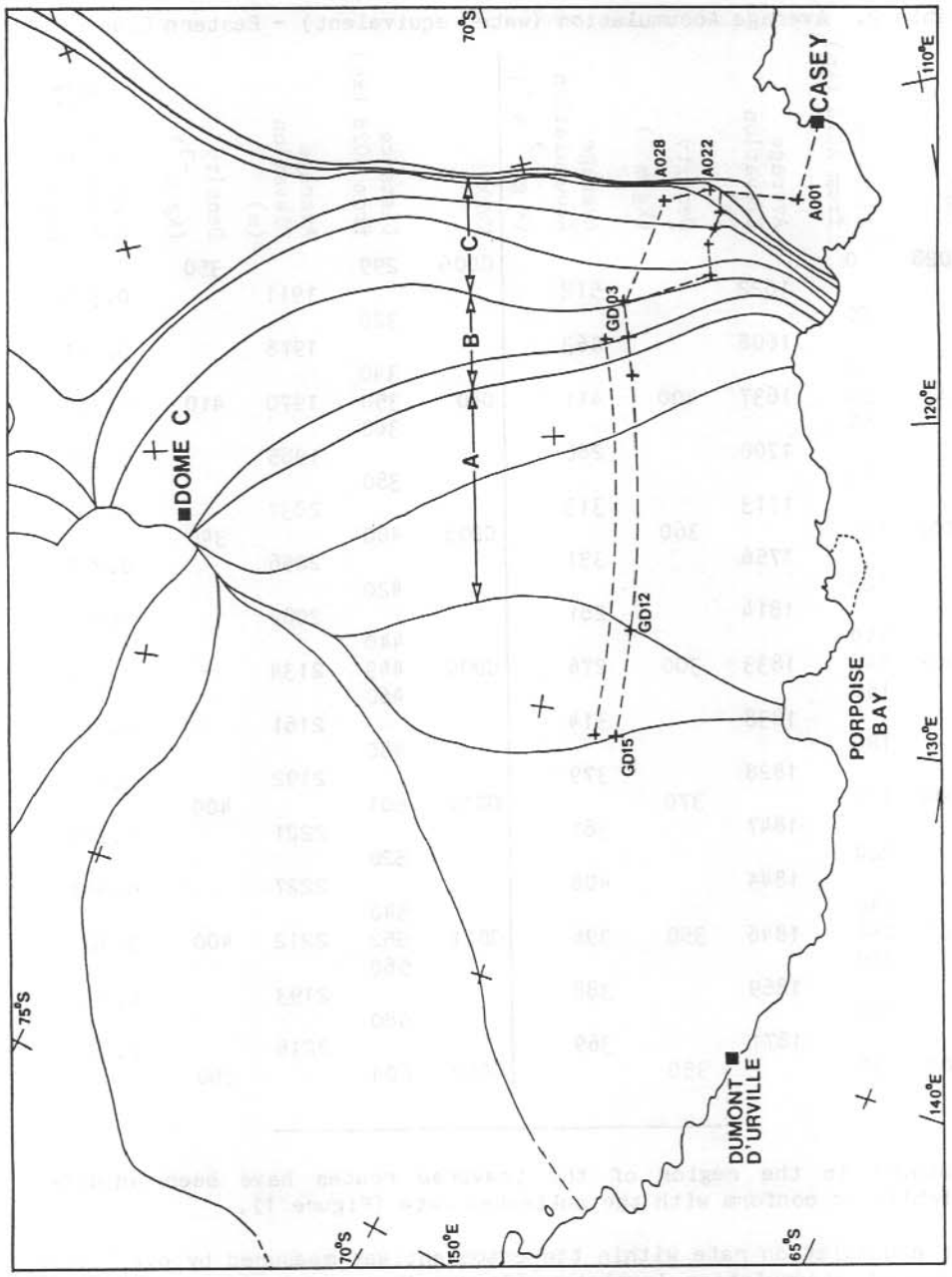

Figure 3. Flowlines and ice drainage basins, Eastern Wilkes Land, defined from elevation contours of Figure 1.

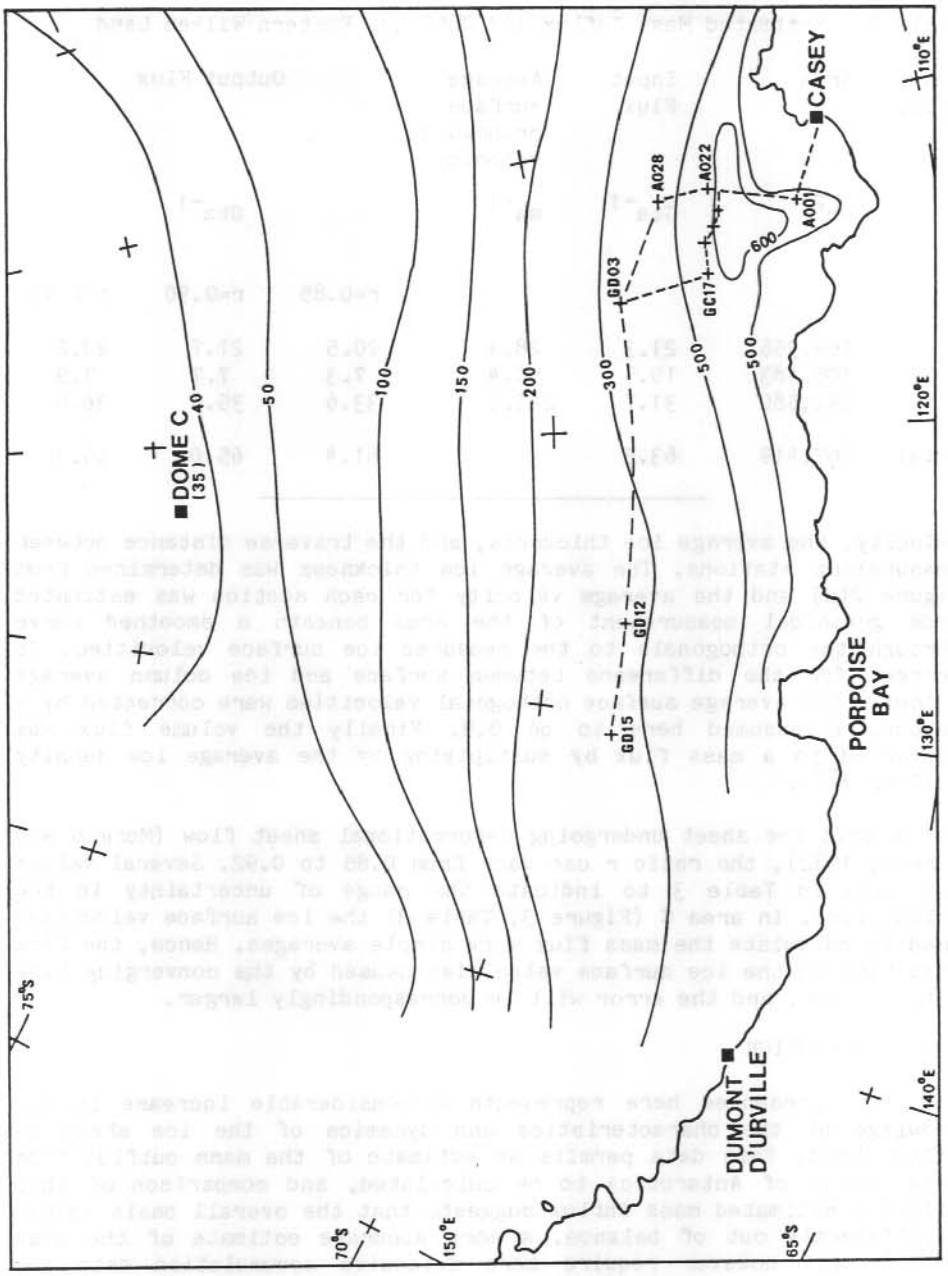

Figure 4. Accumulation isopleths (kg m^{-2} a^{-1}), Eastern Wilkes Land.

Table 3. Estimated Mass Influx and Outflux, Eastern Wilkes Land

Basin (Fig. 3)	Area	Input Flux	Average surface orthogonal velocity	Output Flux		
	km^2	Gta^{-1}	ma^{-1}		Gta^{-1}	
				r=0.85	r=0.90	r=0.92
A	159,356	21.3	28.4	20.5	21.7	22.2
B	105,483	10.5	50.4	7.3	7.7	7.9
C	342,580	31.7	223.5	33.6	35.6	36.0
Total	607,419	63.5		61.4	65.0	66.1

velocity, the average ice thickness, and the traverse distance between measurement stations. The average ice thickness was determined from Figure 2(a) and the average velocity for each section was estimated from graphical measurement of the area beneath a smoothed curve through the orthogonals to the measured ice surface velocities. To correct for the difference between surface and ice column average velocity the average surface orthogonal velocities were corrected by a factor, r assumed here to be 0.9. Finally the volume flux was converted to a mass flux by multiplying by the average ice density ($910\ kg\ m^{-3}$).

For a cold ice sheet undergoing deformational sheet flow (Morgan and others, 1982), the ratio r can vary from 0.85 to 0.92. Several values are used in Table 3 to indicate the range of uncertainty in the calculation. In area C (Figure 3, Table 3) the ice surface velocities used to calculate the mass flux were simple averages. Hence, the fine structure in the ice surface velocities caused by the converging flow will be lost, and the error will be correspondingly larger.

24.4 CONCLUSION

The data presented here represents a considerable increase in our knowlege of the characteristics and dynamics of the ice sheet in Wilkes Land. This data permits an estimate of the mass outflux from this sector of Antarctica to be calculated, and comparison of this with the estimated mass influx suggests that the overall basin is not significantly out of balance. A more accurate estimate of the mass budget will however require more extensive accumulation data and elevation data (to define drainage areas), especially in the interior of the basin.

24.5 ACKNOWLEDGMENTS

The authors thank the 1980 Casey traverse party (led by glaciologist, Peter Hicks) for pioneering work on this line and all ANARE personnel

who participated in the field programs, often under extreme conditions, and without whom none of this work would have been achieved. The long term Australian traverse program is co-ordinated by Neal Young, and his guidance is acknowledged.

REFERENCES

Drewry, D.J. (Ed.), Antarctica: Glaciological and Geophysical Folio. Map 2: The Surface of the Antarctic Ice Sheet. Scott Polar Research Institute, University of Cambridge.

Hendy, M. (unpublished) Glaciology data report, Casey 1981: Eastern 2000 m and associated traverses. Antarctic Division Glaciology Section Internal Report.

Jones, D.J. (unpublished) 1982 Casey traverse glaciological data report. Antarctic Division Glaciology Section Internal Report.

Jones, D.J. (1983) Snow stratigraphy observations in the katabatic wind region of eastern Wilkes Land, Antarctica. ANARE Research Notes, 17.

Morgan, V. (unpublished) ANARE MKV ice radar. Antarctic Division Glaciology Section Inernal Report.

Morgan, V. and Davis, E. (unpublished) ANARE ditigal barometer handbook. Antarctic Division Glaciology Section Internal Report.

Morgan, V.I., Jacka, T.H., Akerman, G. and Clarke, A.L. (1982) Outlet Glacier and Mass Budget Studies in Enderby, Kemp and MacRobertson Lands, Antarctica. Annals of Glaciology, 3, 204-210.

SCAR, (1971) International Antarctic Glaciological Project. SCAR Bulletin, 38, 829-833.

Smith, N. (unpublished) 100 MHz phased array for ice radar. Antarctic Division Glaciology Section Internal Report.

Young, N. (1979) Measured velocities of interior East Antarctica and the state of mass balance within the IAGP area. Journal of Glaciology, 24, (90), 77-87.

Young, N.W., Pourchet, M., Kotlyakov, V.M., Korolev, P.A. and Dyugerov, M.B. (1982) Accumulation distribution in the IAGP area, Antarctica: 90°E. Annals of Glaciology, 3, 333-338.

25. GLACIOLOGICAL MEASUREMENTS IN WESTERN WILKES LAND, ANTARCTICA

T.G. Medhurst
Antarctic Division, Department of Science
Kingston, Tasmania, 7150.

ABSTRACT

During 1983 a new traverse route was established along latitude 68°30'S between longitude 112°04'E (B029) and 94°34' (GM04), a distance of 725 km. Fourteen new ice movement stations were established. Similarly 190 km of traverse route and two new ice movement stations were established inland of the Vanderford Glacier. Surface and bedrock profiles, along with a range of other glaciological measurements were obtained on all routes. A summary of measurements made with relevant comment is given.

25.1 INTRODUCTION

The new traverse route along latitude 68°30'S between B029 and GM04, will be referred to as the Western traverse whilst the route from GF02 to A021 via GC25 will be referred to as the Vanderford offset (Figure 1). Data was collected on these routes during two of five traverses from Casey in 1983. The first, during the months of March and April, established the western route from B029 to GF03. A later traverse, from September to December intersected with the existing Soviet traverse route from Mirny to Pioneerskaya at GM04. On the return journey the Vanderford offset was established in early December.

25.2 TOPOGRAPHY

By following latitude 68°30'S the route ran approximately parallel to the coast at a range of 250-300 km. A surface profile was obtained by barometric levelling between ice movement stations at which heights were measured using satellite doppler position fixing. These stations were generally 50 km apart. Typically, one barometer and chart recorder was stationary at each ice movement station whilst the other was travelling. Elevations along the western route showed a gradual rise from B029 (1670 m) up to GF06 (2300 m). From there the surface fell to GF10 (1970 m), around the centre of the Denman Glacier Valley, before rising relatively steeply to GF12 (2320 m). The 2300 m contour was then approximately followed via GF13 to GM04.

25.3 BEDROCK

Ice depth was measured with the 100 MHz radar which was run continuously on both outward and return journeys giving a permanent record on 35 mm film. A clear record was obtained giving bedrock echoes for more than 90% of the route. Also at every marker a manual reading of ice thickness was recorded. Figure 2 shows surface and bedrock profiles along the western route. This is an initial profile using the ice movement station heights only for the surface profile and 2 km manual readings for ice depths. Maximum ice depth was about 3850 m below GF10, whilst other areas were as shallow as 1000 m. Two

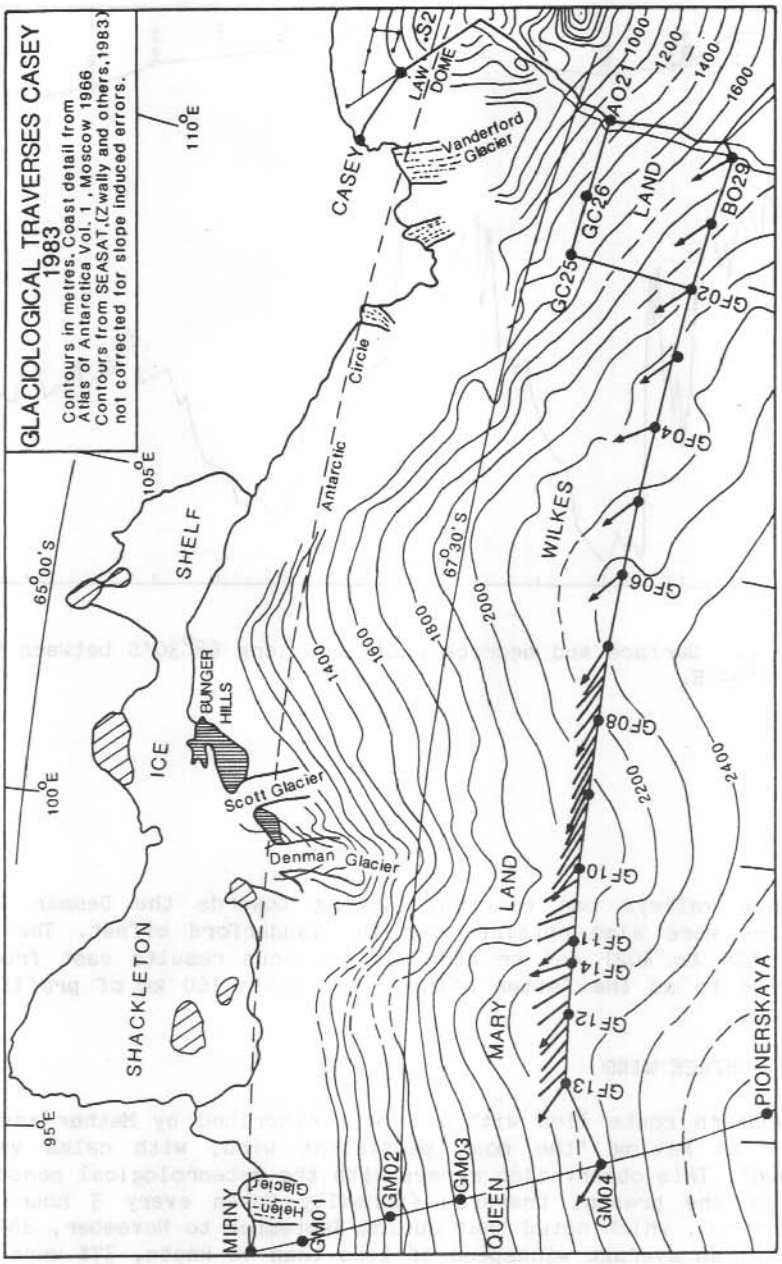

Figure 1. Map of western Wilkes Land and Queen Mary Land depicting the major features of the region, the location of the western traverse route from B029 to GM04 and doppler satellite stations (solid circles). The prevailing wind direction, shown by vectors at 10 or 50 km intervals along the route, was derived from measurements of sastrugi alignment in the spring/summer.

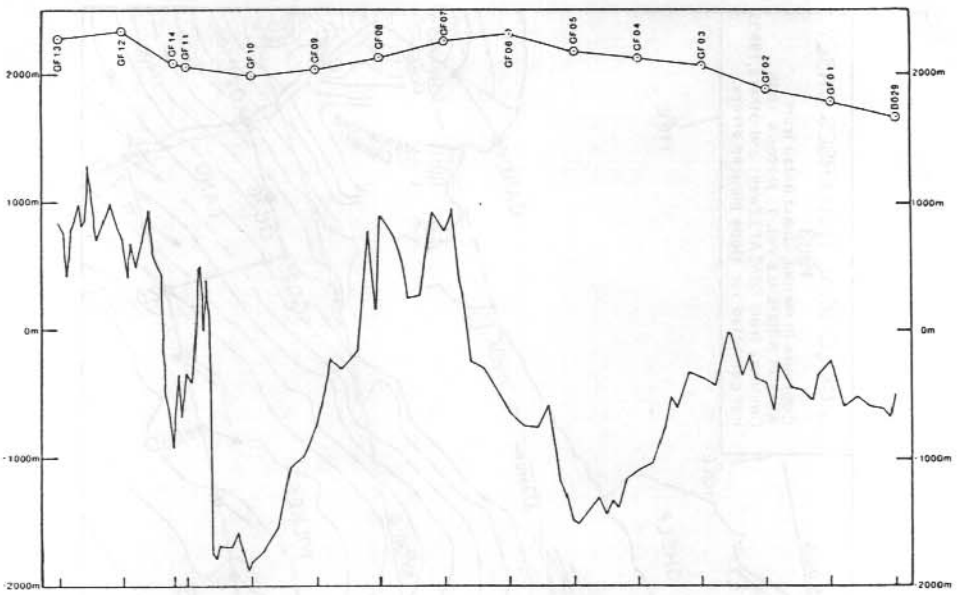

Figure 2. Surface and bedrock profiles along 68°30'S between 95°56'E and 112°04'E.

distinct valleys can be seen flowing towards the Denman Glacier. Profiles were also obtained for the Vanderford offset. The profile from GC25 to A021 can be added to previous results east from A021, referred to as the Totten offset, to obtain 160 km of profile along 67°42'S.

25.4 SURFACE WIND

The western route lies within a belt described by Mather and Miller (1967) as having "the most persistent wind, with calms virtually unknown". This observation agrees with the meteorological measurements made on the present traverse (normally taken every 3 hours whilst stationary), which noted that during September to November, 28% of the days had an average windspeed of less than 10 knots, 37% were between 10 and 20 knots, and the remaining 35% were more than 20 knots. Most of these winds carried drift with them, considerably reducing horizontal visibility. At times large sastrugi or snow dunes up to 2 m high were encountered. However in general the sastrugi was 0.2 -0.8 m in height. Smoother surfaces were found around GF07 and GF08, whilst small surface crevassing up to 0.5 m wide was encountered for 30 km southwest from GF13.

The sastrugi are formed by the wind over a long period of time and can be used as a method of determining the prevailing surface wind direction. Observations were made at least every 50 km, and for 300 km across the head of the Denman Glacier they were made every 10 km. As seen in Figure 1 there is an obvious swing to the west as the wind flows into the Denman Valley. It is assumed that this swing is a combination of the corriolis effect and local topography. This information can be added to existing results, such as those of Mather and Miller (1967) to help determine the overall surface wind system in Antarctica.

25.5 10 M SNOW TEMPERATURES

For the purpose of estimating the mean annual surface temperature, 10 m snow temperature was measured at each ice movement station on the western route. Temperatures ranged from -27.2 to -35.2 ^{o}C. A linear regression of temperature against elevation reveals a temperature elevation gradient of -1.10 ^{o}C/100 m rise in elevation. This figure is comparable with -0.98 ^{o}C/100 m, using data measured along 69^{o}S in eastern Wilkes Land, in 1981 (Hendy, unpublished), and -1.02 ^{o}C/100 m on the Law Dome in 1958 (Cameron, 1964).

25.6 SURFACE DENSITY

Surface density was measured to a depth of 0.2 m every 10 km on all routes. At every 50 km density was measured down the face of a pit 2-3 m deep. Each pit generally covered a minimum of 2 years accumulation. Over the length of the western route the average density of the spring-summer surface was 0.47 gm/cm^{3}. However, it is considered that a more accurate interpretation of the snow density was obtained by averaging the densities measured in each pit and hence covering a full range of seasons. This gives a mean of 0.43 gm/cm^{3}, from a range of individual pit means of 0.37 to 0.50 gm/cm^{3}.

25.7 ACCUMULATION

Accumulation canes were placed every 2 km along all routes. Based on measurements five months apart during 1983, a snow accumulation of 1.2 ma^{-1} (0.48 ma^{-1} water equivalent) was calculated for the western route between B029 and GF03. Estimates of accumulation for the whole western traverse have been made from stratigraphical measurements every 50 km in a 2-3 m pit, along with detailed oxygen isotope sampling (Table 1).

25.8 STRATIGRAPHY

At the face of each pit the following measurements were made.
(a) depth of different snow and ice layers, crystal sizes and hardness (when possible).
(b) density was measured every 100 mm down the face. At least 100 gm of firn was collected for each measurement.
(c) generally 30-40 water samples were taken to determine oxygen isotope ratios, giving a detailed coverage from which annual trends were interpolated.

Table 1. Estimates of accumulation from stratigraphic measurements in a 2-3 m pit.

Station	Density	Accumulation	
	gm/cm^3	$m_{snow}a^{-1}$	$m_{water}a^{-1}$
Around B029 *	0.46	1.39	0.64
GF01	0.40	1.3	0.52
GF02	0.40	1.0	0.40
GF03	0.44	1.0	0.44
GF04	0.49	1.0	0.49
GF05	0.46	0.95	0.44
GF06	0.44	0.9	0.40
GF07	0.43	0.9	0.39
GF08	0.44	0.85	0.37
GF09	0.43	0.8	0.34
GF10	0.42	1.45	0.61
GF11	0.44	1.2	0.53
GF12	0.44	0.7	0.31
GF13	0.50	0.4	0.20
Around GM04*	0.47	0.25	0.12

* B029 and GM04 are known results. Figures shown for B029 are the mean accumulation for 10 km east of A028 (Hendy, unpublished). GM04 figures come from data collected between 1970 and 1973 (Barkov, 1975).

Table 2. Ice movement results

Station	Days between measurement	Velocity vector	
GF02	230	31 ma^{-1}	23 ^oT
GF03	166	25 ma^{-1}	27 ^oT
GF10	23	141 ma-1	359 ^oT

At either end of the western route previously established stations were measured to give

B029	1 218 (3.3 a)	105 ma^{-1}	18 ^oT
GM04	2 480 (6.8 a)	11 ma^{-1}	10 ^oT

25.9 ICE MOVEMENT STATIONS

Position was determined by satellite doppler survey equipment. Typically 50-100 satelite passes were utilised in the final processing of each station. Of the new stations established in 1983 (numbered GF01-GF14 on the western route and GC25 and GC26 on the Vanderford offset), opportunity arose for the measurement of three stations to obtain some estimate of movement prior to a complete remeasure being done in coming years. Stations remeasured are summarised in Table 2.

25.10 OTHER MEASUREMENTS

Other measurements included gravity every 2 km on the outward journey and every 10 km on return, closing at Casey. Total magnetic field intensity was measured every 10 km on all routes. Both sets of results are currently undergoing reduction and analysis.

ACKNOWLEDGMENTS

I thank the 1983 ANARE traverse personnel for their efforts in the field and the other ANARE personnel at Casey who supported the traverse program. Position measurements were made in cooperation with the Division of National Mapping. This cooperation is also acknowleged.

REFERENCES

Barkov, N.I. (1975) Snow Accumulation along the Mirny-Vostok Profile, 1970 through 1973. Antarctic Journal of U.S.A., X, (2), 56-57.

Cameron, R.L. (1964) Glaciological studies and Wilkes station, Budd Coast, Antarctica. Antarctic snow and ice studies. 2. Antarctic research series. Mellor, M. (Ed.), American Geophysical Union. 16.

Hendy, M. (unpublished) Glaciology data report, Casey 1981. Eastern 2000 m and associated traverses. Antarctic Division Glaciology Section Internal Report.

Mather, K.B. and Miller, G.S. (1967) Notes on topographic factors affecting the surface wind in Antarctica, with special reference to Katabatic winds; and bibliography. Technical report, Grant No GA-900 National Science Foundation. Geophysical Institute of the University of Alaska. 45 pages.

Zwally, H.J., Bindschadler, R.A., Brenner, A.C., Martin, T.V. and Thomas, R.H. (1983) Surface elevation contours of Greenland and Antarctic ice sheets. Journal of Geophysical Research, 88, (C3), 1589-1596.

26. GLACIOLOGICAL MEASUREMENTS ON THE 1983/84 SOVIET TRAVERSE FROM MIRNY TO DOME C

T. Hamley
Antarctic Division, Department of Science
Kingston, Tasmania, 7150.

ABSTRACT

An invitation to participate in the 1983/84 Mirny to Dome C traverse provided an opportunity to complete the remeasurement of ice-movement markers already established on four previous visits by Australian glaciologists since 1976/77. Some markers had not been remeasured and others required further remeasurement. Surface ice velocity data from the survey are presented here.

Accumulation data and snow surface samples were also collected.

The major objectives of the program were achieved despite wide ranging difficulties during the traverse.

26.1 INTRODUCTION

Since 1976/77, Australian glaciologists have participated in the Soviet Antarctic oversnow traverse from Mirny to Dome C on five occasions, at the invitation of the Soviet Arctic and Antarctic Institute in Leningrad.

Data gathered from this cooperative glaciology study have been an important contribution to the International Antarctic Glaciology Project (I.A.G.P.), which is broadly aimed at determining the state of balance of the East Antarctic ice sheet. The Mirny to Dome C line is one of four major overland traverse routes within the I.A.G.P. area.

The main glaciological aim of the 1983/84 program was to finalise remeasurements of slow moving inland ice-velocity markers. Some markers had not been remeasured and others required further remeasurement.

Results to come out of the program to date have been compiled by Young (1979), Young and others (1982), and Kotlyakov and others (1983).

26.2 1983/84 MEASUREMENT PROGRAM (MIRNY/DOME C)

The specific reason for the Soviet 1983/84 Dome C traverse was to support their continuing long-term investigation of fluctuations in the earth's interplanetary magnetic field. Overland traverses from Mirny to Dome C are necessary on a yearly basis to maintain "Automatic Remote Magnetic Stations" (ARMS).

During the 1983/84 austral summer the author was in Antarctica for a period of five months, two and a half of which were taken up with the Mirny to Dome C traverse. Approximately one month was spent at Mirny.

Despite wide ranging difficulties during the traverse all major scientific objectives were achieved. Ice velocity measurements were obtained with satellite doppler positioning equipment.

Before leaving Australia, existing markers were assigned a remeasurement priority which determined the length of stay at various stations along the route.

An important part of the program also entailed the remeasurement of an ice movement station establised at Vostok in 1977. This was completed in a two day period prior to leaving on the Dome C traverse.

In addition, snow accumulation readings were taken at all available marker poles, approximately every 2 km between Pionerskaya and Dome C.

Snow surface samples were collected between Mirny and Dome C at spacings of 50 to 100 km. The melted samples were sent to the "Laboratoire de Geochemie Isotopique" in France, for analysis of the stable isotopes of hydrogen and oxygen.

26.3 VELOCITY OF THE INLAND ICE SHEET

The 1983/84 remeasurement successfully concludes the final stage of this Soviet/Australian Mirny to Dome C program. The resulting velocity measurements provide one of the first comprehensive data sets for the inland ice sheet at an approximate elevation of 3000 m. A full compilation of results is currently being prepared in a joint report by Soviet and Australian scientists.

A summary of velocity data resulting from the 83/84 remeasurement is given in Table 1. Surface ice velocity vectors are shown in Figure 1.

Ice velocities inland (i.e. above the 3000 m contour) are typically less than 10 ma^{-1}. This region is characterised by low surface slope and low strain rates. Between the 3000 m and 2500 m contour, ice velocities are typically in the range up to 20 ma^{-1}. Towards the coast (elevations less than 2500 m), ice velocities vary between 20 ma^{-1} and 100 ma^{-1} with evidence of faster ice flow and streaming near Mirny.

Elevation contours shown in Figure 1 were derived from Drewry (1983). General agreement is apparent between the direction of velocity vectors and surface slopes. However a notable exception to this appears at GM15 where strongly divergent flow is clear between GM15 and GM14.

The error range in velocity measurements (Figure 1) is dependent on two factors. First, the accuracy of the satellite doppler position fix and second, the time between measurements. The movement accuracies have been determined in accordance with guide lines suggested by the Division of National Mapping, and represent an assigned error based on the number of satellite passes collected.

Table 1. Satellite doppler stations measured (1983/84 season).

				Solution - Final Processing NSWC - 9 Z2 Satellite Datum					
Station Number	Duration of Velocity Computation (Years)	Days of Occupation	Number of Passes (After Final Processing)	Latitude (DD.MM.SS)	Longitude (DD.MM.SS)	Elevation of Snow Surface (m)	Velocity * (ma^{-1})	Azimuth (^oT)	Comments
GM 90	6.0	353/354,83	18	78 27 56.007	106 50 14.334	3471	2.0 ± 0.6	139	VOSTOK
GM 01	4.9	357/358,83	15	67 00 15.791	93 18 01.193	886	108.5 ± 0.7	25	
GM 03	6.9	360/361,83	17	67 51 31.553	93 45 00.523	1753	24.3 ± 0.7	354	
GM 05	6.8	03/05,84	50	69 44 43.804	95 31 49.860	2745	2.0 ± 0.4	15	PIONERSKAYA
GM 06	6.9	05/06,84	9	69 58 43.274	96 18 30.256	2732	7.9 ± 0.8	41	
GM 12	6.0	52/58,84	23	72 59 48.409	109 20 56.222	2920	6.7 ± 0.7	1	
GM 13	6.9	22/24,84	15	73 14 25.304	110 27 22.348	2960	8.2 ± 0.4	356	
GM 14	4.9	18/20,84	29	72 11 08.422	105 23 07.577	2895	8.6 ± 0.6	56	
GM 15	6.9	13/15,84	30	71 53 49.178	103 18 28.441	2983	5.3 ± 0.7	354	
GM 16	6.9	10/11,84	4	71 18 42.590	100 32 06.635	2928	8.3 ± #	14	
GM 12	5.0	41/43,84	43	74 10 34.298	117 43 17.952	3107	2.2 ± 0.9	317	
GM 22	5.0	31/32,84	51	74 29 30.056	120 57 41.015	3163	2.6 ± 0.9	353	
GM 22	5.0	38/40,84	51	74 29 30.056	120 57 41.015	3163	2.6 ± 0.9	353	
GM 25	5.0	48/50,84	20	73 40 04.256	113 26 46.350	3034	7.7 ± 0.9	325	
GM 28	3.0	27/28,84	34	73 52 39.052	115 06 56.116	3066	5.0 ± 1.1	315	
GM 28	3.0	43/45,84	34	73 52 39.052	115 06 56.116	3066	5.0 ± 1.1	315	
GM 29	2.9	33/36,84	70	74 43 55.179	124 22 03.807	3210	1.3 ± 0.9	324	DOME C
GM 30		02/03,84	20	69 31 53.687	95 20 14.979	2664	-	-	ARMS-61
GM 31		37/38,84	11	74 39 54.785	123 45 37.271	3214	-	-	ARMS-67

Note * Accuracies refer to the estimated error at the 90% confidence interval = 1.650.

Measurement unreliable.

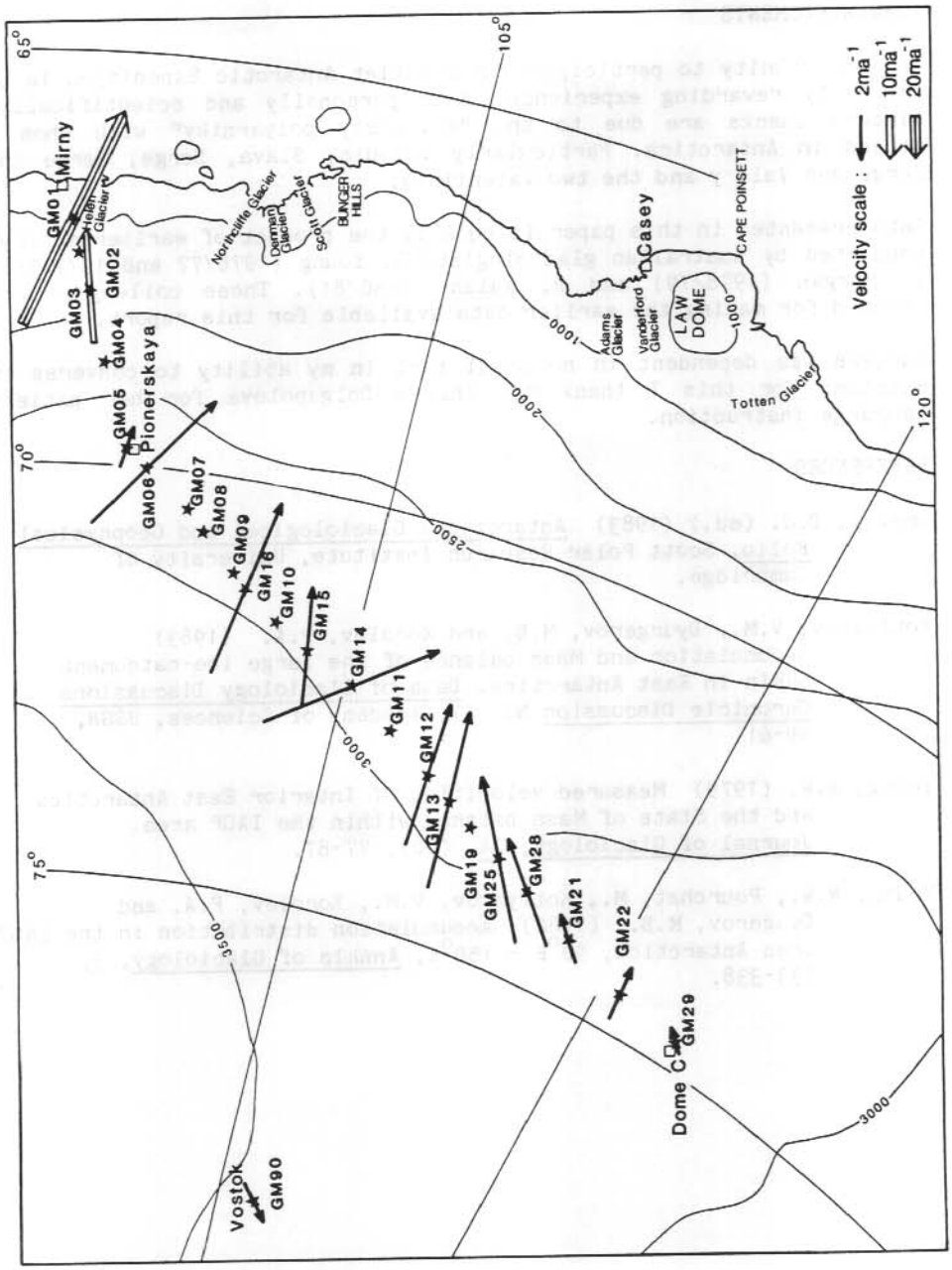

Figure 1. Ice movement vectors, Mirny-Dome C route.

ACKNOWLEDGMENTS

The opportunity to participate in a Soviet Antarctic Expedition is an immensely rewarding experience, both personally and scientifically. Sincere thanks are due to the "sovietsky polyarniky" with whom I worked in Antarctica. Particularly Valodia, Slava, Serge, Serge and Serge and Valery and the two Valentines.

Data presented in this paper is equally the product of earlier surveys conducted by Australian glaciologists N. Young (1976/77 and 1977/78), V. Morgan (1978/79) and R. Walsh (1980/81). These colleagues are thanked for making the earlier data available for this report.

Success was dependent in no small part in my ability to converse in Russian; for this I thank Mrs Zhanna Dolgapolova for her patient language instruction.

REFERENCES

Drewry, D.J. (ed.) (1983) Antarctica: Glaciological and Geophysical Folio. Scott Polar Research Institute, University of Cambridge.

Kotlyakov, V.M., Dyurgerov, M.B. and Korolev, P.A. (1983) Accumulation and Mass balance of the large ice-catchment basin in East Antarctica. Data of Glaciology Discussions Chronicle Discussion No. 47, Academy of Sciences, USSR, 49-61.

Young, N.W. (1979) Measured velocities of Interior East Antarctica and the State of Mass balance within the IAGP area. Journal of Glaciology, 24, (90), 77-87.

Young, N.W., Pourchet, M., Kotlyakov, V.M., Korolev, P.A. and Dyugerov, M.B. (1982) Accumulation distribution in the IAGP area Antarctica, 90°E - 150°E, Annals of Glaciology, 3, 333-338.

27. THE VANDERFORD GLACIER TOPOGRAPHIC SURVEY

D.J. Jones and E. Davis
Antarctic Division, Department of Science
Kingston, Tasmania, 7150.

ABSTRACT

A comprehensive airborne topographic and ice thickness survey of the Vanderford Glacier, 30 km south of Casey, was begun in January, 1983 and continued in December and January, 1983-84.

3500 km^2 of the glacier have now been covered by an approximately 5 km grid. Over about half this area, bedrock topography was measured in detail with an ANARE ice radar; whilst over the remainder, where the ice radar failed to produce a bottom echo, a general coverage was obtained with a gravity meter. Surface topography was recorded continuously as the ice radar always produced a surface echo.

Ice surface velocity measurements at ten locations near the snout of the glacier show that about 5 km^3/a of ice is draining through the Vanderford system.

Bedrock topography shows a very pronounced feature in which the glacier lies and gravity measurements show approximately where the glacier begins to float.

27.1 INTRODUCTION

A comprehensive airborne and ice thickness survey of the Vanderford Glacier, 30 km south of Casey, Antarctica ($66^{o}17'S$, $110^{o}32'E$) (Figure 1), was completed in January, 1984.

3500 km^2 of the glacier was covered by an approximately 5 km grid for surface and bedrock detail. Two additional detail areas were covered by an approximately 1 km grid; one on the glacier near GC02 ($66^{o}54'S$) and the other near the eastern edge of the glacier on the Law Dome.

Bedrock detail was measured over more than half the covered area, whilst in the remainder, the ice radar failed to produce bottom echo. In these areas a gravity meter was used to provide an estimate of ice thickness.

Additional gravity traverses were carried out to calibrate the ice thickness measurements and in an attempt to define the area in which the glacier begins to float.

Ten markers were positioned on the snout of the glacier and later remeasured to provide ice surface velocities.

27.2 DATA COLLECTION

An instrumented Bell 206 helicopter was used for the topographic survey. Precise positioning was provided by Motorola Mini Ranger

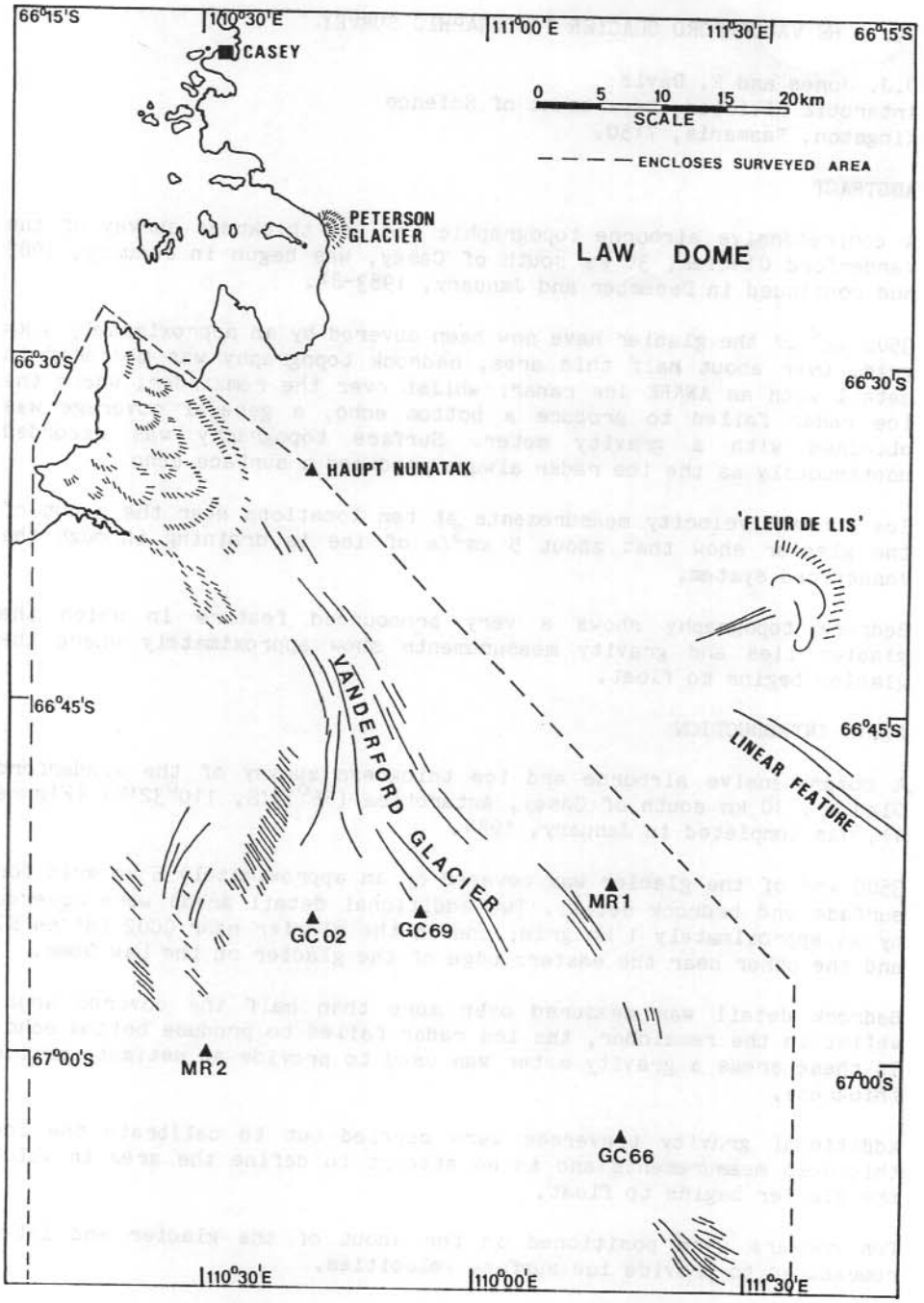

Figure 1. Map of the region south of Casey showing the location of the surveyed area, Vanderford Glacier and other major features, and stations with doppler satellite positions (triangles).

distance measuring equipment, ground stations, a doppler satellite positioning instrument, and accurate barometry.

A LaCoste and Romberg gravity meter was carried in another helicopter and operated manually at selected points on the glacier surface.

Positioning for the velocity and gravity surveys was accomplished with guided precision hovering.

Topographic (bedrock and surface) detail was measured using an ANARE ice radar incorporating an accurate altimeter for surface detail.

Data was logged automatically every 10 seconds on each flight.

27.3 DATA ANALYSIS

Three applications of the data are here considered; total mass flux, gravity reduction for ice thickness, and the location of the grounding line or region in which the glacier begins to float.

Mass flux

From the five measured velocities on the transverse line from Haupt Nunatak, and the known morphology of the area it is possible to draw a smoothed velocity profile across the glacier. It is assumed that the ice velocity approaches zero in the region of Haupt Nunatak and remains constant from about the middle of the stream to the southern edge, as there is an obvious region of high shear at this edge in a distance of less than 500 m, where the glacier and the adjacent ice shelf merge. Since the glacier is floating across most of the transverse the ice velocity is assumed approximately constant throughout the depth. Thus the problem reduces to a numerical integration of ice velocity multiplied by increments of cross sectional area. The latter is derived from an ice thickness contour map.

The resultant mass flux is 4.6 Gt a^{-1}.

Gravity measurements and the grounding line

All gravity measurements have been reduced to a common datum (0 m on NWL-8E) so that the resultant Bouguer anomaly is due to ice thickness, bedrock topography and, to a much lesser extent, ice surface topography. Since the measuring grid spacing is coarse (5 km), an estimate has to be made of the topographic contribution to the Bouguer anomaly. An approximate ice thickness can then be calculated, and this detail added to the contour map of the bedrock. Most of the above anomalies are positive. When they become negative, it is deduced that the "bedrock" is indeed only the ice bottom and that there is matter less dense than rock between the ice bottom and the bedrock, that is, water. This phenomenon occurs over a well defined region of the glacier and is indicated in Figure 3.

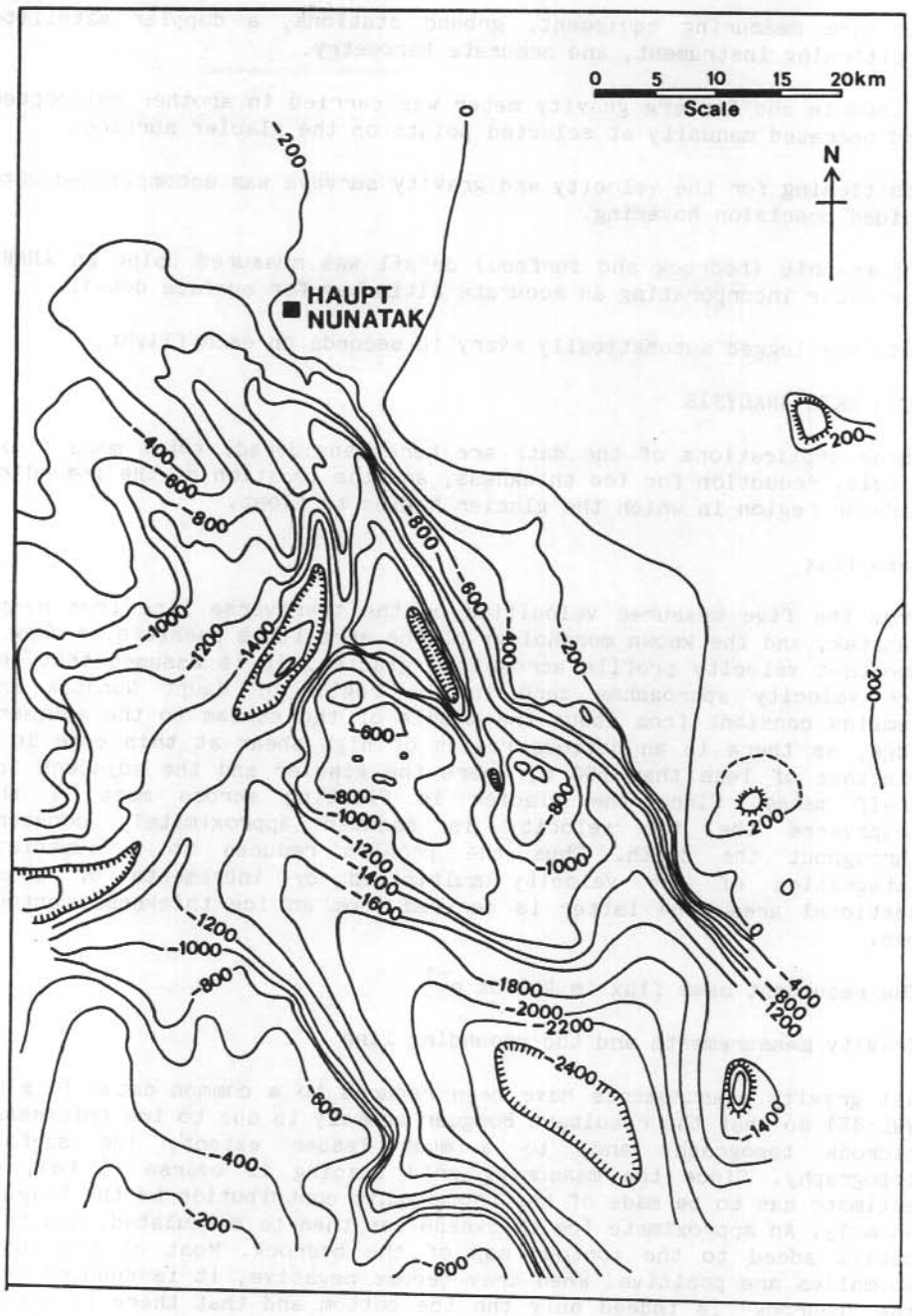

Figure 2. Map of ice bottom relief. Contours are at 200 m interval, and elevations are referenced to the NWL8E ellipsoid (Sea level is equivalent to approximately -18 m). Where the ice is not floating, the bedrock relief is given.

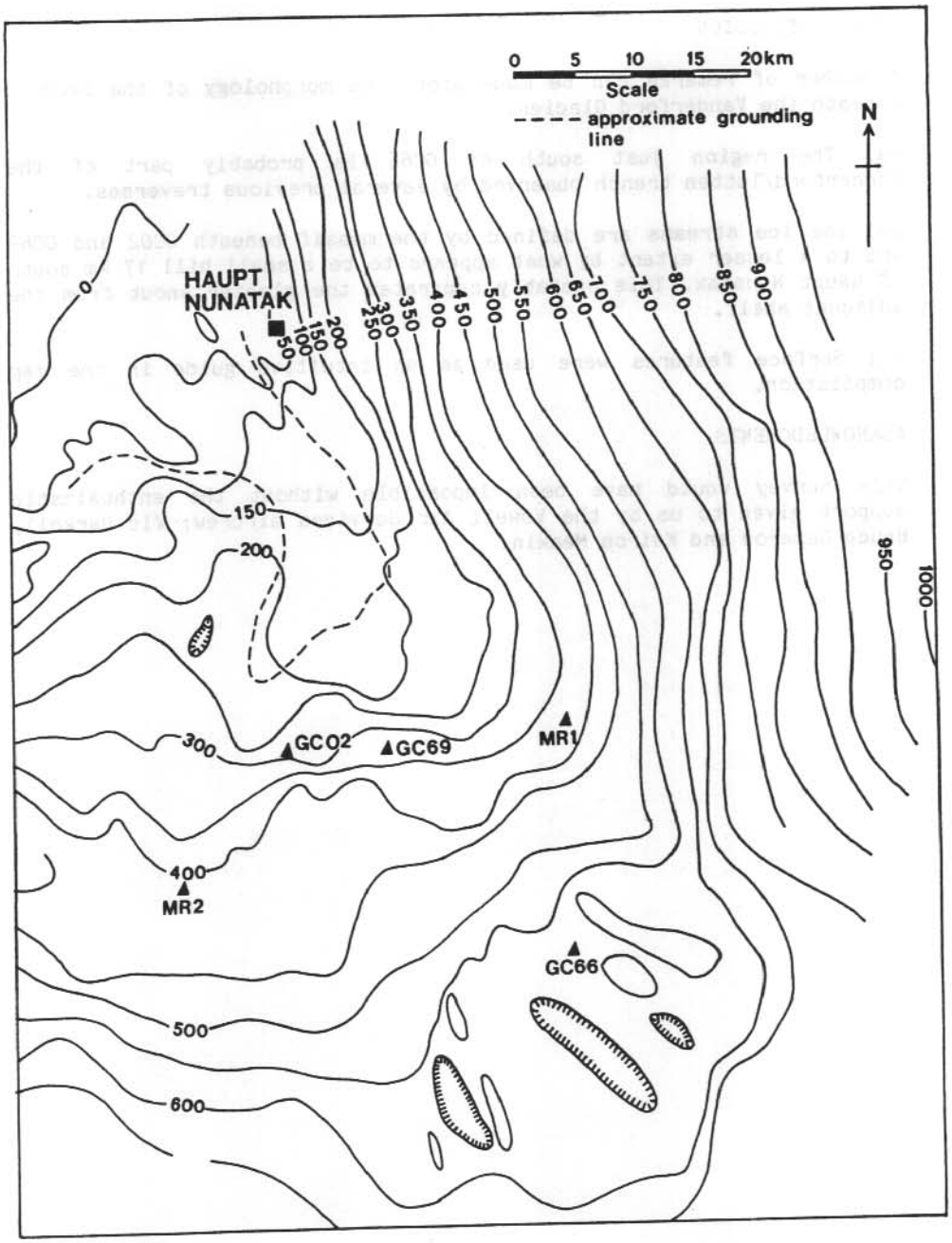

Figure 3. Map of ice surface elevation. Contours are at 50 m interval, and elevations are referenced to the NWL8E ellipsoid. (Sea level is equivalent to approximately -18 m). Enclosed surface depressions are shown by hatching.

27.4 DISCUSSION

A number of remarks can be made about the morphology of the bedrock beneath the Vanderford Glacier.

(a) The region just south of GC66 is probably part of the Vanderford/Totten trench observed by several previous traverses.

(b) The ice streams are defined by the massif beneath GC02 and GC69 and to a lesser extent by what appears to be a small hill 17 km south of Haupt Nunatak. This probably separates the glacier snout from the adjacent shelf.

(c) Surface features were used as an intuitive guide in the map compilation.

ACKNOWLEDGMENTS

This survey would have been impossible without the enthusiastic support given to us by the Vowell Air Services aircrew; Vic Barkell, Bruce Cameron and Keiron Meakin.

F. GLACIOLOGICAL INSTRUMENTATION

The collection of glaciological data in Antarctica often requires the development of specialised equipment and techniques.

Some of these methods and instruments are detailed.

28. INSTRUMENTATION AND OPERATIONAL PROCEDURES USED ON THE VANDERFORD GLACIER SURVEY PROGRAM

E. Davis
Antarctic Division, Department of Science
Kingston, Tasmania, 7150.

ABSTRACT

This note provides a brief overview of instrumentation and procedures used on the 1983/84 austral summer Vanderford Glacier survey program.

28.1 AIMS AND EQUIPMENT

The Vanderford Glacier is situated at approximately 66°30'S and 110°17'E. The total area surveyed was approximately 3000 km^2 and is devoid of notable landmarks (Figure 1).

The aims of the survey were:

a) Surface and subsurface profiling of an additional 2500 km^2 of the Vanderford Glacier (approximately 1000 km^2 had been surveyed the previous summer).
b) Gravity survey in the snout region of the glacier.
c) Ice velocities survey in the snout region of the glacier.
d) Surface and subsurface profiling of an existing grid system on Law Dome.
e) Profiling of the coast between the Vanderford Glacier and Hatch Island (66°S, 109°E).

The following equipment was used:

a) Doppler satellite receiver - JMR, complete with cassette recorder and microprocessor
b) Gravity meter
c) 2 channel distance measuring equipment - Motorola Miniranger
d) Ice radar
e) Barometers
f) Data logger

The Doppler satellite receiver was used to accurately position reference points used throughout the survey. These points included the ground reference stations used by the distance measuring equipment and to a lesser extent the velocity stations set up in previous years.

The gravity meter was used to measure gravity at various points about the glacier. Initially, gravity measurements were taken in the snout area of the glacier, however owing to poor ice radar results, this was later extended to cover more of the survey area.

The Vanderford Glacier area is essentially featureless. Coupled with the vastness of the survey area, along with the need for position accuracy varying from ±100 m to ±5 m, it was necessary to use distance measuring equipment. The 2 channel Motorola Miniranger III DME

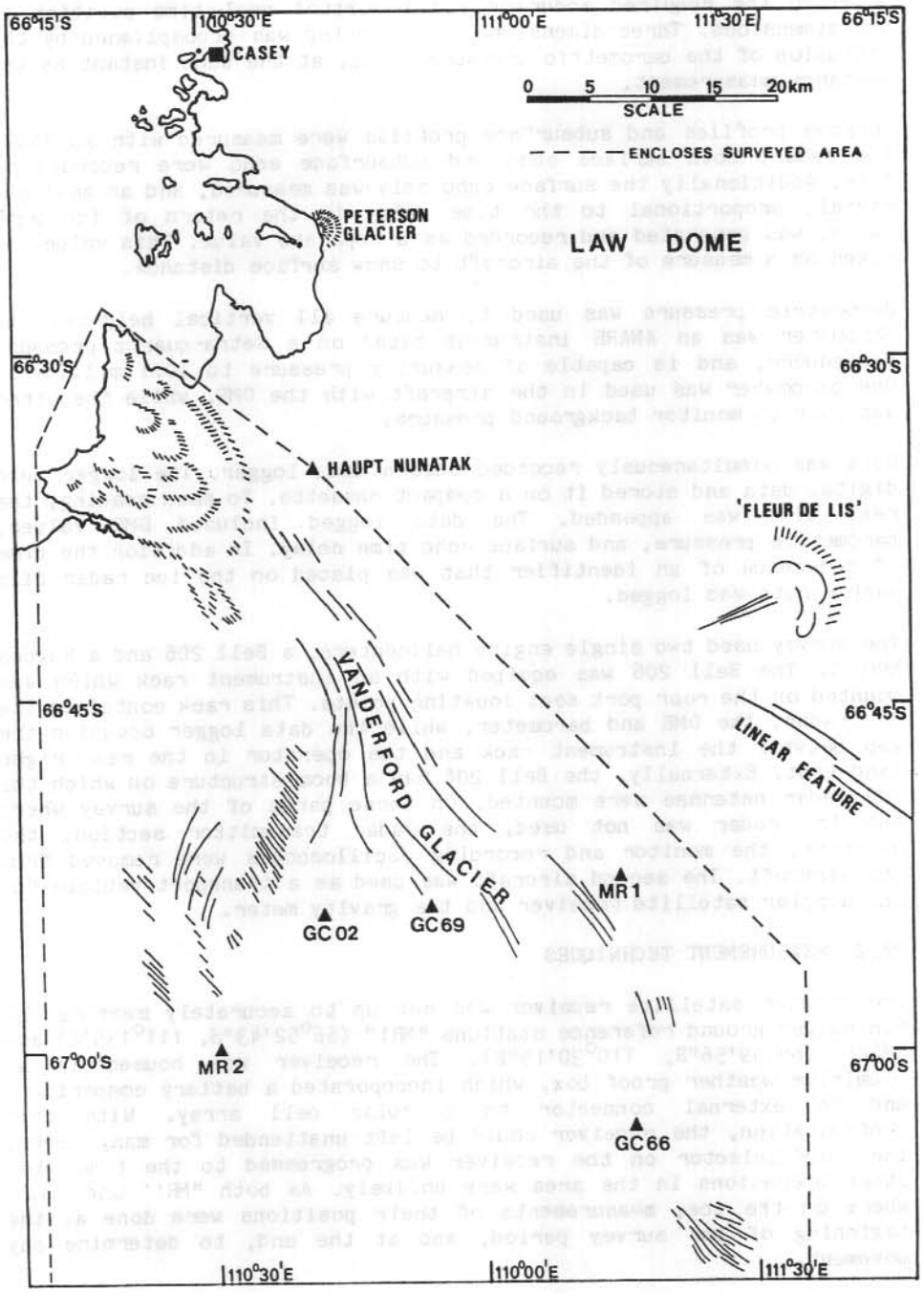

Figure 1. Map of the region south of Casey showing the location of the surveyed area, Vanderford Glacier and other major features, and stations with doppler satellite positions (triangles).

provided the required accuracy and a virtual real time position in two-dimensions. Three-dimensional positioning was accomplished by the inclusion of the barometric pressure value, at the same instant as the distance measurement.

Surface profiles and subsurface profiles were measured with an ANARE ice radar. Both surface echo and subsurface echo were recorded on film. Additionally the surface echo only was measured, and an analogue signal, proportional to the time delay in the return of the echo pulse, was generated and recorded as a separate value. This value was taken as a measure of the aircraft to snow surface distance.

Barometric pressure was used to measure all vertical heights. The Barometer was an ANARE instrument based on a Setra-quartz pressure transducer, and is capable of measuring pressure to ±0.1 millibars. One barometer was used in the aircraft with the DME, while the other was used to monitor background pressure.

Data was simultaneously recorded onto a data logger. The logger read digital data and stored it on a compact cassette. To each reading, the real time was appended. The data logged included DME values, barometric pressure, and surface echo time delay. In addition the time of occurence of an identifier that was placed on the ice radar film each minute was logged.

The survey used two single engine helicopters, a Bell 206 and a Hughes 500 C. The Bell 206 was equiped with an instrument rack which was mounted on the rear port seat locating points. This rack contained the ice radar, the DME and barometer, while the data logger occupied the gap between the instrument rack and the operator in the rear right hand seat. Externally, the Bell 206 had a boom structure on which the ice radar antennae were mounted. On those parts of the survey where the ice radar was not used, the radar transmitter section, the antennae, the monitor and recording oscilloscopes were removed from the aircraft. The second aircraft was used as a transport vehicle for the doppler satellite receiver and the gravity meter.

28.2 MEASUREMENT TECHNIQUES

The doppler satellite receiver was set up to accurately measure the Miniranger ground reference stations "MR1" ($66^{o}52'43"S$, $111^{o}135'E$) and "MR2" ($66^{o}59'56"S$, $110^{o}30'19"E$). The receiver was housed in an aluminium weather proof box, which incorporated a battery compartment and an external connector to a solar cell array. With this configuration, the receiver could be left unattended for many weeks. The Pass Selector on the receiver was programmed to the time when other operations in the area were unlikely. As both "MR1" and "MR2" where on the ice, measurements of their positions were done at the beginning of the survey period, and at the end, to determine any movement.

Surface and subsurface profiling was done with the ice radar. The aircraft in which it was mounted flew a predetermined grid over the area. In-flight navigation was done by plotting the distances given by

the DME. The DME values, barometric pressure (aircraft), surface echo time delay and real time were logged every 10 seconds. The subsurface echo from the radar was recorded on 35 mm film.

Velocity measurements of markers placed at the snout of the glacier were made by accurately measuring their position using the DME when they were first placed, then several weeks later. Since the accuracy required was in the order of several metres, the helicopter with the DME was guided to hover directly overhead by an observer on the ground. After a position value was obtained, the helicopter landed at the marker, so that a barometric pressure for the altitude of the marker could be obtained.

Positioning of gravity measurement points was similar to the velocity marker positioning, except that it was not necessary to hover. While the gravity measurement was being taken, the helicopter with the DME passed slowly overhead to windward. At the estimated instant of being overhead, the position was recorded. A barometric pressure of the gravity measurement site was then taken.

Barometric control was achieved by the recording of the value on the barometer used in the helicopter, at the beginning and end of each flight. Where possible, the same datum was used. A second recording barometer was located at Casey ($66^{o}16S$, $110^{o}32E$) as a backup and cross check.

29. A SHALLOW CORE-COLLECTING MECHANICAL ICE DRILL

E. Wehrle
Antarctic Division, Department of Science
Kingston, Tasmania, 7150.

ABSTRACT

A portable electro-mechanical ice drill is described. The drill is intended to obtain 1 m long ice cores, in a dry hole, to a maximum depth of 200 m. It is to be used on inland Antarctic traverses and thus, must be easy to operate and maintain.

29.1 INTRODUCTION

A portable electro-mechanical shallow ice drill is currently being developed by the Antarctic Division Glaciology Section. It is intended to obtain 1 m long ice-cores in a dry hole to a maximum depth of up to 200 m.

A new drill design concept has been adopted which incorporates a counter-rotating barrel and cutting system. By using two barrels rotating in opposite directions, the resultant torque is minimised and ice chip transport rate increased.

The drill was designed and built during 1982, and tested at three sites on the Law Dome, Antarctica during the austral summer season of 1983/84.

29.2 DESCRIPTION

The shallow drill consists of an upper section approximately 1 m long containing anti torque skates, motor and gearbox; and a lower section approximately 1.8 m long consisting of two counter rotating barrels (Figure 1).

The motor is an 800 watt 'AEG' drill with the handle cut off to enable it to fit inside a tube which is approximately 128 mm in diameter. The electronics contained in the handle were fitted in a separate box within the same compartment. A relay was used for reversing the drill direction.

The motor drives through a 6:1 reduction gearbox and then another gearbox which drives the concentric inner and outer barrels in opposite directions. The barrels can rotate at a rate between 35 and 130 rpm depending on the motor speed.

The lower section of the two counter-rotating barrels is designed to obtain a core 1 m long, with a chamber 0.5 m long above it where ice cuttings are stored.

The outer barrel, which rotates anti-clockwise, is 1.8 m long and made from a combination of fibreglass and Kevlar. On the inside of it, are

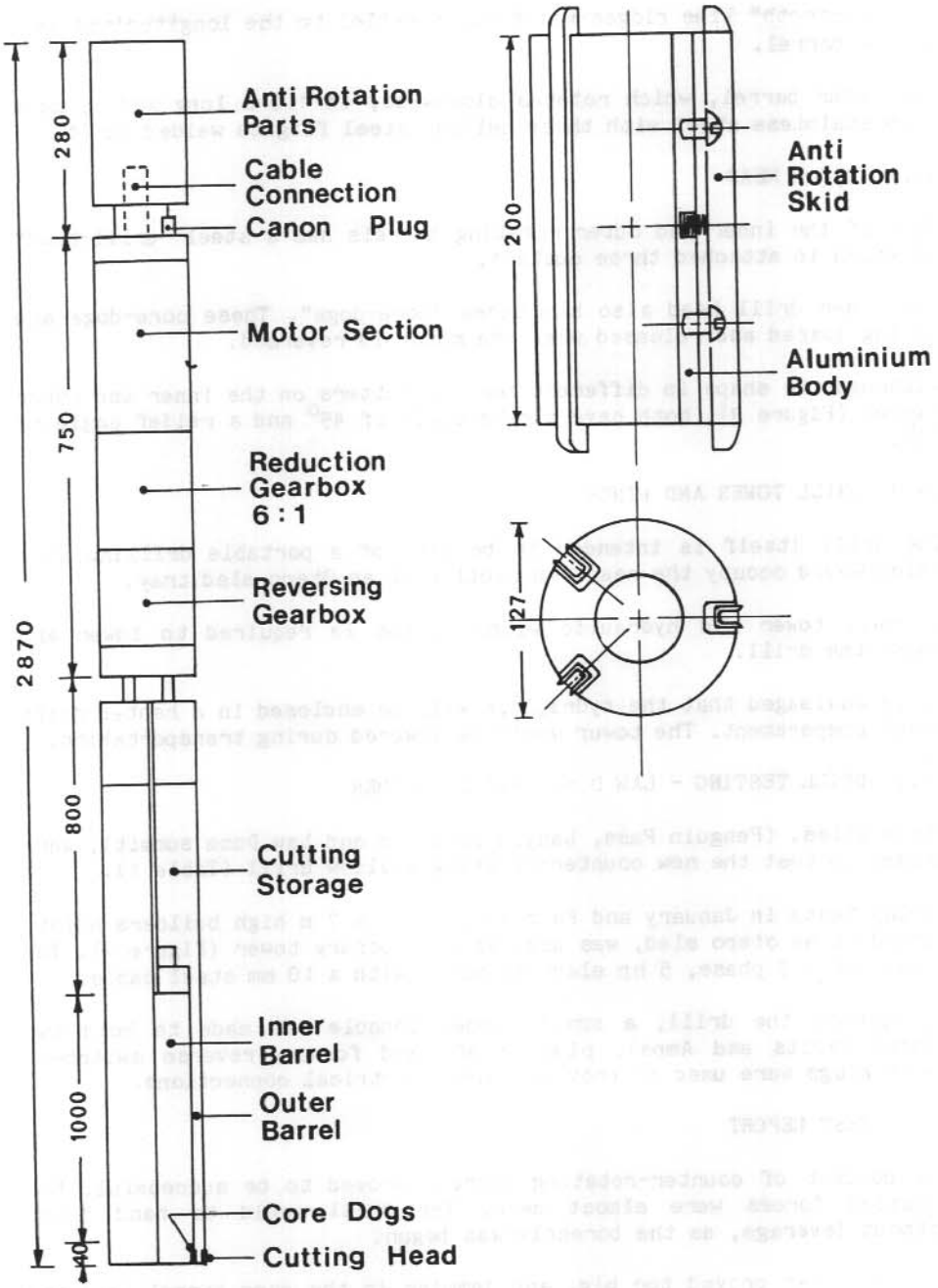

Figure 1. Shallow drill schematic.

24 "saw-tooth" like ridges which run parellel to the longitudinal axis of the barrel.

The inner barrel, which rotates clockwise, is 1.0 m long and is made from stainless steel with three helical steel flights welded to it.

29.3 DRILL HEAD

Each of the inner and outer rotating barrels has a steel "drill-head" to which is attached three cutters.

The inner drill head also has three "core-dogs". These core-dogs are spring loaded and released when the motor is reversed.

Although the shape is different for the cutters on the inner and outer barrel (Figure 3), both have a rake angle of 45^{o} and a relief angle of 10^{o}.

29.4 DRILL TOWER AND WINCH

The drill itself is intended to be part of a portable drilling unit which would occupy the rear 1 m section of an Otaco sled tray.

A small tower and hydraulic winch system is required to lower and raise the drill.

It is envisaged that the hydraulics will be enclosed in a heated drift proof compartment. The tower would be lowered during transportation.

29.5 DRILL TESTING - LAW DOME 1983/84 SUMMER

Three sites, (Penguin Pass, Lanyon Junction and Law Dome summit), were chosen to test the new counter-rotating shallow drill (Table 1).

During tests in January and February, 1984, a 7 m high builders hoist, fitted to an otaco sled, was used as a temporary tower (Figure 4). The hoist had a 3 phase, 5 hp electric motor with a 10 mm steel cable.

To operate the drill, a small wooden consele was made to hold two gauges (volts and Amps), plus on/off and forward/reverse switches. Canon plugs were used to provide quick electrical connections.

29.6 TEST REPORT

The concept of counter-rotating barrels proved to be successful. Net rotation forces were almost zero. The drill could be hand held, without leverage, as the borehole was begun.

Core diameter proved too big, and jamming in the core barrel consumed too much motor power. The gearbox functioned well although a shear pin in the drive shaft broke and was replaced with stronger material. It was thought that the motor load might be decreased by increasing the width of the cutting face. Enlarged cutters were fitted reducing the core diameter to 96 mm, but little improvement resulted.

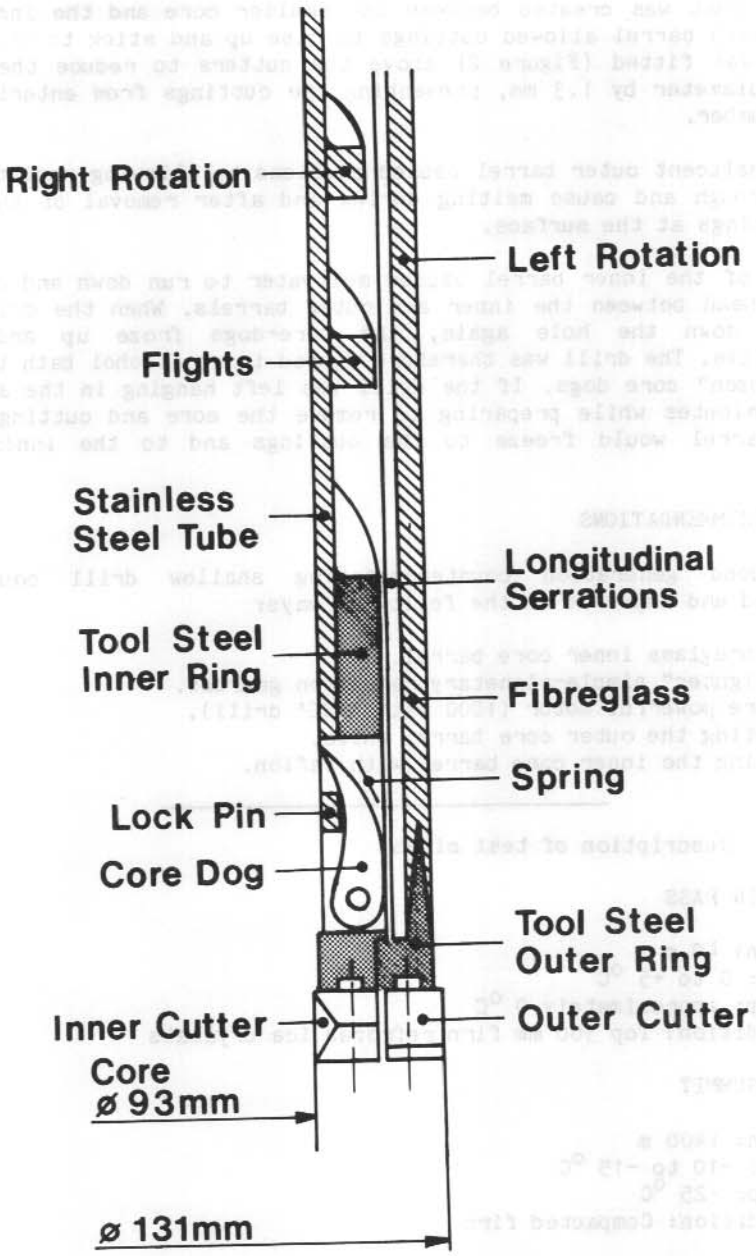

Figure 2. Cross section of the inner and outer core barrel.

The gap that was created between the smaller core and the inside of the (inner) barrel allowed cuttings to rise up and stick to the core. A ring was fitted (Figure 2) above the cutters to reduce the inner barrel diameter by 1.3 mm, preventing the cuttings from entering the core chamber.

The translucent outer barrel caused problems by allowing radiation to pass through and cause melting during and after removal of the core and cuttings at the surface.

Heating of the inner barrel caused meltwater to run down and collect at the head between the inner and outer barrels. When the drill was lowered down the hole again, the core-dogs froze up and were inoperative. The drill was therefore dipped in an alcohol bath to free the "frozen" core dogs. If the drill was left hanging in the sun for say, 5 minutes while preparing to remove the core and cuttings, the outer barrel would freeze to the cuttings and to the inner core barrel.

29.7 RECOMMENDATIONS

The second generation counter-rotating shallow drill could be lightened and improved in the following ways:

(a) A fibreglass inner core barrel.
(b) A "lighter" simple-planetary reduction gearbox.
(c) A more powerful motor (1000 watt 'AEG' drill).
(d) Painting the outer core barrel white.
(e) Coating the inner core barrel with teflon.

Table 1. Description of test sites

1. PENGUIN PASS

Elevation: 40 m
Air Temp: 0 to +5 ^{o}C
Snow Temp: approximately 0 ^{o}C
Snow Condition: Top 300 mm firn refrozen ice crystals

2. DOME SUMMIT

Elevation: 1400 m
Air Temp: -10 to -15 ^{o}C
Snow Temp: -25 ^{o}C
Snow Condition: Compacted firn

3. LANYON JUNCTION

Elevation: 400 m
Air Temp: +3 to -5 ^{o}C
Snow Temp: unknown
Snow Condition: Compacted firn with refrozen melt water layers approximately 10 to 3 mm thick.

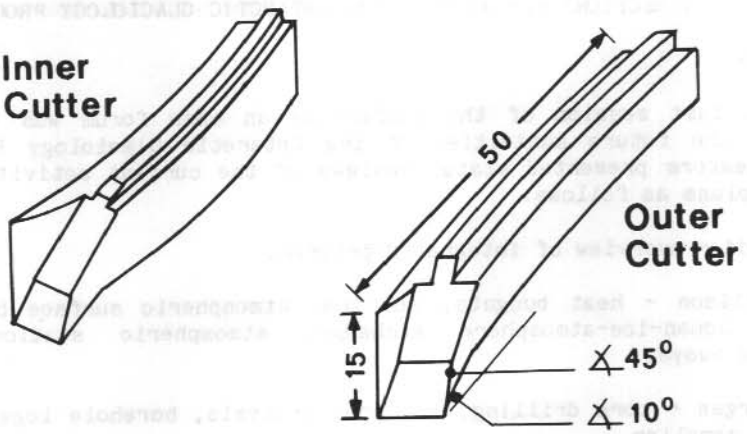

Figure 3. Cutter shapes for the inner and outer core barrel.

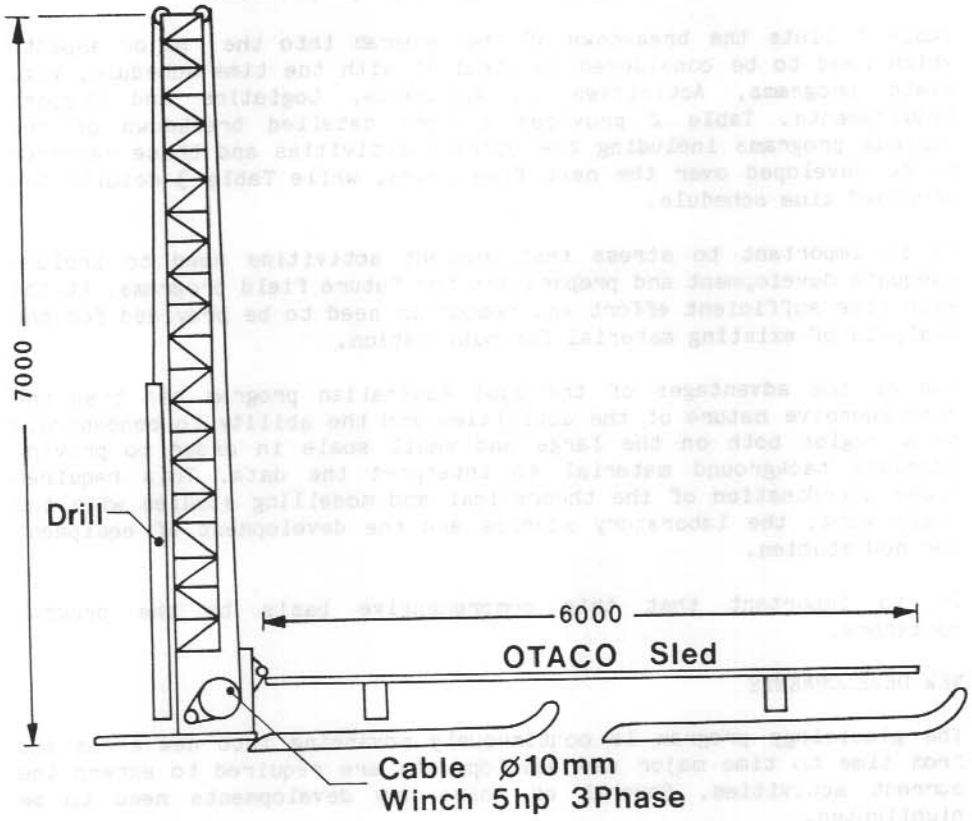

Figure 4. Tower arrangement used in 1983/84 testing program.

G. FUTURE DIRECTIONS FOR AUSTRALIA'S ANTARCTIC GLACIOLOGY PROGRAM

OVERVIEW

For the last session of the conference an open forum was held to discuss the future activities of the Antarctic Glaciology Program. Lead speakers presented status reviews of the current activities and future plans as follows:

W.F. Budd - overview of integrated program.

I.F. Allison - heat budgets, sea ice, atmospheric surface boundary layer, ocean-ice-atmosphere exchange, atmospheric stations and drifting buoys.

V.I. Morgan - core drilling, ice core analysis, borehole logging and surface sampling.

N.W. Young - oversnow traverses, aerial sounding, summer programs for ice movement stations.

T.H. Jacka - Laboratory studies of ice flow properties.

Table 1 lists the breakdown of the program into the major aspects which need to be considered in parallel with the time schedule, viz. Field programs, Activities in Australia, Logistics and Support Requirements. Table 2 provides a more detailed breakdown of the various programs including the current activities and those required to be developed over the next five years, while Table 3 details the proposed time schedule.

It is important to stress that current activities need to include adequate development and preparation for future field programs. At the same time sufficient effort and resources need to be provided for the analysis of existing material for publication.

One of the advantages of the past Australian program has been the comprehensive nature of the activities and the ability to concentrate on a region both on the large and small scale in order to provide adequate background material to interpret the data. This requires close coordination of the theoretical and modelling studies with the field work, the laboratory studies and the development of equipment for new studies.

It is important that this comprehensive basis to the program continues.

NEW DEVELOPMENTS

The glaciology program is continuously advancing into new areas and from time to time major new developments are required to extend the current activities. Several of these new developments need to be highlighted.

(a) Deep core drilling

The thermal drill currently in use is limited to depths not much greater than 500 m, depending on the ice temperatures. Near the coast of Law Dome the ice cored near the bed reaches ages of about 30 000 years but is very compressed. To get ice much older to study climatic change back beyond the last interglacial, it is necessary to develop a drill to operate in fluid. Such a drill has been developed in Denmark and successfully used in Greenland. It is proposed to develop a similar drill for use inland of Casey.

(b) Lambert Basin traverse

As the repeat surveys over the traverse routes inland of Casey to the south, east and west are completed over the next few years the major traverse interest concentrates on the interior Lambert Basin between Mawson and Davis. A further gap in our coverage exists between Davis and Mirny. It is important to plan for these traverses well in advance, and to develop the capability of large traverses from Mawson, as was usual in previous years of the ANARE.

(c) Aerial sounding

Over recent years with the lack of a fixed wing aircraft for aerial sounding the small helicopters have been equipped with sounding equipment. There is still a strong need for the fixed wing aircraft for the sounding and the ability to extend the range of sounding further afield.

(d) Automatic stations

The success of the current automatic station program is encouraging and offers the opportunity for a wide coverage of surface data over the continent in a very cost effective manner. It is important to aim to increase the life of the stations to in excess of 10 years and to arrange that the basic meteorologial data also be channelled routinely into the synoptic network.

(e) Ice core analysis

Work is progressing well on the ice core analyses for isotopes, crystallography and CO_2. Other projects are being carried out in cooperation with the French (radioactivity and gas volumes).

There is still need to develop other techniques including the measurement of conductivity, particulates and chemical analysis. Additional assistance is needed to study chemicals and particulates. In particular for the chemicals, an extraction technique is needed to obtain various elements much as C, Cl, Al and Be for radioactive dating using the new accelerator dating technique. This new technique should allow accurate dating of the core back to 10^6 a and should be available by the time the deep cores are obtained.

Table 1. Australian Antarctic Glaciology Program overview.

A. Field Programs

1. Deep core drilling
2. Aerial sounding
3. Oversnow traverses
4. Automatic stations
5. Sea ice - ocean - atmosphere interaction

B. Activities in Australia

1. Ice core analysis
2. Survey reductions
3. Numerical modelling
4. Instrumentation development

C. Logistics and Support Requirements

1. Aircraft
2. Oversnow
3. Shipping
4. Australian infrastructure

Table 2. Details of glaciology programs.

A. Field Programs

1. Deep core drilling and borehole logging
(New deep coring drill required)

Locations

(i) Law Dome
Summit (1200m to bed)
Other locations on flowline to coast

(ii) Inland deep ice ~600km S of Casey
4.5km to bed.

(iii) Intermediate drilling along traverses.

2. Aerial Sounding

(i) Outlet Glaciers: Vanderford-Totten
Scott-Denman

(ii) Northern PCM, Mawson-Davis, Grove Mts., Amery Ice Shelf.

(iii) Coastal Surveys: Dumont-Casey-Mirny-Davis.
George V and Oates Land.

3. Oversnow Traverses.
Surface elevation, radio-echo sounding, snow accumulation, surface sampling, mean surface temperatures, intermediate drilling (10m-500m).
Routes: Casey-Mirny re-survey
Casey-Dumont re-survey
Inland deep core drilling S of Casey.
Law Dome surveys (3 further years' winters)
Australian-USSR cooperative traverses.
(Mirny-Dome B-Dome A, towards Davis)

Lambert Basin: Mawson-Komsomolskiy Pk-Grove Mts-Davis

4. Automatic Stations
Atmosphere boundary layer, heat budgets, participation in meteorological research (synoptic pressure, temperature and wind)
Locations: Law Dome (3); Inland of Casey (3) south, east and west; Bunger Hills; Chick Is.; Inland of Mawson, Komsomolskiy Pk; Grove Mts.; Amery Ice Shelf; Heard Is.

5. Sea Ice-Ocean-Atmosphere Interaction
Drifting Buoys
Aerial remote sensing and ground truth
ocean profiling (STD)
CO_2 exchange
Icebergs: monitoring observations, instrumented trial tows.

B. Activities in Australia

1. Ice core analysis
Stable isotopes ($^{18}O/^{16}O$)
Crystal structure, size (past temperatures), orientation
Deformation properties
Sonic velocities
Conductivity (volcanic record, annual layers)
Chemical content
Particulates, (volcanic and dust components)
Radio-isotopes-dating

Accelerator Mass-spectrometer (^{39}A, ^{14}C, ^{36}Cl, ^{26}Al, ^{10}Be) dating
Chemical extraction

2. Survey Reductions and Data Analysis
Oversnow traverse data
Aerial sounding (automation of digital processing)
Borehole logging data
Ice movement surveys
Heat budget studies (inland stations, sea ice and ocean observations)
Remote sensing analyses
Climatic data monitoring

3. Numerical Modelling

(i) Ice flow, mass budgets, dynamics, particle trajectories, age distributions.

(ii) Temperature distributions and thermal regime, interpretation of past climates.

(iii) Specific regional models: Law Dome, outlet glaciers, ice shelves, drainage basins, whole Antarctica.

(iv) Past climate-ice sheet-sea level interactions for Antarctica and globally.

(v) Future behaviour of the ice sheet, climate and sea level.

4. Instrumentation Development

(i) Deep coring drill, borehole logging ice core handling and analysis

(ii) Automatic stations and buoys

(iii) Ice radar and aerial sensing equipment

(iv) Laboratory equipment for ice studies.

C. Logistics and Support Requirements

1. Aircraft
Fixed wing instrumented aircraft for aerial sounding and remote sensing in Antarctica (e.g. Twin Otter type)
Intercontinental aircraft for passenger transfer (e.g. Hercules C-130)
Rotary wing aircraft for deployment of ground parties

2. Oversnow Traverse equipment
Tractors, Personnel carriers, caravans, sledges, Support for deep core drilling inland.
Traverse equipment is required for each of Casey and Mawson.

3. Shipping
Depth sounding over the continental shelf, observations of pack ice and icebergs, oceanographic sounding, deployment of buoys, deployment of ground parties and automatic stations.

4. Australian Infrastructure
Core storage and handling facilities
Laboratory analysis equipment
Chemical and dating analyses facilities
Personnel for instrumentation development and data analysis.

Table 3. Proposed future glaciology programs.

	Casey Region				Other
	Traverse	Air Supported	Drilling		
1984	Southern IAGP route. (Remeasure)				Deploy AWS along southern route at 68.5° S, 71.4° S, 74.2° S. Studies of thermal and ice crystal structure of Law Dome.
1984-85		Vanderford Glacier movement survey.	Field drill testing. Law Dome summit site survey.	Deploy 3 buoys Prydz Bay Region.	
1985	Eastern 2000 m route. (Remeasure)				Studies of thermal and ice crystal structure of Law Dome. Deploy AWS at Mawson (67.6° S, 62.9° E) Law Dome (66.7° S, 112.9° E) GD10 (69°, 124.3° E).
1985-86		Totten Glacier Topographic and movement survey.	Law Dome summit site preparation.		Deploy AWS at Commonwealth Bay and Heard Island (opportunity).
1986	Western 2000 m route. Casey - Davis.			Mawson winter sea ice studies in conjunction with S.P.R.I. Cambridge, U.K.	Deploy AWS at GF10 68.5° S, 99.7° E.
1986-87	Possible extension of traverse to Grove Mountains.	Denman Glacier/Shackleton Ice Shelf topographic and movement survey.	Thermal drilling and electromechanical drill testing.	Deploy 3-5 buoys and observations of pack ice characteristics and structure during marine science cruises.	Deploy AWS near Grove Mountains.
1987	Western 2000 m route. Davis - Casey. (Remeasure)				Deploy AWS inland of Davis.
1987-88			Completion of electromechanical drilling to bedrock.		
1988	Law Dome glaciological/ geophysical surveys				Preparation for Mawson - Komsomolskiy Peak - Grove Mts.

Footnote: Cooperative traverse program with Soviet Antarctic Expeditions to be continued on opportunity basis. Proposed route: Mirny - Dome Argus.

1988 - 1993

Traverse 4 - 5 year program of surveys Mawson - Davis in Lambert Basin.

Air supported 1 - 2 season program of topographic and movement surveys in Northern Prince Charles Mountains/Amery Ice Shelf - (after Bunger Hills programs completed). Fixed wing R.E.S. of coastal regions.

Drilling 3 - 4 season/year program of deep drilling in 4000 m ice inland of Casey.